

ISSN 1407-5806

**COMPUTER
MODELLING
AND
NEW TECHNOLOGIES**

**Volume 5
No 1**

2001

Transporta un sakaru institūts
(Transport and Telecommunication Institute)

Computer Modelling and New Technologies

Volume 5, No.1- 2001

ISSN 1407-5806
ISSN 1407-5814
(On-line: www.tsi.lv)

Riga – 2001

EDITORIAL BOARD:

Prof. Igor Kabashkin (Chairman of the Board), *Transport & Telecommunication Institute, Latvia*

Prof. Yuri Shunin (Editor-in-Chief), *Transport & Telecommunication Institute, Latvia*

Prof. Adolfas Baublys, *Vilnius Gedeminas Technical University, Lithuania;*

Dr. Brent Bowen, *University of Nebraska at Omaha , USA;*

Prof. Olgierd Dumbrajs, *Helsinki University of Technology, Finland;*

Prof. Vitaly Yeremeyev, *Transport & Telecommunication Institute, Latvia*

Prof. Juris-Roberts Kalninsh *Social Technologies Institution of Higher Education, Latvia;*

Prof. Arnold Kiv, *Ben-Gurion University of the Negev, Israel*

Prof. Anatoly Kozlov, *Moscow State University of Civil Aviation, Russia;*

Prof. Juris Zakis, *University of Latvia.*

Technical editors:

MS Christina Hamroon, *Transport & Telecommunication Institute, Latvia*

MS Cyril Budilov, *Transport & Telecommunication Institute, Latvia*

Host Organization:

Transport and Telecommunication Institute - Eugene Kopytov, Rector

Co-Sponsor Organization:

PAREX Bank, Latvia - Valery Kargin, President

Supporting Organizations:

Latvian Transport Development and Education Association - Andris Gutmanis, President

Latvian Academy of Sciences - Juris Ekmanis, Vice-President

University of Nebraska at Omaha , USA - Brent Bowen, Director of Aviation Institute

“The Khaim Kordonsky Charitable Foudation”- Inna Kordonsky-Frankel

THE JOURNAL IS DESIGNED FOR PUBLISHING PAPERS CONCERNING THE FOLLOWING FIELDS OF RESEARCH:

- mathematical and computer modelling
- mathematical methods in natural and engineering sciences
- physical and technical sciences
- computer sciences and technologies
- semiconductor electronics and semiconductor technologies
- aviation and aerospace technologies
- electronics and telecommunication
- navigation and radar systems
- telematics and information technologies
- transport and logistics
- economics and management
- social sciences

Articles are presented in the journal in English (preferably), Russian, German and Latvian languages (at the option of authors). All articles are reviewed.

EDITORIAL CORRESPONDENCE

Transporta un sakaru institūts (Transport and Telecommunication Institute)

Lomonosova iela 1, LV-1019, Riga, Latvia. Phone: (+371)-7100593. Fax: (+371)-7100535.

E-mail: journal@tsi.lv, <http://www.tsi.lv>

COMPUTER MODELLING AND NEW TECHNOLOGIES, 2001, Vol. 5, No.1

ISSN 1407-5806, ISSN 1407-5814 (on-line: www.tsi.lv)

Scientific and research journal of Transport and Telecommunication Institute (Riga, Latvia).

The journal is published since 1996.

CONTENT

EDITORS' REMARKS	5
SOLID STATE PHYSICS	7
ADHESION OF SILVER ON THE AL-TERMINATED CORUNDUM (0001) SURFACE: HARTREE-FOCK SIMULATIONS O. SYCHEV, Yu.F. ZHUKOVSKII, E.A. KOTOMIN, Yu.N. SHUNIN	7
A NOVEL RELATION FOR THE EFFECTIVE DIFFUSION COEFFICIENT IN INHOMOGENEOUS MEDIA J.-R. KALNIN, E. KOTOMIN	18
AB INITIO SIMULATIONS OF THE CU/MGO(001) INTERFACE YU.F. ZHUKOVSKII, D. GRYAZNOV, A. FINOGENOV, YU.N. SHUNIN	28
ELECTRONIC STRUCTURE AND RESISTIVITY OF COPPER YU. N. SHUNIN, K. BUDILOV	41
DIFFUSION PROCESSES CAUSED BY PLASMA IMMERSION ION IMPLANTATION AND DEPOSITION (PI ³ &D) A.E. KIV, E.P. BRITAVSKAYA	86
MATHEMATICAL STATISTICS AND RELIABILITY THEORY	90
RELIABILITY MODELS FOR COMMUNICATION CHANNEL OF AIR TRAFFIC CONTROL SYSTEM WITH DIFFERENT TEST STRATEGY I.V. KABASHKIN	90
APPLIED STATISTICS: METHODS AND PROBLEMS IN EDUCATION (in Russian) I.V. YATCKIV	96
CHAOTIC MAP ALGORITHMS AND ENCRYPTION TECHNOLOGY OPTIMIZATION (in Latvian) O. NASKIDAYEV	100
PECULARITIES OF DIAGNOSTIC SYSTEMS WITH ELEMENTS OF ARTIFICIAL INTELLECT (in Russian) E. KOPYTOV, V. LABENDIK, N.KABELEV	119
APPLIED ELECTRONICS	124
HIGH-SELECTION DIGITAL POLYPHASE FILTERS (in Russian) V.P. YEREMEYEV, E.V. MATOSOV, S.G. TIMONIN	124
NEW STRUCTURES OF LOW-SENSE DIGITAL FILTERS (in Russian) V.P. YEREMEYEV, A. GUMENYUK, T. MAMIROV	132
Authors' index	138
Personalia	139
Preparation of publications	143



Editors' Remarks

THE DREAM

Our life is twofold: Sleep hath its own world,
A boundary between the things misnamed
Death and existence: Sleep hath its own world,
And a wide realm of wild reality,
And dreams in their development have breath,
And tears, and tortures, and the touch of Joy:
They leave a weight upon our waking thoughts,
They take a weight from off our waking toils,
They do divide our being; they become
A portion of ourselves as of our time,

1816

George Gordon Byron **Selections. Lyrical Verse**

I'm happy to announce that "**The Khaim Kordonsky Charitable Foundation**" joins in supporting **Computer Modelling and New Technologies** journal. The introduction of *Reliability and Mathematical Statistics* field is essential and important contribution the research community. My father, Professor Khaim Kordonsky developed his life in advancing not only the science of reliability and mathematical statistics, but also the application to the solution of important problems in safety and operation efficiency.

But just as important, he selflessly gave his time and talent to his students and assistants. In supporting your journal I want to continue my father's legacy.

May 28, 2001

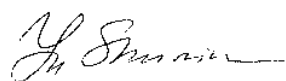
Inna Kordonsky-Frankel,
President of The Khaim Kordonsky
Charitable Foundation

The nature phenomena are accorded and contradict their models at the same time. The problem of scientist to find the best compromise on the way of nature description, and thus, on the complicated way to the truth. This is the way of science.

With this edition (**Volume5, No.1**), which is sponsored now by "**The Khaim Kordonsky Charitable Foundation**" also, we start new activities of our Journal and announce the competition on the best student scientific work presented here for **Khaim Kordonsky Prize**, open a new division "Mathematical Statistics and Reliability Theory".

This edition is the continuation of our publishing activities and the current step in new science fields. We hope our journal will be interesting for research community, and we are open for collaboration both in research and publishing.

EDITORS



Yu. N. Shunin



I.V. Kabashkin

ADHESION OF SILVER ON THE Al-TERMINATED CORUNDUM (0001) SURFACE: HARTREE-FOCK SIMULATIONS

O. SYCHEV^a, Yu.F. ZHUKOVSKI^b, E.A. KOTOMIN^b, Yu.N. SHUNIN^a

^a Department of General and Applied Physics, Transport and Telecommunication Institute,
 1 Lomonosova, LV-1019, Riga, Latvia

^b Institute for Solid State Physics, University of Latvia, 8 Kengaraga, LV-1063 Riga, Latvia

Ab initio Hartree-Fock calculations on the atomic and electronic structure of the Ag/ α -Al₂O₃(0001) (corundum) interface have been performed for a periodic two-dimensional slab model with using *a posteriori* electron correlation corrections. We have considered only Al-terminated corundum (0001) surface as both chemically and stoichiometrically stable. The dependence of the adhesion energy on the interfacial distance has been analyzed for the two most favorable Ag adsorption positions over corundum and for two different metal coverages: a 1/3 monolayer (ML) of the Ag(111) crystallographic plane and a full Ag(111) monolayer. The small adhesion energies per Ag atom (~0.2 eV for 1 ML and ~0.5 eV for 1/3 ML) are accompanied by a minor interfacial charge transfer, thus indicating a *physisorption*. The observed difference of Ag adhesion energies for 1/3 ML and 1 ML coverages arises essentially due to a transition from directed Ag-O bonding towards a more delocalized electronic density distribution. The results of our calculations are compared with available experimental studies and theoretical simulations for several Me/Al₂O₃ interfaces.

Keywords: *Ab initio* Hartree-Fock calculations, electronic structure of the Ag/ α -Al₂O₃ (corundum)

1. Introduction

Well-known in jewelry as sapphire, α -Al₂O₃ (*corundum*) nowadays is one of the most widespread ceramic materials [1], which is used also as a prospective substrate for ultrathin metal film deposition [2] and as a catalyst [3]. Numerous experimental and theoretical studies have been performed for the interfaces between corundum and various metal films including Ag [2,4,5,12-14], Cu [2,4-7,9,12,15], Nb [2,4,5,8,11,16,17], Pt [2,5,14,15], V [2,5,10,15], etc. Recent ultramicroscopic observations using STM and TEM methods have given structural information of almost atomic resolution for several Me/ α -Al₂O₃ interfaces; together with microdiffraction LEED studies they serve as a good test for theoretical simulations [2,4,5]. It may be illustrated for thin copper films grown on α -Al₂O₃(0001) substrate by molecular beam epitaxy (Figs. 1 and 2, respectively). The epitaxial orientation relationship leads to a mismatch of about 7% between the corresponding spacings of the adjacent copper and alumina lattices, i.e. 16 of the Cu(02 $\bar{2}$) planes correspond to 15 corundum (30 $\bar{3}$ 0) planes [6]. In order to minimize the interfacial energy either misfit dislocations can accommodate lattice registry or the two lattices form a strain-free incoherent interface. The latter was mainly observed for the Cu/ α -Al₂O₃ interface (Fig. 1), and its diffraction image (Fig. 2) confirms this conclusion. In the case of the Nb/ α -Al₂O₃ interface, with noticeably smaller lattice mismatch (2%), areas of fully coherent interface (as shown in Fig. 3) may coexist with the so-called semicoherent interface containing misfit dislocations in niobium (due to a larger elasticity of metal as compared to alumina) [8]. Nowadays various high-resolution spectroscopic methods such as HREELS and XPS make it possible to predict both the structural arrangement of a metal layer on corundum substrate [5,9] and details of interfacial interaction [10]. It has been reported that an oxide surface exposed to a metal atom beam results usually in 3D metal islands [2,4], although under some circumstances a layer-by-layer metal film growth can also take place [9]. The actual film growth mode depends on the very delicate balance of energies for these two modes, and also on the rate of the metal deposition [11].

For a better understanding the adhesion nature of metals deposited on the corundum surface, we need detailed information on the atomic structure of the pure substrate [18-25]. Equilibrium structure of corundum (0001) substrate have been optimized using *ab initio* methods realized in both Hartree-Fock (HF) [18,19] and Density Functional Theory (DFT) [20] computational codes. Recent molecular dynamics (MD) simulations on the Al-terminated α -Al₂O₃(0001) surface have estimated an equilibrium surface geometry at several temperatures, in qualitative agreement with previous first-principles calculations [21]. It is generally believed

that the Al-terminated surface is energetically favored over the O-terminated one since the former is closer to a bulk structure [22]. Detailed theoretical studies [23,24] indicate that even under conditions of high oxygen gas partial pressure the Al-terminated corundum surface is stable (contrary to conclusions made in the review paper [25]), while even a small hydrogen concentration on the α - $\text{Al}_2\text{O}_3(0001)$ substrate considerably stabilizes the alternative O-terminated surface.

Since H atoms are not included in our model, the Ag/ α - Al_2O_3 interface with O-termination of substrate is not considered here. All the more so because we earlier simulated the latter [13] when

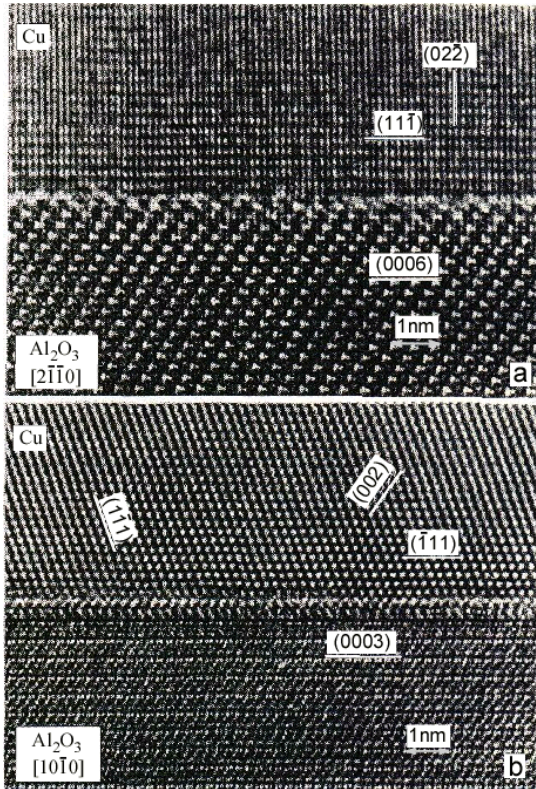


Figure 1. High-resolution TEM images of atomically flat Cu(111)/ α - $\text{Al}_2\text{O}_3(0001)$ interface [6]: (a) along the Cu[211] and α - $\text{Al}_2\text{O}_3[2\bar{1}\bar{1}0]$ zone axes (the clearly resolved Cu(022) planes have a spacing of 1.28 Å); (b) after tilting the same interface area into the Cu [110] and α - $\text{Al}_2\text{O}_3[10\bar{1}0]$ zone axes the $(\bar{1}11)$, $(1\bar{1}1)$ and (002) copper planes are clearly imaged.



Figure 2. LEED pattern of 50 Å Cu film on α - $\text{Al}_2\text{O}_3(0001)$ substrate after annealing to 923 K to give Cu(111) particles [7]. The schematic below shows the Cu(111) spots as small, filled dots, and the clean α - $\text{Al}_2\text{O}_3(0001)$ spots as open circles.

suggesting that silver atoms may replace outer Al^{3+} ions in result of the non-equilibrium metal deposition on corundum surface. The most favorable substrate sites for adsorption of silver atoms have been found in that study as well: (i) on axes containing Al^{3+} ions and crossing *equilateral* triangles formed from O^{2-} ions (*E* sites), and (ii) on *hollow* sites over internal O^{2-} ions (*H* sites). In both cases silver atoms were found to be interacting with substrate rather strongly (3 eV per Ag atom) [13]. Later Verdozzi *et al.* [14] modeled silver and platinum adhesion over an Al-terminated 54-plane corundum slab using plane-wave pseudopotential calculations in the framework of DFT method. Their general conclusion was made that the nature of such an Ag/corundum interaction is *physisorption*, although well-separated metal atoms (1/3 ML) may be more strongly bound (1.1 eV per Ag atom) due to an effect of the surface Madelung potential above the alumina surface. A similar DFT plane-wave study was performed for Nb adhesion on the both Al- and O-terminated surfaces of a corundum (0001) substrate [17]. It was found that Nb-adhesion on the O-terminated surface (13

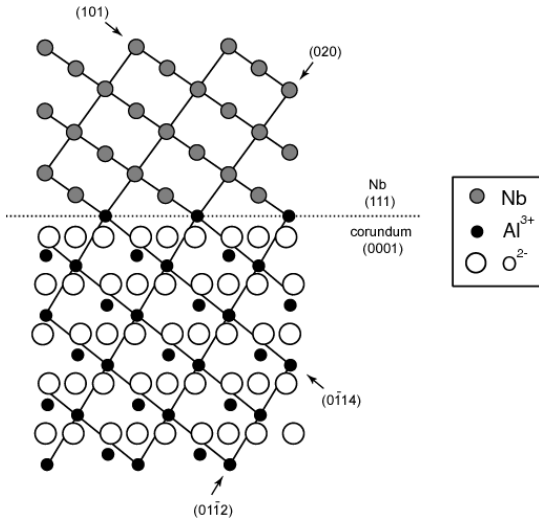


Figure 3. Cross-section of the coherent Nb(111)/ α -Al₂O₃(0001) interface with Al-terminated substrate along the Nb[101] and α -Al₂O₃[2110] zone axes [8].

eV per Nb atom) is much stronger than on the Al-terminated surface (3.4 eV), probably due to the high “energy cost” for forming such a surface [17]. A phenomenological so-called Image Interaction Model (IIM) has also been applied to Nb adhesion on Al-terminated corundum [11]. The optimal adsorption sites for the Nb(111) monolayer were found in agreement with previous *ab initio* calculations, over equilateral O triangles; the adhesion energy per Ag atom for these adsorption sites was found here to be 4 eV.

To clarify the nature of Ag adhesion on an Al-terminated corundum (0001) surface, we present in this paper a quantitative analysis for both parameters of total energy and electronic properties of the interfacial bonding (in terms of the difference electron density and local multipolar components of the charge density). The analysis is based on periodic HF-CC calculations (Hartree-Fock method with electron-correlation corrections) for two different Ag adsorption sites and two different Ag coverages (1/3 ML and 1 ML).

2. Theoretical background

2.1. COMPUTATIONAL DETAILS

We use the HF-CC method as implemented into the computer code CRYSTAL98 [26] with Gaussian-type basis set. This code is well suited for calculations of periodic 2D and 3D systems and incorporates electron correlation corrections. Recently we have described main algorithms and procedures realized in CRYSTAL code in order to perform the HF-CC calculations [27,28]. In the framework of the HF-CC method, we have used mainly Perdew-Wang *a posteriori* corrections [29]. In contrast to our previous study [13], here we have applied the basis sets optimized by Catti *et al.* [30] for both α -Al₂O₃ and MgAl₂O₄ crystals. The Al and O basis sets were modified in Ref. [30] by introducing *d* polarization function and re-optimizing core and valence shells as well as *sp* polarization functions used in previous α -Al₂O₃ studies [18,19]. Re-optimized all-electron 8(*s*)-511(*sp*)-1(*d*) and 8(*s*)-411(*sp*)-1(*d*) basis sets for Al and O, respectively, were found to be effective in lowering the total energy for corundum slabs and describing the electron density distribution more properly, especially around the aluminium atoms [29]. For the Ag atoms, we have used the same basis set as earlier [13], employing the small-core Hay-Wadt pseudo-potential for the atomic core [31] and a 311(*sp*)-31(*d*) basis set with Gaussian-type functions for the valence and virtual shells.

2.2. MODEL OF Ag/ α -Al₂O₃(0001) INTERFACE

For the simulation of silver adhesion on the corundum substrate, we have used a *slab model*, periodic in two dimensions and with finite thickness in the third dimension, perpendicular to the (0001) plane. We have fixed the alumina substrate structure to be the same as in Refs. [13,19]. Slab model of the α -Al₂O₃(0001) substrate belongs to the hexagonal plane group P_{321} (see its top views in Fig. 4). Two-dimensional (2D) surface unit cell is a rhombus with optimized side $a \approx 4.76$ Å. The C_3 , rotation axes normal to the surface and containing Al³⁺ ions form a regular network, which crosses a (111) plane of the face-centered cubic structure (*fcc*) parallel to the (0001) plane. The distance between adjacent aluminium axes is 2.75 Å ($a/\sqrt{3}$). The two rhombic surface unit cells drawn between Al³⁺ axes are shown in Fig. 4. All the O²⁻ ions in the bulk structure are equivalent and the slab structure optimized by Puchin *et al.* [19] forms a periodic network of *equilateral triangles* with sides b_1 , b_2 and b_3 (2.64, 2.74 and 2.87 Å, respectively), as well as versatile triangles positioned

between them (Fig. 4a). Although this optimized structure belongs to the plane group P_{321} , it is slightly distorted as compared to the structure of perfect corundum crystal [18,32] containing only two types of equilateral oxygen triangles (b'_1 and b'_2) and isosceles triangles between them (Figure 4b).

A 9-layer slab terminated by Al^{3+} ions (Figure 5) has been modeled, with a primitive unit cell containing 15 atoms. The oxygen-containing corundum (0001) planes are equivalent, with a distance $c \approx 2.16$ Å between nearest ones. Each oxygen plane can be transformed into neighboring one by a synchronous combination of the 60° rotation around the corresponding C_{3v} axes and a translation by $AA' = a/\sqrt{3}$, so that the two rhombic surface unit cells shown in Figure 4a coincide. Each O plane is associated with two adjacent, less-densely packed Al planes, so that each Al^{3+} ion is positioned either above the center

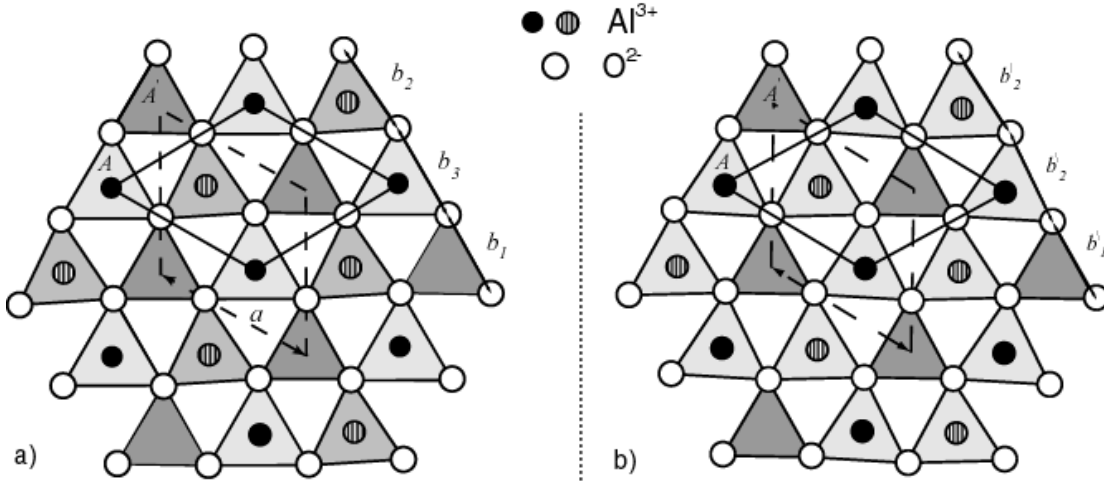


Figure 4. Top views of the oxygen plane of the corundum (0001) substrate as optimized in [19] (a) and in the case of perfect corundum structure [32] (b). The 2D rhombic unit cell with a side a as well as the two neighboring aluminium planes positioned symmetrically above and below oxygen plane (the corresponding Al^{3+} ions are shown as black and striped circles, respectively). (a) The side lengths b_1 , b_2 and b_3 for three different equilateral triangles are given in the text; each of them is shown with own gray-scale color: the larger side, the lighter triangle. The versatile triangles are shown white. (b) There exist only two types of equilateral oxygen triangles with side lengths b'_1 and b'_2 (2.57 Å and 2.84 Å) shown as dark and light, respectively, whereas white triangles between them are isosceles.

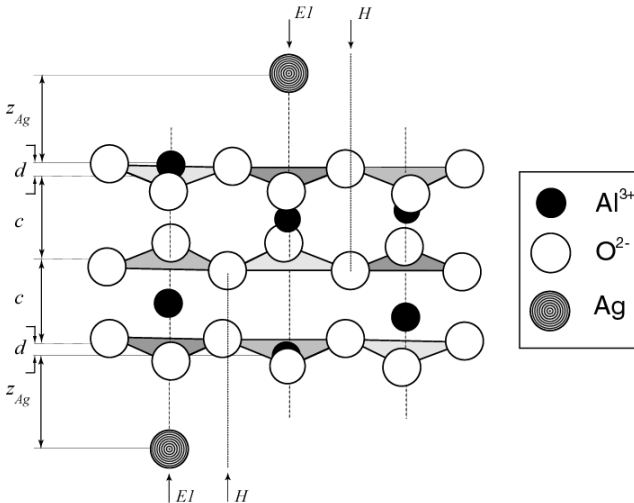


Figure 5. Side view for $\alpha\text{-Al}_2\text{O}_3(0001)$ slab where silver atoms are distributed regularly on the aluminium C_{3v} axes above and below Al-terminated substrate, thus forming a periodic $\sqrt{3} \times \sqrt{3}$ superstructure (1/3 ML coverage). The interlayer structure of the interface is defined by c , d and z_{Ag} parameters. The optimized values for c and d are 2.16 Å and 0.12 Å, respectively, whereas values of z_{Ag} are given in Table 1. The most probable sites of Ag adsorption are found to be H and EI (their explanations are given in text).

of the largest equilateral oxygen triangle or below the middle triangle (at a distance d of 0.84 Å). To reduce maximally the computational effort and exploit the system's symmetry, we have applied a two-side adhesion model, i.e. spatially similar Ag layers have been placed on *both* surfaces of the corundum slab. HF-CC

calculations performed by Puchin *et al.* [19] and other studies of the $\alpha\text{-Al}_2\text{O}_3(0001)$ substrate in the literature [18,20,21] have shown that the external aluminium ions on the isolated Al-terminated substrate relax by 60-80% towards the outermost oxygen plane (Figure 5). Here, we have varied the interfacial distance z_{Ag} as well as the outer distance d for the Al-terminated corundum substrate. We have considered two different coverages, 1/3 ML (Figs. 6a,b) and 1 ML (Figures 6c,d). For 1/3 ML coverage, we have considered two different adsorption patterns: Ag atoms over the smallest equilateral triangles, site $E1$, or Ag over versatile oxygen triangles, *i.e.* above 1/3 of H sites (Fig. 5). As to 1 ML coverage, two different adsorption patterns were considered as well: either above all equilateral triangles (E sites shown in Fig. 6c) or above all H sites (Fig. 6d). For the 1/3 ML coverage one third of an $\text{Ag}(111)$ crystallographic plane is distributed regularly on corundum (0001) substrate forming a periodic $\sqrt{3} \times \sqrt{3}$ superstructure. In our previous simulations of silver adhesion on O-terminated corundum (0001) surface [13], we considered also Ag adsorption above outermost O^{2-} ions, but these were found to be less stable towards silver adhesion. Space and symmetry compatibility between the $\alpha\text{-Al}_2\text{O}_3(0001)$ and $\text{Ag}(111)$ planes mentioned above makes it possible to consider comparatively simple models of the Ag/corundum interface without misfit dislocations (Figures 6a-d).

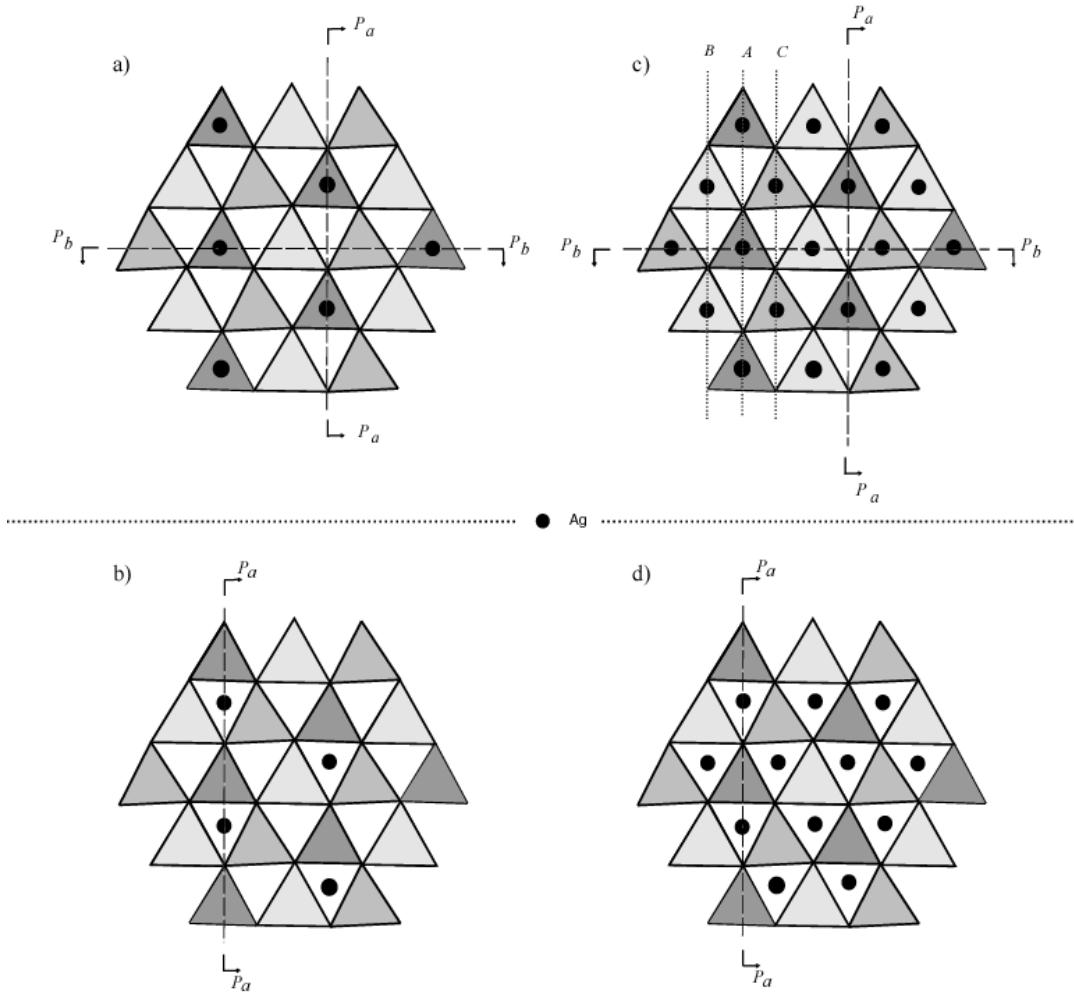


Figure 6. Top views of Ag atom distributions over corundum (0001) surface for the two different coverages: 1/3 ML of the $\text{Ag}(111)$ crystallographic plane (a,b) or 1 Ag ML (c,d). The two different Ag adsorption positions are above equilateral triangles (a,c) and versatile triangles (b,d) forming the outermost oxygen plane. Various planes P - P , which projections are shown on all top views, are used in Fig. 7 to analyze the electron charge density distributions in the cross sections perpendicular to the (0001) surface. Note that (c) shows the top view on steps of the buckled $\text{Ag}(111)$ monolayer over Al-terminated corundum. A lines correspond to foets of silver steps closest to the substrate while C lines correspond to their apexes, respectively (density plot in Fig. 7e shows more clearly a relief of Ag step).

The experimental Ag-Ag equilibrium distance in bulk silver is 2.88 Å and slightly exceeds that between the nearest Al³⁺ axes normal to the α-Al₂O₃(0001) surface (2.75 Å) [32]. Thus, mismatch between the corresponding spacings of the adjacent silver and alumina lattices is about 4.7%, *i.e.* smaller than for Cu/corundum interface, but larger than mismatch between alumina and niobium lattices mentioned in Introduction. This is why for 1 Ag ML positioned over all *E* sites (Figure 6c), some difference between the z_{Ag} coordinates appears (when optimizing the interfacial energy), which can be characterized by height h_{Ag} of steps in the buckled silver monolayer. To simplify the geometry optimization, the heights between the Ag rows *A* and *B* as well as between *B* and *C* (Figure 6c) have been kept equal. Our resulting optimized overlayer becomes a *stepped* Ag(111) monolayer for the adsorption pattern in Fig. 6c. The optimized value of h_{Ag} was found to be around 0.7 Å, similar to the result of Verdozzi *et al.* [14]. The buckled silver monolayer is clearly seen in the corresponding electron density plot (Figure 7e). When 1 Ag ML is placed over all *H* sites (Figure 6d), by necessity silver monolayer forms a flat, slightly *distorted* Ag(111) film, with *three* kinds of distances between nearest Ag atoms: 2.64, 2.74 and 2.87 Å (cf. aforementioned 2.88 Å in the Ag bulk [32]).

2.3. BRIEF DEFINITION OF BASIC PROPERTIES

In TABLE 1 we present parameters of equilibrium geometry, h_{Ag} and z_{Ag} , which were mentioned above. The binding energy per Ag atom, E_{bind} , at the equilibrium distance is also given in Table 1. Here we have calculated E_{bind} using the *universal binding energy relation* [33] (similar to the potential energy curve for diatomic molecule), where E_{bind} is extracted from the potential interface energy curve $E_b(z_{\text{Ag}})$:

$$E_b(z_{\text{Ag}}) = 2nE_{\text{bind}} \left(1 + \frac{z_{\text{Ag}} - z_{\text{Ag}}^{(o)}}{z_{\text{Ag}}} \right) \exp \left[-\frac{z_{\text{Ag}} - z_{\text{Ag}}^{(o)}}{s} \right], \quad (1)$$

where the co-factor 2 appears due to the two-side adhesion, n is a number of Ag atoms per surface unit (one or three, for 1/3 ML and 1 ML coverages, respectively) and s a scaling constant. Obviously, for well-separated Ag and corundum slabs $\lim_{z_{\text{Ag}} \rightarrow \infty} E_b(z_{\text{Ag}}) = 0$. Eq. (1) is used in this paper to obtain the potential

energy curves of interface energy for various substrate coverages and several adsorption sites (Figure 8).

The basis-set-superposition error (BSSE) has also been evaluated according to the standard procedure implemented into CRYSTAL98 code [26]. The BSSE is estimated as the difference between the total energy of the interface system and the energies of each of the two sub-systems with the other sub-system included as “ghost” atoms only. The BSSEs for the binding energies for the Al-terminated slab in Table 1 lie in the range 0.05 to 0.10 eV. The order in which the Ag atoms favor the different adsorption sites is not affected whether we use BSSE corrected or uncorrected binding energies.

To obtain more insight into the nature of the interaction between the corundum surface and the Ag quasi-isolated adatoms (1/3 ML) or the full (111) monolayer, we have calculated a few properties using the CRYSTAL98 code. The Mulliken net atomic charges, *e.g.* Δq_{Ag} , are defined as a difference between the electronic charge of isolated neutral atom (Z_{Ag}) and interfacial atom (q_{Ag}). Projections of atomic dipole moments, $D_{\text{Ag}}^{(z)}$, have been calculated as matrix elements of atomic orbitals (AO) with the operator z (its direction pointing outwards from the surface), and describe an electron density shift perpendicular to the interface. The matrix elements in an AO representation with the operator $2z^2 - x^2 - y^2$ form vertical projections of quadrupole moments $Q_{\text{Ag}}^{(2z^2 - x^2 - y^2)}$. A negative value here means that atom is contracted along the z direction while expanded in the interfacial xy plane and *vice versa*.

To characterize the interaction between atoms inside the metal slab and between the slab and the corundum substrate across the interface better, we have plotted a series of *difference* electron density plots (Fig. 7). Computational algorithm used to construct these plots has been described in our recent paper [27]. The 2D charge distributions $\Delta\rho(\mathbf{r})$ show effects of the interface interaction since they are defined as:

$$\Delta\rho(\mathbf{r}) = \rho_{\text{Ag/corundum slab}}(\mathbf{r}) - [\rho_{\text{Ag slab}}(\mathbf{r}) + \rho_{\text{corundum slab}}(\mathbf{r})], \quad (2)$$

i.e. the total electron density $\rho_{\text{Ag/corundum slab}}(\mathbf{r})$ minus a superposition of the densities for the two isolated metal and corundum slabs with the same geometry as in the interface system ($\rho_{\text{Ag slab}}(\mathbf{r})$ and $\rho_{\text{corundum slab}}(\mathbf{r})$, respectively). The projections for the cross-sections used for these plots are defined in Figure 6.

3. Main results and discussion

Our results for the low and high (1/3 ML and 1 ML) substrate coverages show important characteristics concerning the silver-oxide binding (TABLE 1 and Figures 7,8). The equilibrium Al-O interlayer distance d (Figure 5) is almost unchanged in the Ag/corundum interface when it is optimized simultaneously with z_{Ag} (TABLE 1) as compared to the isolated Al-terminated substrate (0.12 Å versus 0.14 Å, respectively). For 1/3 ML coverage, the energetically most preferable position for silver adhesion is over versatile triangles, *i.e.* atop subsurface O^{2-} ions (Figure 6b). Probably this occurs due to an additional attraction of Ag atoms by the O^{2-} ions of the next subsurface oxygen plane. At the same time, surface projections of the outermost Al^{3+} ions of the corundum substrate are closer to H sites (top the centers of white triangles in Figures 4a and 6), than to the centers of smallest equilateral triangles (dark gray triangles with side length b_1 in the same Figures). This also explains why silver atoms in the former adsorption positions end up further away from the corundum surface (Fig. 8 and Table 1) and why vertical projections of the corresponding multipole moments are smaller.

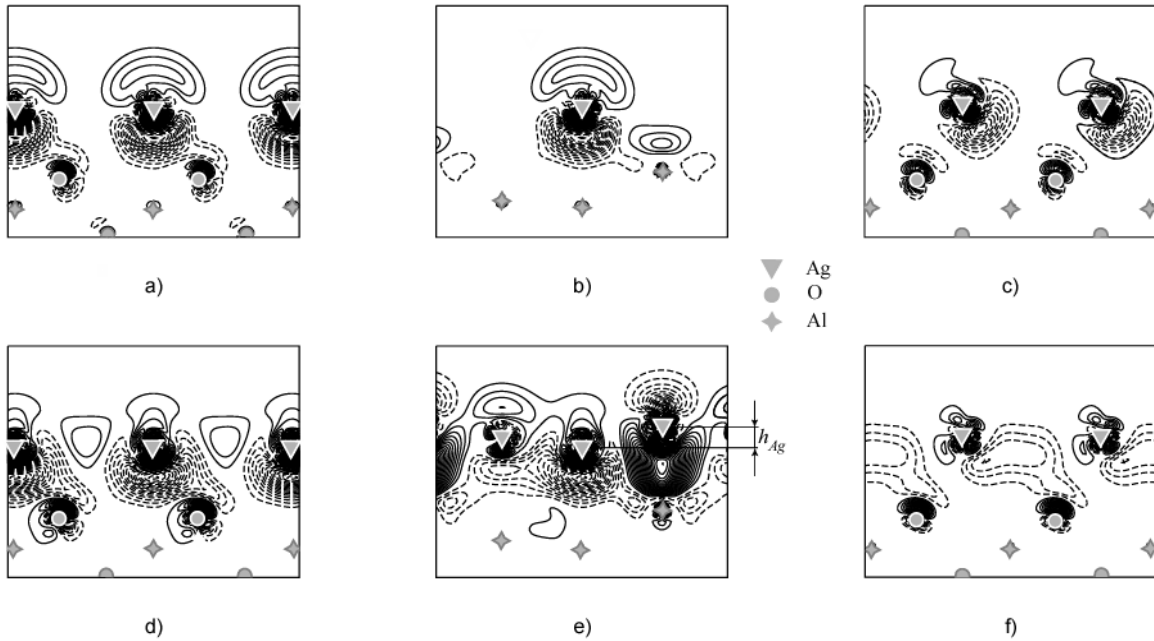


Figure 7. The 2D difference electron density distributions $\Delta\rho(\mathbf{r})$ (see explanation in Section 2) for various configurations of Ag atoms adsorbed on substrate (Fig. 5), with special symbols used to show centers of the crossed atoms and ions: (a,b) the two cross-sections for 1/3 ML of Ag(111) plane over $E1$ sites along P_a-P_a and P_b-P_b directions (Fig. 6a), (c) cross-section for 1/3 ML of Ag(111) plane over H sites along P_a-P_a direction (Fig. 6b); (d,e) two cross-sections for Ag(111) monolayer over all equilateral oxygen triangles along P_a-P_a and P_b-P_b directions (Fig. 6c); (f) section for distorted Ag(111) monolayer over all versatile oxygen triangles along P_a-P_a direction (Fig. 6d). Isodensity curves are drawn from $-1 e \text{ au}^{-3}$ to $+1 e \text{ au}^{-3}$ with an increment of $0.002 e \text{ au}^{-3}$. The full and dashed curves correspond to positive and negative difference electron densities, respectively. Fig. 7e shows a step h_{Ag} of the buckled Ag(111) monolayer (Table 1).

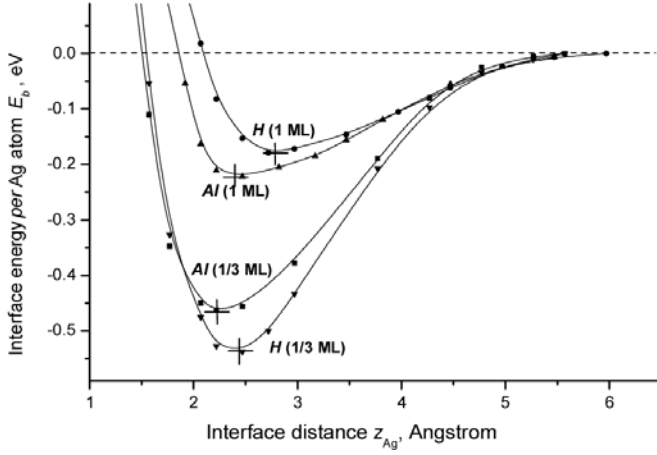


Figure 8. The binding energies $E_b(z_{Ag})$ as a function of the interfacial distance z_{Ag} for the two different adsorption sites E and H (Fig. 5) and two different substrate coverages (1/3 ML and 1 ML). Full lines are drawn using the standard B-spline option.

TABLE 1. Optimized parameters for different slab models of the $Ag/\alpha-Al_2O_3(0001)$ interface. Ag positions over both equilateral and versatile O triangles for different substrate terminations and coverages are shown in Figure 6.

Ag atom over	Substrate coverage by Ag(111)		Distance $z_{Ag}^a)$	Height in steps $h_{Ag}^b)$	Binding energy $E_{bind}^c)$	Mulliken charge on Ag Δq_{Ag}	Projections of multipoles ^{d)}	
							e	$D_{Ag}^{(z)}$
			Å		eV		$e au$	
equilateral O triangles	1/3 ML	our data	2.21	None	0.48	+0.01	0.348	-0.713
		Ref. [14]	1.96	none	1.1	$0 < q_{Ag} < +0.1$	-	-
	1 ML	our data	2.49	0.72	0.21	(A) ^{e)} +0.11	0.696	-0.702
						(B) ^{e)} +0.04	0.175	-1.090
		Ref. [14]	2.13	0.84	0.36	(C) ^{e)} -0.15	-0.472	-0.982
					-	-	-	
versatile O triangles	1/3 ML		2.39	none	0.54	+0.01	0.051	-0.448
	1 ML		2.77	none	0.17	-0.01	-0.013	-0.894

a) Optimized distance between Ag atom closest to a surface and an outer substrate layer (Figure 5).

b) Optimized value of intralayer height between silver atoms in a stepped Ag(111) monolayer (Figure 7e).

c) Values of the interface binding energy per Ag atom are estimated according to universal binding energy relation written as Eq. (1).

d) Normal to surface components of both dipole and quadrupole moments for Ag atom.

e) Charge transfer on a stepped Ag(111) layer calculated for interfacial, middle and outer silver atoms, which lie on A , B , C lines in Fig. 6c, respectively.

There exist certain structural restrictions for Ag atoms over hollow sites to form monolayers and thicker overlayers (Figure 6d). While a periodic network formed by the centers of all equilateral oxygen triangles (crossed by axes containing Al^{3+} ions) completely corresponds to the symmetry of the Ag(111) plane (Fig. 6c), the alternative network over H sites, which repeats the distribution of O^{2-} ions in the subsurface oxygen plane, may be treated as a *distorted* Ag(111) surface. Such a monolayer film is not very stable in an isolated state and its further growth is rather problematic. As to a regular Ag(111) monolayer, its profile is buckled because silver atoms on the corundum substrate tend to preserve the same interatomic distance as in bulk silver, which is somewhat larger than the distance between the nearest centers of equilateral oxygen triangles E . Moreover, periodic change of vertical positions of Al^{3+} ions in corundum (0001) substrate (Figure 5) prevents flat horizontal profile of silver monolayer if Ag atoms are adsorbed in E sites. It may be also illustrated by Fig. 3 for the $Nb/\alpha-Al_2O_3$ interface. The optimized h_{Ag} value of the regular steps in the Ag(111)

monolayer is considerable (0.74 Å). The charge redistribution within the buckled Ag layer (Figure 7e and TABLE 1) contributes to making the equilateral oxygen triangles the preferred adhesion sites for the Ag monolayer. Since the “internal” Ag atoms over A rows (Figure 6c) are slightly positively charged (+0.1 e), they are attracted to the equilateral triangles formed by the O^{2-} ions.

The ratio of the binding energies *per* Ag atom between 1/3 and 1 ML Ag adsorption over equilateral oxygen triangles is 2.3 for our data, namely 0.47 eV versus 0.21 eV (TABLE 1). Verdozzi *et al.* [14] obtained a ratio of 3.1, namely 1.1 eV versus 0.36 eV. The energy ratio about 2-3 probably occurs because each Ag atom in the 1/3 ML interacts directly with *three* nearest O^{2-} ions, while for 1 Ag ML, the number of silver atoms equals that of oxygen ions. Moreover, adjacent Ag atoms in the buckled monolayer form metallic bonds, interacting unfavorably with the oxygen triangles below and reducing the interfacial bonding per Ag atom. This is evident from a comparison of charge distributions for both Ag coverages on the Al-terminated substrate (Figures 7a and 7d): the Ag electron density delocalization on silver atoms is markedly larger for a metal monolayer. On the other hand, if we consider binding energies per rhombic surface unit of the substrate (Figure 4a), they are higher for 1 ML coverage than for 1/3 ML, since one such unit contains three quasi-equivalent adsorption positions.

The relatively large quadrupole moment values, $Q_{Ag}^{(2z^2-x^2-y^2)}$ (Table 1), mainly indicate that silver electronic shells are affected by the outermost Al^{3+} substrate ions. Our results agree well with corresponding physisorption energies for perfect Ag/MgO(100) and (110) interfaces (0.2-0.8 eV per atom) [34], and we find only a negligible charge transfer across the Ag/ α - Al_2O_3 (0001) interface. The charge redistribution (Fig. 7) is mainly limited to electronic charge polarization in the rather close vicinity of the Ag nuclei.

4. Conclusions

In this paper, we have analyzed the dependence of the adhesion energy on the interfacial distance for the two most probable Ag adsorption patterns and for two different coverages of corundum (0001) substrate. Ag adsorption over every third versatile oxygen triangle (*i.e.* H sites) is found to be slightly more preferable energetically than over equilateral oxygen triangles, whose centers are pierced by Al^{3+} -containing C_{3v} axes. A possible explanation could be a favorable interaction between the Ag atoms and O^{2-} ions in next, *subsurface* oxygen plane, which are positioned under versatile O triangles. In contrast, for the dense silver monolayer coverage, the equilateral oxygen triangles (*i.e.* on the C_{3v} , Al^{3+} axes), are more favorable adsorption sites for Ag adsorption than the versatile triangles (above a network of internal O^{2-} ions). The binding energy per Ag atom is by a factor 2-2.5 larger for 1/3 ML coverage than for 1 ML on α - Al_2O_3 (0001) surface. This is probably due to a larger interaction of Ag atom with *three* nearest oxygen ions for 1/3 ML, whereas for 1 ML, each metal atom corresponds to the only oxygen ion, and thus Ag binding turns out to be weaker. Calculated *per surface unit* of corundum, the binding energy is larger for the larger coverage since the Ag atom concentration is three times higher. Unlike for the Ag/MgO interfaces [34], where the electron density localized between the Ag atoms inside the metallic monolayer film, gives rise to a favorable electrostatic attraction with the MgO substrate cations, the analogous Ag-Ag electron density features for the Ag/ α - Al_2O_3 (0001) interface rather result in an electrostatic repulsion with the corundum substrate anions (Figure 7d), due to different crystalline structure of both oxides. At the same time, a presence of enhanced interatomic electron density inside the Ag monolayer indicates a preservation of some metallic properties in silver film as was earlier observed in the Ag/MgO interfaces.

On the whole, for the Al-terminated α - Al_2O_3 (0001), which corresponds to an equilibrium state of the corundum substrate, we observe relatively small adhesion energies per Ag atom and negligible interfacial charge transfer, which clearly indicates a *physisorption*. One can suppose that the outer aluminium ions on the Al-terminated substrate surface “screen” the favorable interaction between the silver atoms and the outermost oxygen triangles. As to buckled profile of silver monolayer, it corresponds to a coherent Ag/ α - Al_2O_3 (0001) interface when existing some mismatch of lattice constants between metallic film and substrate. Common incoherence of metal/oxide interfaces, well observed for instance in Figure 1 for Cu/corundum interface, arises usually for more-or-less thick metal overlayer. Clarifying a mechanism of metal film growth, which we have begun to study [35], one can explain also this transition from coherent to incoherent metal/oxide interface.

Acknowledgements

This study was supported by the EC Excellence Centre of Advanced Material Research and Technology (Contract Nr ICA1-CT-2080-7007). The authors acknowledge computational facilities of the Theoretical Inorganic Chemistry Group (the Ångström Laboratory, Uppsala University) as well as kindly thank K. Hermansson, B. Herschend (both Uppsala University, Sweden) and P.W.M. Jacobs (University of Western Ontario, Canada) for numerous stimulating discussions.

References

- [1] Gitzen W.H. (1970) *Alumina as a Ceramic Material*. Amer. Ceramic Society Publishing: Columbus, OH.
- [2] Noguera C. (1996) *Physics and Chemistry at Oxide Surfaces*. Cambridge: Univ. Press.
- [3] Gates B.C. (1992) *Catalytic Chemistry*. Wiley&Sons: New York.
- [4] Finnis M.W. (1996) *J. Phys.: Cond. Matter*, **8**, 5811.
- [5] Campbell C.T. (1997) *Surf. Sci. Reports*, **27**, 3.
- [6] Dehm G., Rühle M., Ding G., Raj R. (1997) *Phil. Mag. B*, **71**, 1111.
- [7] Guo Q., Möller P.J. (1992), *Acta Phys. Polon. A*, **81**, 647.
- [8] Gutekunst G., Mayer J., Rühle M. (1997) *Phil. Mag. A*, **75**, 1329; 1357.
- [9] Kelber J.A., Niu C., Shepherd K., Jennison D.R., Bogicevic A. (2000) *Surf. Sci.*, **446**, 76.
- [10] Biener J., Baumer M., Madix R.J., Liu P., Nelson E., Kendelewicz T., Brown G. (2000) *Surf. Sci.*, **449**, 50.
- [11] Duffy D.M., Harding J.H., Stoneham A.M. (1996) *Acta Mater.*, **44**, 3293.
- [12] Ndubuisi G.C., Liu J., Cowley J.M., (1992) *Microsc. Res. Tech.*, **20**, 439.
- [13] Zhukovskii Yu.F., Alfredsson M., Hermansson K., Heifets E., Kotomin E.A. (1998) *Nucl. Instr. Meth. Phys. Res. B*, **141**, 73.
- [14] Verdozzi C., Jennison D.R., Schultz P.A., Sears M.P. (1999) *Phys. Rev. Letters*, **82**, 799.
- [15] Alemany P., Boorse R.S., Burlitch J.M., Hoffmann R. (1993) *J. Phys. Chem.*, **97**, 8464.
- [16] Kruse C., Finnis M.W., Milman V.Y., Payne M.C., De Vita A., Gillan M.J. (1994) *J. Am. Ceram. Soc.*, **77**, 451
- [17] Batirev I.G., Alavi A., Finnis M.W., Deutsch T. (1999) *Phys. Rev. Letters*, **82**, 1510.
- [18] Causá M., Dovesi R., Pisani C., Roetti C. (1989) *Surf. Sci.*, **215**, 259; Salasco L., Dovesi R., Orlando R., Causá M., Saunders V.R. (1991) *Mol. Phys.*, **72**, 267.
- [19] Puchin V.E., Gale J.D., Shluger A.L., Kotomin E.A., Günster J., Brause M., Kempter V. (1997) *Surf. Sci.*, **370**, 190.
- [20] Batirev I.G., Alavi A., Finnis M.W. (1999) *Faraday Discuss.*, **114**, 33.
- [21] Baudin M., Hermansson K. (2001) *Surf. Sci.*, **474**, 107.
- [22] Guo J., Ellis D.E., Lam D.J. (1992) *Phys. Rev. B*, **45**, 3204.
- [23] Tepesch P.D., Quong A.A. (2000) *Phys. Stat. Solidi (b)*, **217**, 377.
- [24] Wang X.G., Chaka A., Scheffler M. (2000) *Phys. Rev. Letters*, **84**, 3650.
- [25] Renaud G. (1998) *Surf. Sci. Reports*, **32**, 5.
- [26] Saunders V.R., Dovesi R., Roetti C., Causá M., Harrison N.M., Orlando R., Zicovich-Wilson C.M. (1999) *CRYSTAL98. User Manual*. Univ. Torino: Turin.
- [27] Piskunov S., Zhukovskii Yu.F., Kotomin E.A., Shunin Yu.N. (2000) *Computer Modelling & New Technologies*, **4**, N 2, 7.
- [28] Zhukovskii Yu.F., Gryaznov D., Finogenov A., Shunin Yu.N. (2001) *Computer Modelling & New Technologies*, **5**, N 1, 28.
- [29] Perdew J.P., Wang Y. (1992) *Phys. Rev. B*, **45**, 13244.
- [30] Catti M., Valerio G., Dovesi R., Causá M. (1994) *Phys. Rev. B*, **49**, 14179.
- [31] Hay P.J., Wadt W.R. (1985) *J. Chem. Phys.*, **82**, 284.
- [32] Wyckoff R.W.G., *Crystal Structures (2nd ed.)* (1963) V. 1; (1964) V. 2. Wiley-Interscience: New York.
- [33] Smith J.R., Hong T., Srolovitz D.J. (1994) *Phys. Rev. Letters*, **72**, 4021.

- [34] Zhukovskii Yu.F., Kotomin E.A., Jacobs P.W.M., Stoneham A.M., Harding J.H. (1999) *Surf. Sci.*, **441**, 373.
- [35] Fuks D., Dorfman S., Kotomin E.A., Zhukovskii Yu.F., Stoneham A.M. (2000) *Phys. Rev. Letters*, **85**, 4333.

Received on the 21st of July 2001

A NOVEL RELATION FOR THE EFFECTIVE DIFFUSION COEFFICIENT IN INHOMOGENEOUS MEDIA

J.R. KALNIN^a and E.A. KOTOMIN^{a,b}

^a*Institute of Solid State Physics, 8 Kengaraga str., Riga LV-1063, Latvia*

^b*Max-Planck-Institut für Festkörperforschung, Heisenbergstr. 1, Stuttgart D-70569, Germany*

We suggest a modification of the well-known Maxwell-Garnett equation for the mobility (effective diffusion coefficient) in two-phase media (a matrix with inclusions) which permits the description of a wide range of experimental situations. The novel approach correctly treats the partial trapping of a diffusing particle by an inclusion as well as consequences of an energy barrier for the particle penetration into an inclusion. Computer simulations show that the presented mean-field theory reproduces surprisingly well results for square inclusions without concentration limitation. For inclusions with other shapes (e.g., spherical) the theory works well up to concentrations at which mobile particles become trapped in "pockets" between inclusions.

Key words: inhomogeneous media, diffusion, computer simulation, mean-field theory, particle penetration

1. Introduction

Calculation of transport properties of inhomogeneous materials has a long history, starting with the pioneering papers by Maxwell-Garnett [1]. The composite material is usually modelled as a combination of a host phase (matrix) characterised by the diffusion coefficient of a probe particle, D_2 , and spherical inclusions (the second phase) characterised by the particle diffusion coefficient D_1 , radius r_0 and volume fraction Φ . These two diffusion coefficients are expressed through the hop length l and the average waiting time between the two successive hops τ :

$$D_i = \frac{l_i^2}{2d\tau_i}, \quad i = 1, 2, \quad (1)$$

where d denotes the space dimension (1, 2, or 3).

A very similar problem arises in the description of other transport coefficients (electrical and thermal conductivity, dielectric constant, magnetic permeability, elastic moduli, etc.) in two-phase systems [2-9]. Examples of systems for which it is desired to predict such properties are porous media, polymer blends, foams, and ceramic-metal mixture. In this paper, we consider cases for which the generally accepted relation for the effective diffusion coefficient fails and requires generalisation.

2. Standart Maxwell-Garnett approach

Let us reproduce briefly a typical derivation of what is generally known as the Maxwell-Garnett (MG) formula. Experimentally the matrix with inclusions is characterised by an effective diffusion coefficient, D_{eff} , which is a function of D_1 , D_2 , and Φ . To determine it, one can use the electrostatic analogue. We consider a macroscopically homogeneous material with the diffusion coefficient D_{eff} . Following the original derivation of MG equation, we imagine that the particle concentration c has an average gradient g (similarly to a homogeneous electric field) along some axis.

Then we insert into the material a spherical inclusion of radius r_0 surrounded by a spherical shell of a host material (matrix) with the radius r_1 and assume that the inclusion does not change the concentration field outside, i.e. at $r \geq r_1$. (The radii r_1 and r_0 are defined in such a way that the inclusion's volume fraction

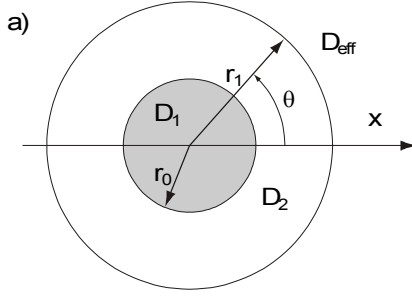


Figure 1. (a) Schematic presentation of the matrix with inclusions in terms of a core-shell model. (b) The case of different-size inclusions.

$\Phi = \frac{r_0^3}{r_1^3}$ is satisfied) (Figure 1a). The effective diffusion coefficient D_{eff} can be determined from the following steady-state equation:

$$\Delta c_{r,\vartheta}(r, \vartheta) = 0, \quad (2)$$

in the coordinates r and ϑ , where ϑ is an angle between \mathbf{r} and the external gradient \mathbf{g} . The appropriate solution of eq.(2) reads

$$c_1(r, \vartheta) = A \cos \vartheta, \quad (0 < r \leq r_0), \quad (3)$$

$$c_2(r, \vartheta) = \left(Br + \frac{E}{r^2} \right) \cos \vartheta, \quad (r_0 < r \leq r_1), \quad (4)$$

$$c_{eff}(r, \vartheta) = -gr \cos \vartheta, \quad (r_1 < r), \quad (5)$$

where $c_i(r, \vartheta)$ is a local particle concentration in inclusions ($i=1$) or in a host material ($i=2$).

Equations for the unknown constants A , B , E and g arise from the boundary conditions for the particle concentrations and fluxes:

$$c_1(r_0, \vartheta) = c_2(r_0, \vartheta) \quad (6)$$

$$D_1 \frac{\partial c_1(r, \vartheta)}{\partial r} \Big|_{r=r_0} = D_2 \frac{\partial c_2(r, \vartheta)}{\partial r} \Big|_{r=r_0} \quad (7)$$

$$c_2(r_1, \vartheta) = c_{eff}(r_1, \vartheta) \quad (8)$$

$$D_2 \frac{\partial c_2(r, \vartheta)}{\partial r} \Big|_{r=r_1} = D_{eff} \frac{\partial c_{eff}(r, \vartheta)}{\partial r} \Big|_{r=r_1} \quad (9)$$

From eqs. (3) to (9) we obtain a set of equations:

$$r_0^3 A - r_0^3 B - E = 0 \quad (10)$$

$$D_1 r_0^3 A - D_2 r_0^3 B + 2D_2 E = 0 \quad (11)$$

$$r_1^3 B + E + r_1^3 g = 0 \quad (12)$$

$$D_2 r_1^3 B + D_{eff} r_1^3 g - 2D_2 E = 0 \quad (13)$$

Using this set of equations, one gets the MG equation sought for:

$$D_{eff} = D_2 \left[1 + \frac{3(D_1 - D_2)\Phi}{D_1 + 2D_2 - (D_1 - D_2)\Phi} \right] \quad (14)$$

In general, for an arbitrary space dimension ($d=1, 2$ and 3) instead of eq.(14) one finds:

$$D_{\text{eff}} = D_2 \left[1 + \frac{d(D_1 - D_2)\Phi}{D_1 + (d-1)D_2 - (D_1 - D_2)\Phi} \right] \quad (15)$$

This result holds not only for a periodic set of the same-size spherical inclusions but also for a random inclusion distribution of different radii r_0^i if the condition $\Phi = \frac{(r_0^i)^d}{(r_i^i)^d}$ (d is space dimension) remains to be fulfilled (Figure 1b). However, the question, at which volume fractions Φ inclusions begin to 'compete' and eq.(15) is no longer valid, remains open and could be solved by a comparison with an analytical theory which takes many-particle effects into account (see, e.g., [7]) and/or by means of direct computer simulations.

3. Disadvantage of MG equation

Consider now several cases when the generally-accepted MG equation (15) gives incorrect results. **A.** Let us begin with a situation when the inclusion is totally impenetrable, i.e. a diffusing particle is reflected at r_0 as could be described by the condition $\left. \frac{\partial c_2(r, \vartheta)}{\partial r} \right|_{r=r_0} = 0$ (consider also the limiting case $\frac{D_1}{D_2} \rightarrow 0$ in eq.(7)). In this situation eq.(15) gives

$$D_{\text{eff}} = D_2 \left[1 - \frac{2\Phi}{1 + \Phi} \right], \quad (d = 2) \quad (16)$$

$$D_{\text{eff}} = D_2 \left[1 - \frac{3\Phi}{2 + \Phi} \right], \quad (d = 3) \quad (17)$$

Such relations are well-known in the reaction-rate theory [11]. The same result may be obtained from eqs.(3) to (9), putting there $c_1(r, \vartheta) = 0$ (as well as $A=0$, see discussion in [10]).

However, eqs.(16) and (17) give an incorrect concentration dependence (see discussion in [6].) The correct Φ -dependence, as we show below, is

$$D_{\text{eff}} = \frac{D_2}{1 - \Phi} D_2 \left[1 - \frac{3\Phi}{2 + \Phi} \right], \quad (d = 3) \quad (18)$$

$$D_{\text{eff}} = \frac{D_2}{1 - \Phi} D_2 \left[1 - \frac{2\Phi}{1 + \Phi} \right], \quad (d = 2) \quad (19)$$

The reason for this incorrectness lies in the use of relation (8). In fact, the concentration of diffusing particles in the matrix cannot be equal to that in the effective medium because in the latter all particles are stirred over a whole system's volume and thus their averaged concentration should be less by the factor of $1 - \Phi$. This indicates that eq.(8) should be corrected as:

$$c_2(r_1, \vartheta) = k_1 c_{\text{eff}}(r_1, \vartheta), \quad (20)$$

i.e., in reality there is a jump in concentration on the core (inclusion) - shell (matrix) boundary, $r = r_1$. The question is, how to get the coefficient k_1 ? We propose to obtain it, as a much better approximation, from the expression for the average equilibrium particle concentration of the system (total particle number divided by total volume)

$$c_{\text{eff}} = c_1 \Phi + c_2 (1 - \Phi). \quad (21)$$

In the particular case of impenetrable inclusions ($c_1 = 0$) we obtain from eq.(21):

$$c_{\text{eff}} = c_2 (1 - \Phi), \quad k_1 = \frac{1}{1 - \Phi}. \quad (22)$$

B. Another restriction of the use eq.(15) arises from the Maxwell's boundary condition $c_1(r_0, \vartheta) = c_2(r_0, \vartheta)$, eq.(6). In fact it can be shown that eq.(15) is valid in the case of different diffusion coefficients in the matrix and the inclusion, $D_1 \neq D_2$, only if the particle velocities in the matrix and inclusions coincide, $\frac{l_1}{\tau_1} = \frac{l_2}{\tau_2}$. In a general case it is necessary to introduce the measurable coefficient k connecting c_1 and c_2 :

$$c_1(r_0, \vartheta) = k c_2(r_0, \vartheta). \quad (23)$$

In order to improve the MG equation, in the above-presented standard derivation of the effective diffusion coefficient, we can use eqs.(20) and (23) instead of the original Maxwell's eqs.(6) and (8). When doing so, instead of standard eq.(15) we arrive at

$$D_{\text{eff}} = D_2 k_1 \left[1 + \frac{d(D_1 k - D_2) \Phi}{k D_1 + (d-1) D_2 - (k D_1 - D_2) \Phi} \right]. \quad (24)$$

In the 1D case this equation coincides with the exact solution [12]. The two coefficients k and k_1 are related through the equilibrium concentrations in inclusions and the matrix and volume fraction Φ according to eqs. (20), (21), (23):

$$k = \frac{c_1}{c_2} \quad (25)$$

and

$$c_2 = k_1 c_{\text{eff}}. \quad (26)$$

From eq.(21) we obtain the volume dependence of the coefficient k_1 :

$$k_1 = \frac{1}{1 - \Phi + \frac{c_1}{c_2} \Phi}. \quad (27)$$

Using eq.(27), one obtains the following relation instead of eq.(24) :

$$D_{\text{eff}} = \frac{D}{1 - \Phi + \frac{c_1}{c_2} \Phi} \left[1 + \frac{d \left(D_1 \frac{c_1}{c_2} - D_2 \right) \Phi}{(d-1) D_2 + \frac{c_1}{c_2} D_1 - \left(D_1 \frac{c_1}{c_2} - D_2 \right) \Phi} \right]. \quad (28)$$

Similarly to the MG theory, this equation reproduces correctly both limiting cases, as Φ strives for zero and unity. Equation (28) is a basic result of our theory. It should be recalled that c_1 and c_2 are average concentrations of diffusing particles in the two phases - the inclusions and the matrix.

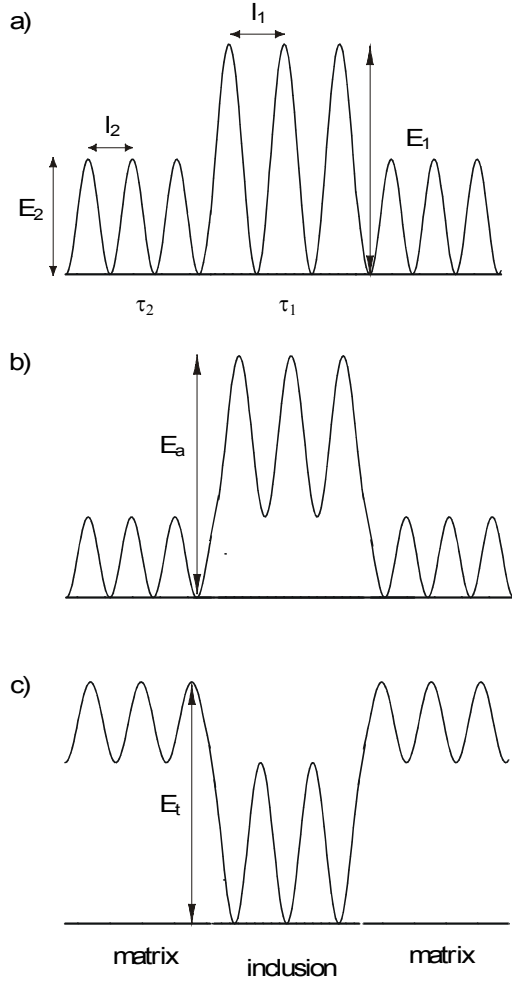


Figure 2. Different cases of energy barriers between the matrix and inclusions, l_i , E_i are a hop length and an activation energy for diffusion in the two phases, $i=1, 2$. (a) An inclusion with the diffusion coefficient in the inclusions smaller than in the matrix; there is no energy barrier between them. (b) An energy barrier E_a for the penetration into inclusion, $p_2 \leq 1$. (c) Partial trapping of particles inside inclusions, $p_1 \leq 1$. The detrapping energy is E_t .

It is convenient to express the ratio c_1/c_2 entering eq.(28) through the kinetic parameters of inclusions and the matrix. In equilibrium, the steady-state situation fluxes of particles to and from inclusions are equal:

$$c_1 \frac{l_1}{\tau_1} = c_2 \frac{l_2}{\tau_2} . \quad (29)$$

Remember that the diffusion coefficients D_1 and D_2 are defined by eq.(1).

Figure 2 shows several important situations for the potential energy profiles of the diffusing particle, modeling its partial trapping by an inclusion (potential energy well) and the (partial) reflection from it due to the energy barrier, respectively. To describe these situations, let us introduce the penetration probabilities p_1 from the inclusion to the matrix and p_2 from the matrix to inclusions, respectively. Thus, in the general case one gets

$$\frac{c_1}{c_2} = \frac{l_2 p_2 \tau_1}{l_1 p_1 \tau_2} . \quad (30)$$

In the case of a potential barrier the penetration probability (per unit time) is defined entirely by the activation energy E_{12} [13]:

$$p_2 = \tau_2 \cdot \exp\left(\frac{-E_{12}}{kT}\right) . \quad (31)$$

The same is true for the particle hop from the inclusion with the probability p_1 . Equations (28) and (30) allow one to describe many diffusion-controlled processes in composite media with trapping and release of mobile particles.

Now let us compare our results with previous theories. In the 1D case eq.(28) reproduces the exact result derived for a periodical inclusion distribution in the Kronig-Penny model with particle reflections (eq. (4) in [12]) which reads in our notations as:

$$D_{\text{eff}} = \left[\frac{\Phi}{D_1 k} + \frac{1-\Phi}{D_2} \right]^{-1} \cdot \frac{1}{1-\Phi + \Phi k} , \quad (32)$$

where $k = c_1/c_2$.

In turn, in the 3D case our eq.(28) for D_{eff} coincides with that obtained in ref. [6] for a particular case of periodic distribution of inclusions using mathematically very complicated formalism of irreversible thermodynamics with chemical potentials. The analytical results presented in ref. [14] also demonstrate the presence of a distinctive co-factor $\left(1 - \Phi + \frac{c_1}{c_2} \Phi\right)^{-1}$ entering the D_{eff} .

In the case of a complete particle reflection from the inclusions ($D_1 = 0$; $c_1/c_2 = 0$) eq.(28) transforms into eqs.(18) and (19) as quoted above. For a small volume fraction of the inclusions, $\Phi \ll 1$, one arrives at

$$D_{eff} = D_2 \left[1 - \frac{\Phi}{2}\right], (d = 3) \tag{33}$$

$$D_{eff} = D_2 [1 - \Phi], (d = 2). \tag{34}$$

Equation (33) was received earlier in ref. [15] whereas eq.(34) was derived in ref. [10] using the effective medium approximation. The expression (33) was also derived calculating the effective self-diffusion constant of the mobile species in solution [16].

Let us consider now several limiting cases for D_{eff} . In the case of impenetrable inclusions (complete reflection of particles, $c_1/c_2 \rightarrow 0$), eq. (28) is simplified:

$$D_{eff} = \frac{D_2(d-1)}{d-1+\Phi}. \tag{35}$$

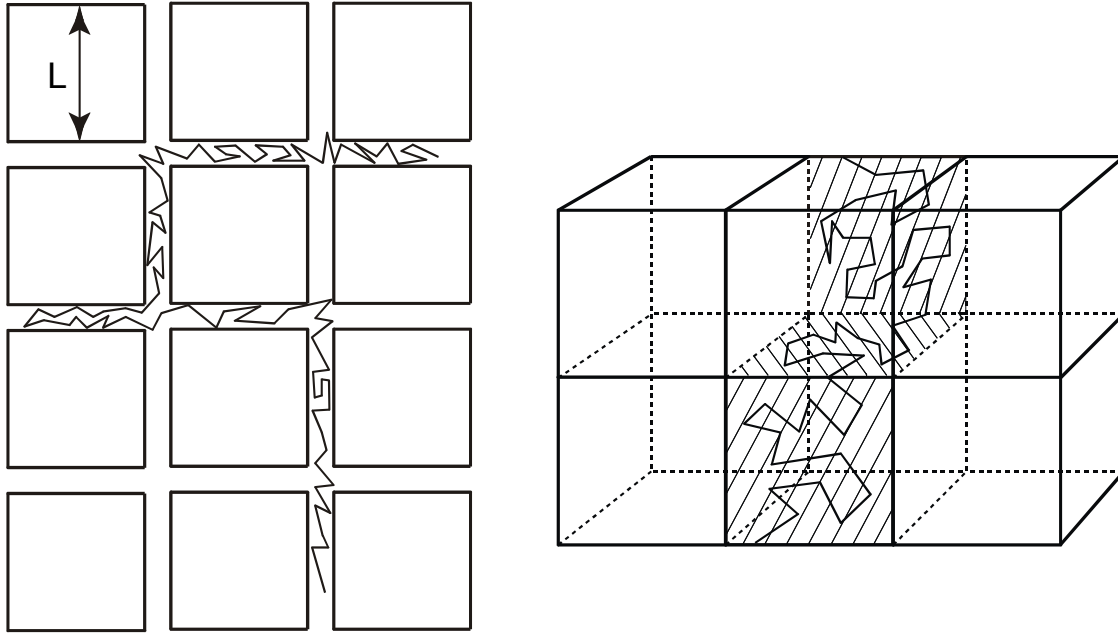


Figure 3. Transformation of the 2D (3D) diffusion into 1D and 2D diffusion as square (cubic) inclusion fractional volume approaches unity ((a) and (b), respectively).

As $\Phi \rightarrow 1$, one gets in 2D and 3D cases $D_{eff} = D_2/2$ and $2D_2/3$, respectively, while the MG equation yields a zero effective diffusion coefficient. This result means that in these limiting cases the particle diffusion becomes in fact one- or two-dimensional as shown in Figure 3 for square and cubic inclusions.

To stress the role of a potential barrier in D_{eff} , let us consider the limiting case of a strong trapping, $c_2/c_1 \rightarrow 0$. From eq.(28) one obtains:

$$D_{\text{eff}} = \frac{D_2}{k\Phi} \cdot \frac{1+d-\Phi}{1-\Phi}, \quad (36)$$

which demonstrates that D_{eff} is independent of the diffusion in inclusions. The same results in the limiting case $D_2/D_1 \rightarrow 0$.

4. Random walk simulations

In order to compare eq.(28) with computer simulations, we have modeled periodical arrays of spherical and square inclusions of the same size in 2D varying the kinetic parameters l_1, τ_1 , and l_2, τ_2 , for particle diffusion in the matrix and inclusions in a very wide range of magnitudes thus simulating very different situations mentioned above. For a periodical distribution of inclusions in the matrix we monitored a particle diffusion and calculated D_{eff} by the standard formula:

$$D_{\text{eff}} = \frac{\langle r^2 \rangle}{2dt}, \quad (37)$$

where t is diffusion time and the mean-square particle displacement during its random walks on the lattice

$$\langle r^2 \rangle = \frac{\sum_{i=1}^N r_i^2}{N}, \quad (38)$$

was averaged over more than (typically) $N=10^5 - 10^6$ runs. The waiting time τ was chosen to be sufficient to satisfy the standard condition: $\langle r^2 \rangle$ is much larger than the squared distance between adjacent inclusions L^2 . For this purpose we used the first-passage algorithm [7]. We modeled cases of both impenetrable and penetrable inclusions. The hop length l was always chosen to be much smaller than both the shortest distance between boundaries of the two nearest inclusions and inclusion radius. Results of computer simulations are discussed below.

5. Simple exactly solvable model

There is one particular case in which D_{eff} could be determined exactly for the two-phase inhomogeneous media in all dimensions: $l_1 = l_2$; $\tau_1 \neq \tau_2$; $D_1 \neq D_2$. That is, the waiting times in the matrix and inclusions differ but hopping lengths are equal (Figure 2a). In this case after N walks we get from eq.(37):

$$D_{\text{eff}} = \frac{\langle r^2 \rangle}{2d(N_1\tau_1 + N_2\tau_2)}. \quad (39)$$

Here N_1 and N_2 are numbers of particle walks in the phases 1 and 2, respectively. For sufficiently large N (diffusing particle visits inclusions many times) one obtains, obviously:

$$N_1 = \Phi N, \quad N_2 = (1-\Phi)N \quad (40)$$

Substituting eq.(40) and $\langle r^2 \rangle = 2dNl^2$ into eq.(39), we receive results well-known for conductivity in inhomogeneous media [5]:

$$\frac{1}{D_{\text{eff}}} = \frac{1}{D_1} \Phi + \frac{1}{D_2} (1-\Phi) \quad (41)$$

Note that this equation is often considered to be valid only for 1D but as we have demonstrated, in fact it could be used in any space dimension. (Compare this equation with eq.(32) where energy barriers for particle penetration to/from inclusions are incorporated.) The same result also follows immediately from our general eq.(28), taking into account that at $l_1 = l_2$:

$$\frac{c_1}{c_2} = \frac{\tau_1}{\tau_2}, \tag{42}$$

which leads to

$$D_{\text{eff}} = \frac{D_2}{1 - \Phi + \frac{\tau_1}{\tau_2} \Phi}. \tag{43}$$

Equation (43) coincides with eq.(41), we just have to replace $\frac{\tau_1}{\tau_2}$ by $\frac{D_1}{D_2}$. The effective diffusion coefficient could be easily related to the fractions of time which mobile the particle spends in matrix (t_2) and inclusions (t_1):

$$D_{\text{eff}} = D_1 \frac{t_1}{t_1 + t_2} + D_2 \frac{t_2}{t_1 + t_2}. \tag{44}$$

From eqs. (28) and (44) one obtains:

$$\frac{t_2}{t_1} = 1 - \frac{1}{A}, \quad A = \frac{k(1-d-\Phi)}{(1-\Phi + k\Phi) \left[k \frac{D_1}{D_2} (1-\Phi) + d - 1 + \Phi \right]} \tag{45}$$

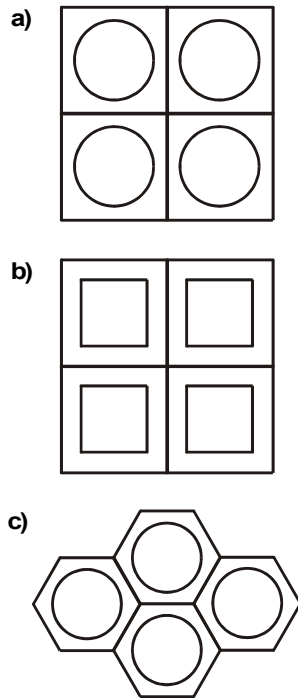


Figure 4. Different types of lattices and inclusions: spherical and square shape inclusions in the square lattice (a, b), spherical inclusions in the hexagonal lattice (c).

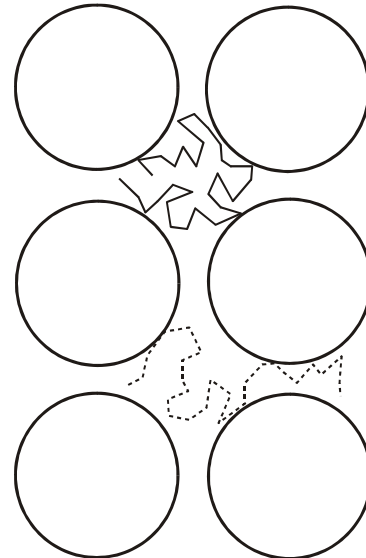


Figure 5. A pocket effect when particles become trapped between inclusions which results in zero effective diffusion coefficient

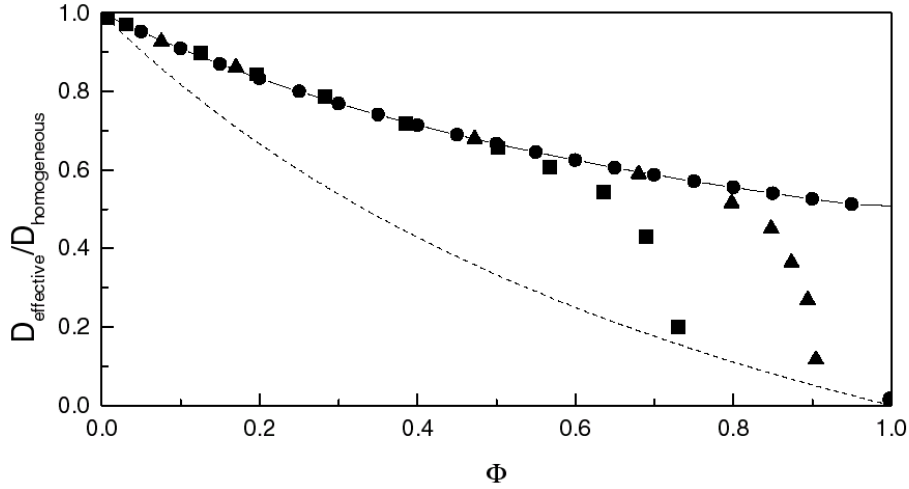


Figure 6. Comparison of generally-accepted Maxwell-Garnett theory (dotted line, eq.(14)) and our eq.(28) (solid line) with 2D computer simulations for periodically distributed rejecting inclusions vs their dimensionless concentration; square symbols are for the spherical inclusions on a square lattice; triangles for the spherical inclusions on a hexagonal lattice, and full circles are for square inclusions on a square lattice.

6. Results of computer simulations

It should be mentioned that at high concentrations of the inclusions their shape becomes important (Figure 4) the effect never discussed earlier in the literature. If inclusions are circular or spherical and touch each other at one point, $D_{eff} \rightarrow 0$ as $\Phi \rightarrow \Phi_{lim}$ (which could be easily be calculated as $\Phi_{lim} = \pi/4$ and $3/\pi$ for circular inclusions in the square lattice and hexagonal lattice, respectively). The reason is that a particle spends most of its time in a "pocket" formed by nearest inclusions (Figure 5).

Let us discuss here results of modeling inclusions of different shapes as shown in Figure 4. (Very preliminary results were presented in ref. [17]). First of all, our computer simulations clearly demonstrated the correctness of our theory in the case of large concentrations of the square inclusions (Figure 6) in a whole range of concentrations and failure of the MG theory. This figure presents also the results of calculations for the effective diffusion coefficient at completely reflecting circular inclusions in the 2D square and hexagonal lattices ($\frac{D_1}{D_2} = 0$, Figure 4a,c). The immediate conclusion can be drawn that the computer simulations also

coincide, with a precision of 1 %, with our theory, eqs.(28) and (35), for the case of spherical inclusions, up to inclusion volume fractions as large as $\Phi = 0.6$ and 0.8 , for square and hexagonal lattices, respectively. The discrepancy at larger volume fractions is due to the just explained "pocket" effect (Figure 5) neglected in the analytical theory. What should be stressed here is that the MG eq.(14) (dotted line) gives a rather incorrect dependence even at small since it neglects differences in the particle concentrations in inclusions and in matrix. This becomes very transparent in the case of impenetrable inclusions.

7. Discussions and conclusions

In this paper a modified Maxwell-Garnett equation (28) was derived which gives surprisingly good description of the mobility in the 2D heterogeneous media with square inclusions. We believe that this is also true for 3D case.) The main advantage of our mean-field theory is its simplicity, transparency and validity for any space dimension in contrast to previous mathematically very complicated approaches based on irreversible thermodynamics with chemical potentials [6], cluster expansion [14] etc. Validity of our universal relation for the effective diffusion coefficient is proved by computer simulations. These latter demonstrated for the first time the effect of inclusion shape at high inclusion concentrations. Note that the concentration

jump on the inclusion boundary, Eq.(25), commonly known as partition coefficient, is not new and was observed in all previous theories (e.g., [14,19,20]). The more so, this partition coefficient was found also experimentally, e.g., for metallic alloys Al-Cu, Al-Ge, Al-In, Al-Sn [19]. The concentration jump is not surprising which becomes obvious in the limiting case of impenetrable inclusions ($c_2 > 0$, $c_1 = 0$). The expression suggested for the effective diffusion coefficient permits treatment of solid-state inhomogeneous systems (composites, ceramics) with very different properties of inclusions and the host matrix, including a partial rejection of diffusing particles from inclusions and a trapping inside inclusions. The more so, it could be useful in quite different fields like mathematical modelling of the release of anti-microbial agent from packaging material to a food product [20], transport through membranes, or self-diffusion of small molecules in colloidal systems containing polymers, proteins, micells etc [6].

8. Acknowledgments

This study has been partly supported by the European Center of Excellence in Advanced Materials Research and technology in Riga, Latvia (contract Nr ICA-I- CT-2000-7007).

References

- [1] Maxwell Garnett J.C. (1904) *Philos. Trans. R. Soc. London* **203**, 385
- [2] Milton G.W. (1990) *Pure and Applied Mathematics XLIII*, 63 and references therein.
- [3] Oshima N. and Nomura S. (1985) *Journal of Composite Materials* **19**, 287
- [4] Bergman D. (1978) *Phys. Rep.* **43**, 377
- [5] Christensen R.M. (1979) *Mechanics of Composite Materials*. Wiley-Interscience, New York;
Christensen R.M. and. Lo K.H.(1979) *Journal of Mechanics and Physics of Solids* **27**, 315
- [6] Jönsson B., Wennerström H., Nilsson P.G., and Line P. (1986) *Colloid and Polymer Science* **264**, 77
- [7] Torquato S. (1991) *J. Stat. Phys.* **65**, 1173
- [8] Jacobs P.W.M., Hooton I.E. (1990) *J.Phys.Chem.Sol.* **51**, 1207
- [9] Catlow C.R.A. (1991) *Phil.Mag. A* **64**, 1011
- [10] Kalnin Yu.R.(1985) Proc Latvian Acad. Sci. physics **No 6**, 13
- [11] Felderhof B.U. and Deutch J.M. (1976) *J.Chem. Phys.* **64**, 4551
- [12] Kalnin Yu.R. and Zapol P. (1995) *Radiation Effects and Defects in Solids* **137**, 295
- [13] Manning J.R. (1968) *Diffusion Kinetics for Atoms in Crystals*. Princeton, Toronto
- [14] Ronis G.M. (1987) *Phys Rev A* **36**, 1908
- [15] Cukier R.I. (1983) *J.Phys.Chem. Solids* **87**, 582
- [16] Bell G.M. (1964) *Trans.Farad.Soc.* **60** 1752
- [17] Kalnin Yu.R. and Kotomin E.A. (1998) *J.Phys: Math.Gen.* **31** 7227
- [18] Vucans J. (1995) **In: Proceedings of IFIP WG 7.2 on Modelling and Optimisation of Distributed Parameter Systems with Applications to Engineering**. Chapman and Hall, p.321
- [19] Smith P.M. and Aziz M.J. (1994) *Acta Metallurgica and Materialia* **42**, 3515
- [20] Han J.H. (2000) *Foodtechnology* **54**, 56

Received on the 2nd of June 2001

***Ab initio* SIMULATIONS OF THE Cu/MgO(001) INTERFACE**

Yu.F. ZHUKOVSKII^a, D. GRYAZNOV^b, A. FINOGENOV^b, Yu.N. SHUNIN^b

^a*Institute of Solid State Physics, University of Latvia, 8 Kengaraga Str., LV-1063 Riga, Latvia*

^b*Department of General and Applied Physics, Transport and Telecommunication Institute,
 1 Lomonosova Str., LV-1019 Riga, Latvia*

We present the first *ab initio* Hartree-Fock simulations on the Cu/MgO interface using CRYSTAL computer code for periodic systems. First, we describe our results for bulk copper and MgO(001) 2D slabs. Then we consider a model of an initial stage of the Cu/MgO(001) interface formation (with 1/4 submonolayer and monolayer substrate coverages). We compare our results with various experimental and theoretical data, in order to clarify the nature of interfacial bonding and its electronic structure. The dominant interfacial effect is found to be physical adhesion of copper associated with polarization and charge redistribution.

Keywords: *Ab initio* Hartree-Fock calculations, CRYSTAL code, electronic structure, Cu/MgO interfaces, copper adhesion

1. Introduction

A number of technological applications of copper continue to grow, especially in microelectronics [1]. In particular, Sun Microsystems Inc. and IBM use copper-containing microelectronic devices in supercomputers. The power of new copper-based microprocessors is derived in part from IBM pioneered copper *wiring*. Copper-based chips offer superior commercial and technical performance as compared to chips that use traditional aluminum wires [2]. Copper possesses a better conductivity than aluminium, which provides a more efficient signal transfer. Thus, copper chips could operate 40% faster than aluminium ones and, moreover, the former are cheaper by 30%. Copper is now expected to replace aluminium as the main conducting material for all types of integrated circuits within the next device generations. Meanwhile, even today copper-based microprocessors are widely used in all kinds of electronic products - from notebook computers to cameras, mobile phones, microwave ovens, etc. [1].

In the light of recent achievements in microelectronics and other high technologies, the necessity in both improving and further development of copper applications is quite actual. There is increasing demand for epitaxially grown copper films on non-conducting substrates widely used in integrated circuits [2,3]. One of the important issues is the fabrication of smooth Cu films to serve as a growth template for device structures, such as tunneling magnetoresistance devices (TMR). MgO substrates in a combination with a Fe/Pt seed layer provide the superior film quality needed. The copper/magnesia interface is also of great importance in other technological applications, including catalysis, metal-matrix composites, recording media, etc. [4]. It is very important to understand both atomic structure and electronic properties of the interfacial region. One example is charge redistribution in the metal film, which has an impact on its conductivity and also affects its catalytic ability [5]. Stability of the metal-oxide interfaces and their technologically important properties markedly depend on the adhesion nature, mechanical support, both heat and carrier transfer across the interface, as well as specific morphology.

Two types of copper/magnesia interfaces have been mainly studied so far, both experimentally and theoretically: Cu/MgO(001) and Cu/MgO(111) [6-19]. In the former case, oxide surface is non-polar, due to successive alternation of Mg²⁺ and O²⁻ ions in each magnesia (001) plane. On the other hand, the MgO(111) surface may be either Mg²⁺- or O²⁻-terminated, thus the interface between copper and magnesia is polar and more strongly bonded than non-polar one [6]. Growth of MgO precipitates in a Cu matrix under an internal oxidation has been observed using high-resolution methods of atom-probe field ion and transmission electron microscopy (AFM and TEM, respectively [7-9]), as well as spatially resolved electron energy loss spectroscopy (HREELS [10,11]). These experimental studies revealed presence of the Cu/MgO(111) interfaces, with the preferable O²⁻-termination of MgO surface, and absence of Cu/MgO(001). On the other hand, the adsorption of copper moieties on the MgO(001) support was analysed in Auger electron spectroscopic (AES) experiments performed by Møller *et al.* [12].

Theoretical studies of copper/magnesia interfaces were mainly performed at the *ab initio* level [6,13-19]. Using Hartree-Fock (HF) method and finite-cluster models, Bacalis and Kunz [13] considered

neutral and ionization states of Cu atom on a perfect and defective MgO(001) substrate. For the perfect MgO, the adsorption energy per copper atom positioned over O^{2-} ion was estimated to be rather weak (0.38 eV). Further simulations [6,14-19] were mainly performed using Density Functional Theory (DFT). Li *et al.* [14] used the DFT method to calculate several finite-cluster models of Cu atom over the MgO(001) surface. In analogous simulations, Rösch *et al.* [15] applied cluster model embedded in a large array of point charges. At the same time, Benedek, Minkoff *et al.* [6] considered results of DFT calculations for the periodic slab models of Cu/MgO(111) and Cu/MgO(001) interfaces and found markedly larger sticking of copper atoms to the (111) surface of magnesia substrate: three-fold larger than that on the (001) surface.

Nevertheless, taking into account noticeable mismatch ($\approx 15\%$) between the lattice constants of MgO and Cu, a couple of recent theoretical studies considered not just a monolayer coverage of substrate by a metal (as in the case of the Ag/MgO(001) interface with almost equal lattice constants for both components [20-25]) but copper *clusters* distributed on densely-packed magnesia substrates. Using Car-Parinello method, which combines DFT and molecular dynamics techniques, Musolino *et al.* [16] have studied the adsorption of small Cu_n clusters ($n \leq 13$) onto a MgO(100) substrate simulated by two-layer slab. It was found that the competition between adsorbate-adsorbate and substrate-adsorbate interactions turns in favor of the former. The interaction between copper atoms inside the clusters determines the metal adsorption process. This is one of the reasons why three-dimensional (3D) structures are preferred as compared to two-dimensional ones (2D): the system gains more energy by bonding copper atoms together than by 2D metal adsorption them on oxygen surface ions. Results [16] show that small copper clusters ($n=1-5$) readily are adsorbed on the MgO surface with binding energies E_{ads} per Cu atom in the 0.4-0.9 eV range, whereas for larger clusters, E_{ads} is always smaller than 0.4 eV per atom. Matveev *et al.* [17] used embedded cluster model of the Cu/MgO(001) interface to simulate both creation of copper clusters on regular magnesia substrate and strong localization of metal atoms in the vicinity of anion oxygen vacancies with two and one trapped electrons (so-called F_s^- and F_s^+ -centers, respectively) [17]. Jug *et al.* [18] applied both *ab initio* DFT and semi-empirical MSINDO calculations to simulate various Cu_n clusters ($n \leq 52$) on a $(8 \times 8 \times 3)$ $Mg_{96}O_{96}$ cluster model of magnesia (001) substrate. It was found that the sticking probability of copper atoms to the MgO surface is reduced with an increase of a number of adsorbed Cu atoms because not all atoms can be adsorbed atop the oxygen ions. Instead, Cu-Cu binding is invoked. At the first step, the growth of a single double layer takes place, on top of which, formation of an *island* from metal atoms is expected. Comprehensive simulation of the Cu/MgO(222) interface has been carried out by Benedek, Seidman *et al.* [19]. Periodic calculations were performed for both regular and semi-regular interfaces that approximate the lattice constant mismatch of the real system: a 5×5 copper layer unit cell (UC) placed on a 4×4 magnesia UC. The terminating O^{2-} -layer as well as the interface Cu-layer exhibits warping albeit on a scale of less than 0.1 Å. It was also found that the interface atoms in relatively coherent regions move toward the interface and those in regions of poorer fit move away from it.

Our study is devoted to periodic slab simulations of the Cu/MgO(001) interface. We focus both submonolayer and monolayer substrate coverages but first analyze isolated copper and magnesia. To go beyond usual periodic DFT simulations on copper/magnesia interfaces [6,16], we perform *ab initio* Hartree-Fock calculations with the electron correlation corrections (HF-CC method) as implemented in CRYSTAL95 code [26]. This was successfully applied for a series of simulations on the Ag/MgO interfaces performed recently at the Institute of Solid State Physics, University of Latvia [23-25]. There were several theoretical calculations of the electronic structure of silver layers deposited on the perfect (001) and (011) magnesia substrates [23] as well as Ag/MgO(001) interface with substrate defects (O^{2-} and Mg^{2+} surface vacancies) [24]. The most recent paper was devoted to a thermodynamic theory of the mechanism for silver film growth on perfect MgO(001) substrate based on results of *ab initio* HF-CC calculations on the interfacial superstructures [25]. A novel approach permits to predict conditions for metal atom aggregation into Ag_n clusters, and to estimate the metal density in them. The calculated high mobility of Ag atoms leads to formation of 3D metal islands, whereas continuous silver layer can arise in result of their further overlap.

1. Theoretical background

2.1. HARTREE-FOCK CALCULATIONS ON PERIODIC SYSTEMS

For a long time the Hartree-Fock method was the most popular technique for a study the electronic structure of atoms, molecules and clusters, whereas a number of periodic systems, especially

crystalline solids, were mainly studied using Kohn-Sham (KS) method in the framework of DFT approach [27]. Moreover, various HF computational procedures has never been too popular among solid state physicists, for at least two reasons [28]:

- standard HF approach performs rather poorly for the electron gas, which is the simplest of all possible periodic systems; moreover, this remains true (or possibly gets even worse) for many properties of real solids;
- the non-local exchange term makes the HF equations more difficult to solve than the KS ones, where the exchange-correlation potential is simply a multiplicative operator, no matter how complicated its determination [29] either as such or as a well defined starting point for more sophisticated techniques.

Nevertheless, in the recent years has it become possible to formulate a fair judgement about the usefulness of the HF approach in solid state physics [30], since the advent of powerful computers and of improved computational schemes, which also include electron correlation corrections. Quite contrary, DFT method, which had played for long time a minor role in molecular quantum chemistry, has become more and more popular in the last years, and DFT related computational schemes are now available in standard *ab initio* molecular codes [31]. The most successful modern HF codes possess a similar structure:

- the linearized Hartree-Fock-Roothaan (HFR) equations are solved by using a few localized functions *per atom* indicated as atomic orbitals (AOs) expressed as linear combinations of Gaussian type functions (GTF) with appropriate exponents and “contraction” coefficients;
- either molecular or crystalline orbitals (MO and CO, respectively), as well as eigenvectors of the Fock matrix are obtained through a self-consistent field (SCF) procedure;
- the correlation corrections to the ground state wave function (*a posteriori* HF-CC approach [32]) are used to evaluate total energy in more adequate way as compared to standard HF procedure;
- the description of excited states are usually performed by means of configuration interaction (CI) or perturbation techniques.

To perform *ab initio* HF-CC simulations on the Cu/MgO(001) interface, we have used the computer code CRYSTAL95 [26] implemented by the Group of Theoretical Chemistry of the University of Torino in collaboration with the Computational Group at the Daresbury Laboratory (a series of computer codes CRYSTAL are under continuous development for about twenty-five years [30,33]). The crystalline-orbital method, upon which CRYSTAL treatment is based, uses a set of localized atom-centered GTFs, $\chi_\mu(\mathbf{r})$, for the n_e -electron-containing unit reference cell (UC) of periodic lattice described by \mathbf{g} translation vectors. The unknown COs are expanded as linear combinations of a set of m Bloch functions (BF) built from these GTFs (CO LCGTF):

$$\varphi_i(\mathbf{k}, \mathbf{r}) = n_e \sum_{\mu=1}^m c_{\mu i}(\mathbf{k}) \sum_{\mathbf{g}} \exp(i\mathbf{k} \cdot \mathbf{g}) \chi_\mu(\mathbf{r} - \mathbf{g}), \quad (1)$$

where \mathbf{k} is a general vector in the first Brillouin zone (BZ). Solution of one-electron Hartree-Fock equations for this crystal

$$\hat{F} \varphi_i(\mathbf{k}, \mathbf{r}) = \varepsilon_i(\mathbf{k}) \varphi_i(\mathbf{k}, \mathbf{r}) \quad (2)$$

defines the energy spectrum of eigenvalues $\varepsilon_i(\mathbf{k})$. BF representation of the Fockian becomes

$$F_{\mu\nu}(\mathbf{k}) = \sum_{\mathbf{g}} \exp(i\mathbf{k} \cdot \mathbf{g}) F_{\mu\nu}(\mathbf{g}), \quad (3)$$

where $F_{\mu\nu}(\mathbf{g})$ is the matrix element of the Fock operator between the μ -th AO located in the *zero* UC ($\mathbf{0}$) and the ν -th AO located in the \mathbf{g} cell (the row index can be limited to the $\mathbf{0}$ cell for translation symmetry) and may be presented as a sum of four different contributions:

$$F_{\mu\nu}(\mathbf{g}) = T_{\mu\nu}(\mathbf{g}) + V_{\mu\nu}(\mathbf{g}) + J_{\mu\nu}(\mathbf{g}) + K_{\mu\nu}(\mathbf{g}), \quad (4)$$

where matrix elements of kinetic (\hat{T}), electron-nuclei (\hat{V}), Coulomb (\hat{J}), and non-local exchange (\hat{K}) operators are defined throughout the first BZ [28]:

$$T_{\mu\nu}(\mathbf{g}) = \int \chi_\mu(\mathbf{r}) \nabla_{\mathbf{r}}^2 \chi_\nu(\mathbf{r} - \mathbf{g}) d\mathbf{r}, \quad (5a)$$

$$V_{\mu\nu}(\mathbf{g}) = \sum_{j=1}^N \sum_{\mathbf{g}'} \int \chi_\mu(\mathbf{r}) \frac{Z_j}{|\mathbf{r} - \mathbf{R}_j - \mathbf{g}'|} \chi_\nu(\mathbf{r} - \mathbf{g}) d\mathbf{r}, \quad (5b)$$

$$J_{\mu\nu}(\mathbf{g}) = \sum_{\lambda\sigma}^m \sum_{\mathbf{g}'} P_{\lambda\sigma}(\mathbf{g}') \sum_{\mathbf{g}''} \iint \chi_{\mu}(\mathbf{r}) \chi_{\nu}(\mathbf{r} - \mathbf{g}) \frac{1}{|\mathbf{r} - \mathbf{r}' - \mathbf{g}''|} \chi_{\lambda}(\mathbf{r}' - \mathbf{g}'') \chi_{\sigma}(\mathbf{r}' - \mathbf{g}' - \mathbf{g}'') d\mathbf{r} d\mathbf{r}', \quad (5c)$$

$$K_{\mu\nu}(\mathbf{g}) = -\frac{1}{2} \sum_{\lambda\sigma}^m \sum_{\mathbf{g}'} P_{\lambda\sigma}(\mathbf{g}') \sum_{\mathbf{g}''} \iint \chi_{\mu}(\mathbf{r}) \chi_{\lambda}(\mathbf{r}' - \mathbf{g}'') \frac{1}{|\mathbf{r} - \mathbf{r}' - \mathbf{g}''|} \chi_{\nu}(\mathbf{r} - \mathbf{g}) \chi_{\sigma}(\mathbf{r}' - \mathbf{g}' - \mathbf{g}'') d\mathbf{r} d\mathbf{r}', \quad (5d)$$

where $\nabla_{\mathbf{r}}$ is a Laplace operator, N , \mathbf{R}_j , and Z_j are number of atoms *per* UC, their radii-vectors and charges, respectively, \mathbf{g}' and \mathbf{g}'' determine lattice summations, whereas elements of density matrix are defined as:

$$P_{\lambda\sigma}(\mathbf{g}') = 2 \int_{\text{Brillouin zone}} \exp(i\mathbf{k} \cdot \mathbf{g}') \left(\sum_i^{n_b} c_{\lambda i}^*(\mathbf{k}) c_{\sigma i}(\mathbf{k}) \theta\{\varepsilon_F - \varepsilon_i(\mathbf{k})\} \right) d\mathbf{k}, \quad (6)$$

where θ is the so-called Heaviside "zero-temperature" occupation function [34], ε_F is the Fermi energy which determines the occupied manifold in \mathbf{k} -space, whereas $c_{\mu i}(\mathbf{k})$ and $\varepsilon_i(\mathbf{k})$ are eigenvectors and eigenvalues of Fock matrix $\|F(\mathbf{k})\|$, respectively. Since summations over all translation vectors, which are used in Eqs. (5b-5d), extend to the infinite set, a special strategy is specified for the treatment of the corresponding infinite series, as well as for the substitution of the integral that appears in Eq. (6) with a weighted sum extended to a finite set of \mathbf{k} -points. CRYSTAL code provides an accurate and efficient solution to these problems [30,33].

Matrices represented in the Bloch basis (" \mathbf{k} space") take a block diagonal form, as Bloch functions are bases for the Irreducible Representations (IR) of the Translation Group (TG). In the case of closed shell systems HFR equations in matrix form are presented as:

$$\|F(\mathbf{k})\| \times \|C(\mathbf{k})\| = \|S(\mathbf{k})\| \times \|C(\mathbf{k})\| \times \|E(\mathbf{k})\|, \quad (7)$$

where $\|C(\mathbf{k})\|$ and $\|E(\mathbf{k})\|$ are matrix of eigenvectors and diagonalized matrix of eigenvalues, respectively, whereas $\|S(\mathbf{k})\|$ contains Fourier transformations of pair-wise overlap integrals:

$$S_{\mu\nu}(\mathbf{k}) = \sum_{\mathbf{g}} \exp(i\mathbf{k} \cdot \mathbf{g}) \int \chi_{\mu}(\mathbf{r}) \chi_{\nu}(\mathbf{r} - \mathbf{g}) d\mathbf{r}, \quad (8)$$

In principle, Eq. (7) should be solved for all the (infinite) $\{k\}$ set of points in the Brillouin zone. Fortunately, only a finite and usually a small subset of these blocks, corresponding to a suitable sampling of \mathbf{k} -points, needs to be diagonalized, because interpolation techniques can be used for eigenvalues and eigenvectors throughout the first Brillouin zone. An expression for the total electron energy *per* UC, which is obtained using variational principle and taking into account representation of the trial HF wave function as a single determinantal function constructed from antisymmetrized spin-orbitals [30], can be written as follows:

$$E_{tot} = \sum_{\mu\nu}^m \sum_{\mathbf{g}} P_{\mu\nu}(\mathbf{g}) [F_{\mu\nu}(\mathbf{g}) + T_{\mu\nu}(\mathbf{g}) + V_{\mu\nu}(\mathbf{g})]. \quad (9)$$

In the case of open shell periodic systems (for instance, paramagnetic species), the so-called unrestricted HF method (UHF) is usually applied, where two matrix equations must be solved self-consistently, for both α and β electrons:

$$\|F^{\alpha}(\mathbf{k})\| \times \|C^{\alpha}(\mathbf{k})\| = \|S(\mathbf{k})\| \times \|C^{\alpha}(\mathbf{k})\| \times \|E^{\alpha}(\mathbf{k})\|, \quad (10a)$$

$$\|F^{\beta}(\mathbf{k})\| \times \|C^{\beta}(\mathbf{k})\| = \|S(\mathbf{k})\| \times \|C^{\beta}(\mathbf{k})\| \times \|E^{\beta}(\mathbf{k})\|. \quad (10b)$$

The total density and spin density matrices are defined in direct space using UHF computational scheme as:

$$\|P(\mathbf{g})\| = \|P^{\alpha}(\mathbf{g})\| + \|P^{\beta}(\mathbf{g})\|, \quad (11a)$$

$$\|P^{spin}(\mathbf{g})\| = \|P^{\alpha}(\mathbf{g})\| - \|P^{\beta}(\mathbf{g})\|, \quad (11b)$$

where $\|P^{\alpha}(\mathbf{g})\|$ and $\|P^{\beta}(\mathbf{g})\|$ are obtained as in Eq. (6) by using the eigenvectors $\|C^{\alpha}(\mathbf{k})\|$ and $\|C^{\beta}(\mathbf{k})\|$ obtained from Eqs. (10a,b), respectively. Elements of Fockians are defined as follows:

$$F_{\mu\nu}^{\alpha}(\mathbf{g}) = F_{\mu\nu}(\mathbf{g}) - K_{\mu\nu}^{spin}(\mathbf{g}), \quad (12a)$$

$$F_{\mu\nu}^{\beta}(\mathbf{g}) = F_{\mu\nu}(\mathbf{g}) + K_{\mu\nu}^{spin}(\mathbf{g}), \quad (12b)$$

where $\|F(\mathbf{g})\|$ matrix is defined as in Eq. (4), the total density matrix $\|P(\mathbf{g})\|$ from Eq. (11a) is used in the Coulomb and exchange terms written in Eqs. (5c,d), whereas $K_{\mu\nu}^{spin}(\mathbf{g})$ is defined as $K_{\mu\nu}(\mathbf{g})$ in Eq. (5d), however, elements of spin density matrix $P_{\mu\nu}^{spin}(\mathbf{g})$ are used there instead of $P_{\mu\nu}(\mathbf{g})$ for total density matrix. An expression for the total electron energy *per* UC according to the UHF procedure is slightly more complicated than that in Eq. (9):

$$E_{tot} = \sum_{\mu\nu}^m \sum_{\mathbf{g}} \left\{ P_{\mu\nu}(\mathbf{g}) \left[F_{\mu\nu}(\mathbf{g}) + T_{\mu\nu}(\mathbf{g}) + V_{\mu\nu}(\mathbf{g}) \right] + P_{\mu\nu}^{spin}(\mathbf{g}) K_{\mu\nu}^{spin}(\mathbf{g}) \right\}. \quad (13)$$

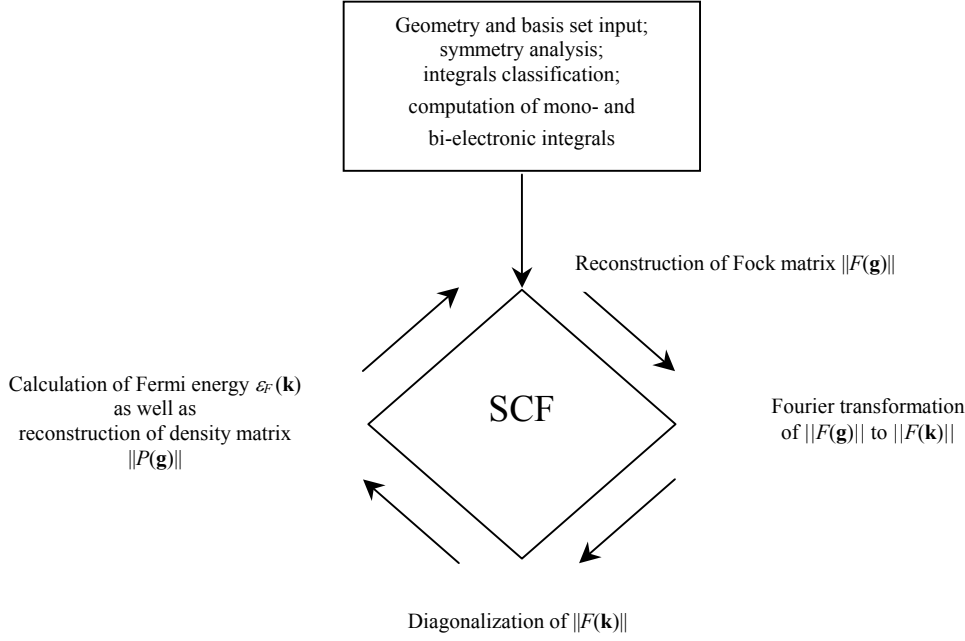


Figure 1. Scheme of implementation of the standard HF method in CRYSTAL code.

Cyclic procedure of the Self-Consistent-Field (SCF) solution for matrix Eqs. (7) and (10a,b) in the framework of CRYSTAL computational scheme [28] is illustrated in Fig. 1. All the relevant quantities (mono- and bi-electronic integrals, overlap and Fock matrices) are computed in the direct configuration space. Just before diagonalization step $\|F(\mathbf{g})\|$ matrix is Fourier transformed to reciprocal space of BF according to Eq. (3), then both eigenvalues $\varepsilon_i(\mathbf{k})$ and eigenvectors $c_{\mu i}(\mathbf{k})$ are combined to generate direct space matrix $\|P(\mathbf{g})\|$ using Eq. (6) for the next SCF cycle. Each of them is completed by total energy calculation using either Eq. (9) or Eq. (13). Two sections of the UHF scheme, corresponding to α and β electrons, are independent until the Fermi energy ε_F calculation and $\|F(\mathbf{g})\|$ matrix reconstruction. It is then possible to force the system into a state with a particular total spin value (S_z), by imposing the corresponding value when the crystalline one-electron energy levels ε_i are populated at each cycle of the SCF step [28]. The whole procedure is completed after n -th SCF cycle when either set tolerance of the total energy *per* UC is achieved, i.e. $|E_{tot}^{(n)} - E_{tot}^{(n-1)}| < \delta E$, or n exceeds set limit of cycles.

To correct E_{tot} for the standard HF method by *a posteriori* estimating the electron correlation energy, CRYSTAL code provides an integration of the applying DFT functional [34]:

$$E_c^{(DFT)} = \int_{\text{unit cell}} \rho(\mathbf{r}) \varepsilon_c[\rho(\mathbf{r})] d\mathbf{r}, \quad (14)$$

where ε_c is a correlation energy per particle, whereas HF electron density $\rho(\mathbf{r})$ is defined as:

$$\rho(\mathbf{r}) = \int_{\text{Brillouin zone}} \sum_i^{\text{occupied states}} |\varphi_i(\mathbf{k}, \mathbf{r})|^2 \theta\{\varepsilon_F - \varepsilon_i(\mathbf{k})\} d\mathbf{k} \quad (15)$$

Several correlation functionals used in the DFT and implemented in the CRYSTAL95 code [26] may be applied in order to evaluate $E_c^{(DFT)}$ as defined by Eq. (14). Thus, a total energy per unit cell using a *a posteriori* HF-CC approximation is expressed as a simple sum of contributions given in Eqs. (9) or (13) and Eq. (14). In calculations we have used both Local Spin Density and non-local Generalized Gradient approximations (LSD and GGA) for the electron correlation corrections. In the former case, $E_c^{(LSD)}$ is defined in terms of the correlation energy per particle ε_{xc} in the homogeneous electron gas with a density $\rho(\mathbf{r})$. In the present study we have used a LSD functional suggested by Vosko, Wilk and Nusair [35]. The GGA correlation functional depends not only on the electron density of homogeneous electron gas but on its gradients as well; to determine $E_c^{(GGA)}$, we have used the Perdew and Wang approximation [36].

To perform *ab initio* calculations of the Cu/MgO(001) interface using CRYSTAL code, we must make a correct choice of the basis set (BS) for local atom-centered Gaussian-type functions $\chi_j(\mathbf{r})$. In this study, we use all-electron BS 8(*s*)-51(*sp*) for O and 8(*s*)-61(*sp*) for Mg, originally optimized by Causá *et al.* [37] and then re-optimized in our previous studies of the Ag/MgO interfaces [23], as well as 8(*s*)-64111(*sp*)-41(*d*) for Cu, originally developed by Doll and Harrison [38] and re-optimized by us in current study, in order to reproduce better the properties of copper bulk. When applying the mentioned BS for oxygen, magnesium, and copper, we could obtain reasonable results for properties of both Cu/MgO(001) interface and its separate components, which are described below, in Sections 3-5.

2.2. SLAB MODEL OF THE Cu/MgO(001) INTERFACE

Both copper and magnesia bulk crystals possess a face-centered cubic (*fcc*) lattice structure, which belongs to the space symmetry group $Fm\bar{3}m$. As mentioned in Introduction, a mismatch of their lattice constants, a_{Cu} (3.6 Å) and a_{MgO} (4.2 Å) [39], is about 15%. Thus, in spite of a space compatibility within the coherent Cu/Mg(001) and Cu/MgO(111) interfaces, their components are either strained (in the case of the copper film on magnesia substrate) or compressed (for magnesia film on the copper substrate). This is why such an interface is very likely completely incoherent or semicoherent (with misfit dislocations) [40]. Nevertheless, this is not relevant for the adsorption of *single* Cu atoms on substrate, therefore a model of 1/4 submonolayer copper coverage (1/4 ML) of the perfect MgO(001) surface (Fig. 2a) is quite justified for a simulation of the interaction between Cu atom and oxide substrate. We also treated monolayer substrate coverage (1 ML), where copper network is indeed strained. The reason for this model (Fig. 2b) is a comparative analysis of the interfacial properties when increasing concentration of metal atoms on oxide substrate in the framework of a periodic slab model.

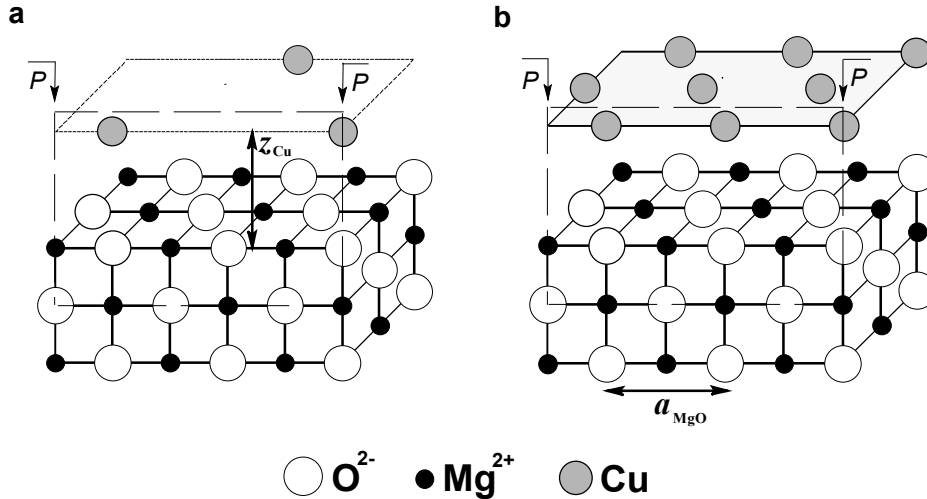


Figure 2. Fragments of the Cu/MgO(001) interface with 1/4 ML (a) and 1 ML (b) substrate coverages where Cu atoms are placed at the distance z_{Cu} above surface O^{2-} ions. Another possible adsorption position of copper atoms on the same substrate is above surface Mg^{2+} ions. Both interface models are sectioned by one and the same plane $P-P$ limited by dashed lines and used for construction of the difference electron density plots shown in Fig. 6.

In our theoretical simulations of the perfect MgO(001) substrate, we have applied three-layer slab which has a 2D periodicity. Since one-side copper coverage of magnesia slab, which we consider, was varied from 1/4 ML to a 1 ML, we have made a series of calculations for a 2×2 extended surface unit cell of MgO(001). Figs. 2a and 2b show copper atom positions over surface O^{2-} ions (we have considered also the interface configurations with Cu atoms sitting over Mg^{2+} ions). For all these structures, we have carried out the total energy optimization. For the metal/oxide system, this means a two-dimensional optimization of the total energy $E_{tot}(a_{MgO}, z_{Cu})$ as a function of the substrate lattice constant a_{MgO} and the interfacial distance z_{Cu} . For the MgO substrate, we optimize the total energy $E_{tot}(a_{MgO})$ as a function of the lattice constant. Similar to our recent simulations on the Ag/MgO(001) interface [23-25], we neglect here magnesia surface relaxation, which was earlier found to be rather small [37]. Dashed planes across slabs (Fig. 2) are used in Section 5 to analyze re-distribution of the electron density in the interfacial region between Cu and MgO(001).

2.3. BASIC PROPERTIES OF COPPER/MAGNESIA INTERFACE AND ITS COMPONENTS

Using CRYSTAL95 code [26], we have calculated a number of properties describing both the Cu/MgO(001) interface as well as copper and magnesia which interact with each other. For these, we have analyzed the cohesive and adhesion properties (optimized lattice constants and interfacial distances as well as cohesive energy and bulk modulus for bulk copper, and interfacial adhesion energy), moreover we have studied charge distribution across copper-magnesia interface (both Mulliken charges and bond populations as well as the difference electron density plots). Some properties may be obtained directly during the HF-CC calculations, whereas to obtain another group of properties, we performed further analysis of the results of CRYSTAL calculations.

To optimize bulk lattice constants a_{Cu} (Fig. 3) and a_{MgO} (Fig. 4), we have varied both interatomic distances retaining $Fm\bar{3}m$ symmetry of the *fcc* crystal (Fig. 2). Details of the corresponding procedure using both quasi-harmonic parabolic approximation for the energy minimum $E_{tot}^{(o)}$ per lattice unit cell (UC) and a least-square method with the second-degree polynomial have been described by us elsewhere [32]. Another important lattice feature is the bulk modulus B , which is defined as [32]:

$$B = n^{-1} a_o^3 \frac{\partial^2 E_{tot}}{\partial V^2}, \quad (16)$$

where n is a co-factor dependent on the type of cubic lattice (for the *fcc* lattice $n = 4$), a_o an equilibrium lattice constant, whereas $V = a^3$ an optimizing volume of UC. The bulk modulus have been estimated through a fitting the curves $E_{tot}(a)$ by a polynomial regression as described in Ref. [32]. The cohesive energy E_{coh} per atom defines the difference between optimized total energy E_{bulk}^{min} per UC and the total energy E_{atom}^{min} of isolated atom surrounded by 12 AO of its nearest *fcc* neighbors, according to the optimized lattice structure (“ghost” atoms contain no charge) [41]:

$$E_{coh} = E_{bulk}^{min} - E_{atom}^{min}. \quad (17)$$

The values of B and E_{coh} have been mainly calculated for bulk copper (Table 1), in order to check correctness of the re-optimized BS for Cu, as was mentioned in subsection 2.1.

To define an optimal value of adhesion energy E_{adh} , according to the so-called universal binding energy relation, UBER (similar to the potential energy curve for a diatomic molecule) [22], we fit the calculated total energy of the interface to the following potential binding energy curve:

$$E_b(z_{Cu}) = E_{adh} k \left(1 + \frac{z_{Cu} - z_{Cu}^{(o)}}{z_{Cu}}\right) \cdot \exp\left(-\frac{z_{Cu} - z_{Cu}^{(o)}}{s}\right) \quad (18)$$

where $z_{Cu}^{(o)}$ is the equilibrium interfacial distance, k the number of Cu atoms per 2×2 magnesia surface unit (one or four, for 1/4 ML and 1 ML coverages, respectively), and s a scaling constant. Note that for well-separated copper and magnesia slabs $\lim_{z_{Cu} \rightarrow \infty} E_b(z_{Cu}) = 0$. Eq. (18) has been used in this paper to fit

the interfacial potential energy curves (Fig. 5) as well as to get values of $z_{Cu}^{(o)}$ and E_{adh} (Table 2) for the two substrate coverages (1/4 ML and 1 ML) and two Cu adsorption sites (above Mg^{2+} and O^{2-} ions). Both charges and bond populations at the Cu/MgO(001) interface (Table 2) may be analyzed directly from outputs of CRYSTAL calculations, in terms of Mulliken population analysis [26]. For more detailed description of the interface charge re-distribution, we have drawn the difference 2D plots of electron

density (Fig. 6) across the Cu/MgO(001) interface shown in Fig. 2. This represents the total interface electron density minus the superposition of atomic densities. To construct these plots, CRYSTAL code uses algorithms described by us recently [32].

3. Simulation on bulk Cu

To begin the simulation of Cu/MgO(001) interface, we must be sure that its components are described properly. Despite the fact that magnesia substrate was earlier simulated using CRYSTAL code quite intensively since 80s [37], and we have used its optimized geometry and BS earlier in a study of Ag/MgO(001) interface [23-25], previous HF simulations of copper-containing materials are rather scarce [38,42]. Moreover, the basis set used for description the metallic copper and its chemical activity [38] was obtained after rather trivial re-optimization of BS for copper ions in magnetic pseudocubic KCuF_3 perovskite [42]. We found that description of the valence Cu $4s$ AO by using only one Gaussian type function, as done in [38], is not sufficient for comprehensive simulations. Three GTFs for this valence state were suggested 15 years ago by Bacalis and Kunz [13]. However, that basis set was applied for a finite cluster model of Cu/MgO interface and, moreover, two of the three functions were too diffuse to apply them directly in our periodical calculations. This is why we have re-optimized BS for copper applied by Doll and Harrison [38], not changing configuration of the LCGTF but only optimizing exponents of the Gaussian functions for the valence $4s$ state as well as virtual $4d$, $5s$ and $6s$ states, in order to achieve a better reproducibility of experimental values for a_{Cu} , B and E_{coh} in the framework of HF-CC method.

TABLE 1. Basic cohesive properties for bulk copper.

Method \ Properties	$a_{\text{Cu}}^{(0)}$, Å	B , Gpa	E_{coh} , eV
standard HF	3.8	113	2.69
HF+CC (LSD)	3.75	106	3.07
HF+CC (GGA)	3.65	105	3.86
Data obtained by Doll and Harrison [38] ^a	3.95 (standard HF) 3.53 (DFT, LSD) 3.63 (DFT, GGA)	69 (standard HF) 195 (DFT, LDA) 155 (DFT, GGA)	0.49 (standard HF) 4.95 (DFT, LSD) 3.89 (DFT, GGA)
Experiment	3.604 [44]	142 [46]	3.51 [45]

^a DFT method, with both LSD or GGA exchange and correlation functionals [29]

Basic results of our simulation on bulk copper are presented in Table 1 and Figure 3. We describe here three data set, which are obtained using the standard HF method (with no corrections) and two different electron correlation corrections implemented in the framework of HF-CC method: LSD (VWN [35]) and GGA (PW [36]), as was explained in subsection 2.1. It is obvious from Table 1 that both corrections improve the quality of obtained results. This may be explained by well-known fact that the standard Hartree-Fock method usually overestimates bond lengths and underestimates the formation energy [43], whereas electron correlation corrections minimize these artifacts, especially GGA. It is also true for the value of cohesive energy (Table 1). This is why for further simulations of both magnesia substrate and Cu/MgO(001) interface we have used only PWGGA correlation corrections. When we compare values of ΔE (Fig. 3) and E_{coh} (Table 1) *per* Cu atom, their difference by a factor 2.2-2.5 may be explained by the different geometries: the former case corresponds to a symmetrical 3D expansion of copper lattice, whereas cohesion energy estimates a simple removal of Cu atom from the lattice, along some one-dimensional trajectory. As to the bulk modulus, its values seem to be underestimated in all three cases, *a posteriori* corrections did not lead to a better agreement with the experimental value [46]. It confirms the corresponding shortcoming observed in [38], although only the standard HF method was applied there, not HF-CC like in our current paper.

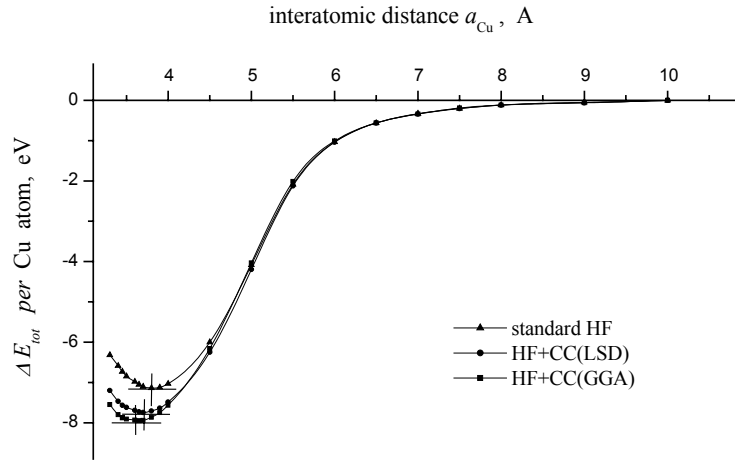


Figure 3. Potential curves $\Delta E_{tot}(a_{Cu}) = E_{tot}(a_{Cu}) - E_{tot}(a_{Cu}^{\infty})$ obtained using three different ways, where $\Delta E_{tot}(a_{Cu}^{\infty}) = \lim_{a_{Cu} \rightarrow \infty} \Delta E_{tot}(a_{Cu}) = 0$. Equilibrium lattice constant $a_{Cu}^{(0)}$ corresponds to an energy minimum of the potential curve.

4. Simulation on the MgO(001) substrate

Magnesia is a typical ionic crystal, during its formation the charge transfer of almost $2e$ between the initially neutral magnesium and oxygen atoms takes place (according to different theoretical estimates for bulk magnesia [47,48], this transfer lies in the range 1.9 - $2.0e$, whereas our calculations give $1.97e$ for both bulk MgO and non-polar MgO(001) substrate). In this study, we mainly use magnesia basis sets, which were described in Refs. [37,47] and mentioned in subsection 2.1. The extended BSs of MgO (8-511G for Mg and 8-411G for O) introduced later [48] include more diffuse polarization functions for $4sp$ and $3d$ virtual states of both magnesium and oxygen. Nevertheless, the basic properties of bulk MgO are not changed noticeably with these new BSs. Thus, we did not see the need to use the extended BS, taking into account the large increase in both computer disk space and CPU time, which would result in such calculations.

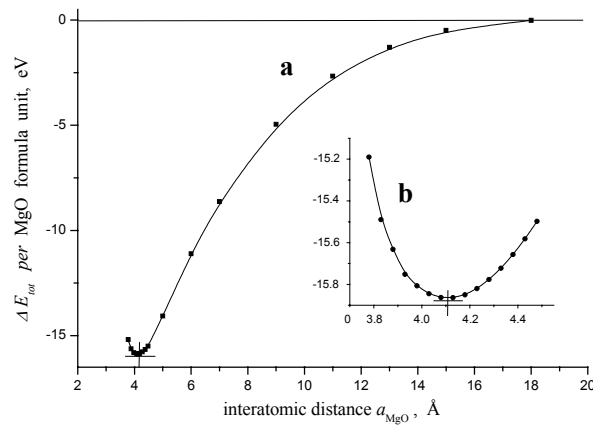


Figure 4. Potential curve $\Delta E_{tot}(a_{MgO}) = E_{tot}(a_{MgO}) - E_{tot}(a_{MgO}^{\infty})$ obtained for the PWGGA electron correlation correction (a) and its fragment, which allows to localize an energy minimum for the lattice constant $a_{MgO}^{(0)}$ (b).

The optimized value of the lattice constant $a_{\text{MgO}}^{(0)}$ for the pure MgO(001) substrate have been determined by us using the potential energy curve for a 2×2 surface supercell (Fig. 4) since the latter is used in further periodic simulation on the copper-magnesia interface. In this case a lattice constant has been found to be slightly smaller than in previous calculations for the bulk unit cell and the surface UC (4.19-4.21 Å [23,37,47,48]). We find $a_{\text{MgO}}^{(0)}$ values to vary in the range 4.09-4.15 Å when using various electron correlation functionals and slab models (three and five (001) layers). One reason for the difference can come from the surface stress, which, like the surface tension of a liquid, tends to reduce the interatomic spacing. This effect can be confirmed by the systematic differences of about 0.02 Å between three-layer and five-layer systems (in the latter case the lattice constant is larger). In any case, we have chosen the value of $a_{\text{MgO}}^{(0)}$ (4.11 Å) optimized for three-layer MgO(001) slab using the PWGGA electron correlation correction (Fig. 4) for further *a posteriori* HF-CC calculations of the copper-magnesia interface. As to the substrate binding energy *per* MgO formula unit (15.87 eV), this is quite close to the corresponding experimental value for the bulk magnesia 10.45 eV [48]. Obviously, for 3D and 2D crystalline systems the binding energies per the same structural unit could differ. Taking into account that the energy of atomization for bulk Cu is about 8 eV (PWGGA *a posteriori* correlation), one can conclude that it would be quite close to ΔE_{tot} per MgO unit in MgO(001) substrate if both estimates were done per “averaged” atom.

5. Simulation on the Cu/MgO(001) interface

5.1. COMPLETE 1 ML SUBSTRATE COVERAGE

There is difference in adsorption nature of both complete and partial copper coverages (Figs. 5,6 and Table 2). Copper monolayer model gives a clear the energetic preference for Cu adsorption over the surface O^{2-} ions (0.24 eV versus 0.16 eV for Cu positions over surface Mg^{2+}). This is in agreement with both previous theoretical simulations on the Cu/MgO(001) interface [6,13-17] and our results for the Ag/MgO(001) interface [23,24]. Theoretical data systematized by Lopez *et al.* [15] show a wide range of E_{adh} values (0.2-1.5 eV *per* copper atom) for Cu adhesion over *O* sites on magnesia substrate obtained using different models and computational methods. However, our current data do not provide so marked preference for the *O* adsorption sites as in the most of cited studies, moreover, the $z_{\text{Cu-O}}^{(0)}$ distances are noticeably overestimated while values of $z_{\text{Cu-Mg}}^{(0)}$ may be considered as underestimated (Table 2). The same comparative analysis [15] reveals a rather narrow interval of the interfacial distances, $z_{\text{Cu-O}}$ (1.85-2.15 Å); therefore, our estimate (2.4 Å) is evidently above it.

TABLE 2. Parameters of the Cu/MgO(001) interface as calculated using HF-CC method (PWGGA correlation corrections) and their comparison with previous results

Cu atom over	Substrate coverage (our and previous calculations)		Interface distance $z_{\text{Cu}}^{(0)}$, Å (Fig. 2)	Adhesion energy $E_{\text{adh}}^{\text{a}}$, eV	Charge transfer $\Delta q_{\text{Cu}}^{\text{b}}$, e
O^{2-} ion	1/4	our data	2.48	0.22	-0.005
	ML	Li <i>et al.</i> [14] ^c	1.9	1.4	0.03
	1	our data	2.40	0.24	-0.009
	ML	Benedek <i>et al.</i> [6] ^d	2.0	1.0	-0.08
Mg^{2+} ion	1/4	our data	2.35	0.62	-0.014
	ML	Li <i>et al.</i> [14] ^c	2.5	0.5	–
	1	our data	2.69	0.16	-0.005
	ML	Benedek <i>et al.</i> [6] ^d	3.20	0.2	-0.06

^a Value of adhesion energy is given *per* Cu atom.

^b A positive sign means excess of the electron density as compared to a neutral atom.

^c Single Cu atom over finite cluster model of MgO(001) was calculated using DFT method (LSD exchange and correlation functionals)

^d DFT (LSD) method was applied to calculate periodic slab model of the Cu/MgO(001) interface with monolayer substrate coverage.

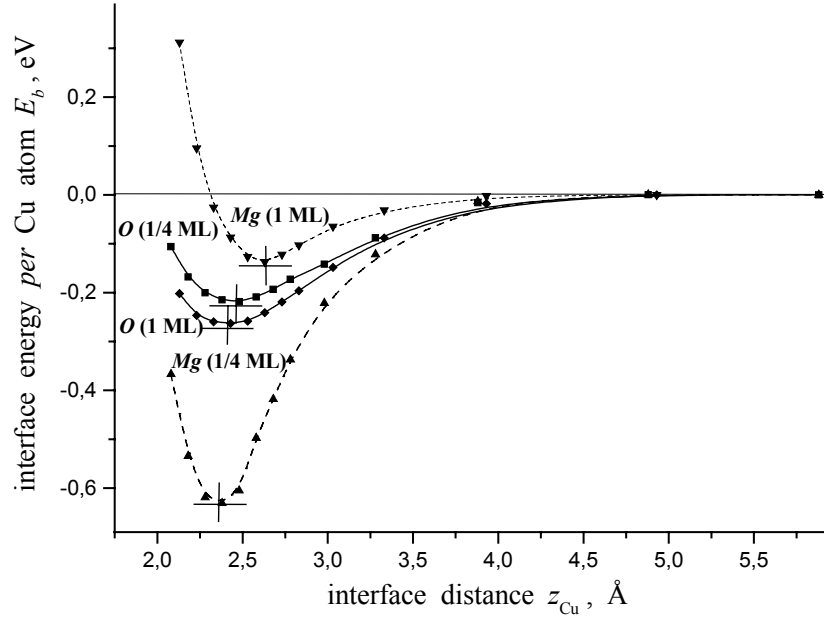


Figure 5. Interfacial energy $E_b(z_{\text{Cu}})$ as a function of the interfacial distance z_{Cu} for the two different adsorption sites Mg and O (Fig. 2) and two different Cu coverages (1/4 ML and 1 ML) on the $MgO(001)$ substrate. PWGGA electron correlation correction has been used to obtain energy values for potential curves. Full lines were drawn using the standard B-spline option.

Our calculations confirm another conclusion of previous studies: negligible chemical bonding across the interface, between copper and magnesia substrate. Thus, the adhesion is physical in its origin. The calculated Mulliken charges on Cu atoms indicate a negligible charge transfer from metal atoms to substrate (Table 2). This agrees with results of periodic simulations [6], whereas finite cluster calculations usually predict a small transfer of electronic charge to copper atom [14]. The electron bond populations across the interface (between metal atoms and substrate ions) are also practically zero. On the other hand, there is a charge redistribution *within* the metal. We have observed a noticeable bond population between nearest Cu atoms ($0.075 e$ per atom) within the metal planes parallel to the interface, which is not sensitive to the adsorption site. This value of bond population is smaller as compared to $Ag/MgO(001)$ interface ($0.1 e$ [23]), which could be caused by a just strained state of Cu monolayer on magnesia substrate mentioned above, lattice constants of silver and magnesia almost coincide. Nevertheless, even such a strained copper monolayer displays a conducting behavior, which is important for microelectronic applications. The Mulliken population analysis gives a reason for Cu adsorption over O^{2-} ions to be favored. This preference comes from the electrostatic *attraction* between the enhanced Cu electron density, concentrated around the hollow position of the copper monolayer, and the substrate Mg^{2+} ion below it (Figure 6b). On the other hand, for the Cu adsorption over the Mg^{2+} ions, there is a *repulsion* between this interatomic electron density and the substrate O^{2-} ion below it. The corresponding difference electron density plots (Figures 6b and 6d for copper adhesion over O and Mg sites, respectively) clearly confirm this effect.

5.2. PARTIAL 1/4 ML SUBSTRATE COVERAGE

In the case of low substrate coverage by metal atoms, there is practically no interatomic electron density concentration between Cu atoms, and therefore its attraction or repulsion with the nearest substrate ion plays no longer any role. For separated Cu adsorption over O^{2-} or Mg^{2+} ions, there is a single nearest substrate neighbor (either O^{2-} or Mg^{2+} ion) and four next-nearest substrate ions of the opposite type (either Mg^{2+} or O^{2-} sites). However, our data for the low substrate coverage by copper are rather unexpected (Figure 5 and Table 2): adsorption energies for isolated Cu atoms are almost three-fold larger for positions over Mg sites than over O^{2-} ions, whereas difference $z_{\text{Cu-O}}^{(0)} - z_{\text{Cu-Mg}}^{(0)} = 0.13 \text{ \AA}$ is quite surprising result as well. This

difference may be partly explained by a definite compensation of electrostatic attraction and repulsion of polarized and slightly charged Cu adatoms with surrounding surface ions in the case of 1/4 ML coverage. It may be suggested that the effect of four surrounding O^{2-} ions is much more essential than that from the oxygen ion below.

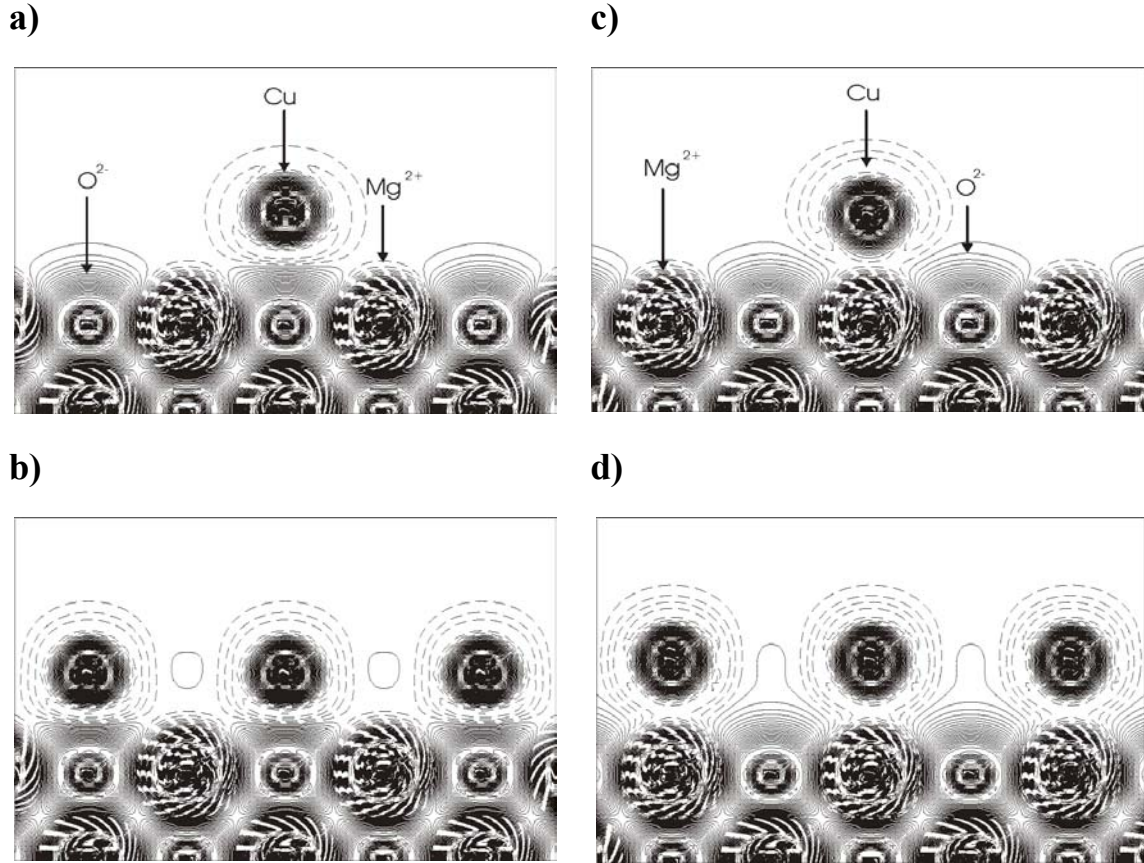


Figure 6. Difference electron density plots $\Delta\rho(r)$ (see explanation in subsection 2.3) for the cross sections shown in Figure 2. (a) and (c) correspond to a 1/4 ML substrate coverage by copper atoms over O and Mg adsorption sites, respectively, whereas (b) and (d) show electron re-distribution in the interface between the copper monolayer and magnesia substrate for the same O and Mg adsorption sites. Isodensity curves are drawn from -1.0 to $+1.0 e \text{ au}^{-3}$ with an increment of $0.0022 e \text{ au}^{-3}$ for atomic difference.

The charge transfer from the isolated copper atom to the substrate is also almost twice as large for Cu positions over Mg sites ($0.09 e$ versus $0.05 e$). A comparative analysis of the difference electron distribution plots (Figs. 6a and 6c) may clearly illustrate these bonding peculiarities of Cu atom adsorbed over surface oxygen and magnesium ions. Their comparison indicates that Cu atoms are more disturbed when sitting atop nearest and interacting with next-nearest O^{2-} ions than to magnesium ions, while electronic shells of Mg^{2+} ions are not affected too much from deposited copper atoms. Meanwhile, a participation of the subsurface substrate ions in interfacial bonding is quite negligible. Thus, the difference electron charge distributions shown in Fig. 6 give the most convincing argument in favor of a decisive role of the interaction between Cu atoms and surface O^{2-} ions in the mechanism of copper adhesion on the magnesia interfaces. Nevertheless, we suppose that the ratio of ≈ 2.8 between the adsorption energies, which favors Cu atom localization atop Mg sites to be rather incorrect. Since we have checked the main configurations of the Cu/MgO(001) interface using extended BS for bulk magnesia [48] and obtained results which qualitatively agree with those we discuss in this paper, the only reasonable explanation of this artifact may be an incompleteness of the copper BS [38]. Thus, our nearest task is the BS further modification, in order to achieve more adequate simulation of the Cu/MgO(001) interface.

6. Conclusions

One general conclusion to be drawn from the *ab initio* Hartree-Fock calculations with correlation corrections is that there is no chemical bonding on the Cu/MgO(001) perfect interface. Contrary, physical adhesion associated with polarization and charge redistribution turns out to be the dominant effect. For copper monolayer, the adhesion energy is enhanced by the interaction of the substrate ions with the additional electron density accumulated near by the interatomic positions of the interfacial Ag layer. This favors copper atoms position above the surface O^{2-} ions on the (001) substrate, similarly to the Ag/MgO(001) case [23,24].

Acknowledgements

This study was partly supported by European Centre of Excellence for Advanced Materials Research and Technology (contract No ICA1-CT-2000-7007). The authors kindly thank K. Doll (Institut für Mathematische Physik, TU Braunschweig, Germany) for the supplying us with basis set of Cu and the manuscript of his paper on CRYSTAL simulations of copper and its chemical activity. The authors appreciate discussions with S. Dorfman (Technion-Israel Institute of Technology, Haifa, Israel), F. Illas (Universitat de Barcelona, Spain), P.W.M. Jacobs (University of Western Ontario, London, Canada), and E.A. Kotomin (University of Latvia).

References

- [1] Murarka S.M., Verner I.V., Gitmann R.J. (2000) *Copper – Fundamental Mechanisms for Microelectronic Applications*. Wiley&Sons, New York.
- [2] Siemroth P., Schülke T. (2000) *Surf. Coat. Technol.* **133-134**, 106.
- [3] Mewes T., Rickart M., Mougín A., Demokritov S.O., Fassbender J., Hillebrands B., Scheib M. (2001) *Surf. Sci.* **481**, 87.
- [4] Noguera C. (1996) *Physics and Chemistry at Oxide Surfaces*. Cambridge University Press, New York.
- [5] Finnis M.W. (1996) *J. Phys.: Cond. Matter* **8**, 5811.
- [6] Benedek R., Minkoff M., Yang L.H. (1996) *Phys. Rev. B* **54**, 7697.
- [7] Lu P., Cosandey F. (1993) *Ultramicrosc.* **40**, 271.
- [8] Shashkov D.A., Seidman D.N. (1995) *Phys. Rev. Letters* **75**, 268.
- [9] Groen H.B., Kooi B.J., Vellinga W.P., De Hosson J.Th.M. (1999) *Phil. Mag. A* **79**, 2083.
- [10] Muller D.A., Shashkov D.A., Benedek R., Yang L.H., Silcox J., Seidman D.N. (1998) *Phys. Rev. Letters* **80**, 4741.
- [11] Imhoff D., Laurent S., Colliex C., Backhaus-Ricoult M. (1999) *J. Eur. Phys.* **5**, 9.
- [12] He J.-W., Møller P.J. (1987) *Surf. Sci.* **180**, 411; Alstrup I., Møller P.J. (1988) *Appl. Surf. Sci.* **33/34**, 143.
- [13] Bacalis N.C., Kunz A.B. (1985) *Phys. Rev. B* **32**, 4857.
- [14] Li Y., Langreth D.C., Pederson M.R. (1995) *Phys. Rev. B* **52**, 6067.
- [15] Pacchioni G., Rösch N. (1996) *J. Chem. Phys.* **104**, 7329; Lopez N., Illas F., Rösch N., Pacchioni G. (1999) *ibid.* **110**, 4873.
- [16] Musolino V., Selloni A., Car R. (1998) *J. Chem. Phys.* **108**, 5044; (1999) *Phys. Rev. Letters* **83**, 3242.
- [17] Matveev A.V., Neyman K.M., Yudanov I.V., Rösch N. (1999) *Surf. Sci.* **426**, 123.
- [18] Geudtner G., Jug K., Köster A.M. (2000) *Surf. Sci.* **467**, 98.
- [19] Benedek R., Seidman D.N., Minkoff M., Yang L.H., Alavi A. (1999) *Phys. Rev. B* **60**, 16094.
- [20] Schönberger U., Andersen O.K., Methfessel M. (1992) *Acta Metal. Mater.* **B 40**, S1.
- [21] Li C., Wu R., Freeman A.J., Wu C.L. (1993) *Phys. Rev. B* **48**, 8317.
- [22] Smith J.R., Hong T., Srolovitz D.J. (1994) *Phys. Rev. Letters*, **72**, 4021; Hong T., Smith J.R., Srolovitz D.J. (1994) *J. Adhes. Sci. Technol.* **8**, 837.
- [23] Heifets E., Zhukovskii Yu.F., Kotomin E.A., Causá M. (1998) *Chem. Phys. Letters* **283**, 395; Zhukovskii Yu.F., Kotomin E.A., Jacobs P.W.M., Stoneham A.M., Harding J.H. (1999) *Surf. Sci.*, **441**, 373.
- [24] Zhukovskii Yu.F., Kotomin E.A., Jacobs P.W.M., Stoneham A.M. (2000) *Phys. Rev. Letters* **84**, 1256; Zhukovskii Yu.F., Kotomin E.A., Jacobs P.W.M., Stoneham A.M., Harding J.H. (2000) *J. Phys.: Cond. Matter* **12**, 55.
- [25] Fuks D., Dorfman S., Kotomin E.A., Zhukovskii Yu.F., Stoneham A.M. (2000) *Phys. Rev. Letters* **85**, 4333.

- [26] Dovesi R., Saunders V.R., Roetti C., Causá M., Harrison N.M., Orlando R., Aprá E. (1996) *CRYSTAL '95 User Manual*. Turin, University of Torino.
- [27] Kohn W., Sham L.J. (1965) *Phys. Rev.* **140A**, 1133.
- [28] Dovesi R., Orlando R., Roetti C., Pisani C., Saunders V.R. (2000) *Phys. Status Solidi b* **217**, 63.
- [29] Zhukovskii Yu.F., Sychev O., Jacobs P.W.M., Shunin Yu.N. (2000) *Computer Modelling and New Technologies* **4**, No. 2, 18.
- [30] Pisani C., Dovesi R., Roetti C. (1988) *Hartree-Fock ab initio Treatment of Crystalline Systems*. (Lecture Notes Chem, Vol. 48), Springer-Verlag, Berlin.
- [31] Frisch M.J. *et al.* (1995) *GAUSSIAN'94, Revision C.3*, Pittsburgh, Gaussian Inc.
- [32] Piskunov S., Zhukovskii Yu.F., Kotomin E.A., Shunin Yu.N. (2000) *Computer Modelling and New Technologies* **4**, No. 2, 7.
- [33] *Quantum-Mechanical ab initio Calculation of the Properties of Crystalline Materials*. (1996) Ed. Pisani C. (Lecture Notes Chem, Vol. 67), Springer-Verlag, Berlin.
- [34] Towler M.D., Zupan A., Causá M. (1996) *Comput. Phys. Commun.* **98**, 181.
- [35] Vosko S.H., Wilk L, Nusair M. (1980) *Canad. J. Phys.* **58**, 1200.
- [36] Perdew J.P., Wang Y. (1992) *Phys. Rev. B* **45**, 13244.
- [37] Causá M., Dovesi R., Pisani C., Roetti C. (1986) *Surf. Sci.* **175**, 551.
- [38] Doll K., Harrison N.M. (2000) *Chem. Phys. Letters* **317**, 282.
- [39] Wyckoff R.W.G. (1963) *Crystal Structures* (2nd ed.), Wiley-Interscience, New York: V. 1; *ibid* (1964); V. 2.
- [40] Gutekunst G., Mayer J., Rühle M. (1997) *Phil. Mag. A* **75** 1329; 1357.
- [41] Boys S.F., Bernardi F. (1970) *Mol. Phys.* **19**, 553.
- [42] Towler M.D., Dovesi R., Saunders V.R. (1995) *Phys. Rev. B* **52**, 10150.
- [43] Henre W.H., Radom L., von Schleyer P.R., Pople J.A. (1986) *Ab Initio Molecular Orbital Theory*. Wiley, New-York.
- [44] Fehrenbach C.M., Bross H. (1993) *Phys. Rev. B* **48**, 17703.
- [45] Overton W.C., Gaffney J. (1955) *Phys. Rev.* **98**, 969.
- [46] Gschneidner K.A. (1964) *Solid State Phys.* **16**, 276.
- [47] Causá M., Dovesi R., Pisani C., Roetti C. (1986) *Phys. Rev. B.* **33**, 1308.
- [48] Catti M., Valerio G., Dovesi R., Causá M. (1994) *Phys. Rev. B.* **49**, 14179.

Received on the 18th of July 2001

ELECTRONIC STRUCTURE AND RESISTIVITY OF COPPER

YU. N. SHUNIN AND K. BUDILOV

The electronic structure and resistivity calculations of are considered. The main attention is paid to the cluster approach for condensed state.

Keywords: atomic potentials, pseudopotentials, cluster approach, effective media approximation, electronic structure and resistivity of copper

“Copper is the first “new” material that is breathing life into the existing well-established silicon realm”.

*Aart de Gues, Chairman and CEO ,
 Synopsys Inc. as quoted in EE Times*

1. Introduction

Copper is a very popular material nowadays. The rapid development of electronics, telecommunications and other high-technological industries lead to the “copper” boom. Copper possesses the highest electrical conductivity of all commonly found metals on earth. This property of copper when added to its inherent strength, formability and corrosion resistance make it and its alloys unique in their usefulness as conductors of electricity.

A basic understanding of the properties of copper and copper alloys can be very useful for the modern electronics. Both physical and mechanical properties play an important role in the selection of an appropriate alloy and its subsequent processing, stamping, drawing, etc.

In 1997, fulfilling a dream of several decades, IBM introduced a technology that allows chip-makers to use copper wires, rather than the traditional aluminium interconnects, to link transistors in chips. This advance gives IBM a significant lead in the race to create the next generation of semiconductors. Every chip has a base layer of transistors, with layers of wiring stacked above to connect the transistors to each other and, ultimately, to the rest of the computer. The transistors at the first level of a chip are a complex construction of silicon, metal, and impurities precisely located to create the millions of minuscule on-or-off switches that make up the brains of a microprocessor. Breakthroughs in chip technology have most often been advances in transistor-making. As scientists kept making smaller, faster transistors and packing them closer together, the interconnect started to present problems. In the semiconductor industry, bigger isn't always better. In fact, the phrase "smaller, faster, and cheaper" is more applicable to computer technology. Aluminium has long been the conductor of choice, but it will soon reach the technological and physical limits of existing technology. Pushing electrons through smaller and smaller conduits becomes harder to do - aluminium just isn't fast enough at these new, smaller sizes. Scientists had seen this problem coming for years and tried to find a way to replace aluminium with one of the three metals that conduct electricity better: copper, silver, or gold. Of course, if that were simple, it would have been done a long time ago. None of those metals is as easy to work with as aluminium in ever-decreasing amounts. Any new material presents fresh challenges, and reliably filling sub-micron holes and channels is a bit like filling the holes of a golf course from an air-plane. What's worse, those metals interact badly with silicon, soaking into it and altering its electrical properties. Not by much, but even a few stray atoms are enough to short-circuit the chip. IBM had to develop a diffusion barrier that could be deposited in silicon wafers along with the copper. By the late 1980s, IBM researchers found one metal that did the trick, paving the way to the breakthrough announced in 1997. Some expert assume that “*Copper in on its way toward becoming the golden metal of the Silicon Age*”.

The following uses for copper are gathered from a several sources as well as from anecdotal comments:

- wire
- coinage metal

- copper compounds such as Fehling's solution are widely used in analytical chemistry in tests for sugar
- the electrical industry is one of the largest users of copper
- copper sulphate is used as an agricultural poison, and water purifier

Additional info about copper usage can be found in electrical industry branch *Appendix*.

The main goals of this work are:

- methods of the electronic structure calculation;
- copper and its electronic properties in the framework of “*liquid metal*” model;
- the strategy of pseudopotential calculation, without using the self-consistent procedure and studied pseudopotentials for copper as main research object;
- the density of electronic states (DOS) for the single scatterer in vacuum, specific resistance for copper and simulated its disorder dependence on the base of calculated pseudopotentials. Started the study of DOS for scatterer in medium for future works as a priority task.

General, atomic and crystallographic Properties and Features of Copper. overview see in Appendix

2. Electronic structure calculation methods overview

In this section we describe the methods, which are now successfully used for electronic structure calculations, discuss some results, define their advantages and limitations.

2.1. GENERAL

The formulation and development of quantum theory in the first half of the 20th century has led to a revolution in our understanding of fundamental physics. Quantum theory has demonstrated a surprising accuracy and predictive power, and the importance of quantum theory in the pure and applied sciences in virtually unchallenged.

The relevant equations to be solved are clearly the equations of quantum mechanics, if we are to attempt to model real processes and real materials. Unfortunately, Schrödinger's equation, the most fundamental equation of wave function based quantum mechanics, cannot be solved analytically for all but the most trivial of systems, most of which are not relevant to the world at large.

Electronic structure calculations - numerical solutions of Schrödinger's equation for a specific system - are distinct from other forms of modelling because they are first-principles in nature. That is, except through the choice of the researcher, the calculations contain no external parameters other than a most basic description of the system. Calculations of this nature enable the speculative study of systems, potentially without reference to experiment. Where a given physical property is physically inaccessible - such as the binding energy of an atom or molecule deeply embedded in a complex host - the availability of reliable qualitative data is a powerful stimulus.

However, the numerical solution of Schrödinger's equation remains a difficult task. Exact solutions of the equation are, in general, only solvable in times scaling exponentially with system size. This scaling precludes exact calculations for all but the smallest and simplest of systems. Approximations may be introduced to reduce the equations to a form that can be solved in polynomial time, but at the penalty of losing some degree of accuracy and predictive power. The treatment of electron-electron interactions is the principle source of difficulty: the physical and chemical properties of a system depend principally on the interaction of the electrons with each other and with the atomic cores. These interactions cannot easily be separated out or treated without approximation.

The most successful electronic structure methods in current use, those of density functional theory and quantum chemistry, have been applied to a wide range of systems relevant to the real world. In practice, the density functional and quantum chemical approaches involve approximations for the electron-electron interactions, limiting the achievable accuracy.

In this work, stochastic methods for the solution of Schrödinger's equation are developed and applied to real systems. Quantum Monte-Carlo (QMC) methods treat electron-electron interactions almost without approximation and with a computational cost scaling cubically with system size. Their accuracy enables an unprecedented degree of confidence to be placed in the results obtained. A number of technical developments are made in the earlier chapters of the thesis, prior to two significant applications: the computation of the one-body density matrix of silicon and several related quantities, and a study of the energetic stability of a series of carbon clusters. The use of Quantum Monte-Carlo methods was essential

in both of these applications, particularly in the study of carbon clusters where no other currently applicable computational method is sufficiently accurate.

2.2. CALCULATION METHODS

Quantum Monte Carlo techniques provide a direct and potentially efficient means for solving the many-body Schrödinger equation of quantum mechanics. Finding accurate solutions of this equation is one of the central problems in physics and chemistry.

The simplest Quantum Monte Carlo technique, variational Monte Carlo (VMC), is based on a direct application of Monte Carlo integration to the calculation of multi-dimensional integrals of expectation values such as the total energy. Monte Carlo methods are statistical and a key result is that the value of integrals computed using Monte Carlo converges faster than by using conventional methods of numerical quadrature, once the problem involves more than a few dimensions. Statistical methods therefore provide a practical means of solving the full many-body Schrödinger equation by direct integration, making only limited and well-controlled approximations.

Comparisons are made with several well-developed approaches for solving the many-body Schrödinger equation in this chapter. Numerous quantum chemical methods and density functional approaches have been developed for solving the "electronic structure problem". A review of several methods currently in general use is given along with an outline of their relative advantages and shortcomings.

2.2.1. The Hamiltonian.

The time independent Schrödinger equation for a system of N particles interacting via the Coulomb interaction is

$$\hat{H}\Psi = E\Psi, \quad (2.1)$$

where

$$\hat{H} = \sum^N \left(-\frac{\hbar^2}{2m} \nabla_i^2 \right) + \frac{1}{2} \sum_{i=1}^N \sum_{j \neq i}^N \left(\frac{1}{4\pi\epsilon_0} \frac{Z_i Z_j}{|\mathbf{r}_i - \mathbf{r}_j|} \right) \quad (2.2)$$

and Ψ is an N-body wave function, \mathbf{r} denotes spatial positions and Z is the charge number of the atom. E denotes the energy of either the ground or an excited state of the system.

Most physical problems of interest consist of a number of interacting electrons and ions. The total number of particles, N, is usually sufficiently large that an exact solution cannot be found. Controlled and well understood approximations are sought to reduce the complexity to a tractable level. Once the equations are solved, a large number of properties may be calculated from the wave function. Errors or approximations made in obtaining the wave function will be manifest in any property derived from the wave function. Where high accuracy is required, considerable attention must be paid to the derivation of the wave function and any approximations made.

2.2.2. The Born-Oppenheimer approximation.

A reasonable approach used in the solution of equation (2.1) is the Born-Oppenheimer approximation. In a system of interacting electrons and nuclei there will usually be little momentum transfer between the two types of particles due to their greatly differing masses. The forces between the particles are of similar magnitude due to their similar charge. If one then assumes that the momentum of the particles are also similar, then the nuclei must have much smaller velocities than the electrons due to their far greater mass. On the time-scale of nuclear motion, one can therefore consider the electrons to relax to a ground-state given by the Hamiltonian (2.2) with the nuclei at fixed locations. This separation of the electronic and nuclear degrees of freedom is known as the Born-Oppenheimer approximation.

It is important to note that this approximation does not limit the techniques described to systems of fixed ions: in principle, once the electronic configuration is known, the nuclear degrees of freedom could also be solved for, giving rise to nuclear motion.

The many-body Hamiltonian, (see, equation (2.2)) , is expressed in form:

$$\hat{H} = \sum_i \left(-\frac{1}{2} \nabla_i^2 \right) + \sum_i \sum_\alpha \left(\frac{Z_\alpha}{|\mathbf{r}_i - \mathbf{d}_\alpha|} \right) + \frac{1}{2} \sum_i \sum_{j \neq i} \left(\frac{1}{|\mathbf{r}_i - \mathbf{r}_j|} \right) + \frac{1}{2} \sum_\alpha \sum_{\beta \neq \alpha} \left(\frac{Z_\alpha Z_\beta}{|\mathbf{d}_\alpha - \mathbf{d}_\beta|} \right), \quad (2.3)$$

where \mathbf{r}_i and \mathbf{d}_α are positions of electrons and ions with the charge Z_α , $e = m_e = 2\pi\hbar = 4\pi\epsilon_0 = 1$ (this means atomic units). The simplified Hamiltonian remains very difficult to solve and no analytic solutions exist for general systems with more than one electron.

2.2.3. The Hartree Fock theory.

Hartree-Fock theory is one the simplest approximate theories for solving the many-body Hamiltonian. It is based on a simple approximation to the true many-body wave function: that the wave function is given by a single Slater determinant of N spin-orbitals:

$$\Psi = \begin{vmatrix} \psi_1(\mathbf{x}_1) & \psi_1(\mathbf{x}_2) & \dots & \psi_1(\mathbf{x}_N) \\ \psi_2(\mathbf{x}_1) & \psi_2(\mathbf{x}_2) & \dots & \psi_2(\mathbf{x}_N) \\ \dots & \dots & \dots & \dots \\ \psi_N(\mathbf{x}_1) & \psi_N(\mathbf{x}_2) & \dots & \psi_N(\mathbf{x}_N) \end{vmatrix}, \quad (2.4)$$

where the variables \mathbf{x} include the coordinates of space and spins.

This wave function may be inserted into the Hamiltonian, equation (2.3), and an expression for the total energy derived. Applying the theorem that the value of a determinant is unchanged by any non-singular linear transformation, we may choose the ψ to be an orthonormal set. We now introduce a Lagrange multiplier ϵ_i to impose the condition that the ψ are normalised, and minimise with respect to the ψ :

$$\frac{\delta}{\delta \Psi} \left[\langle \hat{H} \rangle - \sum_j \epsilon_j \int |\psi_j|^2 d\mathbf{r} \right] \quad (2.5)$$

In the one-electron approximation equations we obtain:

$$-\frac{1}{2} \nabla^2 \psi_i(\mathbf{r}) + V_{\text{ion}}(\mathbf{r}) \psi_i(\mathbf{r}) + U(\mathbf{r}) \psi_i(\mathbf{r}) = \epsilon_i \psi_i(\mathbf{r}), \quad (2.6)$$

where $U(\mathbf{r})$ is a non-local potential and the local ionic potential is denoted by V_{ion} . The one-electron equations resemble single-particle Schrödinger equations. The total Hartree-Fock equations are given by:

$$\epsilon_i \psi_i(\mathbf{r}) = \left(-\frac{1}{2} \nabla^2 + V_{\text{ion}}(\mathbf{r}) \right) \psi_i(\mathbf{r}) + \sum_j \int d\mathbf{r}' \frac{|\psi_j(\mathbf{r}')|^2}{|\mathbf{r} - \mathbf{r}'|} \psi_i(\mathbf{r}) - \sum_j \delta_{\sigma_i \sigma_j} \int d\mathbf{r}' \frac{\psi_j^*(\mathbf{r}') \psi_i(\mathbf{r}')}{|\mathbf{r} - \mathbf{r}'|} \psi_j(\mathbf{r}) \quad (2.7)$$

The right side of the equations consists of four terms. The first and second give rise are the kinetic energy contribution and the electron-ion potential. The third term, or Hartree term, is the simply electrostatic potential arising from the charge distribution of N electrons. As written, the term includes an unphysical self-interaction of electrons when $\mathbf{j}=\mathbf{i}$. This term is cancelled in the fourth, or exchange term. The exchange term takes into account the Pauli principle and the determinantal form of the wave function. The effect of exchange is for electrons of like-spin to avoid each other. Each electron of a given spin is consequently surrounded by an "exchange hole", a small volume around the electron which like-spin electron avoid.

The Hartree-Fock approximation corresponds to the conventional single-electron picture of electronic structure: the distribution of the N electrons is given simply by the sum of one-electron distributions $|\psi|^2$. This allows concepts such as labelling of electrons by angular momentum ("a 3d-electron in a transition metal"), but it must be remembered that this is an artefact of the initial ansatz and that in some systems modifications are required to these ideas.

Hartree-Fock theory, by assuming a single-determinant form for the wave function, neglects correlation between electrons. The electrons are subject to an *average* non-local potential arising from the other electrons, which can lead to a poor description of the electronic structure. Although qualitatively correct in many materials and compounds, Hartree-Fock theory is insufficiently accurate to make accurate quantitative predictions.

2.2.4. Basis set expansions.

In the preceding section, the single-particle Hartree-Fock equations were presented (equation (2.7)). Numerical solutions usually are found by expanding the orbitals in a basis set:

$$\Psi_i = \sum_k^M c_{ik} \phi_k \quad (2.8)$$

The unknown Hartree-Fock orbitals, ψ , are written as a linear expansion in M known basis functions ϕ . Inserting equation (2.8) into equation (2.7) leads to a set of matrix equations for the expansion coefficients, c_{ik} . The problem of solving the Hartree-Fock equations is reduced to a linear algebra problem, which may be solved by techniques such as iterative diagonalisation.

In practice, a basis of plane waves in periodic systems or localised Gaussians in finite systems, is commonly used. The basis set expansion represents an additional limitation of the techniques: unless the basis set expansion has sufficient freedom to encompass the exact solutions for the Hartree-Fock orbitals, ϕ , a compromise solution with a higher Hartree-Fock energy will be found. In practical applications, convergence of the basis set must be studied to verify that the expansion is sufficiently complete.

2.2.5. Post Hartree-Fock techniques.

Going beyond the ansatz of a single-determinant wave function may reduce the limitations of the Hartree-Fock method. There are two broad categories of such approaches: those based on perturbation theory and those based on the variational principle. Among the latter approaches is the configuration interaction method which will be covered here because the focus of this thesis is on obtaining accurate many-body wave functions.

Configuration interaction. Configuration interaction (CI) methods are one of the conceptually simplest methods for solving the many-body Hamiltonian. Although theoretically elegant, in principle exact, and relatively simple to implement, in practice *full* CI can be applied to only the smallest of systems. The basis for CI methods is the simple observation that an *exact* many-body wave function, Ψ , may be written as a linear combination of Slater determinants, \mathbf{D}_k ,

$$\Psi = \sum_{k=0}^{\infty} c_k \mathbf{D}_k, \quad (2.9)$$

where the \mathbf{D}_k fully span the Hilbert space of the wave function. The determinants can be any complete set of N -electron anti-symmetric functions but are typically constructed from Hartree-Fock orbitals such that \mathbf{D}_0 is the ground-state Hartree-Fock determinant.

The Hartree-Fock “reference determinant” \mathbf{D}_0 is by definition the best single-determinant approximation to the exact wave function Ψ . In most electronic systems, the Hartree-Fock energy accounts for the majority of the exact total energy, and the missing correlation energy is small. If the coefficients c_k are normalised then typically $c_0=1$ and all remaining c_k are very small. A very large number of configurations is required to yield energies and wave functions approaching the exact many-body wave function. In practice the expansion must be limited on physical grounds, as the total number of determinants is:

$$k_{\max} = \frac{M!}{N!(M-N)!}, \quad (2.10)$$

where the length of the expansion k_{\max} is given in terms of the number of electrons, N , and the number of basis states, M , in the expansion ($M \gg N$).

The scientific problem in adapting the CI method into a practical one is to obtain the best wave function, and hence lowest CI energy, with the shortest expansion length. A typical approach would be to truncate the expansion after only double or quadruple excitations from the reference determinant, where an excitation consists of replacing a ground state occupied orbital by an unoccupied one. These levels of truncation are the CI singles-doubles (CISD) and CI singles-doubles-triples-quadruples (CISDTQ) methods. A formidable number of terms are still left in the expansion. Accurate applications of the methods are consequently limited due to their computational cost.

When performed within a finite reference space, an additional problem with the method becomes apparent: the methods lack “size-extensivity” and do not perform equally well in systems of differing size. As the size of system increases, the proportion of the electronic correlation energy contained within a fixed reference space (such as all single and double excitations) decreases. The lack of size-extensivity results in a non-cancellation of errors when systems of different sizes are compared, resulting in difficulties when interaction or bonding energies are required. Despite these limitations, CI represents a controlled (and variational) improvement to the ground-state wave function, and may therefore be used in the determinantal parts of trial wave functions in QMC.

2.2.6. Other methods.

The lack of size extensivity and substantial cost of the CI method has led to the development of several related methods. The coupled-cluster (CC) method is one of the most important practical advances over the CI method. Although non-variational, it resolves the problem of size extensivity, and is often very accurate, but more expensive than (limited) CI. The CC method assumes an exponential ansatz for the wave function

$$\Psi_{\text{CC}} = \exp(\hat{T})\Psi_{\text{HF}} , \quad (2.11)$$

where the coupled-cluster wave function is given by an excitation operator acting on a reference wave function, usually the Hartree-Fock determinant $\Psi_{\text{HF}}=D_0$. The operator \hat{T} is generates k -fold excitations from a reference state:

$$\hat{T} = \sum_k \hat{T}_k , \quad (2.12)$$

so that, for example,

$$\hat{T}_2 \Psi_{\text{HF}} = \sum_{ij} t_{ij}^{ab} D_{ij}^{ab} . \quad (2.13)$$

The operator \mathbf{T}_2 generates excitations from pairs of occupied states, \mathbf{ij} , to pairs of virtual states, \mathbf{ab} , from a reference Hartree-Fock determinant \mathbf{D} . The expansion coefficients t_{ij}^{ab} are determined self-consistently. A “coupled-cluster doubles” wave function is written as :

$$\Psi_{\text{CCD}} = \exp(\hat{T}_2)\Psi_{\text{HF}} \quad (2.14)$$

$$\Psi_{\text{CCD}} = D_0 + \sum_{ij} t_{ij}^{ab} D_{ij}^{ab} + \frac{1}{2} \sum_{ij} \sum_{kl} t_{ij}^{ab} t_{kl}^{cd} D_{ijkl}^{abcd} + \dots \quad (2.15)$$

The CC expansion is usually terminated after all double excitations or all quadruple excitations have been included. It may be shown that this expansion is size consistent. By including many excitation terms in the expansion, CC methods are computationally very expensive relative to HF calculations. Formally, CC singles-doubles scales as the sixth power of the number of basis states included in the expansion, and calculations including up to quadruple excitations scale as the tenth power of the number of states. The key limitation of the CC methods are their rapid increase in computational cost with system size. This presently limits the methods to small molecular systems.

Limitations. Hartree-Fock is a simple theory which satisfies the commonly known features of fermion wave functions. The theory generates wave functions that are anti-symmetric with respect to the exchange of two electron positions and includes exchange between like-spin electrons. The cost of a Hartree-Fock calculation formally scales with the cube of the number of basis functions, but depending on implementation the scaling can be between linear and quadratic with system size. It is insufficiently accurate for quantitative predictions of the properties of many compounds. By neglecting electron correlation, interaction energies are typically very poor. A Hartree-Fock wave function is a well-controlled approximation to the many-body wave function, and for this reason Hartree-Fock continues to be widely used: it is often *predictably* accurate or inaccurate, and therefore useful for determining qualitative information such as trends in a structural parameter with system size.

Almost all post Hartree-Fock methods share the combined limitations of a poor scaling with system size and a strong basis set dependence. In practice, post Hartree-Fock methods typically scale with the fourth or higher power of the number of basis states included in the calculation, limiting their application to small systems. The basis states depend on the underlying basis set used in their numeric expansion, equation (2.8), and it is commonly found that use of improved methods requires an improved basis set, further increasing the cost of calculation. CI and CC-based methods effectively transform the electron-correlation problem into a basis set problem, where the basis set is the set of molecular orbitals derived from a Hartree-Fock (or similar) calculation.

Density functional theory. Density functional theory (DFT) is a powerful, formally exact theory. It is distinct from quantum chemical methods in that it is a non-interacting theory and does not yield a correlated N-body wave function. In the Kohn-Sham DFT, the theory is a one-electron theory and shares many similarities with Hartree-Fock. DFT has come to prominence over the last decade as a method *potentially* capable of very accurate results at low cost. In practice, approximations are required to implement the theory, and a significantly variable accuracy results. Calibration studies are therefore required to establish the likely accuracy in a given class of systems.

2.2.7. The Hohenberg-Kohn theorem.

The Hohenberg-Kohn theorem states that if N interacting electrons move in an external potential $V_{\text{ext}}(\mathbf{r})$, the ground-state electron density $n_0(\mathbf{r})$ minimises the functional

$$E[n] = F[n] + \int n(\mathbf{r})V_{\text{ext}}(\mathbf{r})d\mathbf{r} , \quad (2.16)$$

where $F[n]$ is a universal functional of n and the minimum value of the functional E is E_0 the exact ground-state electronic energy.

The proof of equation (2.16) is straightforward. It is a proof only of existence; additional theory is required before a method can be implemented. Levy gave a particularly simple proof of the Hohenberg-Kohn theorem which is as follows:

A functional O is defined as

$$O[n(\mathbf{r})] = \lim_{|\Psi\rangle \rightarrow n(\mathbf{r})} \langle \Psi | \hat{O} | \Psi \rangle , \quad (2.17)$$

where the expectation value is found by searching over all wave functions, Ψ , giving the density $n(\mathbf{r})$ and selecting the wave function which minimises the expectation value of \hat{O} . $F[n(\mathbf{r})]$ is defined by

$$F[n(\mathbf{r})] = \lim_{|\Psi\rangle \rightarrow n(\mathbf{r})} \langle \Psi | \hat{F} | \Psi \rangle , \quad (2.18)$$

so that $\langle \Psi | \hat{F} | \Psi \rangle$, then from the definition of the functional E :

$$E[n] = F[n] + \int n(\mathbf{r})V_{\text{ext}}(\mathbf{r})d\mathbf{r} = \langle \Psi | \hat{F} + V_{\text{ext}} | \Psi \rangle . \quad (2.19)$$

The Hamiltonian is given by $F+V_{\text{ext}}$, and so $E[n(\mathbf{r})]$ must obey the variational principle,

$$E[n(\mathbf{r})] \geq E_0 \quad (2.20)$$

This completes the first part of the proof, which places a lower bound on $E[n(\mathbf{r})]$. From the definition of $F[n(\mathbf{r})]$ equation (2.18) we obtain:

$$F[n_0(\mathbf{r})] \leq \langle \Psi_0 | \hat{F} | \Psi_0 \rangle, \quad (2.21)$$

since Ψ_0 is a trial wave function yielding $n_0(\mathbf{r})$. Combining $\int n(\mathbf{r})V_{\text{ext}}(\mathbf{r})d\mathbf{r}$ with the above equation gives

$$E[n(\mathbf{r})] \leq E_0, \quad (2.22)$$

which in combination with equation (2.19) yields the key result

$$E[n(\mathbf{r})] = E_0, \quad (2.23)$$

completing the proof.

The Kohn-Sham equations. Kohn and Sham derived a coupled set of differential equations enabling the ground state density $n_0(\mathbf{r})$ to be found. Kohn and Sham separated $F[n(\mathbf{r})]$ into three distinct parts, so that the functional E becomes

$$E[n(\mathbf{r})] = T_s[n(\mathbf{r})] + \frac{1}{2} \iint \frac{n(\mathbf{r})n(\mathbf{r}')}{|\mathbf{r}-\mathbf{r}'|} d\mathbf{r}d\mathbf{r}' + E_{\text{XC}}[n(\mathbf{r})] + \int n(\mathbf{r})V_{\text{ext}}(\mathbf{r})d\mathbf{r}, \quad (2.24)$$

where $T_s[n(\mathbf{r})]$ is defined as the kinetic energy of a non-interacting electron gas with density $n(\mathbf{r})$,

$$T_s[n(\mathbf{r})] = -\frac{1}{2} \sum_{i=1}^N \int \psi_i^*(\mathbf{r}) \nabla^2 \psi_i(\mathbf{r}) d\mathbf{r} \quad (2.25)$$

and not the kinetic energy of the real system. Equation (1.26) also defines the exchange-correlation energy functional $E_{\text{XC}}[n]$. Introducing a normalisation constraint on the electron density, $\int n(\mathbf{r})d\mathbf{r} = N$,

we obtain $\frac{\delta}{\delta n(\mathbf{r})} [E[n(\mathbf{r})] - \mu \int n(\mathbf{r})d\mathbf{r}] = 0$, then

$$\frac{\delta E[n(\mathbf{r})]}{\delta n(\mathbf{r})} = \mu \quad (2.26)$$

Equation (1.28) may now be rewritten in terms of an effective potential, $V_{\text{eff}}(\mathbf{r})$,

$$\frac{\delta T_s[n(\mathbf{r})]}{\delta n(\mathbf{r})} + V_{\text{eff}}(\mathbf{r}) = \mu \quad (2.27)$$

where

$$V_{\text{eff}}(\mathbf{r}) = V_{\text{ext}}(\mathbf{r}) + \int \frac{n(\mathbf{r}')}{|\mathbf{r}-\mathbf{r}'|} d\mathbf{r}' + V_{\text{XC}}(\mathbf{r}) \quad (2.28)$$

and

$$V_{\text{XC}}(\mathbf{r}) = \frac{\delta E_{\text{XC}}[n(\mathbf{r})]}{\delta n(\mathbf{r})}. \quad (2.29)$$

Crucially, *non-interacting electrons* moving in an external potential $V_{\text{eff}}(\mathbf{r})$ would result in the same equation (2.28). To find the ground state energy, E_0 , and the ground state density, n_0 , the one electron Schrödinger equation :

$$\left(-\frac{1}{2}\nabla_i^2 + V_{\text{eff}}(\mathbf{r}) - \varepsilon_i\right)\psi_i(\mathbf{r}) = 0 \quad (2.30)$$

should be solved self-consistently with

$$n(\mathbf{r}) = \sum_{i=1}^N |\psi_i(\mathbf{r})|^2, \quad (2.31)$$

and equations (2.27) and (2.28). A self-consistent solution is required due to the dependence of $V_{\text{eff}}(\mathbf{r})$ on $n(\mathbf{r})$. The above equations provide a theoretically exact method for finding the ground state energy of an interacting system provided the form of E_{XC} is known. Unfortunately, the form of E_{XC} is in general unknown and its exact value has been calculated for only a few very simple systems. In electronic structure calculations E_{XC} is most commonly approximated within the local density approximation or generalised-gradient approximation.

The local density approximation. In the local density approximation (LDA), the value of $E_{\text{XC}}[n(\mathbf{r})]$ is approximated by the exchange-correlation energy of an electron in an homogeneous electron gas of the same density $n(\mathbf{r})$, i.e.

$$E_{\text{XC}}^{\text{LDA}}[n(\mathbf{r})] = \int \varepsilon_{\text{XC}}(n(\mathbf{r}))n(\mathbf{r})d\mathbf{n}(\mathbf{r}) \quad (2.32)$$

The most accurate data for $E_{\text{XC}}[n(\mathbf{r})]$ is from Quantum Monte Carlo calculations. The LDA is often surprisingly accurate and for systems with slowly varying charge densities generally gives very good results. The failings of the LDA are now well established: it has a tendency to favour more homogeneous systems and over-binds molecules and solids. In weakly bonded systems these errors are exaggerated and bond lengths are too short. In good systems where the LDA works well, often those mostly consisting of *sp* bonds, geometries are good and bond lengths and angles are accurate to within a few percent. Quantities such as the dielectric and piezoelectric constant are approximately 10% too large.

The principle advantage of LDA-DFT over methods such as Hartree-Fock is that *where the LDA works well* (correlation effects are well accounted for) many experimentally relevant physical properties can be determined to a useful level of accuracy. Difficulties arise where it is not clear whether the LDA is applicable. For example, although the LDA performs well in bulk group-IV semiconductors it is not immediately clear how well it performs at surfaces of these materials.

Limitations. Despite the remarkable success of the LDA, its limitations mean that care must be taken in its application. For systems where the density varies slowly, the LDA tends to perform well, and chemical trends are well reproduced. In strongly correlated systems where an independent particle picture breaks down, the LDA is very inaccurate. The transition metal oxides XO ($X=\text{Fe}, \text{Mn}, \text{Ni}$) are all Mott insulators, but the LDA predicts that they are either semiconductors or metals. The LDA has been applied to high T_c superconductors, but finds several to be metallic, when in reality they are insulating at 0K.

The LDA finds the wrong ground state for in many simpler cases. For example, the LDA finds the wrong ground state for the titanium atom. The LDA does not account for Van der Waals bonding, and gives a very poor description of hydrogen bonding. These phenomena are essential for most of biochemistry: the structure of DNA depends critically on hydrogen bonding, as do the changes in the structure of most molecules on solvation.

The success of the LDA has been shown by QMC calculations to result from a real-space cancellation of errors in the LDA exchange and correlation energies. This is illustrated in figure, where the exchange and correlation energy densities of silicon are compared with an accurate QMC calculation. The cancellation represents a difficulty when improvements to the LDA are attempted, as an improvement in only the exchange or correlation contributions may give worse results.

An obvious approach to improving the LDA is to include gradient corrections, by making E_{XC} a functional of the density and its gradient:

$$E_{\text{XC}}^{\text{GGA}}[n(\mathbf{r})] = \int \varepsilon_{\text{XC}}(n(\mathbf{r}))n(\mathbf{r})d\mathbf{r} + \int F_{\text{XC}}[n(\mathbf{r}), |\nabla n(\mathbf{r})|]d\mathbf{r}, \quad (2.33)$$

where F_{XC} is a correction chosen to satisfy one or several known limits for E_{XC} .

Clearly, there is no unique recipe for F_{XC} , and several dozen functionals have been proposed in the literature. They do not always represent a systematic improvement over the LDA and results must be

carefully compared against experiment. The development of improved functionals is currently a very active area of research and although incremental improvements are likely, it is far from clear whether the research will be successful in providing the substantial increase in accuracy desired.

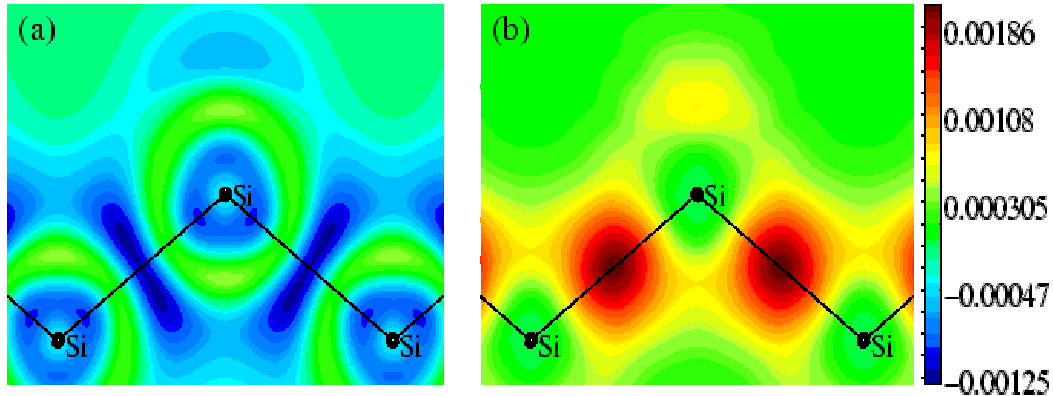


Figure 1. Contour plots of the LDA exchange and correlation energy densities compared with VMC calculations for Si in the diamond structure in the (110) plane: (a) $\epsilon_x^{\text{VMC}}(\mathbf{r}) - \epsilon_x^{\text{LDA}}(\mathbf{r})$; (b) $\epsilon_c^{\text{VMC}}(\mathbf{r}) - \epsilon_c^{\text{LDA}}(\mathbf{r})$. The chain of atoms and bonds are represented schematically. The contours are in atomic units. Note that in the bonding regions between silicon atoms, the error in the exchange energy density tends to cancel with the error in the correlation energy density. Figure courtesy R. Q. Hood.

The main problem of the Hartree-Fock and DFT methods is the underlying treatment of electron correlation. In the Hartree-Fock method, electron correlations beyond a mean field picture are entirely neglected, whereas in DFT they are included approximately via a functional $E_{\text{XC}}[n]$. DFT methods consequently require careful calibration to establish their accuracy (or inaccuracy) on a case by case basis. Both methods provide a relatively inexpensive route to performing computational physics, chemistry and materials science, provided only trends and not highly accurate quantitative predictions are required. Post Hartree-Fock methods are potentially very accurate, but their poor scaling with system size limits their usefulness, restricting their application to small molecules and excluding most topics in condensed matter. Quantum Monte Carlo methods combine favourable scaling with system size with a very accurate treatment of electron correlation. This renders them ideal for correlated studies of large molecules and condensed matter systems when high accuracy is required.

An additional novel and very practical feature of Quantum Monte Carlo methods is that they provide a direct measure of the likely accuracy obtained. This feedback represents a fundamental advance over current density functional and quantum chemical methodology where the accuracy obtained is both unknown and variable. This is clearly advantageous when new systems are investigated, where there is little or no reference data.

3. Pseudopotential for electronic structure calculations

Previously we discussed some methods, which are more or less effectively used for the electronic structure calculations. All these methods are relatively new and have several interpretations in special usage software. The software, which uses these methods, is usually very complex and the approximations and methods are not so clear. Sometimes, calculation results have to be improved and the mechanism of that is not obvious. Also the user interfaces of these programs are not easy to understand as well as the interior, which may need some modifications. But, nevertheless, these programs are used, because no alternative methods are presented. We cannot state that the method, which was described and developed in these papers, can now replace the above-mentioned ones, but with further development and improvement it can become the workable alternative. Who knows, maybe the development of this alternative method will take away all the disadvantages of the other ones. This method is based on the pseudopotential of the atom calculation, using the analytic functions. This approach was successfully used in some calculation previously [1]. As this approach was successfully used for glass-like structure and the thin metal layers have the same structure, we will use this for the study of copper layers properties.

Any calculation of physical characteristics for the solid, which is connected with electron and phonon subsystems, is joined with the calculation and/or plotting of the potentials (potential functions). These potentials must be calculated, taking into account the simulated effects. The first step on this way is to calculate the electronic spectrum of the solid, as a quantum-mechanics object. The practical mean in this situation acquires the single electron approach, i.e. when the movement of every electron in the system is examined in the averaged field of nucleuses and other electrons. This averaged field must account both Coulomb interaction (within the system) and exchange-correlation effects in electron subsystem. In the simplest variant of these task neglect the lattice dynamics of the solid (adiabatic approach) and investigate only the stationary task. But even for this simple task the calculation of electronic spectrum for disordered medium is problematic. In quantum mechanics we can liberate two different stationary calculation approaches.

The first one, when we calculate the eigenvalues, i.e. we must solve the Shrödinger equation $\mathbf{H}\mathbf{u}_i = \varepsilon_i \mathbf{u}_i$ to find the single-electron functions \mathbf{u}_i and the corresponding eigenvalues of energy for single-electron states ε_i . This procedure is usually self-consistent, because the exact shape of the function in the Hamiltonian is unknown and is found on the base of some “seed” potential during the iteration process. The boundary condition for wave functions is their disappearance on infinity. As a result, we get the discreet spectrum of energies, then, on the base of the calculated wave functions the many-electron wave functions and corresponding basis are calculated.

The second class of these tasks is the scattering problems, when the plane wave with the known energy is scattered on the potential $V(\mathbf{r})$ and the Shrödinger equation: $(\Delta + k^2)\psi_{\mathbf{k}}(\mathbf{r}) = V(\mathbf{r})\psi_{\mathbf{k}}(\mathbf{r})$, is solved for boundary conditions, which corresponds the scattered wave: $\psi_{\mathbf{k}}(\mathbf{r}) \rightarrow \exp(ikr) + f(\theta, \varphi)\exp(ikr)/r$.

Originally was supposed, that this problem statement is reasonable only for the positive energies $k^2 = \varepsilon > 0$. But later, this approach was successfully used for the negative energy states of atoms and molecules and the cluster method of multiplex scattering for complex molecules and dopes in solids electronic structure calculation. Later on based on these principles many calculation schemes for both ordered and disordered solids were created. It can be stated that all thin layers have the glass-like structure, so thin copper layers in the way the used in microelectronics can be examined as the mediums with certain order of chaos. On this base we will continue our research.

3.1. GENERAL

The solution of the Shrödinger equation, required for the spectrum determination of atoms, molecules or solids (both ordered and disordered) in a non-relativistic approach, needs the knowledge of the electron self-consistent potential in the summary field of nucleuses and other electrons, so we can proceed to the single-electron task. Usually, this potential is unknown and we need to calculate it. One of the ways to obtain this potential for the free (isolated) atoms is to execute the self-consistent procedure (like Hartee-Fock-Slater) and receive, as a result, the self-consistent potential of an atom and the corresponding wave functions in single-electron approach. It is perfectly clear that the potential of isolated atom is an element of the total solid potential function. But this function cannot be found as a simple superposition of the atoms potentials. Therefore we need a detailed analysis for all the factors that determine atom’s potential. There is a group of methods, which calculate this potential, as a result of eigenvalues task. In the base of all these methods lies the Hartree method, which proposed the single-electron equation for the spin-orbital \mathbf{u}_i of the i -electron in the atom:

$$[-\nabla_1^2 + V_c(1) + V_{xi}(1)]u_i(1) = \varepsilon_i u_i(1), \quad (3.1)$$

where $-\nabla_1^2$ is the kinetic energy operator, $V_c(1)$ is the Coulomb potential energy of the electron in point 1, owing to the interaction with the nucleus and other electrons in the system, $V_{xi}(1)$ is exchange-correlation term, $U_i(1)$ is one of the wave functions. Then, for the atom with charge number Z :

$$V_c(1) = -\frac{2Z}{r} + \sum_j n_j \int u_j^*(2)u_j(2)g_{12}dv_2,$$

where $u_j^*(2)u_j(2)$ is electronic charge density of j -orbital in point 2, $g_{12} = 2/r_{12}$, r_{12} is the distance between point 1 and 2, n_j is the orbital filling number (0 or 1). The term:

$$V_{xi}(1) = -n_j \int u_i^*(2)u_i(2)g_{12}dv_2 ,$$

considers that the electron on *i*-orbital does not interact with himself. Integration is done throughout the volume.

The system of wave functions U_i gives us the possibility to calculate the electronic density of states (DOS) using the Hartree method:

$$\rho(1) = \sum_i n_i u_i^*(1)u_i(1) . \quad (3.2)$$

The single-electron functions, included in well-known determined total wave function are varied and minimize atom's total energy. The use of these wave functions in variational procedure leads to the Hartree-Fock energy:

$$[-\nabla_1^2 + V_c(1)]u_i(1) - \sum_j n_j \int u_j^*(2)u_j(2)g_{12}dv_2 u_j(1) = \varepsilon_i u_i(1) . \quad (3.3)$$

This DOS (3.2) can be used for the representation of exchange-correlation term in statistic approach. The calculation of DOS can be made only numerically. As was mentioned the algorithms of these calculations exist, but the calculation needs a lot of time and powerful system to achieve some results. For some solid systems (like disordered systems, glasses, etc.) these calculations became even more complex, because we need to solve numerically a high-order system of differential equations.

On the other hand, we can't get a structure potential from common potential superposition of the isolated atoms (like in the German-Skillman procedure), because we have to count both Coulomb interaction and bond exchange interaction. So, to calculate the electronic structure of the disordered system, we need to calculate the "crystalline potential" first. The task of electronic density of states calculation forces us to find the simple and effective way to calculate potentials, especially as it is just an intermediate result for the DOS calculation.

The Mattheus-Zeud idea of separate interpretation for nucleus and electronic parts of the potential seems very effective for our task. But the same idea is used in another well-studied method, the $X\alpha$ -Slater method. Slater took into consideration all the major factors that define electron energy in single-electron approach. To be more precise, Slater took the equation (2.2.1) and has written it down in the following form:

$$[-\nabla_1^2 + V_c(1) + V_{xiHF}(1)]u_i(1) = \varepsilon_i u_i(1) , \quad (3.4)$$

where $V_{xiHF} = -\frac{\sum_j n_j \int u_i(1)u_j^2(2)u_j(1)u_i(2)g_{12}dv_2}{u_i^*(1)u_j(1)}$ is the exchange correlation term. The charge,

which creates the V_{xiHF} potential, is called "exchange correlation charge" or "Fermi-hole". After that Slater proposed to replace V_{xiHF} by the weighted average with weights, corresponding to the probability of finding the electron in position 1 on *i* - spin-orbital:

$$[V_{xiHF}]_{AV} = -\frac{\sum_{i\uparrow j\uparrow} n_i n_j \int u_i^*(1)u_j^*(2)u_j(1)u_i(2)g_{12}dv_2}{\sum_{k\uparrow} n_k u_k^*(1)u_k(1)} , \quad (3.5)$$

where arrow means the electron spin position. This formula is true for both "up" and "down" spin positions. The exact solution for equation for the gas of free electrons gives:

$$[V_{xiHF}]_{AV} = -6[3\rho \uparrow(1)/4\pi]^{1/3} = V_{xs}(1) .$$

All these reasoning lead Slater to create the self-consistent field method, which was later modified.

Now it became clear that our main efforts should be directed to the determinations of Coulomb part, as well as the electronic charge distribution near the nucleus that defines the exchange term in $X\alpha$ - Slater method:

$$V_{x\alpha}(1) = \alpha V_{xz}(1) = -6\alpha(3\rho/8\pi)^{1/3}. \quad (3.6)$$

The next step for the DOS can be the introduction of MT-approach of the potential, as this potential will be used to calculate the electronic structure of a solid and what is more a disordered solid, which have no translation symmetry. The MT-approach gives us the possibility to separate the complex potential superposition into the system of isolated potential wells, connected through the constant level of interatomic energy (MT-null). The selection of this MT-null level is also an object of interest, because it's not trivial. Furthermore, the MT-approach gives us some advantages of potential spherical symmetry inside the MT-spheres. That can be very useful in this complex task.

3.2. ATOMIC POTENTIALS.

Let us represent the potential of the neutral atom as the sum of nucleon and electronic parts:

$$V_{cr}(\mathbf{r}) = V_{coul}(\mathbf{r}) + V_{xs}(\mathbf{r}). \quad (3.7)$$

Let us now try to define both items of this sum. For the nucleon (Coulomb) part it is very convenient to use the Gaspar potential, which is the universal approximation of electrostatic screened potential. The advantage of this potential is that it approximates numerical calculations very well, when Thomas-Fermi method is used, in wide range of charge numbers Z and at the same time is an analytic function. It is represented as:

$$V_{coul}^G = -\frac{2Z \exp(-\lambda r / \mu)}{r(1 + Ar / \mu)}, \quad (3.8)$$

where $\lambda=0,1837$, $\mu=0,8853Z^{-1/3}$, $A=1,05$.

After that we can find the electronic charge density from the Poisson equation:

$$V_e(r) = 2Z/r - V^G(r), \quad (3.9)$$

$$\rho(r) = \nabla_r V_e / 8\pi, \quad (3.10)$$

where V_e is the screened part of the potential.

Using the $X\alpha$ -Slater method we can find the exchange term:

$$V_{x\alpha}(1) = -6\alpha(3\rho/8\pi)^{1/3}. \quad (3.11)$$

The α parameter is an adjusting parameter and is chosen accordingly to consist the electron total energies received as a result of Hatree-Fock procedure with energies that were calculated using the $X\alpha$ - Slater method. These calculations were made by Schwartz for the $Z=1,2\dots 41$, but should be noted that for large Z , $\alpha \sim 0.7$ and decreases slowly. This method is very simple, but it has one weak point, the α parameter itself. Therefore, we should mention the modification of this method made by German and Schwartz:

$$V_{X\alpha\beta} = [\alpha + \beta G(\rho)]V_{xs}, \quad (3.12)$$

where

$$G(\rho) = \frac{4}{3} \left(\frac{\nabla \rho}{\rho} \right)^2 - 2 \frac{\nabla^2 \rho}{\rho}, \quad (3.13)$$

$$V_{xs} = -6[3\rho/8\pi]^{1/3}. \quad (3.14)$$

The advantage of this method is the constant parameters α , β for any Z . $\alpha=0,66(6)$ and $\beta=0,003$. The development of these methods can be presented for numerical calculations as follows:

$$V_{cr}(\mathbf{r}) = V_{coul}(\mathbf{r}) + V_{xs}(\mathbf{r}), \quad (3.15)$$

where V_{xs} can be presented either by $X\alpha$ or $X\alpha\beta$ method.

As was mentioned above the Coulomb part of this potential is presented by Gaspar potential:

$$V_{coul}(\mathbf{r}) = -\frac{2Z}{r} f(\mathbf{r}), \quad (3.16)$$

$$f(\mathbf{r}) = \exp(-\lambda r / \mu) / (1 + Ar / \mu). \quad (3.17)$$

The exchange part of this potential also needs some modification to make it more convenient for numerical research:

$$V_{X\alpha} = -6[3\rho/8\pi]^{1/3}, \quad (3.18)$$

where $\rho(\mathbf{r}) = -\nabla_{\mathbf{r}} V^G(\mathbf{r}) = -Zf''(\mathbf{r}) / 4\pi r$, $f'(\mathbf{r}) = -\lambda_{\mu} f(\mathbf{r}) - A_{\mu} f(\mathbf{r})$,

$$f''(\mathbf{r}) = -(\lambda_{\mu} + A_{\mu})f'(\mathbf{r}) + A_{\mu}^2 f(\mathbf{r}), \quad \lambda_{\mu} = \lambda / \mu, \quad A_{\mu} = (A / \mu) / (1 + Ar / \mu).$$

The $X\alpha\beta$ method needs some additional functions to be defined:

$$V_{X\alpha\beta} = [\alpha + \beta G(\rho)] V_{xs}, \quad (3.19)$$

after that we can use the properties of tangent functions to present this exchange potential in other form:

$$V_{X\alpha\beta} = \alpha \left[1 + \text{th} \left(\frac{\beta}{\alpha} G(\rho) \right) \right] V_{xs}, \quad (3.20)$$

where

$$G(\rho) = \frac{4}{3} \left(\frac{\nabla \rho}{\rho} \right)^2 - 2 \frac{\nabla^2 \rho}{\rho}, \quad \nabla_{\mathbf{r}} \rho = Z(f''' - f'' / r) / 4\pi r, \quad \rho'' = Z(f^{IV} - 2f''' / r + 2f'' / r^2) / 4\pi r,$$

$$\nabla^2 \rho = Zf^{IV} / 4\pi r, \quad f''' = -2A_{\mu}^3 f(\mathbf{r}) + 2A_{\mu}^2 f'(\mathbf{r}) - (\lambda_{\mu} + A_{\mu})f''(\mathbf{r}),$$

$$f^{IV} = 6A_{\mu}^4 f(\mathbf{r}) - 6A_{\mu}^3 f'(\mathbf{r}) + 3A_{\mu}^2 f''(\mathbf{r}) - (\lambda_{\mu} + A_{\mu})f'''(\mathbf{r}).$$

In such a way, we have two methods that analytically represent the isolated atom potential; it is very useful in numerical calculations. Using the above-mentioned formulae we will calculate the atomic potentials and compare the results for both methods and for the Hartree-Fock self-consistent potential calculation.

3.3. CRYSTALLINE POTENTIALS

Using the isolated atom potentials in MT-approach in electronic structure calculations for the solids is ill-defined, because we need to take into consideration the influence of the nearest neighbour (short range ordering). Therefore we need to formulate the ‘‘crystalline’’ potential, the term ‘‘crystalline’’ does not mean any translation symmetry, it can be used for disordered solids also. ‘‘Crystalline’’ means that we need to calculate the electron potential in the field of nucleuses and other electrons. But we cannot

just take a simple superposition of neutral atoms, because we need to take in account the behaviour of outer electrons in bonds. The base for this calculation is (as was mentioned in the previous section) the potential of an isolated atom. We can formulate this potential as follows:

$$V_{cr.coul}(r) = V_{coul}(r) + V_{coul}(a - r), \quad (3.21)$$

where a is the interatomic distance. The exchange part of the potential can be presented in the following way:

$$\rho_{cr}(r) = \rho(r) + \rho(a - r), \quad (3.22)$$

where $V_{X\alpha}(r) = -6\alpha[3\rho_{cr}(r)/8\pi]^{1/3}$, $V_{X\alpha\beta} = \alpha \left[1 + \text{th} \left(\frac{\beta}{\alpha} G(\rho) \right) \right] V_{xs}$.

In case of need V_{cr} and ρ_{cr} can be precised by known Levdivine α -functions, to take into consideration several neighbors, but in the first approach it can be ignored. Then the sought potential is presented as:

$$V_{cr}(r) = V_{coul}(r) + V_{xs}(r). \quad (3.23)$$

“Crystalline” potential (2.22) is an analytical function that is very convenient for numerical research.

3.4. POTENTIAL MT-APPROACH

As it was mentioned above, the potential in MT-approach replaces the complex aggregation of overlapping potentials (in fact, one complex potential well) by the system of isolated spherically symmetrical MT-potentials in interatomic medium, which is characterised by the constant potential level (MT-null).

The crystalline potential in MT-approach can be represented as:

$$V_{MT}(r) = V_{cr}(r) - V_{MT0}. \quad (3.24)$$

V_{MT0} characterise the border energy between the localised and non-localised states. The choice of MT-null level is not trivial. For semiconductors, where interatomic bonds are covalent, this level is about $0,5R_{MT}$ Ry, where R_{MT} is the radius of MT-sphere. The radius of this sphere in our case is $\frac{1}{2}a$. For the metals, which are studied in this work, the bond character is not so well-defined, because of electron gas. For it's turn the choice of MT-null in metals in general and copper in particular can be the object of simulation and study. The maximal value for this MT-null parameter can be taken the MT-null level of the semiconductors.

3.5. MAIN RESULTS AND ANALYSIS

For all the calculations where the $X\alpha$ method was used we suppose that $\alpha=1$. The source file for all calculation is available in *Appendix 1*. The program made universal for any structure that will fulfill the method requirements. The “Quick start” Guide on the program can be found in *Appendix 2*.

First of all let us present the basis of all calculations, the potential for $X\alpha$ and $X\alpha\beta$ calculation approach.

The Figure 2 demonstrates the differences in potentials calculated using two methods: $X\alpha$ and $X\alpha\beta$. As we can see, both methods give comparable results, but with the growth of argument the difference became more noticeable. This can possibly be the influence of two factors:

- These calculation was made using the reduced $X\alpha$ method, which is peculiar with the assertion that $\alpha=1$. But the real α coefficient can be different from 1. The real α we suppose is situated between 0.7 and 1. Unfortunately, we have no exact information about α value for copper.
- The other reason that influenced the first graph that $X\alpha\beta$ method is more exact and it better “feels” the presence of neighbor atom. In support of this fact, we can see that $X\alpha\beta$ method react immediately on the border effect (exit from cluster zone, $r > 2.5 \text{ \AA}$).

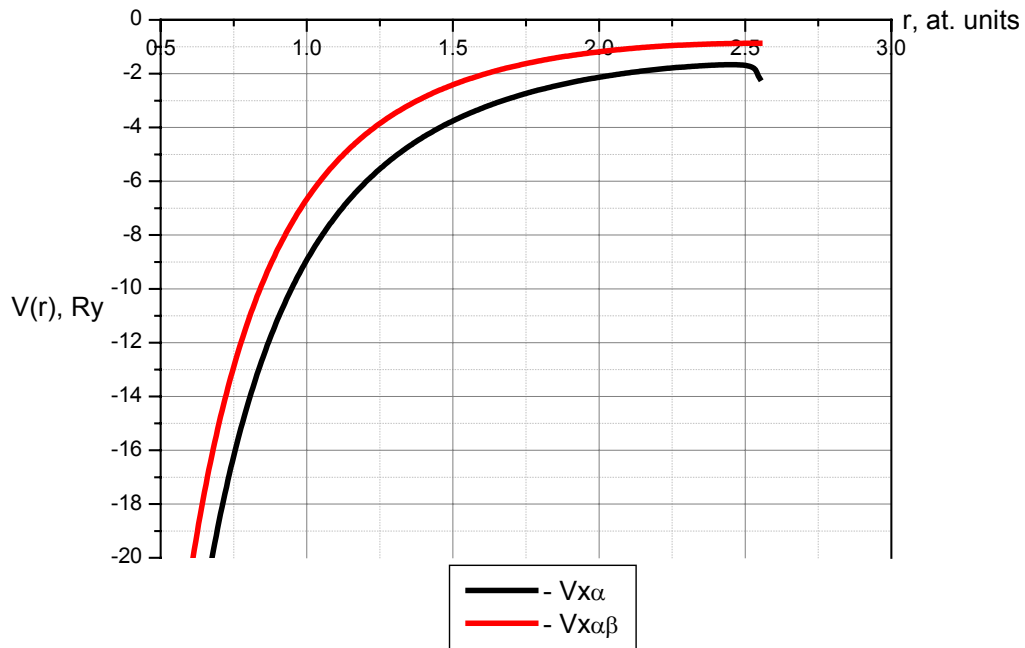


Figure.2. Calculated $V(r)$ in Ry.

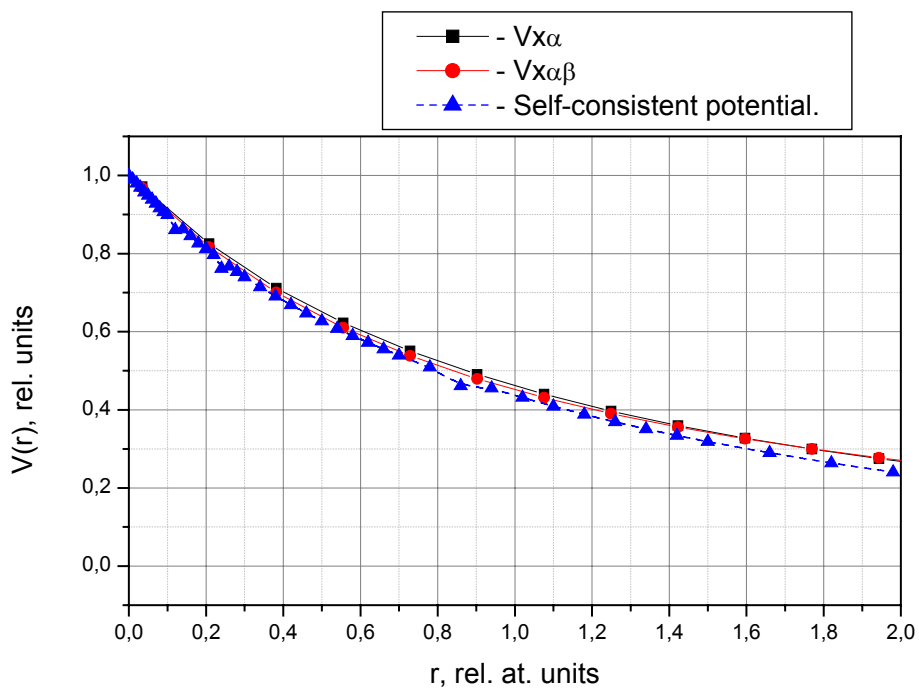


Figure.3. Calculated reduced results in comparison with self-consistent potential.

The second graph illustrates the comparative results of both methods with the self-consistent potential, which was received as a result of Hartree-Fock self-consistent procedure. As we can see from this graph, both methods are in close concordance with the “classical” Hartree-Fock method. This gives us the possibility to use these potentials in future calculations. After short graphs analysis, we can assume

that $X\alpha\beta$ method is more exact, it is also is not dependant from the α coefficient (which, in its place is dependant from Z). Using of this method gives us the possibility to create the universal program for future usage. In conclusion of this analysis we can announce 2 advantages of this method:

- it does not use any experimental constants and this fact makes it usable for poorly studied materials;
- the calculation does not need the prolonged self-consistent procedure (like Hartree-Fock) and it can be successfully used for the simple atomic and molecular structures in some properties calculation (like in spectrum determination).

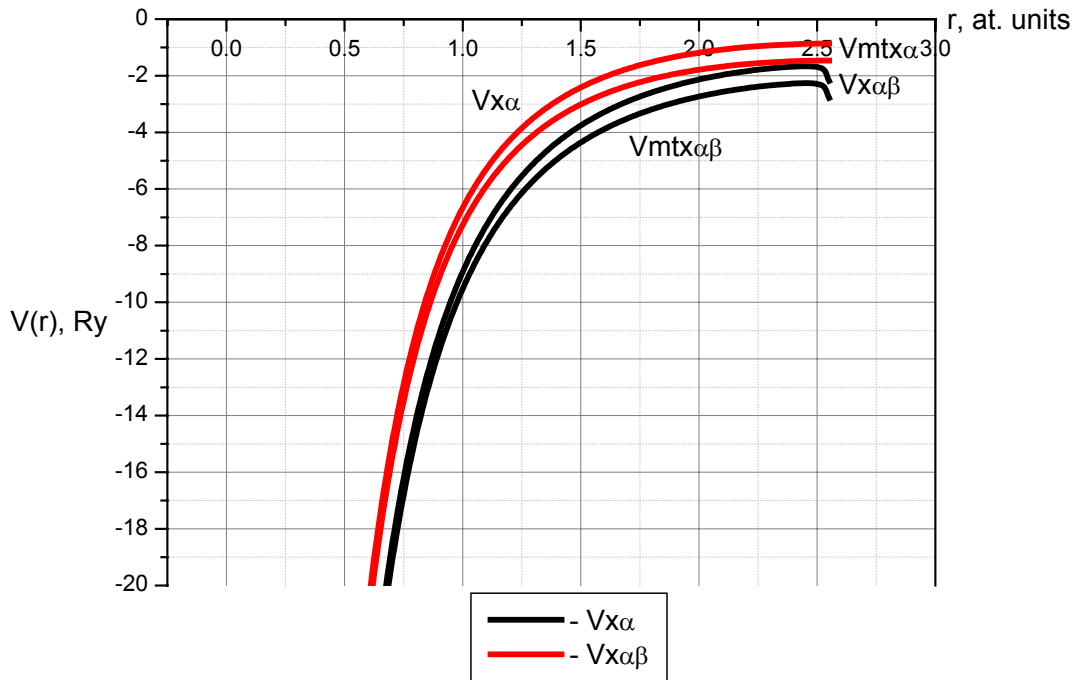


Figure 4. MT-potential for both approaches, MT-level =0,5 Ry.

The Figure 4 in this section presents the comparative results of potentials and potentials in MT-approach. This approach gives us the possibility to “simulate” medium presence. For the semiconductors the MT-level is calculable and well determined, because of purely covalent bond mechanism. For metals, where the presence of free-electron gas complicate the problem we can use this parameter as a variable in future calculations. This will determine the adaptability of this method for metals. The Figure 4 shows us that we lower the MT-potential, like putting it in some potential well, which can be determined as common background potential in medium.

4. Calculations of the density of electronic states and specific resistance for thin copper layers

4.1. PHASE SHIFTS AND LOGARITHMIC DERIVATIVES

There are different models of electromagnetic wave scattering in condensed matter. First of all we will define main positions of our scattering model. We assume that plane electromagnetic wave e^{ikr} interacting with a single atom or medium transforms into studied wave that can be expanded in to wave train as follows:

$$\Psi_{nlm} = \sum_1 R_{nl} Y_1^m . \tag{4.1}$$

The behaviour of an angular component Y_l^m is simple and out of interest, because the scattering is defined by radial component R_{nl} (further R_l). The above-mentioned model is represented on the Figure 5.

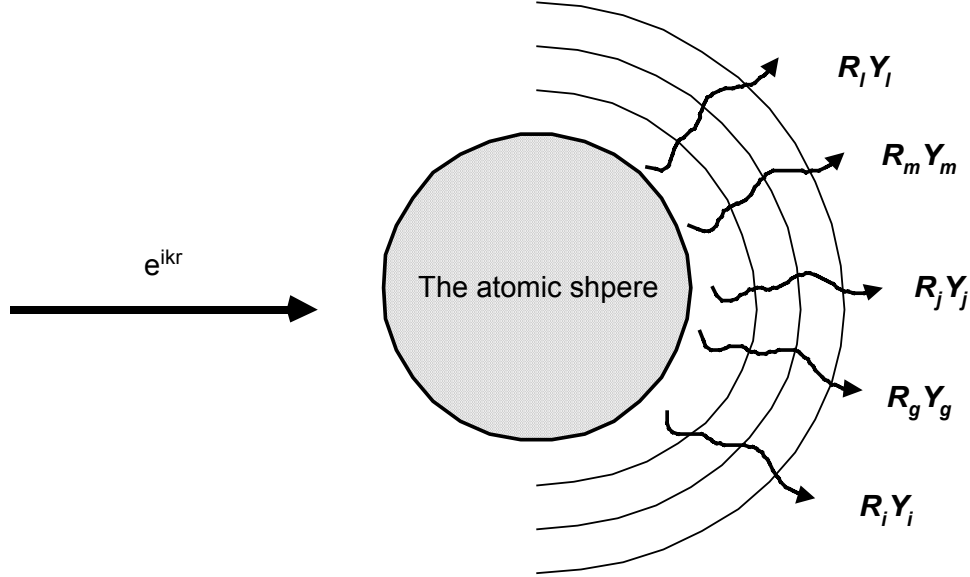


Figure 5. The model of scattering.

The potential (2.23) will be used for logarithmic derivatives calculation $\gamma_l = R_l'(r)/R_l(r)|_{R_{MT}}$ by numerical integration of Shroedinger radial equation:

$$\frac{1}{r^2} \frac{d}{dr} \left(r^2 \frac{dR_l}{dr} \right) + \left[k^2 - \frac{l(l-1)}{r^2} - U(r) \right] R_l = 0. \quad (4.2)$$

The numerical integration was made using the forth-order Runge-Kutta method. The peculiarity of this calculation is that the integration interval $0-R_{MT}$ is divided in two parts: the small values of r , where we have to ensure the singularity of this potential and the solution of this equation is $R_l = r^l f(r)$ and where the equation (4.1) for the $f(r)$ function the (4.2) looks like:

$$f''(r) + \frac{2}{r}(l+1)f'(r) + [k^2 - U(r)]f(r) = 0, \quad (4.3)$$

and the large values of r , the potential weak-change region, where the (4.2) itself was integrated. After we will receive the logarithmic derivatives, we can calculate the phase shifts for the single scatterer in vacuum:

$$\text{tg} \delta_l = \frac{kj_l'(kR_{MT}) - \gamma_l j_l(kR_{MT})}{kn_l'(kR_{MT}) - \gamma_l n_l(kR_{MT})}. \quad (4.4)$$

4.2. CLUSTER: LIQUID METAL MODEL

Expediency of this model examination lies in its simplicity, which gives a possibility, on one hand to demonstrate the methodical part of cluster approach without any technical difficulties, on the other hand to retrieve some convenient for analysis data in an evident form. Besides, the liquid metal model has a plain physical meaning. The term “liquid” means the full structural disorder of the substance involved. To be more precise, the distance up to the nearest neighbour (first coordination sphere) maintains, but the angular coordinates are random. Another condition is that the average density of matter maintains locally also.

So, we take into consideration only the nearest order, in the absence thereof the far order, like it is in the liquid. The term metal doesn't mean that this model can be used only for metals; it was successfully implemented on semiconductors [1]. To implement this model we need to isolate the matter

into a single atom, which will be associated with a crystalline potential in MT-approach (2.23) to consider the influence of the nearest neighbourhood. This means that around the studied atom is spread the neighbor atom and, in fact, we are working on the one-bond distance. The only demand is to maintain the average interatomic distance constant, angular coordinates are random (Figure 6).

This model can be used for the wide range of mediums, where the structural order as is not present, but short-range order is present. These are amorphous semiconductors, glasses, etc. Thin metal layers can also be presented as a glass-like structure.

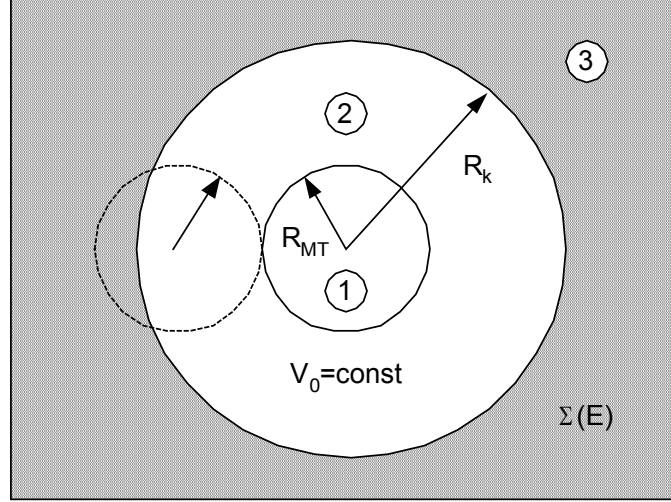


Figure 6. The “liquid metal” model

After that we use the potential to calculate the γ_i , which are, in their turn used to calculate the phase shifts on the R_k , defining the scattering properties of a medium. For the moment we can forget about the potential itself and concentrate on the scattering task, to return to it later, because the possible applications of it are not exhausted. The spherical symmetry of this task allows to use partial decomposition techniques and we can write down the scattered wave outside the MT-sphere (2), where the potential is constant, as:

$$\psi_1^{(2)} = j_1(kr) - tg\delta_1 n_1(kr) \quad (4.5)$$

The region (2) is a sphere of R_k radius is determined from the condition of average matter density preservation. However, to consider the influence of medium we need to “load” the sphere (2) with an effective complex potential, which defines the fading of electromagnetic waves, thereby modeling the disordered medium. The region (3) is under the influence of coherent potential. After that we must sew the wave functions on the border of regions 2 and 3, superposing the Soven condition, which consists in the statement that disordered medium does not allow the forward scattering. The next step is to find the dispersion law of the medium and the density of states.

The calculation of DOS using the means of scattering theory is based on the Fridel sum rule, which is deduced from common physical reasons. Let us examine the electron inside the large sphere with radius R and moving in the presence of spherically symmetrical potential $V(r)$ ($V(r)$ decreases faster than r^{-2}). Then, the scattered partial wave can be written down in well-known asymptotic form:

$$\psi_1(r) = \frac{1}{r} \sin(k'r + \delta_1 - \frac{1}{2}l\pi) . \quad (4.6)$$

Let us demand from the wave function to fade in infinity:

$$\psi(r) \rightarrow 0 \text{ for the } r \rightarrow \infty . \quad (4.7)$$

and we will receive for the given wave number:

$$k' = \left(n + \frac{1}{2}l \right) \frac{\pi}{R} - \frac{\delta_1}{R} , \text{ where } n \text{ is integer.} \quad (4.8)$$

In absence of the scatterer the corresponding wave number is equal to:

$$k = \left(n + \frac{1}{2}l \right) \frac{\pi}{R} . \quad (4.9)$$

Then, we can assume that the difference $k-k'$ is dependent only of δ_i .

$$k' - k = -\delta_l(k') / R . \quad (4.10)$$

Let us point out some interesting properties of $\delta_l(k)$:
 when $k \rightarrow \infty$, $\delta \rightarrow 0$; when $k \rightarrow 0$, $\delta \rightarrow n\pi$; where n is integer or null, n is null for the repulsive or weak-attractive potential.

Now we can examine the s -wave. Assuming that there exists only one bound state for the $V(r)$ potential, then $\delta_0(0) = \pi$ and the difference will be equal to:

$$\nabla k_0 = k_0' - k_0 = -\frac{\pi}{R}, -\frac{2\pi}{R}, \dots, \frac{n\pi}{R}, \quad (4.11)$$

which means that every change in wave number on $\frac{\pi}{R}$ nearby the scattering center new state will appear right up to Fermi level. Then, intending that in many electron system inside the sphere with R radius $V(r)$ is a self-consistent potential energy of every electron in the field of scattering center and Fermi gas, we can calculate the effective electronic charge, which should be added to sphere, to "neutralize" the charge, which appears when the scatterer enters the medium. From (3.33) we can receive:

$$k_F' - k_F = -R^{-1}\delta(k_F'), \quad (4.12)$$

where k_F' , k_F - the Fermi impulses (wave numbers) in presence of the scatterer and without it. Then the number of new bonded states for every partial wave:

$$\frac{R}{\pi}(2l+1)(k_F' - k_F) = -(2l+1)\frac{\delta_l(k_F')}{\pi}, \quad (4.13)$$

where $\delta_l(k_F') \approx \delta_l(k_F)$ since $\delta_l(k_F)$ changes slowly nearby the Fermi level.

Consequently, the total injected charge in sphere is:

$$Z = \frac{1}{\pi} \sum_s \sum_l (2l+1)\delta(k_F) = \frac{2}{\pi} \sum_l (2l+1)\delta_l(k_F), \quad (4.14)$$

where s is the spin quantum number.

Needs to be noticed that this result instantly follows from Levinson theorem, which assume that between scattering phase values for null and infinite energies there is a defined correlation ($\delta_l(0) - \delta_l(\infty) = \pi N_l$, where N_l is the number of bonded states with impulse momentum l), which is the scattering matrix analyticities consequence.

So if we examine the scattering potential with a valence Z in the free electron gas and from the physical reasons we assume that additional states for the electrons, which have to screen the potential are disposed below the unchanged Fermi level, then we come to received in (4.14) phase shifts limitations.

4.3. DENSITY OF ELECTRONIC STATES (DOS) FOR A SINGLE SCATERER IN VACUUM.

Now we will examine the density of states (DOS) that will produce the single potential-scaterer, placed into the spherical "potential box". In that task and later we will use the potential MT-approach. Then, the real potential energy is simulated, as in Figure 6.

Taking into consideration the spherical symmetry for this task, we can use the traditional simplification, connected with partial decomposition techniques and from now on, we will take up only the radial component, do not paying attention to the angular ones.

Let's write down the expression for the greenian, using the specific units, where $\eta = 2m = 1$:

$$(\nabla^2 - V(\mathbf{r}) - E)G(\mathbf{r}, \mathbf{r}') = \delta(\mathbf{r} - \mathbf{r}') \quad (4.15)$$

Considering that:

$$G(\mathbf{r}, \mathbf{r}') = \sum_{lm} Y_{lm}(\mathbf{r}) Y_{lm}(\mathbf{r}') G_l(\mathbf{r}, \mathbf{r}') \text{ and } \int Y_{lm}(\mathbf{r}) Y_{lm}^*(\mathbf{r}) d\Omega = 1,$$

we can pass to the radial equation:

$$-\frac{1}{r^2} \frac{d}{dr} \left(r^2 \frac{dG_l}{dr} \right) + \left(V(r) + \frac{l(l+1)}{r^2} - E \right) G_l(r, r') = \frac{1}{r^2} \delta(r - r') \quad (4.16)$$

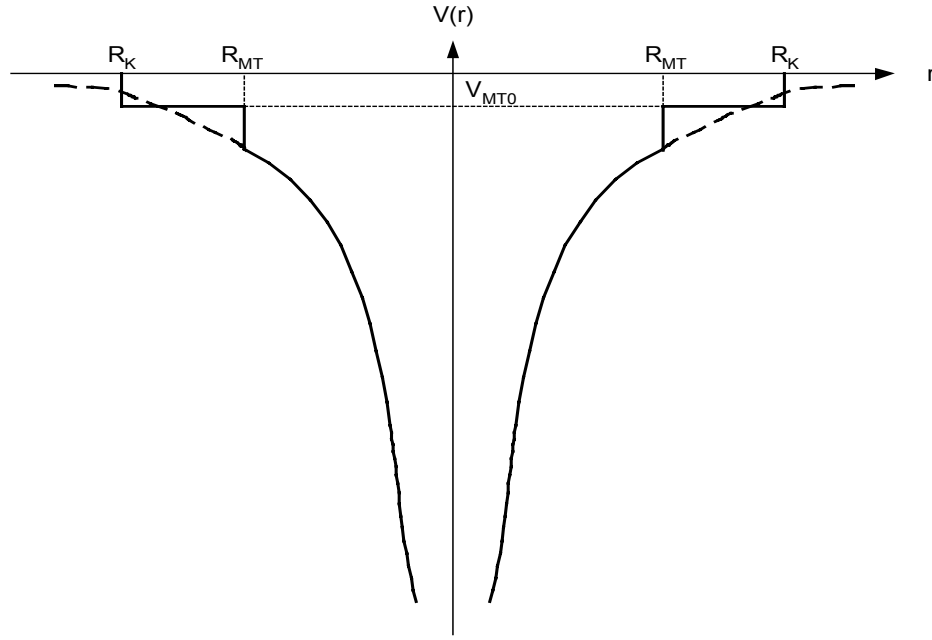


Figure 6. The single MT-potential in vacuum.

We should search for the Green function, which on one hand, will describe the scattered wave outside the MT-sphere and on the other hand, will be the outgoing wave, i.e. satisfied the asymptotic condition in infinity. Then:

$$G_1(r, r') = kF_1(kr_>)J_1(kr_<) \quad (4.17)$$

$J_1(kr_<)$ is the certain partial wave, $F_1(kr_>)$ is the function, which should be find to satisfy the greenian condition.

We will look for the F_l function in the following form:

$$F_l = N_l + A_l J_l \quad (4.18)$$

where A_l – complex coefficient and F_l is a linear combination of the following functions:

$$J_l = \cos \delta_l j_l(kr) - \sin \delta_l n_l(kr) \quad (4.19)$$

$$N_l = -\cos \delta_l n_l(kr) + \sin \delta_l j_l(kr) \quad (4.20)$$

(N_l and J_l – have a phase shift $\pi/2$). Besides, we need to preserve the right normalization for G_l function. That is equivalent to the wronskian preservation and can note that:

$$W(j_l, n_l) = j_l' n_l - n_l' j_l = W(J_l F_l) = J_l' F_l - F_l' J_l = \frac{1}{k^2 r^2} \quad (4.21)$$

and the real part of F_l must satisfy the (3.21).

If we will examine the ε -point region in detail and integrate (3.39), we will pass to:

$$\lim_{\varepsilon \rightarrow 0} \left[\int_{r'-\varepsilon}^{r'+\varepsilon} \frac{1}{r^2} \frac{d}{dr} \left[r^2 \frac{dG(r, r')}{dr} \right] r^2 dr + \int_{r'-\varepsilon}^{r'+\varepsilon} \left[k^2 - V(r) - \frac{l(l+1)}{r^2} \right] r_0^2 |r| \right] = k^2 r^2 (F'J - FJ') \quad (4.22)$$

It was already stated that F_l must be an outgoing wave. If we will choose $A_l = i$, we will certain that:

$$F_l = N_l + iJ_l = \cos \delta_l (-n_l + j_l i) + i \sin \delta_l (-n_l + j_l i) = e^{i\delta_l} |r_0^{(l)}(kr) \sim \frac{e^{ikr}}{kr}, \quad (4.23)$$

i.e. $A_l = i$ – satisfies the stated condition.

Now using the well-known expression for the density of electronic states:

$$\rho(E) = \frac{2k}{\pi} \text{Sp} \text{Im} G(E) = \frac{2}{\pi} \int d\bar{r} \text{Im} G(r, r, E) \quad (4.24)$$

after that, we integrate by angular coordinates and receive:

$$\rho(E) = \frac{2k}{\pi} \sum_l (2l+1) \int_0^R r^2 dr J_l^2(kr) . \quad (4.25)$$

We can check the received (4.25) expression on the “empty lattice” example (absence of scatterer in a potential “box”). So, $J_l = j_l$ and, using the identity:

$$\sum_l (2l+1) j_l^2 = 1 , \quad (4.26)$$

we can state:

$$\rho(E) = \frac{2k}{\pi} \sum_l (2l+1) \int_0^R r^2 dr j_l^2 = \frac{2k}{\pi} \frac{R^3}{3} = \frac{kV}{2\pi^2} \sim \sqrt{E} . \quad (4.27)$$

The result (4.27) corresponds the density of electronic states in a free non-interactive electron system. After that the integral in (3.25) can be presented as:

$$\int_0^R r^2 J_l^2(kr) dr = -R^2 J_l^2(R) \frac{d\gamma_l(E, R)}{dE} . \quad (4.28)$$

And finally, the searched correlation for the density of electronic states inside the sphere with R radius in a presence of the scatterer can be written down as follows:

$$\rho(E) = \frac{2}{\pi} \sum_l (2l+1) \left[\frac{d\delta_l}{dE} - \frac{R^2 J_l^2(kR)}{2} \frac{\partial \gamma_l(k, \delta_l)}{\partial k} \right] , \quad (4.29)$$

where the first item corresponds the scatterer contribution to DOS, the second considers the effect of undisturbed movement.

4.4. DENSITY OF ELECTRONIC STATES (DOS) FOR A SINGLE SCATERER IN MEDIUM.

Let us now place the spherical “potential box”, which was studied in the previous part in vacuum into the medium, the properties of which are simulated by the energetically independent effective potential, or coherent potential (*Figure 7*). The presence of this effective medium urges to provide the attenuation of outgoing electronic wave. If we will pay attention to the asymptotic $h_l^{(+)}(kr) \sim e^{ikr} / kr$ in (4.23), then the attenuation of the wave is natural to associate with the complex wave number and hence to describe the outgoing wave in effective medium on infinity as $h_l^{(+)}(kr) \sim e^{ikr} / kr$. But, as the function $F_l = N_l + A_l J_l$ (A_l – complex coefficient dependent from energy) also describes the outgoing wave, then we should look for A_l from the logarithmic derivatives equality condition for $h_l^{(+)}$ and $F_l = N_l + A_l J_l$:

$$k \frac{N_l'(kR) + A_l J_l'(kR)}{N_l + A_l J_l} = k \frac{h_l^{(+)'}(kR)}{h_l^{(+)}(kR)} , \quad (4.30)$$

where R - the border of spherical “potential box”, or in other words, one-atom cluster.

But the search for A_l is impossible till the moment, we know the dispersion law for the effective medium $E-k$. It is worth to note, that the term “dispersion law” should be used very carefully, because in that case (analogous with crystals) it means the conservation of quasi-momentum also. In disordered mediums the conservation of momentum law is not implemented, and the usage of this term is only a tradition.

The effective medium consistency condition is the fact, that the system does not allow the forward scattering:

$$\langle t \rangle_{\text{medium}} = 0 \quad (4.31)$$

Since it is impossible to calculate the t -matrix of the whole system t_{sys} we are forced to replace that matrix with a t -matrix of the examined “one-atom” cluster t_k , because it is accurately known. The justification for that approach could be the fact that if we’ll remove a small cluster from the large disordered medium then the scattering properties of the whole system will not change. That is:

$$\langle t \rangle_{\text{rst_medium}} = 0, \quad (4.32)$$

this means that:

$$\langle t \rangle_k = 0. \quad (4.33)$$

$$\begin{aligned} \text{Im } A_1 &= \text{Im} \left[i \frac{(1-Q_1)(1+Q_1)^*}{(1+Q_1)(1+Q_1)^*} \right] = \text{Im} \left[i \frac{1+Q_1-Q_1^*-Q_1 Q_1^*}{|1+Q_1|^2} \right] = \\ &= \left[i \frac{1+X+iY-X+iY-|Q_1|^2}{|1+Q_1|^2} \right] = \frac{1-|Q_1|^2}{|1+Q_1|^2} \end{aligned} \quad (4.40)$$

This correlation gives us a possibility to state some useful properties of A_l , and to link them with the electronic wave F_1 behaviour on the cluster border:

- If $Q_l=0$, then, there is no reflection, $\text{Im}A_l=1$ and (4.36) change over to (4.29);
- If $Q_l=1$, then, there is a full reflection, $\text{Im}A_l=0$ and density of electronic states (DOS) is equal to zero (3.36); that could correspond to the system's transparency band;
- If $Q_l=-1$, that leads to the origination of bound states.

4.5. RESISTANCE OF LIQUID METALS IN ZIMAN APPROACH

Another possible application for the MT-approach potential calculated is the possibility to estimate the specific conductivity calculation, using the Ziman theory [2].

If dispersing centers are the atoms of liquid metal (or amorphous metal film), their distribution is not completely random, the amplitude of scattering from two atoms located one from another on a distance, circumscribed by a radius - vector R , is equal:

$$[1 + \exp(iqR)] f(\theta), \quad (4.41)$$

where q is equal to $k - k'$. Thus, if to neglect repeated scattering, the conductivity is given by expression

$$\sigma = \frac{Se^2L}{12\pi^3\eta}, \text{ where:}$$

$$\frac{1}{L} = \frac{1}{v\tau} = N \int S(q)(1 - \cos\theta)I(\theta)2\pi \sin\theta d\theta. \quad (4.42)$$

Here N - number of atoms in 1 sm^3 , a $S(q)$ - structural factor, defined as

$$S(q) = N^{-1} \int [1 + \exp(iqR)]^2 P(R) d^3X, \quad (4.43)$$

where $P(R)$ - conjugate cumulative distribution function, $P(R)d^3X$ is the probability that in volume d^3X on a distance R from the given atom is the one. Using for $f(\theta)$ the Born approximations and following the calculations in [3] for a specific resistance ρ , we can write down the formula:

$$\rho = \frac{3\pi}{\eta^2 e^2 v_F^2 \Omega} \int_0^{2k_F} \frac{|v(q)|^2 S(q) q^3 dq}{4k_F^4}, \quad (4.44)$$

where $v(q) = \int V(r) \exp(iqR) d^3X / \Omega$,

and the integral undertakes on volume Ω .

The *Figure 8* schematically illustrates a course of function $S(q)$ and $v(q)$. The possibility of application of the theory of perturbations is determined by the circumstance, that the magnitude $v(q)$ is small in area, where $S(q)$ is great.

Thus, the theory of scattering of electrons in liquid metal is identical to the theory of scattering of X-rays or neutrons in a liquid. The first indication that the resistance of liquid metals can be calculated that way, was made in work [4] and [5]. Ziman renewed this idea, by taking advantage for $V(r)$ by new representation of atomic pseudo-potential, and has conducted detail comparison to experiment; one of the most successful applications of the Ziman theory is the study of resistance temperature dependence. For univalent metals this dependence is strong, and the resistance grows with temperature; for bivalent materials this dependence is weak and resistance decreases with temperature. This difference in a structural factor $S(q)$ behaviour for one- and bivalent metals has the following explanation.

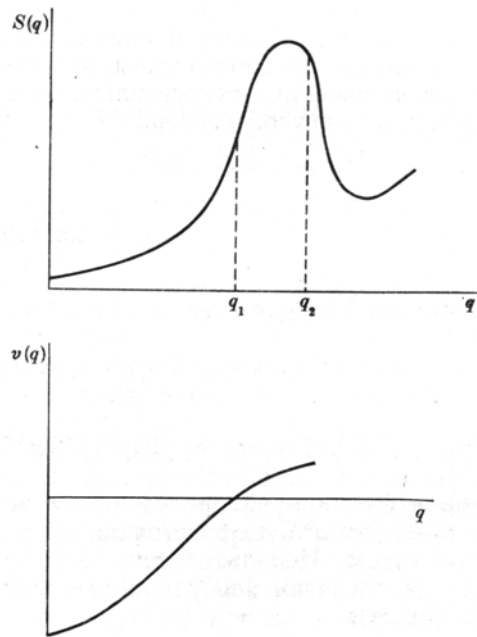


Figure 8. Structural factor and pseudopotential $v(q)$ for a liquid metal.

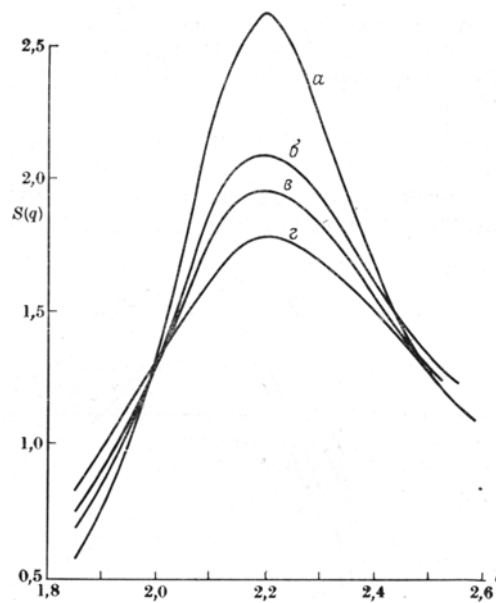


Figure 9. $S(q)$ function for the liquid Pb.

In a Figure 8, constructed on the base of scattering studies for neutrons, the function $S(q)$ for liquid lead for various temperatures is shown. It is clear, that at univalent metals the resistance is determined by a left-hand side of peak, and as $v(q)$ passes through zero close to $q=2k_F$ (Fig.3.4), that, apparently, that part of a curve $S(q)$, which is located much below the maximum. It was observed, that the resistance of univalent liquid metals for constant volume is proportional to absolute temperature; that specifies that the factor $S(q)$ also is proportional T in an interval, where $|v(q)|^2$ has a value noticeably distinct from zero. For very small q the structural factor $S(q)$ is given by the Orstein-Tzernike formula:

$$S(q) = \frac{kT}{\beta\Omega_0}, \tag{4.45}$$

where β - volumetric module of compression and Ω - atomic volume. This formula describes the contribution macroscopic fluctuations of denseness and is fair for liquids or solids. But it should not be fulfilled close $q=2k_F$ even for univalent metals, and the fig. 3.5 demonstrates, that it is so. Large polemic

recently took place on the problem, whether can the linear dependence ρ from T be explained with the help of experimental data for $S(q)$. In work [4] and [6] is stated, that for liquid natrium the value of $d(\ln(\rho))/dT$, calculated on observational data for $S(q)$, makes a half of an experimentally observable value. We suppose, that the observable linear dependence ρ from T is stipulated by that factor, that for univalent metals $|v(q)|^2$ will be converted in zero close $q = 2k_F$.

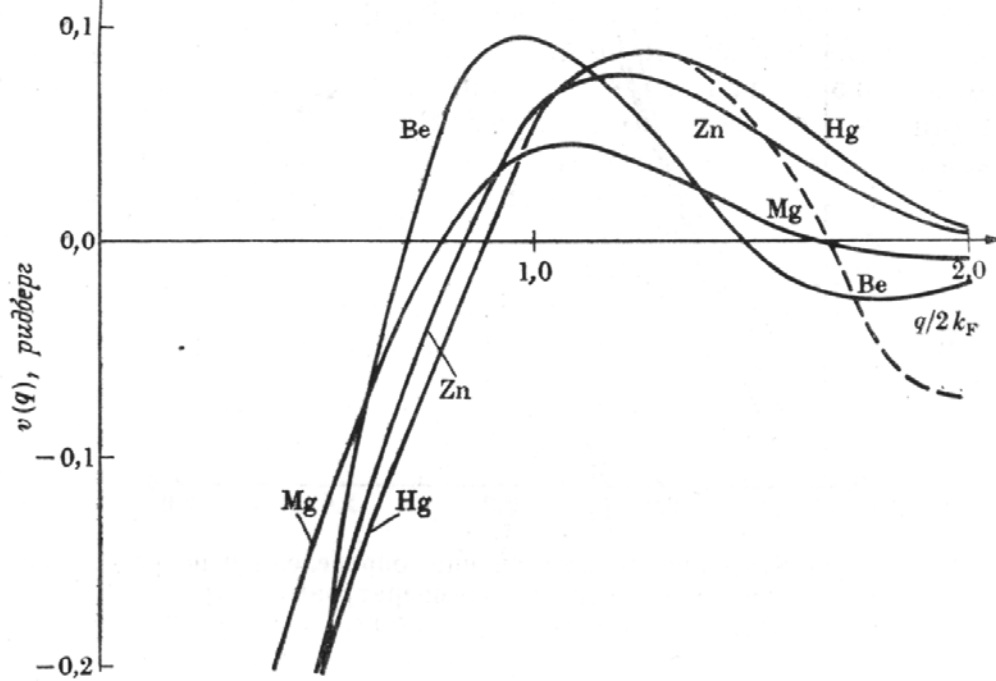


Figure 10. Pseudopotentials $v(q)$ (in Ry) for some metals calculated by Animalou and Heine.

The difficulty in use of the theory for numerical studies of conductivity is connected to indeterminacy as $S(q)$, and in particular $v(q)$, and also with doubtful fitness of a Born approximation. In a Figure 10 some values $v(q)$, calculated Animalou and Heine [7] are shown. All curves pass through zero in a neighborhood of a maximum $S(q)$, due to what the conductivity is rather sensitive to a position $v(q)$, that in details is shown by some calculations, where various aspects of function $v(q)$ were used.

The zero value for $v(q)$ means, that for the defined angle θ the scattering disappears, the amplitude of scattering appropriate to phase shifts of the s - and p -type functions has a form of $A + B\cos(\theta)$. In a Born approximation A and B are real, but it not so if to take exact phase shifts.

Therefore success of the theory permitting to receive a good approximation for a resistance, specifies that the Born approximation appears sufficient, and the phase shifts are really small. On the other hand, the phase shifts for separate atom should satisfy to a rule of Fridel sums.

Heine in his work [8] specifies, that would be irregular to take exact phase shifts, to calculate $I(\theta)$ and to substitute an outcome in the equation (3.22); the scattering on small angles in the correspondence with a Fridel rule can never be small, and the theory of repeated scattering would give single-error corrections compared to basic magnitude. The theory of perturbations works only because for small q the magnitude $S(q)$ is small, and for large q is small $v(q)$.

The similar reasoning allows establishing the difference between univalent and multivalent metals. In univalent metals the magnitude $S(q)$ is small approximately down to $q = 2k_F$, so that specific resistance is small on a comparison with what it would be, if the atoms were arranged chaotically. In multivalent metals both these magnitudes of a resistance are comparable.

5. Main Results and Analysis

The source file for all calculation is available in *Appendix 1*. The program made universal for any structure that will fulfil the method requirements. The program made universal for any structure that will fulfill the method requirements. The "Quick start" Guide on the program can be found in *Appendix 2*.

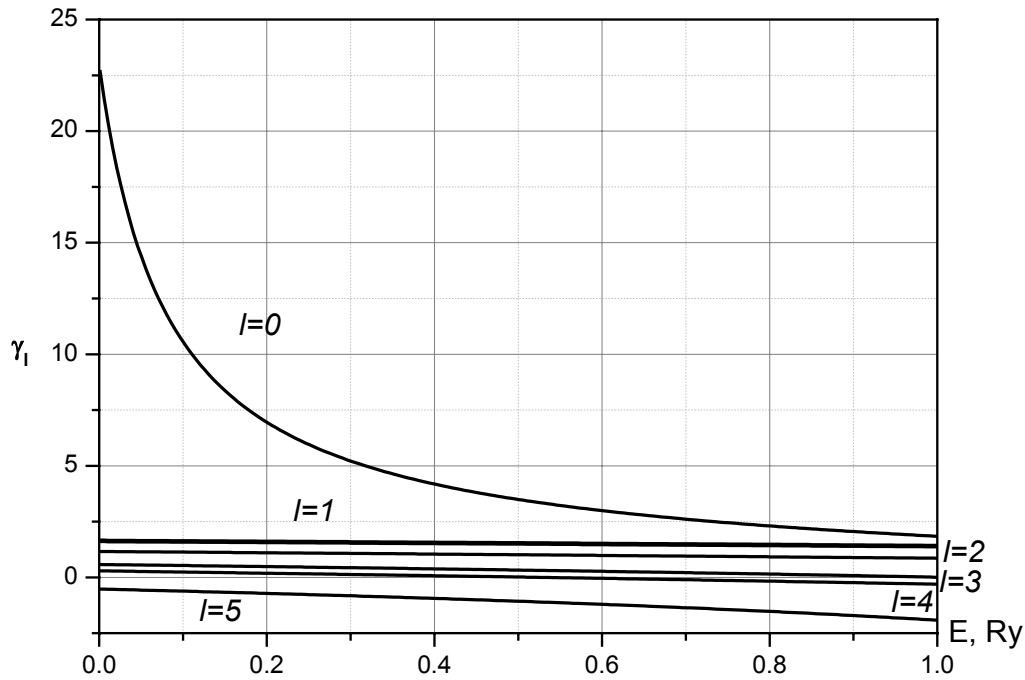


Figure 11. Logarithmic derivatives. MT-level=0,5 Ry.

This graph clearly illustrates the behaviour of logarithmic derivatives. Unfortunately, the only thing we can state about these functions is the fact that they must be smooth decay functions. As we can see this condition is fulfilled. Phase shifts are functions that are dependant of logarithmic derivatives. This dependence is realised through the tangent function. This function is not very convenient for the numerical calculations, because we will have a discontinuous jump in the place where tangent function changes its sign. But we know that these functions must be smooth, so we had to track the sign of tangent and in the place of jump and translocate the argument on \mathbf{PI} .

As we can see from the result on the calculation, the major contribution to the DOS give phase shifts with l numbers $0,1,2$. This result fully juxtaposes to the theory. Theoretical and experimental studies show that main scattering can be characterised by 1st three phase shifts. This can confirm the validity of our calculations.

As it is clear from the obtained graph, the density of electronic states (DOS) behaves how it was supposed in theory. The parabolic character of the given association shows, that we deal with metal. Thus, the obtained outcome is suitable for further use. However, there is one problem, is the MT-approximation of a potential is applicable for metals and how to choose the MT-zero level. For this purpose, we shall estimate the following graph, which shows variations of DOS at a modification of an MT-potential.

The analysis of the calculated graph gives us an opportunity to understand the behaviour DOS at a modification of an MT-potential. Varying this parameter we wanted to achieve such DOS dependence, which on an energy width would correspond the experimental data and previous studies. Thus, it would be possible to evaluate an MT-level for copper, and in further researches, probably advance this part of work. Thus, hereafter it would be possible to formulate the concept of an MT-potential for metals as a material class, not only copper.

In this case, it is possible to state, that MT-zero for copper is about 0,45 Ry, since the width of DOS graph (positive part) should be hardly less than 0,3 Ry. Later, in our calculations we will abide by this MT-level for copper.

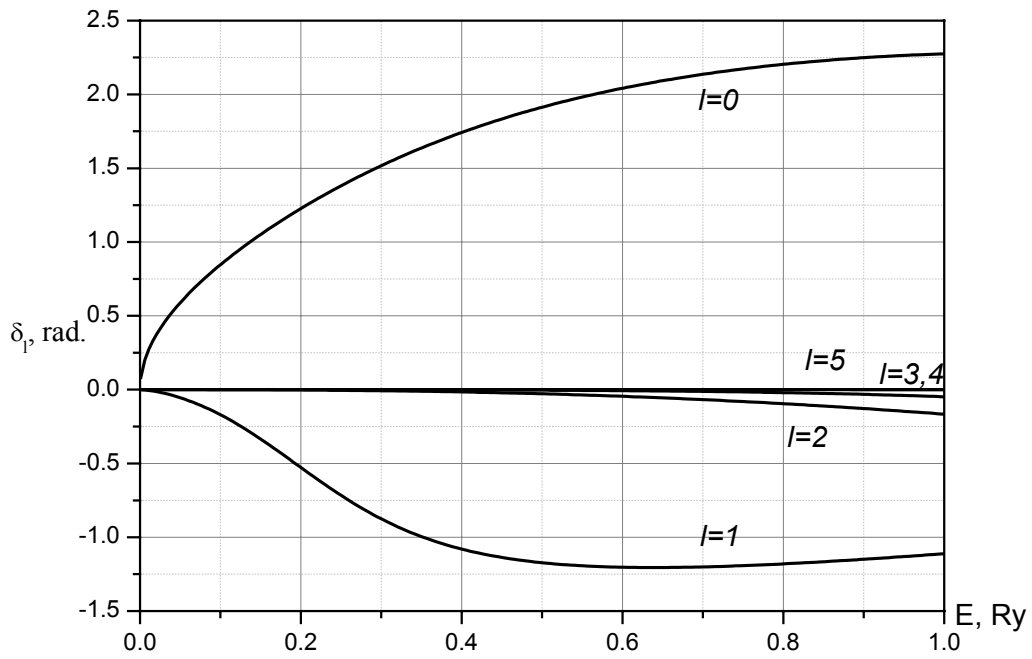


Figure 12. Phase shifts. MT-level=0,5 Ry.

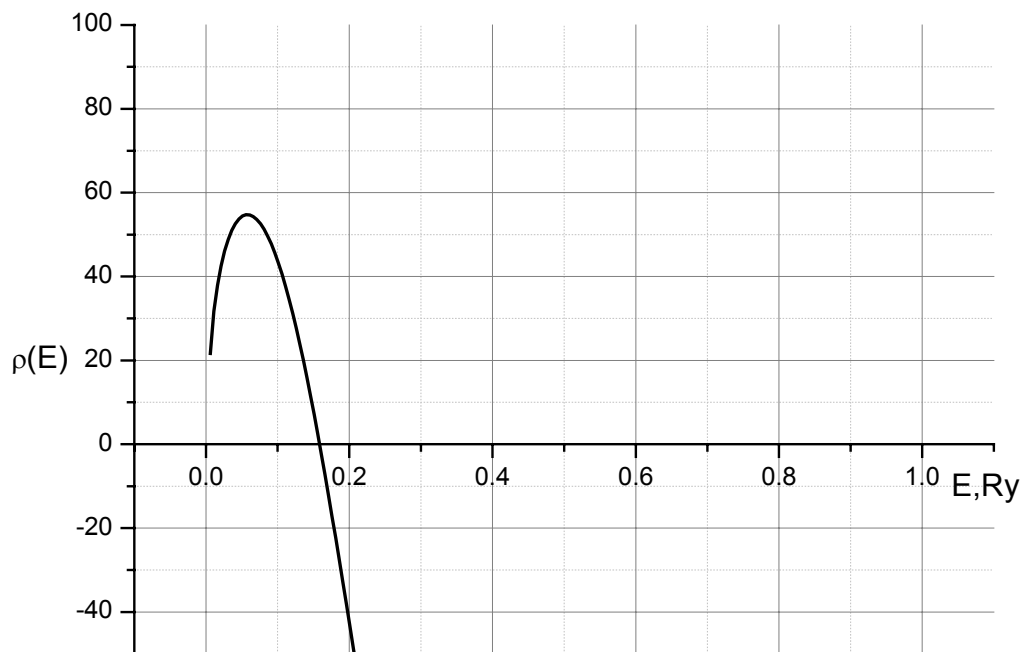


Figure 13. DOS for scatterer in vacuum. MT-level = 0,5 Ry.

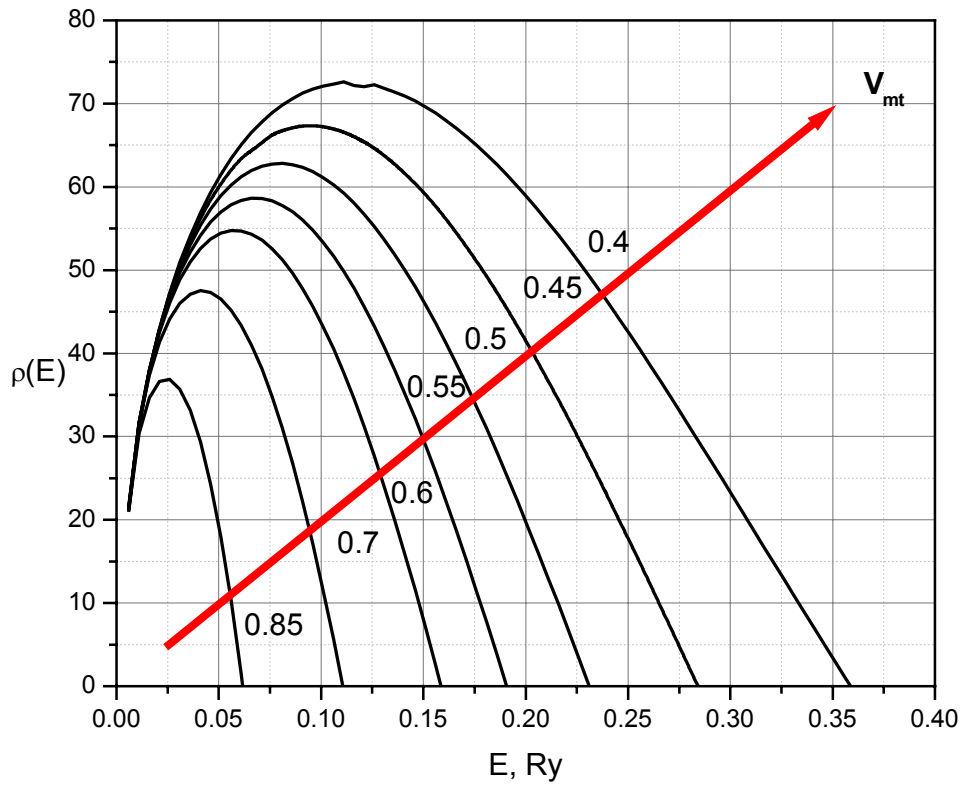


Figure 14. DOS for scatterer in vacuum. MT-level is an object of examination.

For the future task, like DOS for scatterer in medium calculation we need to find $\text{Im}A_l$. The search for this complex coefficient needs the knowledge of complex k wave numbers, which can be presented as $k=k_r+k_l$ and these numbers must be the (4.34) equation solution. In other words, we need to plot the dispersion curves for the scatterer in medium on the cluster border. To plot these curves, we must solve the (4.34) equation, where δ_l – phase shifts on the cluster border, which are calculated as usual (4.35). The γ_l on the cluster border can be found from the following formula:

$$\gamma_l(E, R_K) = k \frac{\cos \delta_l j_l'(kR_K) - \sin \delta_l n_l'(kR_K)}{\cos \delta_l j_l(kR_K) - \sin \delta_l n_l(kR_K)}$$

The equation (4.34) was numerically expanded into its real and imaginary part and after that, a system of two equations was solved using the Newton-Rafson method with a fixed energy level. The calculated graphs have parabolic character, which is fully compatible with other results (ex. [1]) and gives us evidence to suppose that future results will be also reliable. These curves will be essential for the DOS calculation for scatterer in medium for both one-atom cluster and many-atomic cluster.

Now, let's pass to the next set of graphs, the next step in calculation. This set corresponds to the specific resistance calculation. As it was mentioned above, we have to calculate potential in k space – $V(\mathbf{q})$ and the structural factor $S(\mathbf{q})$.

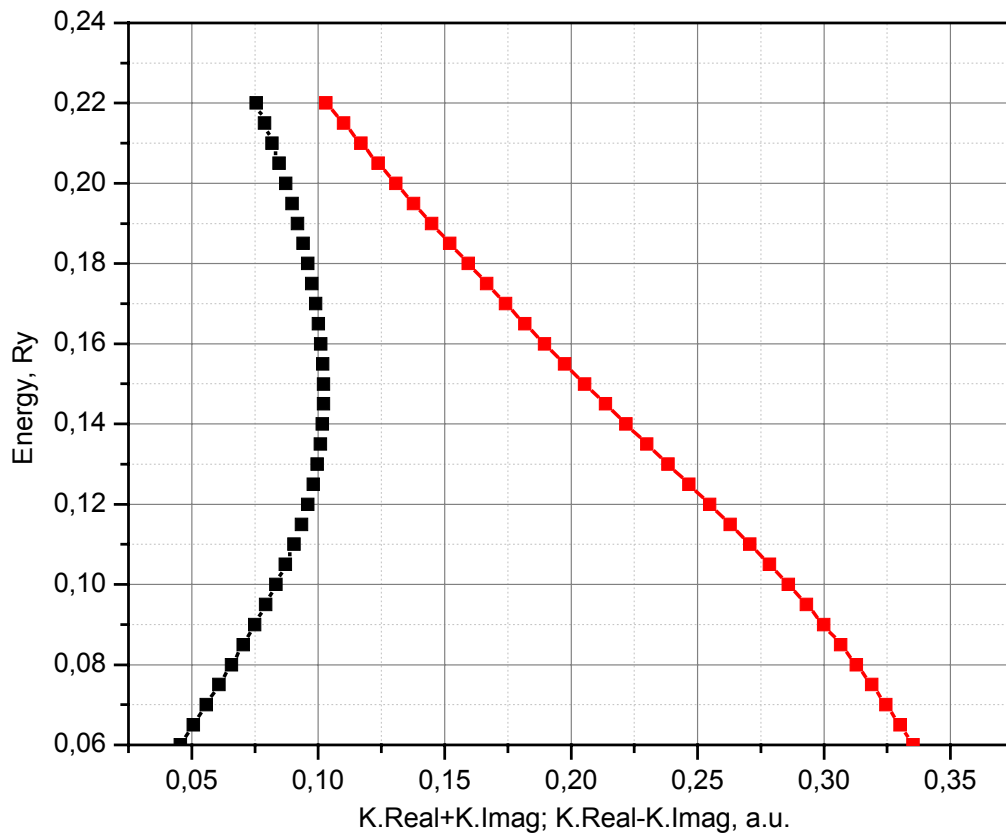


Figure 15. Dispersion curves on the cluster border.

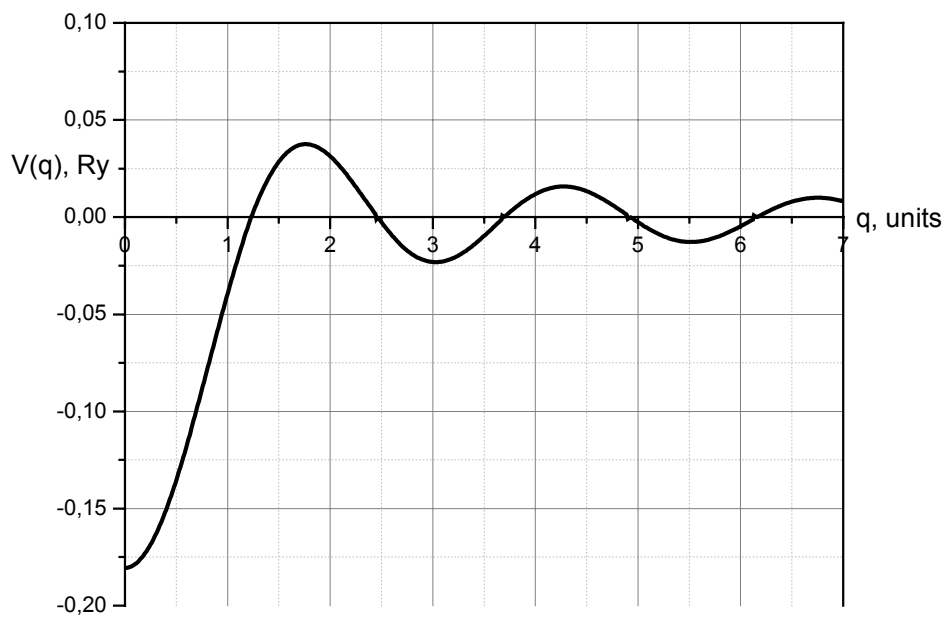


Figure 16. $v(q)$ potential. MT-level=0,45 Ry.

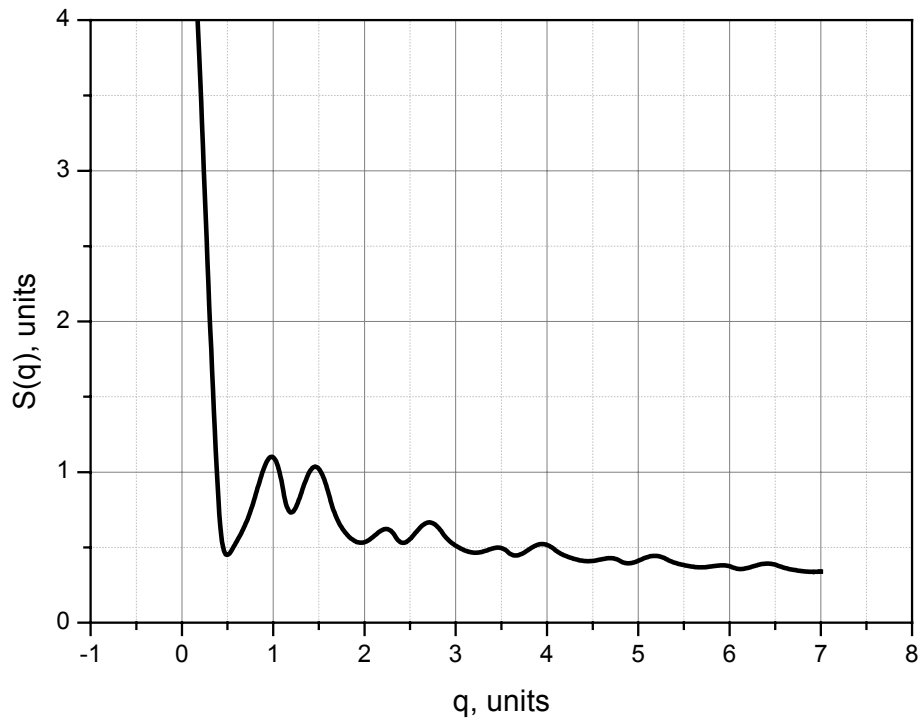


Figure 17. $S(q)$ structural factor. MT-level=0,45 Ry.

It is reasonable to analyze the previous two graphs together. Let's, first of all take a look on the graph $V(q)$. This graph can be compared with Animalou and Heine results (Figure 11). This quick comparison gives us the possibility to state that our calculation process and results are correct. From this graph we can also estimate the k_F value for univalent copper. This value corresponds to the first null of the function $V(q)$. This value, if estimated from graph, is about 1.28 \AA . Some other studies gives the value of 1.4 \AA . This difference is a result of different approaches and methods usage during the $V(r)$ potential calculation. This result can be also stated as a success of this study.

It is also very interesting to examine the $S(q)$ graph. In the calculation of the structural factor we used the one-atom cluster and supposed that the probability distribution function, which is a part of the structural factor (4.33) $P(R)$ is a Gaussian with the following form:

$$P(R) = \exp\left(-\frac{(r - 2R_{MT})^2}{\sigma^2}\right).$$

We suppose that we will definitely find a neighbour at the $2R_{MT}$ distance from the examined atom. Sigma also is an interesting parameter, because it can help us to control ordering in the system. The next graph shows the behavior of structural factor with the disorder growth in the system. As we can see, the peaks are degrading with the growth of σ .

This graph shows us the specific resistance behaviour with disorder growth in the system. It is obvious that this result is correct. The growth of disorder causes the localisation of free electron gas, this localisation in its turn causes the specific resistance growth.

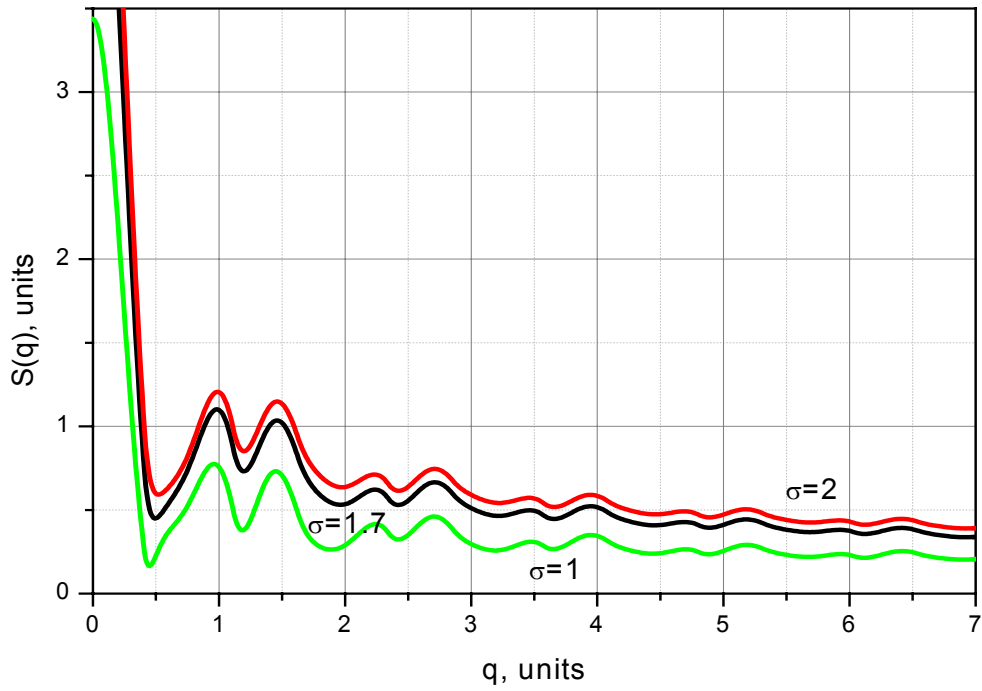


Figure 17. $S(q)$ structural factor dependence from Sigma. MT-level=0,45 Ry.

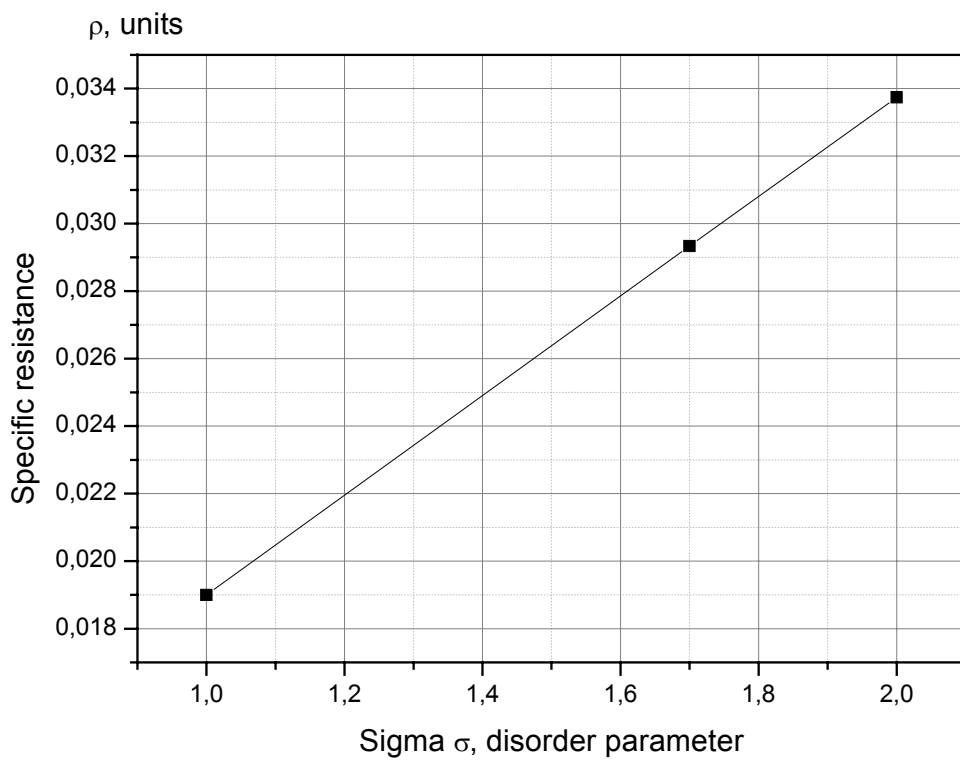


Figure 18. ρ – specific resistance. Sigma varies. MT-level=0,45 Ry.

6. Conclusion and main results

We can state that this work was a success. The main goal of this work was achieved. We studied methods of electronic structure numerical research. One of these methods was developed and successfully used in copper study. As a result of this part, the graph of pseudo potentials can be presented and their comparison with self-consistent calculations. The “liquid metal” model was studied also. Now we can state that we can use both “liquid metal” model and potential MT-approach for copper layers, but the MT-level choice strategy for metals in general needs to be developed later.

Another success of this works is DOS calculation on the base of pseudopotentials. These calculations show us that there are alternative, low-resource using methods of electronic structure calculation. Although, still a lot of research is to be done for this method successful development. The next valuable result may be the DOS for scatterer in medium calculation.

The developed method has clear perspectives for the electronic structure of defect states and other close-order defects calculation. On the base of calculated DOS function we could in future calculate electric and heat conductivity to compare them with experimental results.

The other consecutive step is the examination of “many-atom” cluster, which will bring us on the new level of disordered matter understanding. This calculation will lead to the properties of matter as is, it could also be a mechanism of cluster approach adaptability evaluation for the metals in general and copper specifically.

Another valuable result is specific resistance calculation simulation, the value of it in C units for copper layers lies between $\rho=1.67...1.9 \text{ Ohm/m}$. So we can state that calculation procedure is correct and it is another success.

The further development of the presented method can possibly simplify the electronic structure calculation procedure and, as a result, provides great money and time economy for the different poorly studied materials analysis.

References

- [1] Shunin Yu. N. (1982) Calculation of electronic density of states of disordered covalent compounds. Dr. Thesis. RCAEI-Physics Institute of Latv. Academy of Sciences, Riga. 200 p.
- [2] Mott N.F., Devis E.A. (1979) Electronic processes in non-crystalline materials. Clarendon Press, Oxford
- [3] Ziman J.M. (1979) *Models of Disorder*. Cambridge University Press, London-N.Y.-Melbourne 600 p.
- [4] Shunin Yu. N. Potentials and pseudopotentials (1998) *RAU Sci. Reports* **2**, 34-49
- [5] Shunin Yu. N. (1999) Total energy of solids in local density approximation. *Computer Modelling&New Technologies* **3**, 19-24
- [6] Madelung O. (1972) *Festkorpertheorie. 1,2*. Springer Verlag, Berlin-Heidelberg-N.Y. 413 S.
- [7] Global Design News. June 1999.126 p.
- [8] Kohn W., Rostoker N. (1954) Solution of Shroedinger equation in Periodic Lattices with Application to Metallic Lithium. *Phys. Rev.* **94**, 1111-1120.

APPENDIX 1. CALCULATION PROGRAM CODE (C++, MS VISUAL STUDIO 6.0)

Only calculation part is presented, the interface part may be different, so it does not.

```
#include "stdafx.h"
#include "calculus.h"
#include <stdio.h>
#include <conio.h>
#include <math.h>
#include <stdlib.h>
#include <string.h>
#define M_PI 3.141592653589793

/* Build: 09.06.01,success. <Vacuum OK> */

//////////Complex procedures definitions//////////
#include <complex>
using namespace std;
typedef complex<double> COMPLEX;
//////////
const
```

```

double A=1.05;
double Beta=0.003;
double AlphaB=0.66;
double Lambda=0.1837;
double mu=0.8853;
double r,dTheta,result,Theta,q,ar,rmx,Vmto,Rmt,En,dx,Alfa;
double Vo6,Vo6a,Vmt,Vmta,Rho_vac;
double Gamma[8][3000],Delta[8][3000];
double Vqi[3000],Sqi[3000];
int z,i,imax,l,k;
char fname[256];
FILE *datafile,*dfile,*datfile,*dtfile;

/////////////////////////////////////////////////////////////////
///////////////////////////////////////////////////////////////// Bessel-Neiman functions block/////////////////////////////////////////////////////////////////
/////////////////////////////////////////////////////////////////

double j(int l,double k, double R) {
    double result;
    if (l==0) {
        result=sin(k*R)/(k*R);
    }
    else if (l==1) {
        result=(sin(k*R)/(k*R)-cos(k*R))/(k*R);
    }
    else {
        result=j(l-1,k,R)*(2*l-1)/(k*R)-j(l-2,k,R);
    }
}

return(result);
}

double n(int l,double k,double R) {
    double result;
    if (l==0) {
        result=cos(k*R)/(k*R);
    }
    else if (l==1) {
        result=(cos(k*R)/(k*R)+sin(k*R))/(k*R);
    }
    else {
        result=n(l-1,k,R)*(2*l-1)/(k*R)-n(l-2,k,R);
    }
}

return(result);
}

double dj(int l,double k, double R) {
    double result;
    if (l==0) {
        result=-sin(k*R)/(k*R)-cos(k*R)/(k*R);
    }
    else {
        result=j(l,k,R)*(l-1)/(k*R)-j(l+1,k,R);
    }
}

return(result);
}

double dn(int l,double k,double R) {
    double result;
    if (l==0) {
        result=(cos(k*R)/(k*R)+sin(k*R))/(k*R);
    }
    else {
        result=n(l,k,R)*(l-1)/(k*R)-n(l+1,k,R);
    }
}

return(result);
}

/////////////////////////////////////////////////////////////////
double Quad(double r)
{ return(r*r); }
double mju(int par1) { /*Par1->Parameter 1, Z, atomic number*/
return(mu/pow(par1,0.333333333));
}
double lmju(void){
return(Lambda/mju(z));
}
double Am(void){

```

```

return((A/mju(z))/(1+(A*r/mju(z))));
}
double f(double r) {
double func;
func=(exp(-Lambda*r/mju(z))/(1+(A*r/mju(z))));
return(func);
}
double fprim(void) {
double func1;
func1=-lmju()*f(r)-Am()*f(r);
return(func1);
}
double fp2(void) {
double func2;
func2=-(lmju()+Am())*fprim()+Am()*Am()*f(r);
return(func2);
}
double fp3(void) {
double func3;
func3=-2*Am()*Am()*Am()*f(r)+2*Am()*Am()*fprim()-(lmju()+Am())*fp2();
return(func3);
}
double fp4(void) {
double func4;
func4=6*Am()*Am()*Am()*Am()*f(r)-6*Am()*Am()*Am()*fprim()+3*Am()*Am()*fp2()-(lmju()+Am())*fp3();
return(func4);
}
double rho(double r) {
double rf;
rf=(-z/(4*M_PI*r)*fp2());
return(rf);
}
double rho1(double r) {
double rfunc2;
rfunc2=(z/(4*M_PI*r))*(fp3()-fp2()/r);
return(rfunc2);
}
double rho2(double r) {
return((z/(4*M_PI*r))*(fp4()-2*fp3()/r+2*fp2()/(r*r)));
}
double Pot_Gash(double r) {
double result;
result=-2*z/r*f(r);
return(result);
}
////////////////////////////////////////////////////////////////////////////////////////////////////////////////////////////////
// Isolated atom calculus.//////////////////////////////////////////////////////////////////////////////////////////////////////////////////////////////////
////////////////////////////////////////////////////////////////////////////////////////////////////////////////////////////////

double G(double r) {
double Gfunc;
Gfunc=4/3*(rho1(r)/rho(r))*(rho1(r)/rho(r))-2*rho2(r)/rho(r);
return(Gfunc);
}

double Vxs(double r) {
double Vfunc,param;
param=(3*rho(r)/(8*M_PI));
if (param>=0)
    Vfunc=-6*pow(param,0.3333333);
else
    Vfunc=6*pow(fabs(param),0.3333333);
return(Vfunc);}

double Vo6m(double r) {
double result;
result=-AlphaB*(1+tanh(Beta/AlphaB*Gat(r)))*Vxs(r);
return(result);
}

double Vo6ma(double r) {
double result_a;

```

```

        result_a=-6*Alfa*pow((3*rho(r)/(8*M_PI)),0.3333333);
return(result);
}

int Calc_atomic(int A_number, double Alpha,double rmax, double dr, CString strFname, BOOL ctype, BOOL restype) {
    r=0.01;
    i=0;
    z=A_number;
    sprintf(fname,"%s",strFname);
    datafile=fopen(strcat(fname,".dat"),"w");

        while(r<=rmax) {
            Vo6=Pot_Gash(r)+Vo6m(r);
            Vo6a=Pot_Gash(r)+Vo6ma(r);

            switch(restype) {
            case 0:
                fprintf(datafile,ctype?"%f %f %f %f\n":"%f %f\n",r,Vo6a,r/mju(z),Vo6a*r/(2*z));
                break;
            case 1:
                fprintf(datafile,ctype?"%f %f %f %f\n":"%f %f\n",r,Vo6,r/mju(z),Vo6*r/(2*z));
                break;
            case 2:
                fprintf(datafile,ctype?"%f %f %f %f %f\n":"%f %f
%f\n",r,Vo6,Vo6a,r/mju(z),Vo6*r/(2*z),Vo6a*r/(2*z));
                break;
            }

            r=r+dr;
        }

        fclose(datafile);
        rmx=rmax;
return 0;}

//////////////////////////////////////
// Atom system (+1 neighbour) calculus.//////////////////////////////////////
//////////////////////////////////////

double Gat(double r) {
    double Gfunc;
        Gfunc=4/3*((rho1(r)-rho1(ar-r))/(rho(r)-rho(ar-r))*((rho1(r)-rho(ar-r))/(rho(r)-rho(ar-r)))-2*(rho2(r)-rho2(ar-r))/(rho(r)-
rho(ar-r)));
    return(Gfunc);
}

double Vxsat(double r) {
    double Vfunc,param;
    param=(3*(rho(r)+rho(ar-r))/(8*M_PI));
        if (param>=0)
            Vfunc=-6*pow(param,0.3333333);
        else
            Vfunc=6*pow(fabs(param),0.3333333);
return(Vfunc);}

double Vo6m_at(double r) {
    double result;
        result=-AlphaB*(1+tanh(Beta/AlphaB*Gat(r)))*Vxsat(r);
return(result);
}

double Vo6ma_at(double r) {
    double result_a;
        result_a=-6*Alfa*pow(fabs((3*(rho(r)+rho(ar-r))/(8*M_PI))),0.3333333);
return(result);
}

int Calc_struct(int A_number, double Alpha,double rmax, double dr,double lvl_mt, CString strFname, BOOL ctype, BOOL restype)
{
    r=0.01;
    i=0;
    z=A_number;
    sprintf(fname,"%s",strFname);
    datafile=fopen(strcat(fname,".dat"),"w");
}

```

```

    sprintf(fname,"%s",strFname);
    datfile=fopen(strcat(fname,"_mt.dat"),"w");
    ar=2*(rmax/0.529);
    Rmt=rmax/0.529;
    Vmto=lv1_mt;
    do
    {
        Alfa=Alpha;
        Vo6=Pot_Gash(r)+Pot_Gash(ar-r)+Vo6m_at(r);
        Vo6a=Pot_Gash(r)+Pot_Gash(ar-r)+Vo6ma_at(r);
        Vmt=Vo6-Vmto;
        Vmta=Vo6a-Vmto;

        switch(restype)
        {
            case 0:
                fprintf(datafile,ctype?"%f %f %f %f\n":"%f
%f\n",r,Vo6a,r/mju(z),Vo6a*r/(2*z));
                fprintf(datfile,ctype?"%f %f %f %f\n":"%f
%f\n",r,Vmta,r/mju(z),Vmta*r/(2*z));
                break;
            case 1:
                fprintf(datafile,ctype?"%f %f %f %f\n":"%f
%f\n",r,Vo6,r/mju(z),Vo6*r/(2*z));
                fprintf(datfile,ctype?"%f %f %f %f\n":"%f
%f\n",r,Vmt,r/mju(z),Vmt*r/(2*z));
                break;
            case 2:
                fprintf(datafile,ctype?"%f %f %f %f %f %f\n":"%f %f
%f\n",r,Vo6,Vo6a,r/mju(z),Vo6*r/(2*z),Vo6a*r/(2*z));
                fprintf(datfile,ctype?"%f %f %f %f %f %f\n":"%f %f
%f\n",r,Vmt,Vmta,r/mju(z),Vmt*r/(2*z),Vmta*r/(2*z));
                break;
        }

        r=r+dr;
    } while(r<=ar/2);
    dx=dr;
    fclose(datafile);
    fclose(datfile);
    rmx=ar/2;

return 0;}

int Fourier(CString strFname, double qmax, double dq, double dr) {
dTheta=0.01;
COMPLEX Fnc;
double Rk,Tst,Vq,qrem,Vmt2;
int norma,qi;
COMPLEX Int1,Int2;

sprintf(fname,"%s",strFname);
dfile=fopen(strcat(fname,"_ft.dat"),"w");

norma=-1;
qrem=0;
q=0;
qi=0;

do {
r=0.01;
Tst=0;
Fnc=COMPLEX(0,0);
do {
    Theta=0;
    Fnc=COMPLEX(0,0);
    do {
        Int1=exp(COMPLEX(0,q*r*cos(Theta)))*sin(Theta);
        Int2=exp(COMPLEX(0,q*r*cos(Theta+dTheta)))*sin(Theta+dTheta);
        Fnc=Fnc+(Int1+Int2)*dTheta/COMPLEX(2,0);
        Theta=Theta+dTheta;
        Tst=abs(Fnc);
    } while (Theta<M_PI);
}

```

```

Vmt=Pot_Gash(r)+Pot_Gash(ar-r)+Vo6m_at(r)-Vmt0;
Vmt2=Pot_Gash(r+dr)+Pot_Gash(ar-r+dr)+Vo6m_at(r+dr)-Vmt0;
Rk=abs(Fnc)*atan(arg(Fnc));
Tst=Tst+(Vmt*r-Vmt2*(r+dr))*dr/2*Rk;

r=r+dr;
} while(r<=Rmt);
Vq=3/(2*Rmt*Rmt*Rmt)*Tst;
if (Vq<=dq/10&&(q-qrem)>0.3) {
    norma=norma*(-1);
    qrem=q;}

if (norma<0) {
fprintf(dfile,"%f %f\n",q,-Vq);
}
else {
fprintf(dfile,"%f %f\n",q,Vq);
}
Vqi[q]=Vq;
q=q+dq;
qi++;
} while (q<=qmax);

fclose(dfile);
return 0;
}

double f1(double xp,double yp,double zp) {
float U,result;

U=(Pot_Gash(xp)+Pot_Gash(ar-xp)+Vo6ma_at(xp)-Vmt0);
result=(U-En)*yp-(2/xp)*(1+1)*zp;
return(result);
}

double f2(double xp,double yp,double zp) {
float U,result;

U=(Pot_Gash(xp)+Pot_Gash(ar-xp)+Vo6ma_at(xp)-Vmt0);
result=((1*(1+1))/(xp*xp)+U-En)*yp-2*zp/xp;

return(result);
}

double Shroedinger(void) {
double h,dy,dz;
double x[3000], y[3000], z[3000];
double k1,k2,k3,l1,l2,l3;
int i;
h=0.01;
x[0]=dx;y[0]=1;z[0]=0; // Initial conditions; z=y'.
i=1;
while(x[i-1]<rmx) {
if (x[i-1]<=1) {
    k1=h*z[i-1];
    l1=h*f1(x[i-1],y[i-1],z[i-1]);
    k2=h*(z[i-1]+1/3);
    l2=h*f1(x[i-1]+h/3,y[i-1]+k1/3,k2/h);
    k3=h*(z[i-1]+2*12/3);
    l3=h*f1(x[i-1]+2*h/3,y[i-1]+2*k1/3+2*h*11/9,k3/h);

    dy=k1/4+3*k3/4;
    dz=l1/4+3*l3/4;

    x[i]=x[i-1]+h;
    y[i]=y[i-1]+dy;
    z[i]=z[i-1]+dz;
}
else {

```

```

k1=h*z[i-1];
l1=h*f2(x[i-1],y[i-1],z[i-1]);
k2=h*(z[i-1]+1/3);
l2=h*f2(x[i-1]+h/3,y[i-1]+k1/3,k2/h);
k3=h*(z[i-1]+2*I2/3);
l3=h*f2(x[i-1]+2*h/3,y[i-1]+2*k1/3+2*h*11/9,k3/h);

dy=k1/4+3*k3/4;
dz=l1/4+3*l3/4;

x[i]=x[i-1]+h;
y[i]=y[i-1]+dy;
z[i]=z[i-1]+dz;
    }
i++;
}

return(z[i-1]/y[i-1]);
}

Gamma_calc(CString strFname,int lmax, double Emax, double dE) {
char strTemp[256];

for(l=0;l<=lmax;l++) {
    sprintf(fname,"%s",strFname);
    sprintf(strTemp,"%i",l);
    strcat(fname,strTemp);
    dfile=fopen(strcat(fname,"_gamma.dat"),"w");
    k=0;
    do {
        En=0.001+k*dE;
        Gamma[l][k]=Shroedinger();
        fprintf(dfile,"%f %f\n",En,Gamma[l][k]);
        k++;
    } while(En<=Emax);

    fclose(dfile);
}
return 0;
}

int Delta_calc(CString strFname,int lmax, double Emax, double dE) {
double q;
double tang[3000];
bool c5,c6;
char strTemp[256];

for(l=0;l<=lmax;l++) {
    sprintf(fname,"%s",strFname);
    sprintf(strTemp,"%i",l);
    strcat(fname,strTemp);
    dfile=fopen(strcat(fname,"_delta.dat"),"w");
    En=0.001;
    k=0;
    do {
        En=0.001+k*dE;
        q=sqrt(En);
        tang[k]=(q*dj(l,q,Rmt)-Gamma[l][k]*j(l,q,Rmt))/(q*dn(l,q,Rmt)-Gamma[l][k]*n(l,q,Rmt));
        Delta[l][k]=atan(tang[k]);
        c5=Delta[l][k]>0&&Delta[l][k-1]<0&&fabs(Delta[l][k]-Delta[l][k-1])>1;
        c6=Delta[l][k]<0&&Delta[l][k-1]>0&&fabs(Delta[l][k]-Delta[l][k-1])>1;
        if (c5) {
            tang[k]=(q*dj(l,q,Rmt)-Gamma[l][k]*j(l,q,Rmt))/(q*dn(l,q,Rmt)-
Gamma[l][k]*n(l,q,Rmt));
            Delta[l][k]=atan(tang[k])-M_PI;
        }
        if (c6) {
            tang[k]=(q*dj(l,q,Rmt)-Gamma[l][k]*j(l,q,Rmt))/(q*dn(l,q,Rmt)-
Gamma[l][k]*n(l,q,Rmt));
            Delta[l][k]=atan(tang[k])+M_PI;
        }
        fprintf(dfile,"%f %f\n",En,Delta[l][k]);
        k++;
    }
}
}

```

```

        } while(En<=Emax);

        fclose(dfile);
    }
return 0;
}

double J_l(int l,double q, double R) {
double result;
result=cos(Delta[l][k])*j(l,q,R)-sin(Delta[l][k])*n(l,q,R) ;
return(result);
}

int Rho_calc(CString strFname,int lmax, double Emax, double dE) {
double q,sum;
En=0.001+dE;
Rho_vac=0;
sprintf(fname,"%s",strFname);
dfile=fopen(strcat(fname,"_rho_vac.dat"),"w");
sprintf(fname,"%s",strFname);
datfile=fopen(strcat(fname,"_rho_vac_prc.dat"),"w");
k=1;
    do {
        for(l=0;l<=lmax;l++) {
            q=sqrt(En);
            sum=(2/M_PI)*(2*l+1)*((Delta[l][k+1]+Delta[l][k-1])/(2*dE)-
(Rmt*Rmt*J_l(l,q,Rmt)*J_l(l,q,Rmt))/2*(((Gamma[l][k+1]-Gamma[l][k-1])*2*q)/(2*dE)));
            Rho_vac=Rho_vac + sum;
            fprintf(datfile,"%f %f\n",En,Rho_vac);
        }
        fprintf(dfile,"%f %f\n",En,Rho_vac);
        k++;
        En=0.001+k*dE;
        Rho_vac=0;
    } while(En<=Emax-dE);
fclose(dfile);
fclose(datfile);
return 0;
}

int SFactor(CString strFname, double qmax, double dq, double dr, double Sgm) {
dTheta=0.01;
COMPLEX Fnc,Fnct,Fnct1;
double Rk,Tst,Sq,Pr,Pr1,Sigma;
int qi;

sprintf(fname,"%s",strFname);
dfile=fopen(strcat(fname,"_str.dat"),"w");
q=0;
qi=0;
Sigma=Sgm;
if (Sigma==0) Sigma=1.5;
do {
    r=0.01;
    Tst=0;
    Fnc=COMPLEX(0,0);
    do {
        Theta=0;
        Fnc=COMPLEX(0,0);
        do {
            Fnct=exp(COMPLEX(0,q*r*cos(Theta)));
            Fnct1=exp(COMPLEX(0,q*r*cos(Theta+dTheta)));
            Fnc=Fnc+(Fnct*Fnct+COMPLEX(2,0)*Fnct+Fnct1*Fnct1+COMPLEX(2,0)*Fnct1)*0.5*dTheta;
            Theta=Theta+dTheta;
        } while (Theta<M_PI);

        Pr=exp(-(r-2*Rmt)*(r-2*Rmt)/(Sigma*Sigma));
        Pr1=exp(-(r+dr-2*Rmt)*(r+dr-2*Rmt)/(Sigma*Sigma));
        Rk=abs(Fnc);
        Tst=Tst+(Pr*r+Pr1*(r+dr))*0.5*dr*Rk;
    }
}

```

```

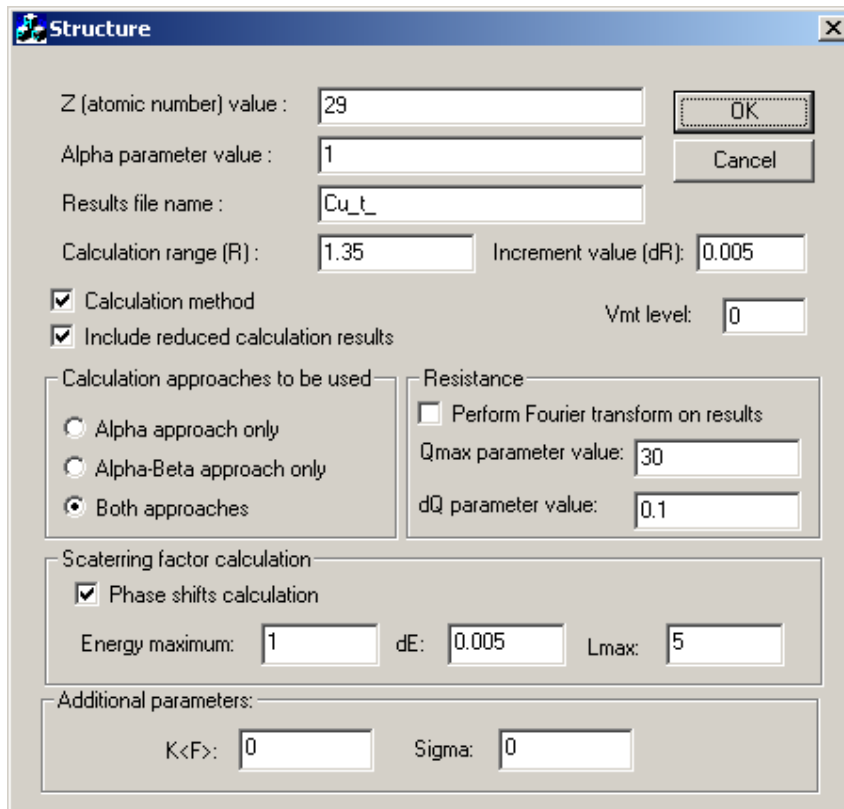
r=r+dr;
} while(r<=2*Rmt);
Sq=3/(2*Rmt*Rmt*Rmt)*Tst;
fprintf(dfile,"%f %f\n",q,Sq);
Sq[i]=Sq;
q=q+dq;
qi++;
} while (q<=qmax);

fclose(dfile);
return 0;
}

int Resistance(CString strFname,double dq, double kFrm) {
double res,retrn,kf;
double e,h,vf;
e=0.511/13.6; // MeV
h=0.659; /*10E-15
vf=1;
i=0;
q=0.0;
res=0;
kf=kFrm;
if (kf==0) kf=1.44;
while(q<=kf) {
res=res+(Vqi[i]*Vqi[i]*Sq[i]*q*q+Vqi[i+1]*Vqi[i+1]*Sq[i+1]*(q+dq)*(q+dq)*(q+dq))*dq/2;
q=q+dq;
i++;
}
retrn=res/(4*q*q*q*q)*(3*M_PI/((4/3*M_PI*Rmt*Rmt*Rmt)*h*h*e*vf*vf));
sprintf(fname,"%s",strFname);
dfile=fopen(strcat(fname,"_res.dat"),"w");
fprintf(dfile,"%f\n",retrn);
fclose(dfile);
return 0;
}
}

```

APPENDIX 2. “QUICK START” GUIDE.



This section covers main parameters of the program and defines main calculation procedures used.

Common parameters:

Z (atomic number) – this parameter is essential for the pseudopotential calculations, defined by the Mendeleev table.

α (alpha parameter) – this parameter is used in Xα-Slater calculation of the pseudopotential.

Results file name – defines file name and path for the calculation results to be stored, for every calculation part is created an individual file.

Calculation range (or Atomic radius) – defines the up-limit in integration on *r* parameter.

Calculation method checkbox changes calculation objects: isolated atom (*Calculation range*) or atom in medium (*Atomic radius*).

Increment value(dR) – integration step.

V_{mt} level – simulation parameter, defines the MT-level.

Reduced calculation results – includes in main (potential) file relational (to the maximum) calculation results.

Calculation approaches to be used – defines the calculation approaches for potential calculation.

Resistance – group box, defines the calculation parameters for the specific resistance calculation.

Q_{max} – defines the up-integration level in *q*-space.

dQ - integration step in *q*-space.

Scattering factor calculation – group box, defines the calculation parameters for the DOS calculation.

E_{max}(Energy maximum) – defines the up-integration level on energy axis.

dE - integration step on energy axis.

L_{max} – defines the number of partial contributions to be taken into consideration.

Additional parameters – group box, defines the additional calculation parameters.

K_F – defines the Fermi level in *q*-space for the material.

Sigma - defines disorder parameter for the structural factor.

All integration procedures were made using the trapezoid method, therefore we do not recommend the number of point > 775, after this value the integration mistake will grow rapidly.

The numerical solution of Shroedinger equation is made using forth-order Runge-Kutt method.

APPENDIX

A. Copper properties overview

TABLE A1. General and Atomic Properties of Copper

Atomic Number	29
Atomic Weight	63.546
Atomic Diameter	2.551×10^{-10} m
Melting Point	1356 K
Boiling Point	2868 K
Density at 293 K	8.94×10^3 kg/m ³
Electronic Structure	3d ¹⁰ 4s
Valence States	2,1
Fermi Energy	7.0 eV
Fermi Surface	Spherical, necks at [111]
Hall Coefficient	-5.12×10^{-11} m ³ /(A·S)
Magnetic State	diamagnetic
Heat of Fusion	134 J/g
Heat of Vaporization	3630 J/g
Heat of Sublimation at 1299 K	3730 J/g

TABLE A2. Crystallographic Features of Copper

Type of Structure	A1
Space Group	O _h ⁵ - Fm3m
Crystal Structure	face-centered cubic
Number of Atoms per Unit Cell	4
Lattice Parameters at 293 K Distance of	3.6147×10^{-10} m
Closest Atomic Approach (Burgers vector) at 293	2.556×10^{-10} m
Goldschmidt Atomic Radii (12-fold coordination)	1.28×10^{-10} m
Atomic Volume	1.182×10^{-29} m ³

TABLE A3. Some additional info on copper.

Bulk properties	
Density of solid [kg m^{-3}]	8920.
Molar volume [cm^3]	7.11
Velocity of sound [m s^{-1}]	3570.
Elastic properties	
Youngs modulus [GPa]:	130
Rigidity modulus [GPa]:	48
Bulk modulus [GPa]:	140
Poissons ratio [no units]:	0.34
Hardnesses	
Mineral hardness [no units]	3.0.
Brinell hardness [MN m^{-2}]	874
Vickers hardness [MN m^{-2}]	369
Electrical properties	
Electrical resistivity [$/10^{-8} \text{ W m}$; or mW cm]	1.7
Optical properties	
Reflectivity [%]	90
Crystal Structure	
Space group:	Fm-3m
Space group number:	225
Structure:	ccp (cubic close-packed).

Received on the 1st of September 2001

DIFFUSION PROCESSES CAUSED BY PLASMA IMMERSION ION IMPLANTATION AND DEPOSITION (PI³&D)

A.E. KIV and E.P. BRITAVSKAYA

*Department of Materials Engineering, Ben-Gurion University of the Negev, Beer-Sheva,
 74895, Israel, e-mail: kiv@bgumail.bgu.ac.il*

Plasmon-activation processes accompanying PI³&D are considered. It is shown that an interaction of low-energy ions with solid surfaces leads to generation of plasmons, which relax by local transferring to crystal lattice the necessary thermal energy for diffusion activation.

Keywords: plasmons, low energy ion implantation

1. Introduction

The PI³&D technique opens new routs for modification of surface properties of three-dimensional objects by accelerated plasma ions treatment and allows to form thin surface layers of allows with unique characteristics [1,2].

The mechanisms of PI³&D are more complex comparing to those involved in conventional ion implantation technique. This is because of the particular characteristics of plasma ions with regard to their energetic and charge distributions, because the high ion beam densities, and because the combined effect of the implantation and deposition processes during PI³. Substantial damage of the atomic lattice caused by the penetration of the plasma ions reduces its stability and lead to the formation of new crystalline phases or even amorphous zones. The incorporation of the implanted ions into atomic lattice also results in formation of regions of high compressive stresses close to the surface. All these changes in the near surface layers caused by PI³ can produce a significant hardening and strengthening effect, and the mechanical properties of the material can be substantially modified. In principle, by means of PIII&D technology it is possible to increase significantly the fatigue lifetime, to enhance the oxidation resistance, to improve the tribological properties, and to modify a wide range of other materials parameters. Radiation-induced diffusion [3] plays an important role in the processes of PI³&D. In this paper we presented results explaining plasmon-induced activation processes, which influence on the final picture of PI³&D. In Sections 2 and 3 we discuss the questions of plasmons formation and their parameters. In Section 4 plasmon-induced processes of diffusion are considered.

2. Formation of plasmons in processes of PI³&D

Penetration of charged particles to solids leads to formation of plasmons [4]. The plasma oscillations frequency is determined by characteristics of the valent electrons, but in the case of transition metals the deep electrons also participate in the formation of plasma oscillations (PO). PO may be caused also by local charges Z appearing in the processes of irradiation of the matter by charge particles. In the last case the probability of plasmons generation $W \neq 0$, if the life time of the local charges $\tau > 1/\omega_p$ (ω_p is the frequency of plasmons). The equation of dispersion for the long wave plasma oscillations is

$$\omega^2(\mathbf{k}) = \omega_p^2 + \frac{\gamma}{mn_0} k^2, \quad (1)$$

where γ is the elastic modulus of the electronic gas, m is the electronic mass, n_0 is the electronic density, \mathbf{k} is the wave vector and

$$\omega_p^2 = 4\pi e^2 n_0 / m. \quad (2)$$

The value of the plasmon energy is $\varepsilon_p = \hbar\omega \approx 10eV$. The values of ε_p for some metals are presented in the TABLE 1.

TABLE 1

Metal	Be	Al	Mg	Cu	Ag
$\eta\omega_p, eV$	19	15	10	20	23

The probability that the local charge Z , which aroused in the irradiated specimen, will result the plasmon generation is:

$$W = \sum_q \frac{2\pi Z^2}{\Omega \eta \omega_p} \frac{1}{q^2}, \quad (3)$$

where Ω is the specific atom volume. The final expression is:

$$W = \frac{Z^2 e^2 k_1}{\pi \varepsilon_p}, \quad (4)$$

where $k_1 = \frac{\omega_p}{V_F}$ is the limit wave vector of plasmons, V_F is the velocity of Fermi electrons. For

$\varepsilon_p = \eta\omega \approx 10eV$ and $k_1 \sim 10^7 \text{ sm}^{-1}$ we have $W \approx 0.05 \cdot Z^2$.

The relaxation of plasmons is caused by their interaction with phonons, impurities and various structural imperfections. The decay of plasmons leads to an energy release in a local volume and in the short time τ_r , which is less than all relaxation times in the crystal. Thus we may consider a phenomena, caused by the plasmon energy releasing, as a point flash-up of an energy in a crystal. In metals the thermal conductivity coefficient of electrons is so large that for the time of electron-lattice relaxation the energy transferred to the electron subsystem is spreading over the large distances. On the other hand, the lattice thermal conductivity coefficient is small, and we get in the lattice subsystem a high temperature splash in a short time interval. The relaxation of this local energy splash results in activation of diffusion processes and structural transformations in the crystal.

3. Mechanisms of plasmon relaxation

The relaxation of high temperature splash in the crystal lattice may be investigated on the basis of equations [5]:

$$c_e \frac{\partial T_e}{\partial t} = k_e \Delta T_e - \alpha (T_e - T_j), \quad (5a)$$

$$c_j \frac{\partial T_j}{\partial t} = k_j \Delta T_j - \alpha (T_j - T_e) \quad (5b)$$

which are differed from the usual equations of thermal conductivity by second terms on the right side. $c_{e,j}$ is

a heat capacity and $\chi_{e,j} = \frac{k_{e,j}}{c_{e,j}}$ is a coefficient of the temperature conductivity. Indexes "e" and "j" relate to

electron and atom subsystems. " α " characterizes the energy exchange between mentioned subsystems.

The equations (5) may be solved in limit cases of different correlation of relaxation times τ_e and τ_j in electronic and lattice subsystems accordingly.

Here we present the qualitative analysis of the system (5). The initial conditions are:

$$T_e(t=0) = \frac{\varepsilon_e}{c_e} f(r), \quad (6a)$$

$$T_j(t=0) = \frac{\varepsilon_j}{c_j} f(r). \quad (6b)$$

$f(r)$ characterizes the energy distribution in the energy source region.

On the basis of (5) and (6) and by using the principle of dimensions one can write:

$$T_e \rho^3 \approx \frac{\varepsilon_e}{c_e}, \quad (7a)$$

$$T_j \rho^3 \approx \frac{\varepsilon_j}{c_j}. \quad (7b)$$

Here it was assumed that the specific gravity is equal to one.

In fact, equations (7) mean that the plasmon energy transfer to the internal energy of one of e, j subsystems. The energy relaxation in the electronic subsystem finishes for $10^{-16} - 10^{-17}$ s. Any structural transformations are impossible during this time interval. The relaxation time for lattice subsystem $10^{-11} - 10^{-12}$ sec. This time is enough for diffusion processes activation and structural changes in the system arising. The last effects may be large in spite of $\varepsilon_j / \varepsilon_e \approx 3 - 5\%$.

Now we shall discuss the evolution of energy flash up in the electronic subsystem and shall discuss a possibility to get a solution of equations (6). We start from the suggestion that $t_e \ll t_j$. While we shall investigate the time intervals, when it is possible to neglect the lattice temperature changes, it reasonable to use a new variable $\theta = T_e - T_j$ and then to rewrite (5) as:

$$c_e \frac{\partial \theta}{\partial t} = k \Delta \theta - \alpha \theta. \quad (8)$$

The last equation describes now the electron temperature changes. It may be shown that for $T = \text{const}$ $\rho(t)$ has a form :

$$\rho^3 = \frac{\varepsilon}{\pi c_e \theta} \tau \left(\ln \frac{1}{\tau} - \beta \tau \right), \quad (9)$$

where $\beta = t_\theta / t_e$, $\tau = t / t_\theta$ and $t_\theta = \varepsilon / 4\pi c_e \chi_e \theta$. (Here is $\varepsilon \approx \varepsilon_e$).

(9) is considered only for $\tau < \tau_1$, where τ_1 is a solution of an equation:

$$\ln \frac{1}{\tau} = \beta \tau. \quad (10)$$

The dependence $\rho^3(\tau)$ may be seen in the Figure 1.

It is convenient for the further analysis to introduce the four-dimensional space-time volume in which the temperature is larger then the given one:

$$\Omega = \rho^3 t. \quad (11)$$

Another expression for Ω is:

$$\Omega_e = \frac{\varepsilon_e^2}{c_e^2 T_e^2 k_e \Gamma} \quad (12)$$

Ω_e may be also represented as:

$$\Omega_e = \int_0^{\tau_1} \rho^3(\tau) \tau d\tau \quad (13)$$

Then the calculations give:

$$\Omega_e \approx \frac{\varepsilon^2}{16\pi k_e c_e^2 \theta^2} \left(1 - \frac{4}{3} \beta \right), \theta \gg \frac{\varepsilon}{4\pi k_e t_p c_e}, \quad (14a)$$

$$\Omega_e \approx \frac{5}{12} \frac{\varepsilon^3}{(4\pi k_c r^2)^2 c_e^3 \theta^3 t_p}, \theta \ll \frac{\varepsilon}{4\pi r k_e t_p c_e}. \quad (14b)$$

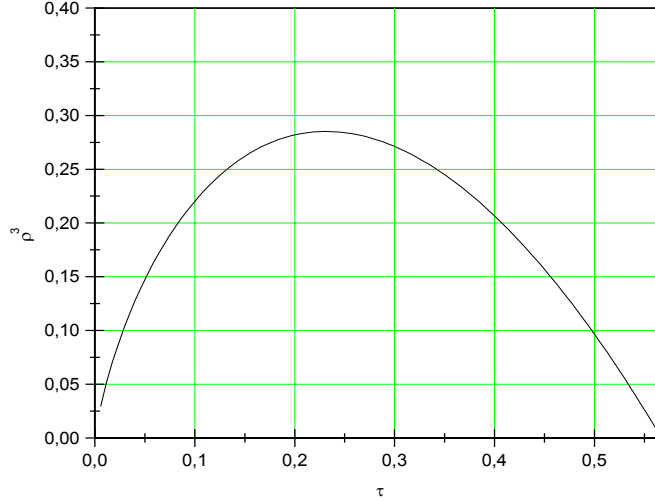


Figure 1. The dependence $\rho^3(\tau)$

The dependence $\theta(t)$ found may be substituted to the equations (5) and by this way the function $T_j(t)$ in the given volume Ω_j may be obtained.

Estimations show that the changes of T_j as a result of heat exchange between an electronic and lattice subsystems are not larger than 100° and cannot lead to activation of lattice processes. This effect can influence only on some kinetic characteristics (for

example, heat conductivity). The lattice processes may be activated in the case of the direct transfer of energy to the lattice subsystem. One of these processes is the radiation - enhanced diffusion.

4. Radiation - enhanced diffusion

The releasing of plasmon energy in the local volume of a crystal and the local increasing of the lattice temperature leads to activation of processes of defect formation and migration. The resulting effect is determined by the value of the temperature flash up and by the time of its relaxation. We suggest that the temperature flash up relaxation may be described by the equation of heat conductivity. The diffusion coefficient change stimulated by plasmon relaxation may be calculated as :

$$D^* = D_0 \int_{r_0}^{\infty} dt 4\pi r^2 \int_0^{\infty} dt \left\{ \exp\left(-\frac{U}{kT_j(r,t)}\right) - \exp\left(-\frac{U}{kT_0}\right) \right\}, \quad (15)$$

where D_0 is the pre-exponential factor in the diffusion coefficient, r_0 is the radius of the region where the plasmon energy released, U is the diffusion barrier. T_0 is the initial temperature of the crystal.

The integral (15) may be calculated if to use the following approximation of temperature distribution [6]:

$$T(r,t) \approx \frac{Q}{(4\pi)^{3/2} c} \frac{1}{(\chi t)^{3/2}} \text{ if } \frac{2}{\sqrt{\chi t}} > r, \quad (16a)$$

$$T(r,t) \approx 0 \text{ if } \frac{2}{\sqrt{\chi t}} < r. \quad (16b)$$

Q is the amount of heat, which is realized in the temperature-flash region. Then we obtain:

$$D^* / D = 0.016 \frac{D}{\chi} \left(\frac{Q}{U} \right)^{5/3}. \quad (17)$$

In many cases $D \approx \chi$ quantitatively, and the increasing of diffusion coefficient caused by plasmon relaxation may be of two-three orders.

5. Conclusion

The PI³&D process is linked with complex interaction of the plasma ions with solids. For the low energy ions inelastic processes become the most important in PI³&D. In particular, these are processes of plasma excitations inside of solids. The interaction of low energy plasma ion beams with surface layers leads to generation of the surface plasmons, which transfer their energy to the lattice excitations and accordingly to acceleration of diffusion and other solid-state reactions. For the plasmon enhanced diffusion one can write an expression:

$$D = W\tau_0 v \delta, \quad (18)$$

where W is given in Section 2, τ_0 is the time interval between two jumps, v is the velocity of diffusing atom moving between two equilibrium positions, δ is the distance between the nearest equilibrium positions. It is seen that D may be enough large (10^{-10} cm²/s) to determine the important processes in PI³&D.

References

- [1] Brown G. (1994) *Rev. Sci. Instrum.* **10**, 3061
- [2] Anders S., Raoux S., Krishman K., MacGill R. A. and Brown I.G. (1996) *J. Appl. Phys.* **79**, 6785
- [3] Indenbom V. L., Kiv. A E. (1984) *Radiation Stimulated Diffusion in Solids*. **In:** Proc. Intern. Conf. on Radiation Effects, Tbilisi, p. 111.
- [4] Maradudin A. (1985). Interaction of Polaritons and Plasmons with Surfaces. **In:** Surface polarilons. Eds. V M.Agranevich, D.L. Mills
- [5] Lifshits I. M., Kaganov M.I., Tanatarov L.V. (1959) *Atom Energy* **6**, 391
- [6] Zeitz F., , Koehler J. S. (1956) *Displacements of Atoms during Irradiation in Solid State Physics*. Eds. F. Zeitz and D. Tumbull. Vol. 2, N.Y., 307-442
- [7] Zener C. (1962). *Elasticity and unelasticity in metals*. Chicago
- [8] Mansur L.K. (1978) *Nucl. Technol.* **40**, 5-34.

Received on the 1st of June 2001

RELIABILITY MODELS FOR COMMUNICATION CHANNEL OF AIR TRAFFIC CONTROL SYSTEM WITH DIFFERENT TEST STRATEGY

I.V. KABASHKIN

*Transport and Telecommunication Institute
 Lomonosova 1, Riga, LV-1019, Latvia;
 phone.: (+371)-7100594, Fax: (+371)-7100535, E-mail: kiv@tsi.lv*

Communication is one of the most important domains of air traffic control system from flight safety point of view. The most fundamental and difficult problem is providing reliability and fault tolerance of such systems. Paper investigates reliability of repairable voice communication channels (air/ground and ground/ground) of air traffic control systems with periodical sessions of communications. Three different test strategies is described:

- Communication channel does not have built-in-test equipment.
- Communication channel has built-in-test equipment with diagnosis procedures during communication sessions.
- Communication channel has periodical test in the pauses between communication sessions.

Marcovian models are studied and communication channel availability is examined for each of above mentioned test strategies. Some numerical examples of real communication systems are presented.

Keywords: communication channels, traffic control systems

1. Introduction

Communication is one of the most important domains of air traffic control system (ATC) from flight safety point of view. The most fundamental and difficult problem is providing reliability and fault tolerance of such systems.

Today the redundancy is the main method of reliability improvement of ATC communication channels (CC). The reliability of the redundant systems in the present time is quite well investigated, however, concerning the controller channels this task has a specific aspects, which are caused by the used method of the CC failure fixation and test strategy of the technical condition of ground-based communication radio aids.

This paper investigates reliability of repairable voice communication channels (air/ground and ground/ground) of air traffic control systems with periodical sessions of communications for different test strategies.

2. Notation

ATC	Air Traffic Control
CC	Communication Channel
MTBF	Mean Time Between Failures
MTTR	Mean Time to Repair
λ	Failure Rate
μ	Repair Rate
A	Availability
h_i	Probability of being in state H_i
T_k	Periodicity of test operations with parameter of Poisson flow $\omega=1/T_k$
t_k	Time of test operations
τ	Parameter of exponential distribution of t_k
t_{f1}	Time of failure fixation by human operator

$v_1=1/t_{f1}$	Parameter of exponential distribution of t_{f1}
t_{f2}	Time of failure fixation by automatic test system
$v_2=1/t_{f2}$	Parameter of exponential distribution of t_{f2}
T_c	Periodicity of communication demands with parameter of Poisson flow $\varphi=1/T_c$
t_c	Time of communication session
$\psi=1/t_c$	Parameter of exponential distribution of t_c
t_n	Mean time of test interruption in the case of communication session begins
$v_3=1/t_n$	Parameter of exponential distribution of t_n
t_R	Time of repeat demand on communication in the channel with failure
η	Parameter of exponential distribution of t_R

3. Reliability of communication channel with different test strategies

3.1. STRATEGY 1. COMMUNICATION CHANNEL DOES NOT HAVE BUILT-IN-TEST EQUIPMENT

In the case when the test equipment is absence the CC failure is detected by controller during the process of operation. In this case the process of the CC failure detection is possible to clarify by the time diagram (Figure 1). Communication channel with completely good set of the equipment starts functioning in the moment of time t_0 . After some operation time T_0 in the moment of time t_1 the failure of the main set of the on-ground communication radio aids happens. However, due to the absence of the automatic test system the fixation of the failure does not happen. After some time T_c in the moment t_2 controller obtains the requirement on communication, for example, in the form of any request from the aircraft. Controller does not know about the malfunction of the operation of the communication channel. He transmits the answer on the request to the aircraft. In this case the crew does not receive the answer and after some time T_R makes the repetitive request. The delivery of the repetitive request in moment t_3 is the information about the malfunction of CC for the controller. In such case controller goes over to the operation with the reserve on-ground communication equipment in this way fixing the failure of the main set of the equipment. The similar process repeats in case the refuse of the reserve radio station too.

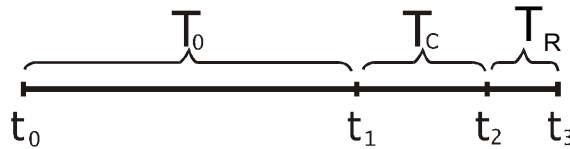


Figure 1. Time diagram of failure detection

The behavior of the examined system is described by the state transition diagram (Fig.2), where: H_1 – completely good state of the CC equipment; H_2 – communication session in CC; H_3 – failure of the main CC system; H_4 – communication session in the CC with failure of the main on-ground communication radio aid; H_5 – repeat demand on communication in CC with failure of equipment; H_6 – detection of the failure state of the main on-ground communication radio aid, switch over to the reserve one.

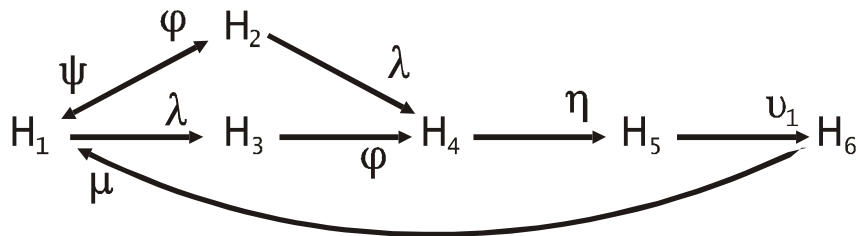


Figure 2. State transition diagram for test strategy 1.

Solving the Kolmogorov equation system describing the operation of the examined channel it is possible to define A_1 availability of the controller channel with the first test strategy

$$A_1 = (1+a_1)/(1+a_1+a_2), \tag{1}$$

where $a_1 = \lambda[\gamma_1(1+\beta)+1/\varphi]$, $a_2 = \beta$, $\gamma_1 = 1/\mu + 1/\eta + 1/\nu_1$, $\beta = \varphi/(\lambda + \psi)$.

Comparing the equation (1) with the equation for the A_0 availability of the ideal system (immediate failure detection, immediate switchover, non-failure switch) [Barloy, 1965], it is possible to get certain that $A_1 = A_0$ with non-limited increase of the intensity of communication φ and the reduction of the failure detection time ($\nu_1 \rightarrow \infty$).

It is possible to evaluate the deterioration of the reliability in the real ATC communication channel in comparison with the ideal one with the help of reliability deterioration coefficient $V_1 = (1 - A_1)/(1 - A_0)$. The function of influence of average time between communication session T_c and average switch time t_{r1} for ATC communication channel are submitted on Figure 3 (line 1- for $t_{r1} = 2$ minute and line 2- for $t_{r1} = 10$ seconds).

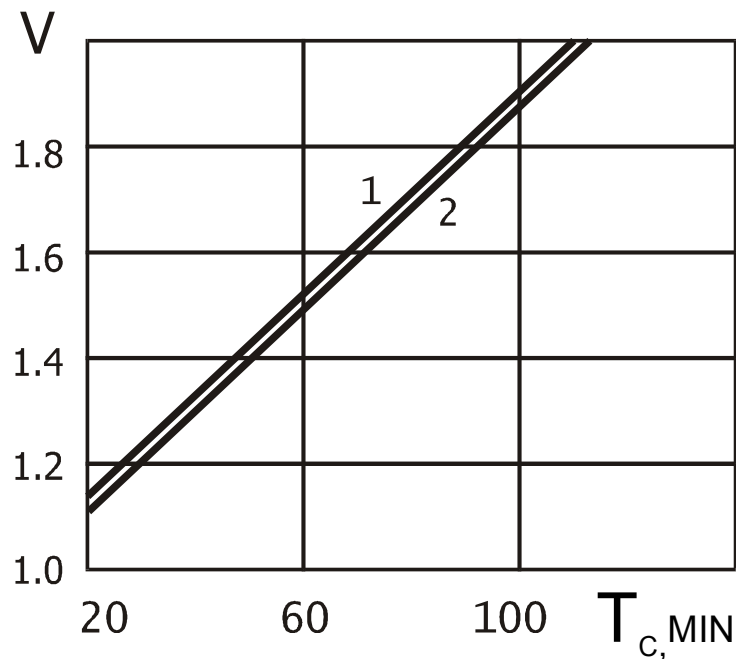


Figure 3. Deterioration of the reliability in the real ATC communication channel with test strategy 1

3.2. STRATEGY 2. COMMUNICATION CHANNEL HAS BUILT-IN-TEST EQUIPMENT WITH DIAGNOSIS PROCEDURES DURING COMMUNICATION SESSIONS

At present many of the ground-based airport radio centers have built-in test equipment, which carry out test in the period of the communication sessions. The behavior of the examined system with the mentioned test strategy is possible to describe by the graph of states submitted on Fig 4, where the entered earlier symbols of states are saved.

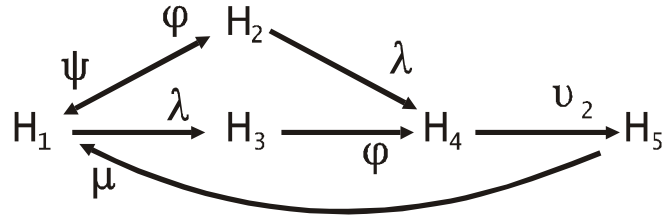


Figure 4. State transition diagram for test strategy 2.

The availability A_2 of the controller channel with the second test strategy may be defined by solution of the Kolmogorov equation system, which is describing the mentioned graph:

$$A_2 = (1 + a_1) / (1 + a_1 + a_2),$$

$$a_1 = \lambda[\gamma_2(1 + \beta) + 1/\varphi], \quad a_2 = \beta, \quad \beta = \varphi / (\lambda + \psi), \quad \gamma_2 = 1/\mu + 1/v_2.$$

The analysis of the reliability deterioration coefficient $V_2 = (1 - A_2) / (1 - A_0)$ shows the dependency similar to the one submitted on Figure 3.

3.3. STRATEGY 3. COMMUNICATION CHANNEL HAS A PERIODICAL TEST IN THE PAUSES BETWEEN COMMUNICATION SESSIONS

In this case process of CC operation could be described by the following states: H_1 – good condition of CC equipment, absence of the communication session and test operations; H_2 – test in the channel without communication session; H_3 – communication session; H_4 – demand on communication in the test period; H_5 – failure of CC equipment in the pause of communication; H_6 – test of system with failure; H_7 – demand on communication in the channel with failure of equipment; H_8 – failure fact fixation by automatic test system or by human operator. On Fig. 5 there is a state transition diagram of the examined system.

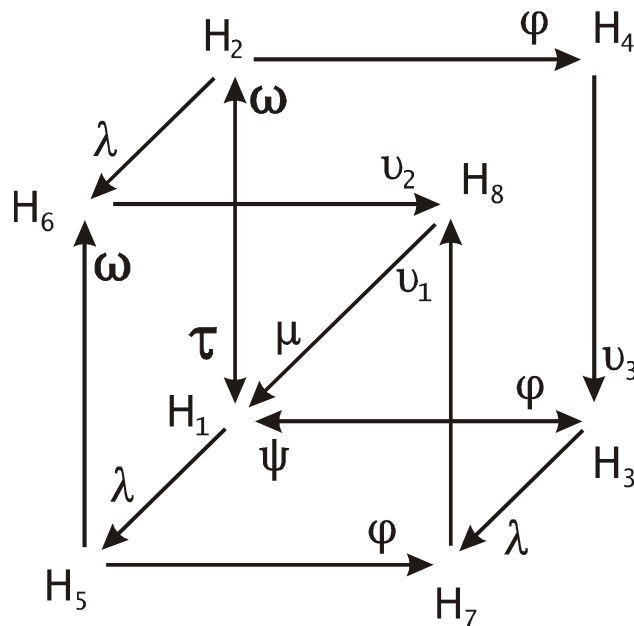


Figure 5. State transition diagram for test strategy 3.

The availability A_3 of the examined CC is defined by equation:

$$A_3 = \sum_{i=1}^3 h_i$$

Forming and solving the Kolmogorov equation system describing the graph of the states it is possible to define probabilities $h_i, i=1, \dots, 8$, and the availability A_3 :

$$A_3 = (1+a_2)/(1+a_1+a_2),$$

where

$$a_1 = \omega/(\lambda+\varphi+\tau) [\lambda(1/\mu+1/v_2)+\varphi/v_3+\lambda\varphi/(\lambda+\psi)(1/\mu+1/v_1)] + \lambda/(\omega+\varphi) [1+\omega(1/\mu+1/v_2)+\varphi(1/\mu+1/v_1)+\varphi/(\lambda+\psi)(1+\lambda/v_1),$$

$$a_2 = (\lambda+\varphi)^{-1} [\omega(\lambda+\varphi+\psi)/(\lambda+\varphi+\tau)+\varphi]$$

The reliability deterioration of the real CC may be evaluated by the coefficient $V_3=(1-A_3)/(1-A_0)$. The analysis of the $V_3(\omega)$ shows that it is a unimodal function with the extremes in ω_{opt} point.

The expression for the definition of $T_{k\ opt}=1/\omega_{opt}$ is possible to find out from the condition $dA_3/d\omega=0$. In general case the expression for the definition $T_{k\ opt}$ has quite a cumbersome look, but, for the practical crucial case of the highly reliable systems ($\lambda \ll \mu$) with the short time of the failure fixation ($\mu \ll v_1, \mu \ll v_2$) the following approximate expression is justified for the definition of the optimal test periodicity:

$$T_{k\ opt}^{-1} = v_3 \varphi^{-1} \{ \lambda + [(\lambda - \varphi^2/v_3)^2 + \lambda \varphi \tau/v_3]^{1/2} \} - \varphi$$

Example. Let's examine the CC availability of the ATC system in the airport area. The channel radio stations are operating in the day night operation regime. The sessions of communication are carried out in the random moments of time. The failures of the radio stations could be fixed by the objective technical test aids executing the periodical test, or subjectively according to the controller's evaluation. On Fig.6 there are $V(T_k)$ dependencies for various MTBF T_0 and typical average meanings of the characteristics of the ATC communication channel.

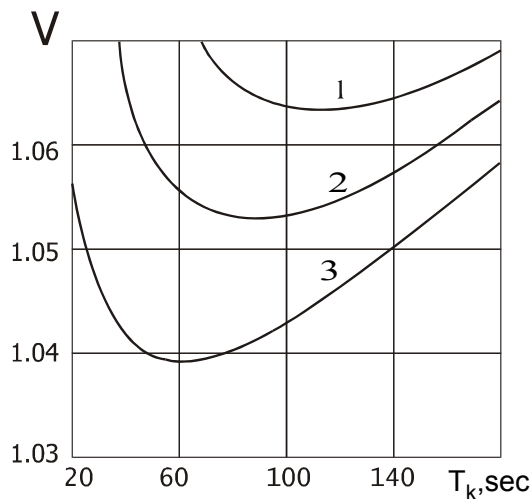


Figure 6. Function $V(T_k)$ for $T_0=3000$ h (1), $T_0=2000$ h (2), $T_0=1000$ h (3)

On Figures 7 and 8 there are functions $T_{k\ opt}(T_0)$ for the various T_c periodicity of communication session and time of test interruption t_n .

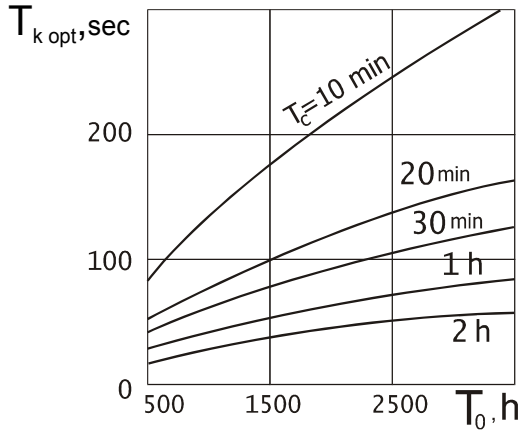


Figure 7. Functions $T_{k\text{ opt}}(T_0, T_c)$

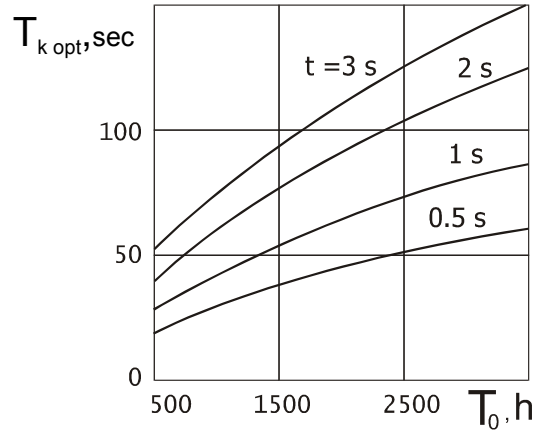


Figure 8. Functions $T_{k\text{ opt}}(T_0, t_n)$

4. Conclusion

- In the ATC communication channel availability for the third test strategy is more than decimal better as compared with the first and second ones.
- The availability of the in case of the third test strategy is unimodal function of test period.
- The optimal test period in the third test strategy increases with the increase of MTBF, the duration of test and time of its interruption. It is reduced with the increase of the intensity of communication and staying practically invariant to the MTTR, duration of the communication session and failure fixation time.

References

- [1] Barloy B.E., Proshan F., Hunter L.C. (1965) *Mathematical Theory of Reliability*. John Wiley & Sons.

Received on the 15th of June 2001

ПРИКЛАДНАЯ СТАТИСТИКА: МЕТОДЫ И ПРОБЛЕМЫ В ОБУЧЕНИИ

И.В. ЯЦКИВ

*Институт транспорта и связи, факультет компьютерных наук и информационных технологий,
ул. Ломоносова 1, LV-1019, Рига, Латвия, ivl@tsi.lv*

Рассматриваются методические проблемы преподавания курса *Статистика*, некоторые задачи прикладной статистики.
Ключевые слова: STATISTIKA, SSPS, методика преподавания курса *Статистика*

1. Введение

Когда начинаешь читать курс лекций по методам компьютерной обработки статистических данных, всегда найдется слушатель, который захочет блеснуть остроумием и напомнить аудитории знаменитую и уже набившую оскомину фразу Марка Твена о трех видах лжи – лжи, явной лжи и математической статистике. Однако, он своим напоминанием только поможет лектору, превратив тщательно планируемую первую лекцию в «как-будто спонтанную» полемику с классиком, который своим остроумным утверждением только подтвердил необходимость вдумчивого изучения статистических данных и грамотного использования результатов их обработки. Область, из которой можно пачками черпать примеры некорректного использования статистического анализа - наша пресса. Читая ее, воочию видишь: прогнозы, вероятность осуществления которых равна нулю; результаты статистических опросов, построенные на нерепрезентативных выборках и т.д. Так и хочется взвыть от некомпетентности тех, кто их составлял, формулировал выводы на их основе, а главное - от наивности читателей, которые готовы в них верить.

2. Мотивация в обучении прикладной статистике

Прикладная статистика – это раздел математики, который сейчас однозначно нужен любому специалисту нефилологического профиля: от компьютерщика, администратора сетей до менеджера по персоналу, бизнес-администратора. Но осознание необходимости этой науки приходит не сразу. Начнем со специалистов компьютерных наук. К сожалению, они самые строптивые в восприятии статистики. Поэтому им уже на первом курсе во «введении в специальность» надо на хороших примерах показать, что конечной целью создания любого программного продукта является реализация некоего существующего в условиях неопределенности процесса, что случайные последовательности находят множество полезных применений и прежде всего в моделировании реальных ситуаций. (На крайний случай мы всегда имеем другого классика под рукой – Дональда Э. Кнута [1]), почти половина второго тома книги которого «Искусство программирования» посвящена генерированию и тестированию случайных последовательностей). Но это первая сторона медали, вторая – хотелось бы, чтобы специалисты, читающие программирование не забывали говорить студентам еще об одной важной области применения статистики - о надежности программного обеспечения и вероятностных моделях, используемых для оценки его надежности. Программное обеспечение также является объектом, подверженным случайным сбоям. Musa & Okumoto [6] определили надежность программного обеспечения как вероятность безотказного функционирования компьютерных программ в специфических условиях в течении указанного периода времени. Разработано большое количество моделей в этой области, которые прежде всего используют авторегрессию, байесовские функции и другие статистические модели (достаточно полный обзор - в статье Nozer D.Singpurwalla and Simon P.Wilson [2]).

Отсутствие своевременной мотивации студентов неизбежно приведет к «насаждению» курса прикладной статистики. Мотивацию эту прежде всего должны провести предметники-программисты. Им студенты поверят быстрее, чем лектору по прикладной статистике. Но мы, преподаватели часто забываем об этом и тащим одеяло на себя, доказывая, что только наш

предмет самый важный. Вспомните, преподаватели по «software», когда в последний раз вы упомянули математический предмет в качестве необходимого для студента-компьютерщика? А затем посмотрите на свои планы, директора программ, - достаточно ли там курсовых работ или домашних заданий по математическим предметам?

А что же столь популярные сегодня экономисты и управленцы? Оказывается их тоже достаточно трудно убедить в необходимости изрядной доли математики в их специальности. Им бы хотелось, чтобы статистика сводилась к среднему и таблицам частот (думаю, что не обижу их – это не их вина, их все время дезинформировали, когда звали на эти специальности и говорили, что математики здесь- минимум). К счастью время таких специалистов прошло. Прогнозируете ли вы аналитически развитие вашей фирмы, или строите микро- и макроэкономические модели, или составляете бизнес-план, статистические модели вам понадобятся прежде всего. Тут - классификация объектов, теория временных рядов и регрессионные модели, как правило, нелинейные в экономических приложениях. Все то, что сейчас принято называть красивым и модным словом «эконометрика». Но если посмотреть в корень этой науки, то это все те же прикладные статистические методы с ориентацией на экономические приложения.

И повторюсь, к сожалению, многие преподаватели по профилирующим предметам менеджмента и экономики даже и слышать не хотят, что студентам нужны не только детерминированные модели. Хотелось бы привести цитату из книги двух крупнейших специалистов С.А.Айвазяна и В.С.Мхитаряна [3] (многие годы читающих статистические дисциплины на факультетах экономики в МГУ, МЭСИ): "...В качестве обязательных компонентов в блоке математико-статистического инструментария (современных учебных планов подготовки экономистов) представлены курсы по *элементарным методам статистического анализа данных, теории вероятностей, математической статистике, прикладной статистике (или многомерным статистическим методам), эконометрике*".

3. Теоретическая часть курса

Позволю себе утверждение, что любой язык программирования можно освоить самостоятельно, теорию микро- и макроэкономического анализа тоже, но провести грамотный статистический анализ без полученных в этой области теоретических основ невозможно. В ответ можно услышать возражение о множестве пакетов статистического анализа, имеющихся на рынке: от простейших электронных таблиц до специализированных ARIMA, Cluster и универсальных SPSS, StatGraphics, Statistica и т.д. - вводи данные и получай результаты! Однако, используя их без достаточной теоретической подготовки, вы и получите тот третий вид лжи, о котором упоминал Марк Твен.

Приведу пример из теории регрессионного анализа: при подборе простой парной регрессии получаем незначимый коэффициент множественной детерминации и, принимая первое пришедшее на ум решение - удалить свободный член из модели, получаем качество намного превышающее предыдущее. Ура - результат есть! Однако, оказывается физический смысл у этой модели отсутствует и применять ее на практике опасно.

Отмечу, что обычно курс по прикладной статистике с использованием пакетов статистического анализа следует за курсами теории вероятностей и основам математической статистики. Поэтому в лекционной части курса по прикладной статистике преподавателю необходимо обратить внимание на следующие моменты.

А. Научить студента формально описывать статистические задачи, находить те допущения и ограничения, которые приводят к использованию именно этого критерия, именно этой статистической модели.

В. Не заставлять запоминать отдельные критерии, а учить понимать их физический смысл и отсюда - слабые и сильные стороны этих критериев.

С. Все время проводить межуровневые связи между методами и процедурами. Классический пример – дисперсионный анализ, который может использоваться и как отдельная процедура, и как универсальный аппарат анализа качества других моделей (в задачах классификации, регрессии и т.д.). Или другой пример, показывающий взаимосвязь статистических процедур, когда при простом транспонировании матрицы исходных данных в задаче факторного анализа можно перейти к задаче классификации.

Д. Акцентировать внимание на анализе результатов и умении формулировать выводы. (Что именно при этих данных и при этом уровне допустимой ошибки гипотеза не может быть отвергнута, модель не может считаться некачественной и т.д.) Объяснять нюансы в сочетаниях:

«не можем отвергнуть» и «принимаем гипотезу». Обращать внимание на предположения на которых базируется статистическая процедура.

Учить пониманию модели, объяснению полученных результатов - это должно составлять основу теоретической части курса.

Какие же ключевые точки в самой теории:

- основополагающая роль законов больших чисел;
- важнейшее значение нормального закона распределения;
- возможность применения различных методов при решении одной и той же проблемы и как следствие возможность различных результатов для одних и тех же данных при использовании различных методов анализа;
- основные понятия процедур проверки статистических гипотез: значимость и мощность, критическая область и др;
- факторы, влияющие на точность оценок и возможность управления ими.

4. Практическая часть курса

Практическая часть курса должна состоять из лабораторного практикума и обязательного проекта. Лабораторный практикум составляется из небольших заданий, которые студент выполняет под руководством преподавателя, и которые должны хорошо интерпретировать теорию и показывать проблемы, возникающие при использовании статистических пакетов. Этот лабораторный практикум призван разъяснять отдельные детали статистических процедур. Какой пакет будет выбран для иллюстрации процедур не столь существенно, главное - его совместимость со всеми Windows-приложениями и достаточная универсальность. В идеале, в лаборатории студент может сам выбрать один из предлагаемых пакетов, и преподаватель назначит ему консультанта из числа магистрантов. Особое внимание надо обратить на графическое представление данных. Необходимо научить студента увидеть по графику направление дальнейших исследований данных.

Большое значение имеет проект. Назначение проекта - помочь студенту осмыслить и решить статистическую задачу от ее постановки и до выработки решений на ее основе. Студенты выбирают тему проекта из тех, которые им предлагает преподаватель, или формулируют сами, учитывая собственные интересы. Причем проект они выполняют в команде из двух-трех человек, в непланируемое в аудиториях время, самостоятельно осуществляя поиск необходимых данных, сбор, обработку и анализ. Обязательное представление результатов проекта на семинарах с использованием слайдов разовьет у студентов способности к презентации и полемике. Краткое резюме своего проекта студенты должны представить участникам семинара заранее, что бы те могли подготовиться к более компетентному обсуждению. Причем вопросы, выносимые на обсуждение, могут быть от «Как?» до «Для чего?».

Сформулировать темы проектов легче для студентов экономистов и менеджеров - много статистики и тем, лежащих на поверхности: прогнозирование уровня инфляции, уровня расходов на питание, анализ зависимости цен на недвижимость и т.д. У студентов вызывают всегда интерес модели, связанные с институтской жизнью – построить модель для оценки вероятности провала на экзамене по статистике и т.д.

Труднее для программистов – для них можно предложить темы, связанные с анализом статистических процедур на сходимость и оценку времени счета (т.е. исследование алгоритмов), анализом статистики по сбоям сети. Также может быть найден прекрасный выход для их программистских устремлений. Как правило, студенты-программисты любят выступать критиками интерфейса прикладных пакетов. Можно предложить им самим реализовать какую-либо статистическую процедуру (например, процедуру пошагового подбора регрессионной модели), а пакет использовать для верификации разработанной программы.

5. Элементы академичности в преподавании статистики

Часто у студентов складывается впечатление, что в статистике все уже сделано и стоит вопрос только за реализацией отдельных идей. В этом случае очень важно, чтобы преподаватель всегда акцентировал внимание на проблемах, которые остаются неоткрытыми в той или иной области или указывал новые возможности, которые открыл для того или иного раздела науки компьютерный век (например, компьютерные интенсивные методы). Так магистрантам по

направлению компьютерные науки, изучающим курс «Компьютерная статистика», большую пользу приносят семинары с темами по современным достижениям в области статистики. Такими темами могут быть «Применение аппарата нейронных сетей для решения задачи распознавания образов», «Применение компьютерных интенсивных методов для оценки надежности системы», «Использование методов кластерного анализа в алгоритмах работы поисковых серверов». Один из семинаров может быть посвящен обсуждению статей, в которых рассматриваются тенденции развития современной прикладной статистики (например, статей А.И.Орлова [4] или П.Н. Дубнера [5]).

6. Анкетирование

Конечно, для любого преподавателя важным моментом является осмысление результатов прочтения своего курса. Мне кажется очень интересной анкета, которую приводит в своей статье Wise [7]. Основные вопросы, на которые предлагают ответить студентам следующие.

- Какое мнение имели о прикладной статистике студенты до изучения курса и после него (отрицательное или положительное)?
- Произошли ли значительные изменения после изучения курса?
- Изменилось ли их представление о применении статистики в их профессиональной области после изучения курса?
- Есть ли значительная разница в успехах при обучении статистике между студентами, имеющими свой собственный компьютер и не имеющими? (Понятно, что положительный ответ на этот вопрос означает, что необходимо повысить уровень компьютерной оснащенности студентов в институте).

Ответы на эти вопросы, требуют тщательного изучения и осмысления на различных уровнях: от лектора – до директоров программ.

7. Заключение

В заключении хочется отметить трудность в освоении предмета статистики. Причин этому много. От объективных - например, не всегда мы имеем абитуриентов (студентов) с хорошей математической подготовкой. До субъективных: не установлен необходимый контакт лектор-студент. Но методика, которую применяет лектор, должна быть робастной к этим вариантам изменений “исходных данных”. Он должен провести студента последовательно, через следующие уровни понимания предмета. Первый состоит в освоении основных статистических терминов и методов. Второй – в знании и умении применять статистический аппарат, используя прикладные пакеты анализа данных. Третий – в умении грамотно построить модель, адекватно отражающую реальность и воспользоваться результатами статистического анализа в управлении.

Литература

- [1] Кнут Д.Э. (2000). *Искусство программирования. том 2. Получисленные алгоритмы.* 3-е изд., Пер. с англ.. Издательский дом «Вильямс», Москва . 832с.
- [2] Singpurwalla N.D., Wilson S.P. (1994). Software Reliability Modeling. *International Statistical Review* **62**, 289-317.
- [3] Айвазян С.А., Мхитарян В.С. (1998) *Прикладная статистика и основы эконометрики.* Учебник для вузов. Юнити, Москва, 1022с.
- [4] Орлов А.И. *Современная прикладная статистика.* <http://phिसica.boom.ru/pri/art5.html>
- [5] Дубнер П.Н. *Ловушки анализа данных.* http://infoscope.forth.ru/Statistics/reading_book/pitfalls/index.html
- [6] Musa, J.D. & Okumoto, K. (1984). A Logarithmic Poisson Execution Time Model for Software Reliability Measurement. *Proceedings of the 7th International Conference on Software Engineering*, Orlando, 230-237.
- [7] Wise S.L. (1985) The development and validation of a scale measuring attitudes toward statistics, *Educ. Psychol. Meas.* **45**, 401-405

Received on the 31st of July 2001

HAOTISKIE ATSPUGUŠANAS ALGORITMI UN ŠIFRĒŠANAS TEHNOLOĢIJU OPTIMIZĀCIJA

O. NASKIDAJEVS

*Transporta un sakaru institūts, vispārīgās un lietišķās fizikas departaments
 Lomonosova 1, LV-1019, Rīga, Latvija, e-mail: shunin@tsi.lv*

Šodien eksistē daudz dažādu kriptosistēmu un šifrēšanas/atšifrēšanas metožu. Šajā darbā ir parādītas kā tradicionālās un modernās kriptosistēmas – *Cēzara* (simetriskā kriptosistēma ar parasto ielikšanu), *Vižinera* (simetriskā kriptosistēma ar sarežģītu ielikšanu), *DES* (moderna simetriska kriptosistēma), *RSA* (moderna asimetriska kriptosistēma) un citas, tā arī kriptosistēmas ar *determinētu haotisku loģistikas atspoguļošanas modeļu* izmantošanu, kuras tuvākajā nākotnē būs populāras. Visas augšminētās kriptosistēmas ir detalizēti parādītas un tās priekšrocības atzīmētas. Atkarībā no kriptosistēmu priekšrocībām un trūkumiem katru no kriptosistēmām ir jāizmanto definēta jomā pēc drošības prasībām. *DES* un *determinētu haotisku loģistikas atspoguļošanas modeļu* kriptosistēmas ir visdrošākās datu šifrēšanas un autentifikācijas gadījumos, *RSA* – datu šifrēšanas un ciparu paraksta nodrošināšanas gadījumos. *Loģistikas atspoguļošanas modeļu* haotiskais raksturs var būt par priekšrocību šifrēšanā, jo sistēma no viena stāvokļa citā ir definēta ar dažādiem vienādojumiem un sākumu parametri tiek izvēlēti gadījumā. Sistēma izbeidz savu darbību atkarībā no raksturotā stāvokļa – viena punkta vai vairāku punktu veidošanas. Eksistē trīs atraktoru tipi :1) fiksētais punkts, 2) ierobežots cikls vai periodiskums, 3) determinētais haoss. Jautājums, cik grūti ir lauzt *determinētu haotisku loģistikas atspoguļošanas modeļu* kriptosistēmu ir aprakstīts un nokomentēts šajā darbā. Datoru stacijām ir jāizmēģina dažādus parametrus augšminētās kriptosistēmas uzlaušanai – dažādas sākumu iterācijas, dažādu parametru vērtības, dažādus sākumu nosacījumus, dažādu precizitāti, dažādus decimāla skaitļus un pozīcijas un, galēji, dažādas funkcijas, kas var ģenerēt determinētu haosu. *Determinētu haotisku loģistikas atspoguļošanas modeļu* pamatā izveidotais programmnodrošinājums šifrē un atšifrē visu veidu datus un atbilst visām modernām prasībām datu aizsargāšanai no nesankcionētas pieejas.

Noteicošie vārdi: kriptosistēmas, loģistikas atspoguļošanas modeļi, determinētais haoss, šifrēšanas/atšifrēšanas metodes

Сегодня существует много разнообразных криптосистем и алгоритмов шифрования/расшифрования. В данной работе рассматриваются как традиционные и современные криптосистемы – *Цезаря* (симметрическая криптосистема с простой вставкой), *Винижера* (симметрическая криптосистема со сложной вставкой), *DES* (современная симметрическая криптосистема), *RSA* (современная асимметрическая криптосистема) и другие, так и криптосистемы, основанные на *моделях детерминированных хаотических логических отображений*, которые в скором будущем будут популярны. Все вышеупомянутые криптосистемы детально рассмотрены и показаны их преимущества. В зависимости от преимуществ и недостатков криптосистем каждая из них должна применяться в определенной области согласно требованиям о безопасности. *DES* криптосистемы и криптосистемы с *моделями детерминированных хаотических логических отображений* наиболее надежны при шифровании данных и аутентификации, *RSA* - при шифровании данных и обеспечении электронной подписи. Хаотический характер *моделей детерминированных хаотических логических отображений* однозначно может быть применим в криптографии с преимуществом по отношению к другим, потому что состояния системы определяется различными уравнениями, а начальное состояние системы выбирается случайным. Обычно система заканчивается состоянием с одним положением или набором положений. Существует три типа аттракторов: 1) фиксированная точка, 2) ограниченный цикл или периодичность, 3) детерминированный хаос. Сложность взлома криптосистемы на основе *моделей детерминированных хаотических логических отображений* обсуждается в данной работе с приведением окончательных выводов. При применении компьютерных систем для взлома вышеупомянутой криптосистемы необходимо перебирать различные параметры – различные начальные итерации, различные значения параметров, различные начальные условия, различную точность, различный набор и расположение чисел и, наконец, различные функции, которые могут моделировать детерминированный хаос. Написанное программное обеспечение, основанное на *моделях детерминированных хаотических логических отображений*, шифрует и расшифровывает любой вид данных и удовлетворяет всем современным требованиям по защите данных от несанкционированного доступа.

Ключевые слова: криптосистемы, логические отображения, детерминированный хаос, методы шифрования/дешифрования.

Today a lot of different cryptosystems and encryption/decryption methods exist. In this paper both traditional and modern cryptosystems – *Ceaser* (symmetric cryptosystem with simple insertion), *Vinigere* (symmetric cryptosystem with complex insertion), *DES* (modern symmetric cryptosystem), *RSA* (modern asymmetric cryptosystem) and others, as cryptosystems based on the *determined chaotic logistic growth models*, are shown. All mentioned cryptosystems are shown in details and their benefits are also remarked. Depending on the cryptosystem advantages and disadvantages each of these cryptosystems must be used in defined area due to the security requirements. *DES* and *determined chaotic logistic growth model* cryptosystems is more reliable to use for data encryption and authentication, *RSA* – data encryption and digital signature. The chaotic character of logistic growth models can be used to advantage in cryptography, because the system from one state to another is determined by a different equations, and the initial state of the system is randomly selected. The system often ends up in a state described by one point or a set of points. There are three types of attractors:

1) a fixed-point, 2) a limit cycle or a periodic, 3) a deterministic chaotic. The question of how difficultly it is to break the cryptosystem, where determined chaotic logistic growth models are used, is discussed here and clear remarks are made. Computers should be used to break the system described above by trying out different parameters - different initial iterations, different parameter values, different initial conditions, different precisions, different numbers and positions of decimals and, finally, different functions that can create

deterministic chaos should all be tried. The created software, based on determined chaotic logistic growth models, encrypts and decrypts all kind of data and satisfies all necessary modern conditions for data protection from unauthenticated access.

Keywords: cryptosystems, encryption/decryption methods, logistic growth models, determined chaos

1. Šifrēšanas tehnoloģiju optimizācija

1.1. DETERMINĒTIE HAOTISKIE LOĢISTIKAS ATSPUGUĻOŠANAS MODEĻI.

Vienādojumu pētīšana, kuri veido haosu, ir jauns virziens zinātnē pēdējos 30 gadus. Teorētiskie pamati tika izstrādāti XIX gadsimtā, bet praktiskā realizācija bija iespējama tikai XX gadsimtā, jo tādu procesu pētīšana prasa daudz kalkulešanu un nav iespējams pilnvērtīgi tos veikt bez datoru palīdzības. Pirmais, kurš veica skaitliskos eksperimentus, bija *Edwards Lorenz 1963.* gadā, veidojot haotisko laika apstākļu modeli. Atkarībā no izmantotiem modeļiem un parametru izmaiņas ir iespējams sasniegt cikliskā vai haotiskā veidā. Tās dod iespēju pētīt un izstrādāt dažādus risinājumus vairākas jomās. Viena no tām ir kriptogrāfija, vai datu šifrēšana un atšifrēšana, nodrošinot lielu kriptozturību un ātrdarbību. Pamatā tiek izmantotas determinētie haotiskie loģistikas atspoguļošanas modeļi, vai loģistikas atspoguļošanas modeļi saīsināti. Tāds nosaukums nāca no pirmā pielietojuma šiem modeļiem, kad bija mēģināts veikt iedzīvotāju pieaugums. Šajā darbā mērķis ir izpētīt ciklisko un haotisko modeļu raksturojumus ar praktisko pielietojumu kriptosistēmu izstrādāšanā.

1.2. VERHALSTA LOĢISTIKAS ATSPUGUĻOŠANAS MODELIS.

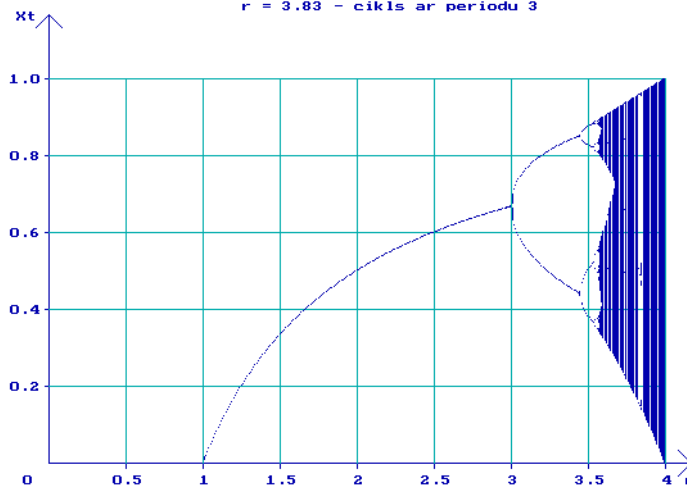
Loģistikas atspoguļošanas modeļi ir vairāki un ir plaši izskatīti literatūrā, līdz ar ko īpaša uzmanība būs pievērsta tikai dažiem no tiem, jo tas ir pilnīgi pietiekami, lai parādītu šo modeļu pielietojumu tādā svarīgā jomā, kā kriptogrāfija. Pamatā tiek izmantots *P. F. Verhulst* modelis

$$x_{t+1} = rx_t(1-x_t), \tag{1}$$

kur x_t ir skaitliskais stāvoklis iterācijas t brīdī, r – auguma parametrs, t – iterācijas daudzums. Grafisks attēls ir redzams *Zīmējumā 1.*

Bifurkācijas diagramma

$r = 3.00$ – cikls ar periodu 2
 $r = 3.45$ – cikls ar periodu 4
 $r = 3.55$ – cikls ar periodu 8
 $r = 3.57$ – iestājas haoss
 $r = 3.83$ – cikls ar periodu 3



Zīmējums 1. Bifurkācijas diagramma Verhulsta modelim ar $0 < r \leq 4$, $0 \leq x_t \leq 1$.

Analizējot loģistikas atspoguļošanas modeļus ir pieņemts vērtēt tos pēc atraktora tipa un stabilitātes kritērijiem. Ja sistēma pāriet no viena stāvokļa citā pēc vienādojuma noteikumiem ar dažādu sakumu nosacījumu parametriem, tad sākot no kādas iterācijas lieluma sistēmas stāvoklis var būt aprakstīts ar vienu punktu vai punktu kopas, kas tiek saukt par atraktoru. Atraktora punkti tiek saukti par atraktora pamatu. Eksistē trīs atraktora tipi:

- fiksētais punkts,
- ierobežots cikls vai periodiskums,
- determinētais haoss.

Analizējot *P. F. Verhulst* modeli var secināt, ka fiksētais punkts ir sasniedzams robežās $1 < r < 3$, periodiskums - $3 < r < 3,57$, determinētais haoss - $3,57 < r \leq 4$. Gadījumā, ja $r > 4$, tad sistēma pāriet negatīvā bezgalīgumā. Kad pieauguma process sākās no fiksēta x_0 , r (sākuma parametri) un paiet t iterācijas, sistēma tiek sagatavotā tālākām pētīšanām, atkarībā no pētījuma raksturojuma. Parametrs x_0 nodrošina x_t vērtības sagatavošanu, r – sistēmas stāvokli vienā no trim atraktoriem. Piemēram, ja $x_0 = 0.36$, $r = 2.51$, tad x_t ir redzami *tabulā 1*. Sākot ar $t = 21$ sistēma iestājas pirmā atraktora stāvoklī (fiksētais punkts) un neatkarība no iterāciju daudzuma parametrs $x_t = 0.6015936$ vienmēr būs patstāvīgs. Otra (ierobežots cikls vai periodiskums) atraktora stāvoklis ir parādīts *tabulās 2, 3 un 4*. Katra tabula atspoguļo savu atraktora raksturu, jo ir dažāds periodiskums – 2 ($3 < r < 3.45$), 4 ($3.45 < r < 3.55$) un 8 ($3.55 < r < 3.57$) attiecīgi. Var redzēt, ka pirmā gadījumā, kad $r = 3.41$, x_t ir nemainīgi 0.4494620 un 0.8437913 attiecīgi no $t=129$, otrā, kad $r = 3.49$, x_t ir 0.8291274 , 0.4944462 , 0.8723924 un 0.3885205 no $t = 49$ un trešā, kad $r = 3.559$, x_t ir 0.8896760 , 0.3493251 , 0.8089503 , 0.5500424 , 0.8808374 , 0.3735629 , 0.8328546 , 0.4954406 no $t = 75$, un trešā atraktora stāvoklī, parādīts *tabulā 5* ar $r = 3.61$, ir determinētais haosa raksturs, kur jau sākot no $t = 0$ katrs x_t ir atšķirīgs.

TABULA 1.

Atraktors: fiksētais punkts, $r = 2.51, t = 21$							
X ₀	0.3600000	X ₂₀	0.6015937	X ₄₀	0.6015936	X ₆₀	0.6015936
X ₁	0.5783040	X ₂₁	0.6015936	X ₄₁	0.6015936	X ₆₁	0.6015936
X ₂	0.6121099	X ₂₂	0.6015936	X ₄₂	0.6015936	X ₆₂	0.6015936
X ₃	0.5959527	X ₂₃	0.6015936	X ₄₃	0.6015936	X ₆₃	0.6015936
X ₄	0.6043906	X ₂₄	0.6015936	X ₄₄	0.6015936	X ₆₄	0.6015936
X ₅	0.6001475	X ₂₅	0.6015936	X ₄₅	0.6015936	X ₆₅	0.6015936
X ₆	0.6023259	X ₂₆	0.6015936	X ₄₆	0.6015936	X ₆₆	0.6015936
X ₇	0.6012188	X ₂₇	0.6015936	X ₄₇	0.6015936	X ₆₇	0.6015936
X ₈	0.6017844	X ₂₈	0.6015936	X ₄₈	0.6015936	X ₆₈	0.6015936
X ₉	0.6014962	X ₂₉	0.6015936	X ₄₉	0.6015936	X ₆₉	0.6015936
X ₁₀	0.6016433	X ₃₀	0.6015936	X ₅₀	0.6015936	X ₇₀	0.6015936
X ₁₁	0.6015683	X ₃₁	0.6015936	X ₅₁	0.6015936	X ₇₁	0.6015936
X ₁₂	0.6016065	X ₃₂	0.6015936	X ₅₂	0.6015936	X ₇₂	0.6015936
X ₁₃	0.6015870	X ₃₃	0.6015936	X ₅₃	0.6015936	X ₇₃	0.6015936
X ₁₄	0.6015970	X ₃₄	0.6015936	X ₅₄	0.6015936	X ₇₄	0.6015936
X ₁₅	0.6015919	X ₃₅	0.6015936	X ₅₅	0.6015936	X ₇₅	0.6015936
X ₁₆	0.6015945	X ₃₆	0.6015936	X ₅₆	0.6015936	X ₇₆	0.6015936
X ₁₇	0.6015932	X ₃₇	0.6015936	X ₅₇	0.6015936	X ₇₇	0.6015936
X ₁₈	0.6015939	X ₃₈	0.6015936	X ₅₈	0.6015936	X ₇₈	0.6015936
X ₁₉	0.6015935	X ₃₉	0.6015936	X ₅₉	0.6015936	X ₇₉	0.6015936

TABULA 2.

Cikliskais atraktors ar periodu 2, $r = 3.41, t = 129$													
X ₀	0.3600000	X ₂₀	0.4528682	X ₄₀	0.4498607	X ₆₀	0.4495110	X ₈₀	0.4494695	X ₁₀₀	0.4494646	X ₁₂₀	0.4494640
X ₁	0.7856640	X ₂₁	0.8449250	X ₄₁	0.8439274	X ₆₁	0.8438074	X ₈₁	0.8437931	X ₁₀₁	0.8437914	X ₁₂₁	0.8437912
X ₂	0.5742306	X ₂₂	0.4468012	X ₄₂	0.4491444	X ₆₂	0.4494259	X ₈₂	0.4494594	X ₁₀₂	0.4494634	X ₁₂₂	0.4494639

X ₃	0.8337103	X ₂₃	0.8428493	X ₄₃	0.8436808	X ₆₃	0.8437781	X ₈₃	0.8437897	X ₁₀₃	0.8437910	X ₁₂₃	0.8437912
X ₄	0.4727537	X ₂₄	0.4516693	X ₄₄	0.4497229	X ₆₄	0.4494946	X ₈₄	0.4494676	X ₁₀₄	0.4494643	X ₁₂₄	0.4494640
X ₅	0.8499686	X ₂₅	0.8445347	X ₄₅	0.8438802	X ₆₅	0.8438018	X ₈₅	0.8437925	X ₁₀₅	0.8437914	X ₁₂₅	0.8437912
X ₆	0.4348501	X ₂₆	0.4477187	X ₄₆	0.4492552	X ₆₆	0.4494391	X ₈₆	0.4494610	X ₁₀₆	0.4494636	X ₁₂₆	0.4494639
X ₇	0.8380262	X ₂₇	0.8431793	X ₄₇	0.8437191	X ₆₇	0.8437827	X ₈₇	0.8437902	X ₁₀₇	0.8437911	X ₁₂₇	0.8437912
X ₈	0.4628676	X ₂₈	0.4508973	X ₄₈	0.4496329	X ₆₈	0.4494840	X ₈₈	0.4494663	X ₁₀₈	0.4494642	X ₁₂₈	0.4494640
X ₉	0.8477982	X ₂₉	0.8442782	X ₄₉	0.8438494	X ₆₉	0.8437981	X ₈₉	0.8437920	X ₁₀₉	0.8437913	X ₁₂₉	0.8437912
X ₁₀	0.4400141	X ₃₀	0.4483212	X ₅₀	0.4493276	X ₇₀	0.4494477	X ₉₀	0.4494620	X ₁₁₀	0.4494637	X ₁₃₀	0.4494639
X ₁₁	0.8402298	X ₃₁	0.8433929	X ₅₁	0.8437442	X ₇₁	0.8437856	X ₉₁	0.8437906	X ₁₁₁	0.8437911	X ₁₃₁	0.8437912
X ₁₂	0.4577710	X ₃₂	0.4503972	X ₅₂	0.4495743	X ₇₂	0.4494770	X ₉₂	0.4494655	X ₁₁₂	0.4494641	X ₁₃₂	0.4494639
X ₁₃	0.8464190	X ₃₃	0.8441099	X ₅₃	0.8438292	X ₇₃	0.8437957	X ₉₃	0.8437918	X ₁₁₃	0.8437913	X ₁₃₃	0.8437912
X ₁₄	0.4432791	X ₃₄	0.4487163	X ₅₄	0.4493748	X ₇₄	0.4494533	X ₉₄	0.4494627	X ₁₁₄	0.4494638	X ₁₃₄	0.4494639
X ₁₅	0.8415292	X ₃₅	0.8435317	X ₅₅	0.8437605	X ₇₅	0.8437876	X ₉₅	0.8437908	X ₁₁₅	0.8437912	X ₁₃₅	0.8437912
X ₁₆	0.4547502	X ₃₆	0.4500723	X ₅₆	0.4495360	X ₇₆	0.4494725	X ₉₆	0.4494649	X ₁₁₆	0.4494640	X ₁₃₆	0.4494639
X ₁₇	0.8455179	X ₃₇	0.8439996	X ₅₇	0.8438160	X ₇₇	0.8437942	X ₉₇	0.8437916	X ₁₁₇	0.8437913	X ₁₃₇	0.8437912
X ₁₈	0.4454053	X ₃₈	0.4489751	X ₅₈	0.4494057	X ₇₈	0.4494570	X ₉₈	0.4494631	X ₁₁₈	0.4494638	X ₁₃₈	0.4494639
X ₁₉	0.8423362	X ₃₉	0.8436219	X ₅₉	0.8437712	X ₇₉	0.8437888	X ₉₉	0.8437909	X ₁₁₉	0.8437912	X ₁₃₉	0.8437912

TABULA 3.

Cikliskais atraktors ar periodu 4, $r = 3.49$, $t = 49$

X ₀	0.3600000	X ₂₀	0.3895296	X ₄₀	0.3885208	X ₆₀	0.3885205
X ₁	0.8040960	X ₂₁	0.8299091	X ₄₁	0.8291276	X ₆₁	0.8291274
X ₂	0.5497644	X ₂₂	0.4926484	X ₄₂	0.4944458	X ₆₂	0.4944462
X ₃	0.8638570	X ₂₃	0.8723114	X ₄₃	0.8723923	X ₆₃	0.8723924
X ₄	0.4104522	X ₂₄	0.3887310	X ₄₄	0.3885206	X ₆₄	0.3885205
X ₅	0.8445143	X ₂₅	0.8292910	X ₄₅	0.8291275	X ₆₅	0.8291274
X ₆	0.4582715	X ₂₆	0.4940703	X ₄₆	0.4944462	X ₆₆	0.4944462
X ₇	0.8664230	X ₂₇	0.8723773	X ₄₇	0.8723924	X ₆₇	0.8723924
X ₈	0.4039124	X ₂₈	0.3885597	X ₄₈	0.3885205	X ₆₈	0.3885205
X ₉	0.8402774	X ₂₉	0.8291579	X ₄₉	0.8291274	X ₆₉	0.8291274
X ₁₀	0.4683973	X ₃₀	0.4943762	X ₅₀	0.4944462	X ₇₀	0.4944462
X ₁₁	0.8690144	X ₃₁	0.8723896	X ₅₁	0.8723924	X ₇₁	0.8723924
X ₁₂	0.3972609	X ₃₂	0.3885276	X ₅₂	0.3885205	X ₇₂	0.3885205
X ₁₃	0.8356619	X ₃₃	0.8291329	X ₅₃	0.8291274	X ₇₃	0.8291274
X ₁₄	0.4792854	X ₃₄	0.4944335	X ₅₄	0.4944462	X ₇₄	0.4944462
X ₁₅	0.8710025	X ₃₅	0.8723919	X ₅₅	0.8723924	X ₇₅	0.8723924
X ₁₆	0.3921265	X ₃₆	0.3885218	X ₅₆	0.3885205	X ₇₆	0.3885205
X ₁₇	0.8318880	X ₃₇	0.8291284	X ₅₇	0.8291274	X ₇₇	0.8291274
X ₁₈	0.4880778	X ₃₈	0.4944439	X ₅₈	0.4944462	X ₇₈	0.4944462
X ₁₉	0.8720039	X ₃₉	0.8723923	X ₅₉	0.8723924	X ₇₉	0.8723924

TABULA 4.

Cikliskais atraktors ar periodu 8, $r = 3.559$, $t = 75$

X ₀	0.3600000	X ₂₀	0.3512763	X ₄₀	0.3735638	X ₆₀	0.3493251	X ₈₀	0.3735629	X ₁₀₀	0.3493251
X ₁	0.8199936	X ₂₁	0.8110294	X ₄₁	0.8328554	X ₆₁	0.8089503	X ₈₁	0.8328546	X ₁₀₁	0.8089503
X ₂	0.5253230	X ₂₂	0.5454548	X ₄₂	0.4954387	X ₆₂	0.5500423	X ₈₂	0.4954406	X ₁₀₂	0.5500424
X ₃	0.8874678	X ₂₃	0.8823966	X ₄₃	0.8896760	X ₆₃	0.8808374	X ₈₃	0.8896760	X ₁₀₃	0.8808374
X ₄	0.3554328	X ₂₄	0.3693275	X ₄₄	0.3493253	X ₆₄	0.3735628	X ₈₄	0.3493251	X ₁₀₄	0.3735629
X ₅	0.8153680	X ₂₅	0.8289790	X ₄₅	0.8089505	X ₆₅	0.8328545	X ₈₅	0.8089503	X ₁₀₅	0.8328546

X ₆	0.5357826	X ₂₆	0.5045694	X ₄₆	0.5500420	X ₆₆	0.4954408	X ₈₆	0.5500424	X ₁₀₆	0.4954406
X ₇	0.8851931	X ₂₇	0.8896757	X ₄₇	0.8808375	X ₆₇	0.8896760	X ₈₇	0.8808374	X ₁₀₇	0.8896760
X ₈	0.3616880	X ₂₈	0.3493260	X ₄₈	0.3735625	X ₆₈	0.3493251	X ₈₈	0.3735629	X ₁₀₈	0.3493251
X ₉	0.8216655	X ₂₉	0.8089513	X ₄₉	0.8328542	X ₆₉	0.8089503	X ₈₉	0.8328546	X ₁₀₉	0.8089503
X ₁₀	0.5215048	X ₃₀	0.5500403	X ₅₀	0.4954415	X ₇₀	0.5500425	X ₉₀	0.4954406	X ₁₁₀	0.5500424
X ₁₁	0.8881041	X ₃₁	0.8808382	X ₅₁	0.8896760	X ₇₁	0.8808374	X ₉₁	0.8896760	X ₁₁₁	0.8808374
X ₁₂	0.3536763	X ₃₂	0.3735608	X ₅₂	0.3493250	X ₇₂	0.3735629	X ₉₂	0.3493251	X ₁₁₂	0.3735629
X ₁₃	0.8135496	X ₃₃	0.8328528	X ₅₃	0.8089502	X ₇₃	0.8328546	X ₉₃	0.8089503	X ₁₁₃	0.8328546
X ₁₄	0.5398528	X ₃₄	0.4954450	X ₅₄	0.5500426	X ₇₄	0.4954405	X ₉₄	0.5500424	X ₁₁₄	0.4954406
X ₁₅	0.8840974	X ₃₅	0.8896762	X ₅₅	0.8808373	X ₇₅	0.8896760	X ₉₅	0.8808374	X ₁₁₅	0.8896760
X ₁₆	0.3646877	X ₃₆	0.3493247	X ₅₆	0.3735631	X ₇₆	0.3493251	X ₉₆	0.3735629	X ₁₁₆	0.3493251
X ₁₇	0.8245868	X ₃₇	0.8089499	X ₅₇	0.8328548	X ₇₇	0.8089503	X ₉₇	0.8328546	X ₁₁₇	0.8089503
X ₁₈	0.5147859	X ₃₈	0.5500433	X ₅₈	0.4954403	X ₇₈	0.5500424	X ₉₈	0.4954406	X ₁₁₈	0.5500424
X ₁₉	0.8889719	X ₃₉	0.8808371	X ₅₉	0.8896760	X ₇₉	0.8808374	X ₉₉	0.8896760	X ₁₁₉	0.8808374

TABULA 5.

Determinētais haotiskais atraktors, $r = 3.61, t = 0$													
X ₀	0.3600000	X ₂₀	0.4426432	X ₄₀	0.3425239	X ₆₀	0.3404588	X ₈₀	0.3389355	X ₁₀₀	0.5167856	X ₁₂₀	0.5157232
X ₁	0.8317440	X ₂₁	0.8906238	X ₄₁	0.8129766	X ₆₁	0.8106132	X ₈₁	0.8088502	X ₁₀₁	0.9014829	X ₁₂₁	0.9016075
X ₂	0.5052048	X ₂₂	0.3516611	X ₄₂	0.5488847	X ₆₂	0.5542051	X ₈₂	0.5581477	X ₁₀₂	0.3206096	X ₁₂₂	0.3202481
X ₃	0.9024022	X ₂₃	0.8230640	X ₄₃	0.8938731	X ₆₃	0.8918931	X ₈₃	0.8902940	X ₁₀₃	0.7863269	X ₁₂₃	0.7858582
X ₄	0.3179416	X ₂₄	0.5257230	X ₄₄	0.3424589	X ₆₄	0.3480754	X ₈₄	0.3525907	X ₁₀₄	0.6065411	X ₁₂₄	0.6075091
X ₅	0.7828456	X ₂₅	0.9001114	X ₄₅	0.8129027	X ₆₅	0.8191773	X ₈₅	0.8240565	X ₁₀₅	0.8615229	X ₁₂₅	0.8607748
X ₆	0.6136941	X ₂₆	0.3245784	X ₄₆	0.5490517	X ₆₆	0.5347344	X ₈₆	0.5234043	X ₁₀₆	0.4306774	X ₁₂₆	0.4326278
X ₇	0.8558359	X ₂₇	0.7914104	X ₄₇	0.8938141	X ₆₇	0.8981446	X ₈₇	0.9005226	X ₁₀₇	0.8851517	X ₁₂₇	0.8861142
X ₈	0.4454048	X ₂₈	0.5959388	X ₄₈	0.3426268	X ₆₈	0.3302459	X ₈₈	0.3233898	X ₁₀₈	0.3669860	X ₁₂₈	0.3643062
X ₉	0.8917399	X ₂₉	0.8692726	X ₄₉	0.8130935	X ₆₉	0.7984726	X ₈₉	0.7898999	X ₁₀₉	0.8386293	X ₁₂₉	0.8360297
X ₁₀	0.3485089	X ₃₀	0.4102321	X ₅₀	0.5486205	X ₇₀	0.5808999	X ₉₀	0.5991085	X ₁₁₀	0.4885421	X ₁₃₀	0.4948733
X ₁₁	0.8196521	X ₃₁	0.8734096	X ₅₁	0.8939661	X ₇₁	0.8788733	X ₉₁	0.8670408	X ₁₁₁	0.9020261	X ₁₃₁	0.9024051
X ₁₂	0.5336394	X ₃₂	0.3991405	X ₅₂	0.3421944	X ₇₂	0.3843026	X ₉₂	0.4161646	X ₁₁₂	0.3190339	X ₁₃₂	0.3179331
X ₁₃	0.8984149	X ₃₃	0.8657768	X ₅₃	0.8126015	X ₇₃	0.8541770	X ₉₃	0.8771276	X ₁₁₃	0.7842771	X ₁₃₃	0.7828345
X ₁₄	0.3294687	X ₃₄	0.4195085	X ₅₄	0.5497318	X ₇₄	0.4496568	X ₉₄	0.3890670	X ₁₁₄	0.6107634	X ₁₃₄	0.6137168
X ₁₅	0.7975179	X ₃₅	0.8791113	X ₅₅	0.8935716	X ₇₅	0.8933507	X ₉₅	0.8580749	X ₁₁₅	0.8582106	X ₁₃₅	0.8558172
X ₁₆	0.5829540	X ₃₆	0.3836515	X ₅₆	0.3433162	X ₇₆	0.3439436	X ₉₆	0.4396344	X ₁₁₆	0.4392834	X ₁₃₆	0.4454527
X ₁₇	0.8776583	X ₃₇	0.8536315	X ₅₇	0.8138751	X ₇₇	0.8145835	X ₉₇	0.8893451	X ₁₁₇	0.8891917	X ₁₃₇	0.8917588
X ₁₈	0.3876210	X ₃₈	0.4510506	X ₅₈	0.5468515	X ₇₈	0.5452443	X ₉₈	0.3552614	X ₁₁₈	0.3556926	X ₁₃₈	0.3484555
X ₁₉	0.8569092	X ₃₉	0.8938503	X ₅₉	0.8945758	X ₇₉	0.8951102	X ₉₉	0.8268732	X ₁₁₉	0.8273230	X ₁₃₉	0.8195937

Tabulās ir parādītās x_t veidošanas atkarībā no sākuma parametriem un ir redzama izmaiņas tendence, kad sākot ar $r = 3$ fiksēta punkta atraktors paliek nestabils (*zim. 1.*) un izveidojās divi jauni punkti, formējot stabili ciklisku atraktoru ar periodu 2. Šis fenomens tiek saukts par perioda dubultošanu. Ar tālāko parametra r palielināšanu cikliskais atraktors ar periodu 2 paliek nestabils un veidojas jauni 4 punkti, veidojot stabili ciklisku atraktoru ar periodu 4, tālāk ar periodu 8, 16, 32, 64 un tā tas notiek ar soli 2^{k+1} līdz brīdim, kad $r = 3.57$ un izveidotie punkti ir tik daudz, kad sistēmā jau nav redzama cikliska punktu palielināšana un veidojas haotiskais atraktors. Haoss ir determinēts un atkarībā no sākuma parametriem veidojās punktu kopa, kurā punkti cikliski neatkārtojas. Tā ir haotiskā atraktora būtiska priekšrocība kriptosistēmu izstrādāšanai, kad nav iespējams paredzēt nākamo punktu un atliek tikai visu simbolu pārlūkšana. Detalizētāk tas tiks parādīts nākamajās nodaļās. Ir daži izņēmumi, kad haotiskajā atraktorā parādās daži cikliskie periodi, bet tas īpaši

neietekmē uz kopējā haotiskā atraktora fona. Piemēram, kad $r = 3.83$, parādās cikls ar periodu 3, bet tas ir ļoti mazā haotiskā atraktora joslā.

1.2. CITI LOĢISTIKAS ATSPUGUĻOŠANAS MODEĻI.

Verhulsta loģistikas atspoguļošanas modelis ir pirmais no pārējiem pieciem loģistikas atspoguļošanas modeļiem, kuri bija izmeklēti. Visi ir parādīti zemāk ar atraktoru robežu norādi.

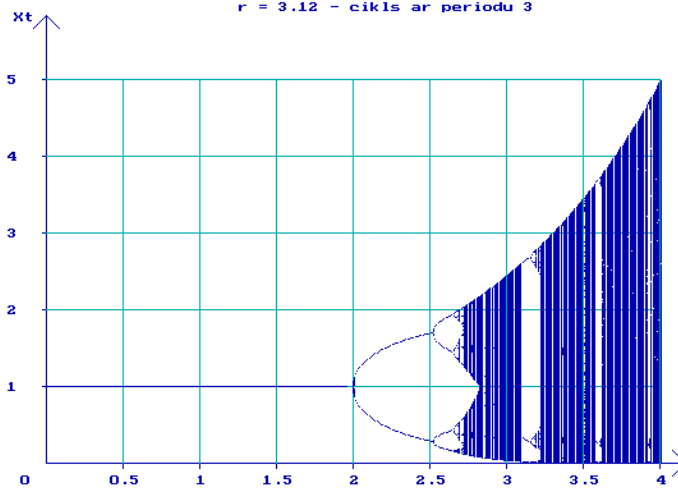
Eksponenciālais modelis

$$x_{t+1} = x_t \exp(r(1-x_t))$$

(2)

Bifurkācijas diagramma

$r = 2.00$ - cikls ar periodu 2
 $r = 2.53$ - cikls ar periodu 4
 $r = 2.66$ - cikls ar periodu 8
 $r = 2.70$ - iestajas haoss
 $r = 3.12$ - cikls ar periodu 3



Zīmējums 2. Bifurkācijas diagramma eksponenciālam modelim ar $0 < r \leq 4$, $0 \leq x_t \leq 5$.

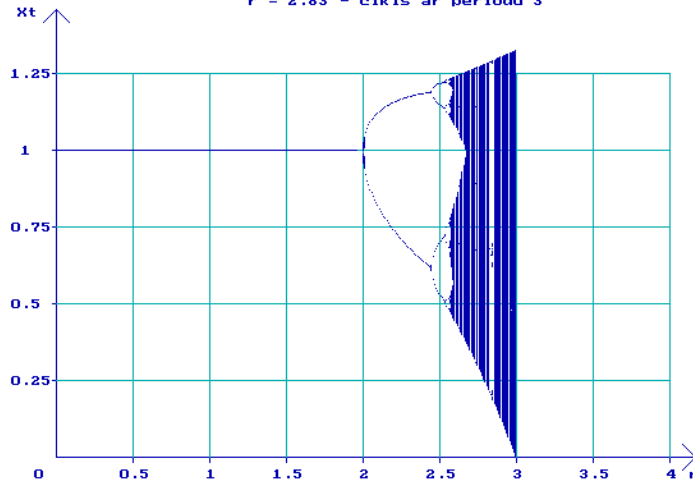
Polinominālais modelis

$$x_{t+1} = x_t(1+r(1-x_t))$$

(3)

Bifurkācijas diagramma

- r = 2.00 - cikls ar periodu 2
- r = 2.45 - cikls ar periodu 4
- r = 2.55 - cikls ar periodu 8
- r = 2.57 - iestajas haoss
- r = 2.83 - cikls ar periodu 3



Zīmējums 3. Bifurkācijas diagramma polinominālam modelim ar $0 < r \leq 3, 0 \leq x_t \leq 1.3$.

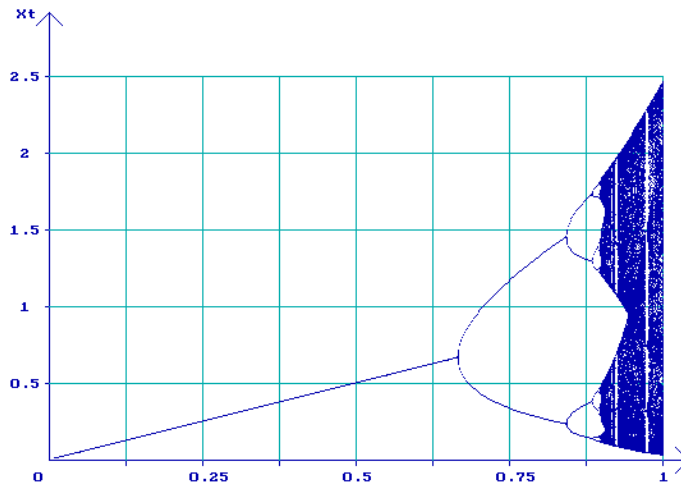
Blackman-Fisher-Pry modelis

$$x_{t+1} = x_t \exp(r(L - x_t))$$

(4)

Bifurkācijas diagramma

- L = 0.67 - cikls ar periodu 2
- L = 0.85 - cikls ar periodu 4
- L = 0.89 - cikls ar periodu 8
- L = 0.90 - iestajas haoss



Zīmējums 4. Bifurkācijas diagramma Blackman-Fisher-Pry modelim ar $0 < L \leq 1, 0 \leq x_t \leq 2.5, r = 3$.

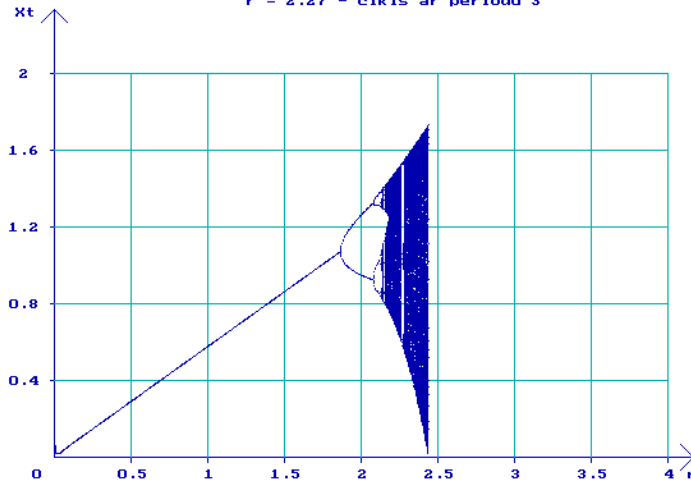
MacLaurin power modelis

$$x_{t+1} = x_t(1 + rx_t - 1.75x_t^2)$$

(5)

Bifurkācijas diagramma

r = 1.88 - cikls ar periodu 2
 r = 2.09 - cikls ar periodu 4
 r = 2.13 - cikls ar periodu 8
 r = 2.14 - iestajas haoss
 r = 2.27 - cikls ar periodu 3



Zīmējums 5. Bifurkācijas diagramma MacLaurin power modelim ar $0 < r < 2.5$, $0 \leq x_t \leq 1.75$.

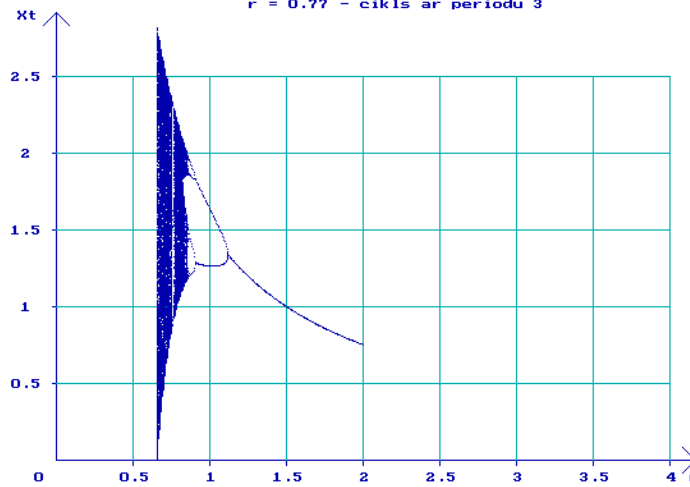
Otrais MacLaurin power modelis

$$x_{t+1} = x_t(1 + 1.5x_t - rx_t^2)$$

(6)

Bifurkācijas diagramma

r = 1.12 - cikls ar periodu 2
 r = 0.90 - cikls ar periodu 4
 r = 0.87 - cikls ar periodu 8
 r = 0.86 - iestajas haoss
 r = 0.77 - cikls ar periodu 3



Zīmējums 6. Bifurkācijas diagramma otram MacLaurin power modelim ar $0.6 < r < 1.4$, $0 \leq x_t \leq 2.8$.

TABULA 6.

Loģistikas atspoguļošanas modeļu visu atraktoru stāvokļi							
	Loģistikas atspoguļošanas modelis	Analizēto parametru intervāls	Atraktora fiksēta punkta reģiona sākums	Iestājas cikls ar periodu 2	Iestājas cikls ar periodu 4	Iestājas cikls ar periodu 8	Iestājas haoss
1	$x_{t+1}=rx_t(1-x_t)$	$r \in (0,4)$	1,01	3,00	3,45	3,55	3,57
2	$x_{t+1}=x_t \exp(r(1-x_t))$	$r \in [0,4]$	0,00	2,00	2,53	2,66	2,70
3	$x_{t+1}=x_t(1+r(1-x_t))$	$r \in (0,3)$	0,01	2,00	2,45	2,55	2,57
4	$x_{t+1}=x_t \exp(r(L-x_t))$	$L \in [0,1], r = 3$	0,00	0,67	0,85	0,89	0,90
5	$x_{t+1}=x_t(1+rx_{t-1}-1,75x_t^2)$	$r \in (0,2,5]$	0,01	1,88	2,09	2,13	2,14
6	$x_{t+1}=x_t(1+1,5x_{t-1}-rx_t^2)$	$r \in [0,6, 2]$	2,00	1,12	0,90	0,87	0,86

TABULA 7.

Loģistikas atspoguļošanas modeļu determinētu haotisku atraktoru stāvokļi				
	Modeļa nosaukums	Loģistikas atspoguļošanas modeļa vienādojums	Haosa iestāšanās parametru intervāls	Iespējamās kombinācijas r parametram
1	<i>Verhulsta</i>	$x_{t+1}=rx_t(1-x_t)$	$r \in (3,57,4)$	$0,43 \cdot 10^8$
2	<i>Eksponenciālais</i>	$x_{t+1}=x_t \exp(r(1-x_t))$	$r \in [2,70,4]$	$1,30 \cdot 10^8$
3	<i>Polinominālais</i>	$x_{t+1}=x_t(1+r(1-x_t))$	$r \in (2,57,3)$	$0,43 \cdot 10^8$
4	<i>Blackman-Fisher-Pry</i>	$x_{t+1}=x_t \exp(3(L-x_t))$	$L \in [0,90,1]$	$0,10 \cdot 10^8$
5	<i>MacLaurin power</i>	$x_{t+1}=x_t(1+rx_{t-1}-1,75x_t^2)$	$r \in [2,14,2,50]$	$0,36 \cdot 10^8$
6	<i>Otrs MacLaurin power</i>	$x_{t+1}=x_t(1+1,5x_{t-1}-rx_t^2)$	$r \in [0,6, 0,86]$	$0,26 \cdot 10^8$

Lai veiktu objektīvu analīzi, darbā tiek parādītas arī citi loģistikas atspoguļošanas modeļi, kuru atraktoru stāvokļi ir parādīti *tabulā 6* un attiecošās bifurkācija, raksturojušas katru no loģistikas atspoguļošanas modeļiem, ir arī parādītas zemāk. Kriptosistēmas izstrādāšanai vissvarīgākā daļa ir tieši haotiskā atraktora robežās, jo tas ļaus nodrošināt ļoti augstu kriptozturību. Aptuvena haotiskā atraktoru robežas r parametram ar iespējamo kombināciju daudzumu katram loģistikas atspoguļošanas modelim, kas tika izmantots programmnodrošinājuma izstrādē, ir parādītas *tabulā 7*. Kombinācijas daudzums ir atkarīgs no vairākiem sākuma parametriem, katrs no kuriem detalizētāk tiks apspriest nākamajā nodaļā.

2. Šifrēšanas tehnoloģiju optimizācijas algoritms

Kriptosistēmas algoritma izstrāde, balstoties pārsvarā uz haotiskā atraktora īpašībām atkarībā no sākuma parametriem veido punktu kopu, kurā punkti cikliski neatkārtojas, dod iespēju optimizēt esošās simetriskās kriptosistēmas, izveidojot jaunu virzienu simetriskās kriptosistēmas vidū. Galvenās prasības jeb kurai kriptosistēmai ir:

- liels atslēgas garums (no 70 bitiem),
- algoritma atklātums (zināms kriptanalītiķim).

Izstrādātā kriptosistēma atbilst šīm prasībām. Lai paskaidrotu smalkāk, tiek izmantota *Verhulsta* loģistikas atspoguļošanas modelis (1).

Pirmais solis – ir nepieciešams aprakstīt sākumu parametrus x_0, r, t, l, p , katrs no kuriem būs kriptosistēmas slepenā atslēga, kopā veidojot vienu atslēgu.

TABULA 8.

Sākuma parametrs	t	x_0	r	l	p
Robežas	$1 \dots 10^6$	$(0,000001 \dots 1,000000) (10^6)$	$1,00000001 \dots 4,00000000 (10^8)$	$1 \dots 12$	$1 \dots 12$
Izvēlētais parametrs	150	0,36	2,56, 3,26, 3,51, 3,56, 3,66	6	4

Otrais solis – izvēlēties simbolu daudzumu, kuri aizvietos atvērto tekstu. Universālam gadījumam tiek piedāvāts izmantot *ASCII* tabulu ar 256 simboliem (*Pielikums A*).

Trešais solis – ģenerēt x_t t reizes. Sākot ar $i = t + 1$ veikt nobīdes parametra k kalkulēšanu pēc sekojoša principa

$$k = x_{i,6,4} \text{ mod } 256, \tag{6}$$

Definējot E_i kā šifrējama simbols, D_i - šifrētais E_i simbols, $ASCII(E_i)$ - E_i simbola $ASCII$ kods un $ASCII(D_i)$ - D_i simbola $ASCII$ kods tiek veikta sekojoša simbolu aizvietošanas operācija, nodrošinot simbola šifrēšanu $ASCII(D_i) = ASCII(E_i) + k$, (7)

Izmantojot dažādus parametrus r ir iegūti dažādi rezultāti, kuri ir atspoguļoti tabulās 9, 10, 11, 12 un 13.

TABULA 9.

Atraktors fiksētais punkts, $r = 2.56$									
i	t	x_t	l	p	k	E_i	$ASCII(E_i)$	$ASCII(D_i)$	D_i
1	151	0,609375	609375	9375	159	1	49	208	ll
2	152	0,609375	609375	9375	159	1	49	208	ll
3	153	0,609375	609375	9375	159	1	49	208	ll
4	154	0,609375	609375	9375	159	1	49	208	ll
5	155	0,609375	609375	9375	159	1	49	208	ll
6	156	0,609375	609375	9375	159	1	49	208	ll
7	157	0,609375	609375	9375	159	1	49	208	ll
8	158	0,609375	609375	9375	159	1	49	208	ll
9	159	0,609375	609375	9375	159	1	49	208	ll
10	160	0,609375	609375	9375	159	1	49	208	ll

TABULA 10.

Cikliskais atraktors ar periodu 2, $r = 3.26$									
i	t	x_t	l	p	k	E_i	$ASCII(E_i)$	$ASCII(D_i)$	D_i
1	151	0,814789	814789	4789	181	1	49	230	μ
2	152	0,491959	491959	1959	167	1	49	216	≠
3	153	0,814789	814789	4789	181	1	49	230	μ
4	154	0,491959	491959	1959	167	1	49	216	≠
5	155	0,814789	814789	4789	181	1	49	230	μ
6	156	0,491959	491959	1959	167	1	49	216	≠
7	157	0,814789	814789	4789	181	1	49	230	μ
8	158	0,491959	491959	1959	167	1	49	216	≠
9	159	0,814789	814789	4789	181	1	49	230	μ
10	160	0,491959	491959	1959	167	1	49	216	≠

TABULA 11.

Cikliskais atraktors ar periodu 4, $r = 3.51$									
i	t	x_t	l	p	k	E_i	$ASCII(E_i)$	$ASCII(D_i)$	D_i
1	151	0,877341	877341	7341	173	1	49	222	
2	152	0,377722	377722	7722	42	1	49	91	
3	153	0,825018	825018	5018	154	1	49	203	π
4	154	0,506713	506713	6713	57	1	49	106	j
5	155	0,877341	877341	7341	173	1	49	222	
6	156	0,377722	377722	7722	42	1	49	91	
7	157	0,825018	825018	5018	154	1	49	203	π
8	158	0,506713	506713	6713	57	1	49	106	j
9	159	0,877341	877341	7341	173	1	49	222	
10	160	0,377722	377722	7722	42	1	49	91	

TABULA 12.

Cikliskais atraktors ar periodu 8, $r = 3.56$									
i	t	x_t	l	p	k	E_i	$ASCII(E_i)$	$ASCII(D_i)$	D_i
1	151	0,880783	880783	0783	15	1	49	64	@
2	152	0,373813	373813	3813	229	1	49	22	—
3	153	0,833314	833314	3314	242	1	49	35	#
4	154	0,494490	494490	4490	138	1	49	187	π
5	155	0,889891	889891	9891	163	1	49	212	⊥
6	156	0,348824	348824	8824	120	1	49	169	—
7	157	0,808639	808639	8639	191	1	49	240	≡
8	158	0,550881	550881	0881	113	1	49	162	ó
9	159	0,880783	880783	0783	15	1	49	64	@
10	160	0,373813	373813	3813	229	1	49	22	—

TABULA 13.

Determinētais haotiskais atraktors, $r = 3.66$									
i	t	x_t	l	p	k	E_i	ASCII(E_i)	ASCII(D_i)	D_i
1	151	0,747938	747938	7938	2	1	49	51	3
2	152	0,690006	690006	0006	6	1	49	55	7
3	153	0,782864	782864	2864	48	1	49	97	a
4	154	0,622154	622154	2154	106	1	49	155	é
5	155	0,860386	860386	0386	130	1	49	179	
6	156	0,439645	439645	9645	173	1	49	222	
7	157	0,901667	901667	1667	131	1	49	180	-
8	158	0,324506	324506	4506	154	1	49	203	⌘
9	159	0,802280	802280	2280	232	1	49	25	↓
10	160	0,580574	580574	0574	62	1	49	111	o

Rezultātā var redzēt, ka visdrošākais šifrtēksts ir determinētā haotiskā atraktora robežās (*tabulā 13*), kur simbols ‘ l ’ tiek katru reizi aizvietots ar citu simbolu. Analizējot pārējās tabulas var manīt, ka drošība samazinās ar tabulas numuru samazināšanos un visbīstamākā no drošības viedokļa ir saņemtais rezultāts *tabulā 9*, kur simbols ‘ l ’ katru reizi tiek aizvietots ar vienu un to pašu simbolu. Tas ir parastās apmaiņas Cēzara šifrs, kurš šodien izmantojās tikai apmācībās. *Tabulā 10, 11* un *12* ir redzams jau komplicētāks rezultāts, kur simbols ‘ l ’ tiek aizvietots ar periodu $2, 4$ un 8 attiecoši. Tas ir sarežģītu apmaiņas šifrs ar soli $2, 4$ un 8 attiecoši un varētu būt kā Vižnera šifrēšanas sistēmas atsevišķs gadījums. Atšifrēšana notiek pretējā virzienā.

Tādā pašā veida tiek nodrošināta algoritma darbība arī pārējiem loģistikas atspoguļošanas modeļiem. *Pielikumā B* ir parādīti detalizētāks teksta faila šifrēšanas rezultāti visiem modeļiem. Programmnodrošinājums *CRYPTO* dod iespēju šifrēt un atšifrēt jeb kādu faila datu formātu un apjomu abos virzienos ar kopējo atslēgas garumu līdz 72 bitiem.

3. Šifrēšanas tehnoloģiju optimizācijas algoritma rezultātu pētīšana

3.1. KRIPTOIZTURĪBA

Vis svarīgākais kriptosistēmas parametrs ir kriptozturība. Izstrādāta programmnodrošinājums *CRYPTO* uz loģistikas atspoguļošanas modeļu pamata nodrošina 5 slepenas atslēgas – sakumu parametri. Katrs no parametriem ir parādīts *tabulā 14*.

TABULA 14.

Katra atslēgas (sākuma parametra) kombināciju daudzums.					
Loģistikas atspoguļošanas modelis	Iespējamās kombinācijas x_0 parametram	Iespējamās kombinācijas r parametram	Iespējamās kombinācijas l parametram	Iespējamās kombinācijas p parametram	Iespējamās kombinācijas $iterācijas$ parametram
$x_{t+1}=rx_t(1-x_t)$	10^6	$0,43 \cdot 10^8$	12	12	10^6
$x_{t+1}=x_t \exp(r(1-x_t))$	10^6	$1,30 \cdot 10^8$	12	12	10^6
$x_{t+1}=x_t(1+r(1-x_t))$	10^6	$0,43 \cdot 10^8$	12	12	10^6
$x_{t+1}=x_t \exp(3(L-x_t))$	10^6	$0,10 \cdot 10^8$	12	12	10^6
$x_{t+1}=x_t(1+rx_t-1,75x_t^2)$	10^6	$0,36 \cdot 10^8$	12	12	10^6
$x_{t+1}=x_t(1+1,5x_t-rx_t^2)$	10^6	$0,26 \cdot 10^8$	12	12	10^6

Kriptozturība ir atkarīga no atslēgas garuma. Piedāvātajā algoritmā datu šifrēšanai un atšifrēšanai izmantojas 5 slepenas atslēgas. Katra no tām nodrošina kādu atslēgu kombinācijas daudzumu, kas varētu būt pārveidots bits, *tabula 15*.

TABULA 15.

Katras atslēgas (sākuma parametra) garums.					
Loģistikas atspoguļošanas modelis	Atslēgas garums x_0 parametram, bitos	Atslēgas garums r parametram, bitos	Atslēgas garums l parametram, bitos	Atslēgas garums p parametram, bitos	Atslēgas garums iterācijas parametram, bitos
$x_{t+1}=rx_t(1-x_t)$	20	25	3	3	20
$x_{t+1}=x_t \exp(r(1-x_t))$	20	26	3	3	20
$x_{t+1}=x_t(1+r(1-x_t))$	20	25	3	3	20
$x_{t+1}=x_t \exp(3(L-x_t))$	20	23	3	3	20
$x_{t+1}=x_t(1+rx_t-1,75x_t^2)$	20	25	3	3	20
$x_{t+1}=x_t(1+1,5x_t-rx_t^2)$	20	24	3	3	20

Kopsummā 5 atslēgas nodrošina līdz 72 bitiem garu atslēgu, kas tiek izmantota datu šifrēšanai un atšifrēšanai, tabula 16. Tas ir ļoti labs rādītājs, jo šodien absolūts drošs atslēgas garums ir 75 biti.

TABULA 16.

Programmnodrošinājuma CRYPTO atslēgas raksturojums.		
Loģistikas atspoguļošanas modelis	Kopējais atslēgu kombināciju daudzums	Kopējais atslēgas garums, bitos
$x_{t+1}=rx_t(1-x_t)$	$6,192 \cdot 10^{21}$	72
$x_{t+1}=x_t \exp(r(1-x_t))$	$18,720 \cdot 10^{21}$	73
$x_{t+1}=x_t(1+r(1-x_t))$	$6,192 \cdot 10^{21}$	72
$x_{t+1}=x_t \exp(3(L-x_t))$	$1,440 \cdot 10^{21}$	70
$x_{t+1}=x_t(1+rx_t-1,75x_t^2)$	$5,184 \cdot 10^{21}$	72
$x_{t+1}=x_t(1+1,5x_t-rx_t^2)$	$3,744 \cdot 10^{21}$	71

Analizējot algoritma teorētisko puse var manīt, ka atslēgas garumu teorētiski var palielināt tik daudz, cik atļauj datoru sistēmas jauda un programmnodrošinājuma iespējas. Pēc noklusēšanas tiek uzskatīts, ka prasības ir līdzīgas norādītām tabulā 17.

TABULA 17.

Katras atslēgas (sākuma parametra) teorētiskais kombināciju daudzums.					
Loģistikas atspoguļošanas modelis	Iespējamās kombinācijas x_0 parametram	Iespējamās kombinācijas r parametram	Iespējamās kombinācijas l parametram	Iespējamās kombinācijas p parametram	Iespējamās kombinācijas iterācijas parametram
$x_{t+1}=rx_t(1-x_t)$	10^{39}	$0,43 \cdot 10^{39}$	39	39	10^{39}
$x_{t+1}=x_t \exp(r(1-x_t))$	10^{39}	$1,30 \cdot 10^{39}$	39	39	10^{39}
$x_{t+1}=x_t(1+r(1-x_t))$	10^{39}	$0,43 \cdot 10^{39}$	39	39	10^{39}
$x_{t+1}=x_t \exp(3(L-x_t))$	10^{39}	$0,10 \cdot 10^{39}$	39	39	10^{39}
$x_{t+1}=x_t(1+rx_t-1,75x_t^2)$	10^{39}	$0,36 \cdot 10^{39}$	39	39	10^{39}
$x_{t+1}=x_t(1+1,5x_t-rx_t^2)$	10^{39}	$0,26 \cdot 10^{39}$	39	39	10^{39}

Pārrēķinot atslēgu teorētisko kombināciju daudzumu bitos, saņemam rezultātus, kuri ir atspoguļoti tabulā 18

TABULA 18.

Katras atslēgas (sākuma parametra) teorētiskais garums.					
Loģistikas atspoguļošanas modelis	Atslēgas garums x_0 parametram, bitos	Atslēgas garums r parametram, bitos	Atslēgas garums l parametram, bitos	Atslēgas garums p parametram, bitos	Atslēgas garums iterācijas parametram, bitos
$x_{t+1}=rx_t(1-x_t)$	128	128	5	5	128
$x_{t+1}=x_t \exp(r(1-x_t))$	128	129	5	5	128
$x_{t+1}=x_t(1+r(1-x_t))$	128	128	5	5	128
$x_{t+1}=x_t \exp(3(L-x_t))$	128	126	5	5	128

$x_{t+1}=x_t(1+rx_t-1,75x_t^2)$	128	128	5	5	128
$x_{t+1}=x_t(1+1,5x_t-rx_t^2)$	128	127	5	5	128

Kopsummā 5 atslēgas nodrošina līdz 399 bitiem garu atslēgu, kas tiek izmantota datu šifrēšanai un atšifrēšanai, *tabula 19*. Tas ir burvīgs rādītājs, jo, kā jau tika minēts iepriekš, šodien absolūts drošs atslēgas garums ir 75 biti, bet lai viņš paliktu drošs arī nākamos 20 gadus, tad atslēgas garumam jābūt no 90 bitiem. Iegūtais rezultāts pieckārši pārsniedz šodienas prasības.

TABULA 19.

Programmnodrošinājuma <i>CRYPTO</i> teorētiskais atslēgu raksturojums.		
Loģistikas atspoguļošanas modelis	Kopējais atslēgu kombināciju daudzums	Kopējais atslēgas garums, bits
$x_{t+1}=rx_t(1-x_t)$	$6,5403 \cdot 10^{119}$	398
$x_{t+1}=x_t \exp(r(1-x_t))$	$19,7330 \cdot 10^{119}$	399
$x_{t+1}=x_t(1+r(1-x_t))$	$6,5403 \cdot 10^{119}$	398
$x_{t+1}=x_t \exp(3(L-x_t))$	$1,5210 \cdot 10^{119}$	395
$x_{t+1}=x_t(1+rx_t-1,75x_t^2)$	$5,4756 \cdot 10^{119}$	397
$x_{t+1}=x_t(1+1,5x_t-rx_t^2)$	$3,9546 \cdot 10^{119}$	397

Uzlaust šifrtēkstu, izmantojot sākumu parametrus no determinētā haotiskā atraktora (vai slepenās atslēgas), ir iespējams tikai tādos gadījumos, kad ir zināms atvērta teksta attēls un pieejami jaudīgi un ļoti dārgi instrumenti (datorsistēmu kompleksi, veidoti uz *SIS - specializētās integrālās shēmas* vērtībā virs 300 000 000 USD). *Tabulas 20 un 21* satur informāciju par jaudīgiem datoru sistēmu kompleksiem un tās spējas uzlaust slepenās atslēgas ar pilnu pārlikšanu.

TABULA 20.

Jaudīgu datorsistēmu saraksts				
Valsts	Jauda (Mflops)	Instalācija	Mikroprocesoru daudzums	Datora nosaukums
ASV	1 068 000	1997	7264	Intel ASCI Red
Japāna	368 200	1996	2048	Hitachi/Tsukuba CP-PACS/2048
Lielbritānija	264 000	1997	696	SGI/Cray T3E900 LC696-128
Vācija	176 000	1996	512	SGI/Cray T3E LC512-128
Francija	115 500	1997	256	SGI/Cray T3E750 LC256-128

TABULA 21.

Nepieciešamais laiks (gados) jaudīgām datorsistēmām visu atslēgu pārlūkšanai							
Datora nosaukums	Jauda (flops)	56 biti = $7,2 \cdot 10^{16}$ atslēgām	64 biti = $1,8 \cdot 10^{19}$ atslēgām	70 biti = $1,8 \cdot 10^{21}$ atslēgām	75 biti = $3,78 \cdot 10^{22}$ atslēgām	90 biti = $1,24 \cdot 10^{27}$ atslēgām	256 biti = $1,15 \cdot 10^{77}$ atslēgām
Intel ASCI Red	$1,068 \cdot 10^{12}$	0,002	0,534	35	1122	$36,8 \cdot 10^6$	$3,4 \cdot 10^{57}$
Hitachi/Tsukuba CP-PACS	$3,68 \cdot 10^{11}$	0,006	1,55	101,7	3257	$106 \cdot 10^6$	$9,9 \cdot 10^{57}$
SGI/Cray T3E	$2,65 \cdot 10^{11}$	0,008	2,15	141	4523	$148 \cdot 10^6$	$1,37 \cdot 10^{58}$
Fujitsu Numerical Wind Tunnel	$2,3 \cdot 10^{11}$	0,0099	2,48	162	5211	$170 \cdot 10^6$	$1,58 \cdot 10^{58}$
Hitachi SR2201	$2,2 \cdot 10^{11}$	0,0103	2,56	170	5448	$179 \cdot 10^6$	$1,66 \cdot 10^{58}$

Kā redzams, sākot ar 70 bitu atslēgas garumu slepenās atslēgas atklāšana ar pilnu pārlīkšanu ir iespējama tikai pēc vairākiem gadiem. Tāpat ir jāņem vērā tas fakts, ka katru gadu datoru sistēmu kompleksi paliek visjaudīgāki un slepenās atslēgas atklāšanas laiks varētu būt samazināts. Pēc kriptanalītiķu pēdējiem datiem, tuvākajos 20 gados atslēgas garumam jābūt no 90 bitiem, lai informāciju 20 gadu laikā būtu pasargāta no nesankcionētas pieejas.

3.2. ĀTRDARBĪBA.

Algoritma ātrdarbība bija pētīta vairāku failu kriptēšanas laikā un var nākt pie secinājuma, ka ātrdarbība ir laba, jo šifrēšanas process notiek ar katru simbolu atsevišķi ļoti īsā laikā. Rezultāti ir parādīti tabulā 22.

TABULA 22.

Programmnodrošinājuma CRYPTO ātrdarbība (datu šifrēšana un atšifrēšana) sekundēs, izmantojot Pentium III 450 Mhz					
Loģistikas atspoguļošanas modelis	1 MB fails, s	500 kB fails, s	200 kB fails, s	100 kB fails, s	20 kB fails, s
$x_{t+1}=rx_t(1-x_t)$	45,16	22,58	9,03	4,52	0,90
$x_{t+1}=x_t \exp(r(1-x_t))$	53,87	26,94	10,77	5,39	1,08
$x_{t+1}=x_t(1+r(1-x_t))$	45,16	22,58	9,03	4,52	0,90
$x_{t+1}=x_t \exp(3(L-x_t))$	53,87	26,94	10,77	5,39	1,08
$x_{t+1}=x_t(1+rx_t-1,75x_t^2)$	45,16	22,58	9,03	4,52	0,90
$x_{t+1}=x_t(1+1,5x_t-rx_t^2)$	45,16	22,58	9,03	4,52	0,90

4. Secinājumi

Vienādojumu pētīšana, kuri veido haosu, ir jauns virziens zinātnē pēdējos 30 gadus. Ir detalizēti izpētīti determinētie haotiskie loģistikas atspoguļošanas modeļi (*Verhulsta, eksponenciāls, polinominālais, Blackman-Fisher-Pry, MacLaurin power un otrs MacLaurin power*). Balstoties uz plašām iespējām, ko var nodrošināts determinētais haotiskais atraktors, ir izstrādāts jauns simetriskais kriptosistēmas algoritms un programmnodrošinājums CRYPTO. Ir izanalizēta algoritma kriptozturība, parādītas priekšrocības virs pārējam kriptosistēmām, īpaša uzmanība ir veltīta slepenu atslēgu veidošanai. Bifurkācijas diagrammu analīze dod iespēju vizuāli redzēt atraktoru raksturojumus, palīdzot ātri atrisināt iespējamās problēmas pētīšanas laikā. Atkarībā no izmantotiem modeļiem un parametru izmaiņas ir iespējams sasniegt cikliskā vai haotiska veida atraktorus, kur determinētais haosa atraktors nodrošina visaugstāku drošības kriptozturību. Sasniegtais atslēgas garums ir līdz 70 bitiem, teorētiski to ir iespējams palielināt līdz pat 400 bitiem, kas piekārsi pārsniedz šodienas prasības. Uzlaust šifrtēkstu, izmantojot sākumu parametrus no šī atraktora (vai slepenās atslēgas), ir iespējams tikai tādos gadījumos, kad ir zināms atvērta teksta attēls un pieejami jaudīgi un ļoti dārgi instrumenti.

Algoritma analīze un salīdzināšana ar citiem moderniem simetriskiem šifrēšanas algoritmiem rāda, ka haotiskais atraktors spēj nodrošināt līdzīgu un augstāku pēc kvalitātes šifrtēksta kriptozturību. Pēc kriptanalītiķu pēdējiem datiem, tuvākajos 20 gados atslēgas garumam jābūt no 90 bitiem. Izstrādātais algoritms var būt pielietojams ikdienā pēc tā modificēšanas saskaņā ar ISO standartizācijas prasībām, programmnodrošinājuma uzlabošanu un speciālu iekārtas veidošanu.

5. Noslēgums

Šajā darbā tika parādīta svarīga informācijas tehnoloģiju nozares daļa – informācijas nodrošināšana no nesankcionētas pieejas. Ar katru gadu šī problēma ir visaktuālāka un tirgu parādās vairākas jaunas šifrēšanas algoritmu realizācijas. Viena no tādām realizācijām ir atspoguļota šajā darbā. Tika veikta izpēte par visām esošām šodien kriptosistēmām un izanalizētas tās priekšrocības un trūkumi. Balstoties uz apkopotās informācijas, tika izstrādāts jauns simetriskais datu šifrēšanas un atšifrēšanas algoritms ar determinētu haotisku loģistikas atspoguļošanas modeļu (*Verhulsta, eksponenciālā, polinominālā, Blackman-Fisher-Pry,*

MacLaurin power un otra MacLaurin power) palīdzību. Algoritma īpašība ir 5 atslēgu izmantošana, kas nodrošina augstu algoritma kriptozturību.

Izstrādāta kryptosistēma atbilst simetriskās kriptosistēmas prasībām, jo tiek izmantota viena un tā paša atslēgas izmantošana kā šifrēšanā, tā arī atšifrēšanā. Parasta šifra izejošā tekstā katrs simbols tiek aizvietots ar simbolu no tā paša alfabēta vienmērīgi visa teksta garumā. Simbola aizvietošana ir atkarīga no atraktoru izmantošanas konkrētā gadījumā, vai sākumu nosacījumiem. Visvienkāršākā šifrēšanas metode izstrādātā kriptosistēmā balstās uz *Cēzara* šifru, pēc tam *Vižiniera* un beidzot ar haotisku simbolu aizvietošanas raksturu, kas ir iespējams tikai haotiskā atraktora robežās. Izstrādātais algoritms pilnīgi der kā šifrēšanai, tā arī datu autentificēšanai. Dati tiek aizsargāti no iepazīšanās ar šifrēšanu, bet datu izmaiņas tiek pārbaudītas ar autentifikāciju, kuru algoritmu var pielietot kā pie atvērta teksta, tā arī pret šifrētu.

Darbā ir parādītas arī asimetriskās kriptosistēmas (*RSA*, *El Hamala* un citas), kur datu šifrēšanai izmantojās viena atslēga, bet atšifrēšanai otra. Pirmā atslēga var būt atklāta un publicēta visu sistēmu lietotāju izmantošanai datu šifrēšanai. Atšifrēt datus ar atklātu atslēgu nav iespējams. Datu atšifrēšanai saņēmējs izmanto otro atslēgu, kura ir slepena. Atšifrēšanas atslēga nevar būt definēta no šifrēšanas atslēgas. Tas nodrošina elektroniskā paraksta funkcionēšanu, kas ir būtisks trūkums visām simetriskām kriptosistēmām.

Aizsardzības līmenis ir atkarīgs no vairākiem faktoriem: kriptosistēmas kvalitāte, tās izmantošanas programmatūrā un iekārtās (īpaši tās drošība atslēgu izvēles veids), iespējamo kopējo atslēgu daudzums. Atslēgu garums tiek mērīts bitos, bet visu iespējamo atslēgu pārlikšanas grūtība pieaug eksponenciāli ar bitu pieaugumu. Modernās tehnoloģijas nodrošina drošu šifrēšanu gandrīz par tādu pašu izmaksu, kā vāju, līdz ar ko visparastākais, vispiesardzīgākais un visekonomiskākais risinājums ir izmantot vienotu šifrēšanas līmeni. Izstrādāts programmnodrošinājums *CRYPTO* ir spējīgs to nodrošināt un šifrēt jeb kādu datu formātu un apjomu ar kopējās atslēgas garumu līdz 70 bitiem. Determinētais haotiskais atraktors teorētiski ir spējīgs nodrošināt visiem determinētiem haotiskiem loģistikas atspoguļošanas modeļiem ļoti augstu līmeņa kriptozturību līdz pat 400 bitiem ar 5 slepenām atslēgām, vai sākumu parametriem.

Kā papildinājums simetrisku un asimetrisku kriptosistēmu drošības palielināšanai ir izstrādāta kombinētā (hibrīdu) šifrēšanas metode, kas ļauj apvienot augstās slepenības priekšrocības, kas nāk no kriptosistēmas ar atklātu atslēgu, un simetrisku kriptosistēmu ar slepeno atslēgu augstas ātrdarbības priekšrocībām.

Eksistē dažādas iespējas kriptosistēmu uzlaušanai sākot no parastiem datoriem un beidzot ar lielu datorkompleksu palīdzību. Ir pierādīts, ka šodien vairāki algoritmi ir vēl spēcīgs, bet ar katru mēnesi zaudē savu spēku, jo datoru jaudas palielinās katru gadu un atrast nepieciešamo atslēgu ir visvienkāršāk. Piemēram, jau šodien *DES* algoritmu ir ļoti vienkārši uzlaust no korporatīva vai valsts uzbrukuma. Lai pasargātu informāciju vairākus gadus simetriskām sistēmām iesaka izmantot atslēgas garumu no 90 bitiem. Tas pats attiecas arī uz kriptosistēmu izstrādi. Izstrādātais programmnodrošinājums atbilst šīm prasībām pēc koda modificēšanas un var būt komerciāli pielietojams ikdienā pēc tā modificēšanas saskaņā ar *ISO* standartizācijas prasībām, programmnodrošinājuma uzlabošanu un speciālu iekārtas veidošanu, kas nodrošinātu algoritma realizāciju iekārtas līmenī.

Literatūra

- [1] Анин Б. (1997) О шифровании и дешифровании. *Конфидент*, №1, 71-79
- [2] Аснис И.Л. (1994) Краткий обзор криптосистем с открытым ключом. *Защита информации*, №2, 35-39
- [3] Баричев С. Криптография без секретов, (1998) <http://infoart.kazan.ru/it/talk/crypto/index.htm>, 4-11. Введение в криптографию (авторизованный перевод статьи Дж. Чандлер "Cryptography 101") http://www.citforum.ru/internet/securities/crypto_1.shtml.
- [4] Долгирев В.А. и др. (1995) Проблемы широкого применения криптографических средств защиты информации. Доклад на 4 международной конференции "Региональная информатика-95", СПб, 1995, Россия, Санкт-Петербург, НТЦ "СПЕКТР", СПбГЭТУ, СПбГУ, 1-6
- [5] Жельников В.А. (1997) *Криптография от папируса до компьютера*. АБФ, 336 с.
- [6] Кочер П. Временной анализ реализаций Диффи-Хеллмана, RSA, DSS и других систем, (1995) <http://www.ssl.stu.neva.ru/psw/crypto/timing.html>, 11-15
- [7] Лебедев А. Г. (1997) Нужны ли "шифровальные средства". *Банковские технологии*, №1, 60-66

- [8] Методы и средства защиты информации" (*курс лекций*) (2000) Авторские права: Беляев А.В. Имущественные права: ЧФ СПбГТУ <http://www.citforum.ru/internet/infsecure/index.shtml>
- [9] Мошонкин А.Г. (1994) Что такое шифрование с открытым ключом? *Защита информации*, №1, 37-41
- [10] Отчет группы криптографов и компьютерных исследователей. О минимальной длине ключа для симметричных шифров, обеспечивающей необходимую степень стойкости (1999) <http://www.ssl.stu.neva.ru/psw/crypto/aptr.html>, 1-5
- [11] Пудовченко Ю.Е. (1999) Максимальная силовая атака на основе максимально распределенных вычислений. <http://www.ssl.stu.neva.ru/psw/crypto/bptr.html>, 5-7
- [12] Пудовченко Ю.Е. (1998) Когда наступит время подбирать ключи. <http://www.ssl.stu.neva.ru/psw/crypto/bptv.html>, 6-18
- [13] Райвест Р.Л. (1997) Многоуровневая криптография, *Конфидент*, №1, 35-67
- [14] Романец Ю.В. и др. (1999) *Защита информации в компьютерных системах и сетях*. Радио и связь, Москва, 12-125
- [15] Ростовцев А.Г., Михайлова Н.В.. (1998) Методы криптоанализа классических шифров. <http://www.ssl.stu.neva.ru/psw/crypto/pptp.html>, 2-15
- [16] Семьянов П.А. (1999) Почему криптосистемы ненадежны? <http://www.ssl.stu.neva.ru/>, 9-11. Смит Г. С. (1997) Программы шифрования данных. *Мир ПК*, №3, 59-68.
- [17] Теория и практика обеспечения информационной безопасности. (1996) Под редакцией Зегжды П.Д. -, Яхтмен, Москва. <http://www.ssl.stu.neva.ru/ssl/koi/publications/book-6.html>, 4-7.
- [18] Чмора А. Л. (1997) Практическая криптостойкость RSA: оценки и прогнозы. *Мир связи*, №10, 56-61
- [19] Schneier B. (1998) Why Cryptography Is Harder Than It Looks, <http://www.counterpane.com/whycrypto.html>, 6-29
- [20] Kinnunen T. (1993) On the way to chaos. Sarja/Series D-6, Publ. Turku School of Economics and Business Administration. Turku, 104-159

Pielikums A

ASCII tabula

	0	1	2	3	4	5	6	7	8	9	10	11	12	13	14	15
0	nul	␣	␣	♥	♦	♣	♠	•	◻	◊	♂	♀	♪	♫	☼	
16	▶	◀	↑	!!	¶	§	—	↓	↑	↓	→	←	↔	▲	▼	
32		!	“	#	\$	%	&	’	()	*	+	.	-	.	/
48	0	1	2	3	4	5	6	7	8	9	:	;	<	=	>	?
64	@	A	B	C	D	E	F	G	H	I	J	K	L	M	N	O
80	P	Q	R	S	T	U	V	W	X	Y	Z	[\]	^	~
96	`	a	b	c	d	e	f	g	h	i	j	k	l	m	n	o
112	p	q	r	s	t	u	v	w	x	y	z	{		}	~	Δ
128	Ç	ú	é	â	ä	å	ç	ê	ë	è	í	î	ï	Ä	Å	
144	É	æ	Æ	ô	ö	ù	û	ÿ	Û	Ü	ç	£	¥	Ps	f	
160	á	í	ó	ú	ñ	Ñ	ª	º	¿	¬	½	¼	¡	«	»	
176	☼	☼	☼													
192	Ł	ł	ł	ł	ł	ł	ł	ł	ł	ł	ł	ł	ł	ł	ł	ł
208	ll	ll	ll	ll	ll	ll	ll	ll	ll	ll	ll	ll	ll	ll	ll	ll
224	α	β	Γ	π	Σ	σ	μ	τ	□	θ	Ω	δ	ω	ø	ε	∩
240	≡	±	≥	≤	[]	÷	≈	°	•	.	√	°	²	▪	

Pielikums B

Detalizēti parādīti katra loģistikas atspoguļošanas modeļa (Verhulsta modelis, eksponenciālam modelis, polinomiālam modelis, Blackman-Fisher-Pry modelis, MacLaurin power modelis, otrs MacLaurin power modelis) teksta faila *teksts.txt* šifrēšanas rezultāts ar sākuma nosacījumiem $x_0 = 0,36$, $t = 15000$, $l = 12$, $p = 6$. Visiem modeļiem tika mainīts parametrs r četros gadījumos, lai parādītu šifrkta raksturu sekojošos atraktoros: fiksētais punkts, ar periodu 2, ar periodu 4 un determinēto haosu. Parādītajos rezultātos ir redzama tendence, ka šifrksts ir izturīgāks, tuvojoties determinēta haosa zonai.

Faila *teksts.txt* saturs:

AA

- [1] How to save FAR properties
- [2] How to switch keyboard to national language
- [3] Why FAR does not accept Windows 95 clipboard pasting
- [4] How to make panels half-screen
- [5] How to switch panels time format to 12-hour
- [6] How to show seconds in file time
- [7] How to show all folders in uppercase
- [8] I want wide panel with 4 name columns
- [9] I want network names and disk labels in "Change drive" menu

1. Verhulsta modelis

r = 2,56 (Atraktors fiksētais punkts)

Θ | πΦδδσ ΓΠΒΣΔ | Πάβ | Θεβσάβββ | βτβδ | ... áá ΛΠ=á | Πάβσ+σá | ... áá ΛΠ=á | Πάβσ

r = 3,26 (Cikliskais atraktors ar periodu 2)

... áá ΛΠ=á | Πάβσ+σá | ... áá ΛΠ=á | Πάβσ
... áá ΛΠ=á | Πάβσ+σá | ... áá ΛΠ=á | Πάβσ

r = 3,51 (Cikliskais atraktors ar periodu 4)

... áá ΛΠ=á | Πάβσ+σá | ... áá ΛΠ=á | Πάβσ
... áá ΛΠ=á | Πάβσ+σá | ... áá ΛΠ=á | Πάβσ

r = 3,66 (Determinētais haotiskais atraktors)

... áá ΛΠ=á | Πάβσ+σá | ... áá ΛΠ=á | Πάβσ
... áá ΛΠ=á | Πάβσ+σá | ... áá ΛΠ=á | Πάβσ

2. Eksponenciālais modelis

r = 1,21 (Atraktors fiksētais punkts)

... áá ΛΠ=á | Πάβσ+σá | ... áá ΛΠ=á | Πάβσ
... áá ΛΠ=á | Πάβσ+σá | ... áá ΛΠ=á | Πάβσ

r = 2,36 (Cikliskais atraktors ar periodu 2)

... áá ΛΠ=á | Πάβσ+σá | ... áá ΛΠ=á | Πάβσ
... áá ΛΠ=á | Πάβσ+σá | ... áá ΛΠ=á | Πάβσ

r = 2,56 (Cikliskais atraktors ar periodu 4)

... áá ΛΠ=á | Πάβσ+σá | ... áá ΛΠ=á | Πάβσ
... áá ΛΠ=á | Πάβσ+σá | ... áá ΛΠ=á | Πάβσ

r = 2,96 (Determinētais haotiskais atraktors)

... áá ΛΠ=á | Πάβσ+σá | ... áá ΛΠ=á | Πάβσ
... áá ΛΠ=á | Πάβσ+σá | ... áá ΛΠ=á | Πάβσ

3. Polinomiālais modelis

r = 1,21 (Atraktors fiksētais punkts)

... áá ΛΠ=á | Πάβσ+σá | ... áá ΛΠ=á | Πάβσ
... áá ΛΠ=á | Πάβσ+σá | ... áá ΛΠ=á | Πάβσ

ОСОБЕННОСТИ ДИАГНОСТИЧЕСКИХ СИСТЕМ С ЭЛЕМЕНТАМИ ИСКУССТВЕННОГО ИНТЕЛЛЕКТА

Е. КОПЫТОВ, В. ЛАБЕНДИК, Н. КАБЕЛЕВ

Институт транспорта и связи
 ул. Ломоносова 1, корпус 4, LV-1019, Рига, Латвия

При всем многообразии задач, решаемых в современных системах диагностирования авиационной техники, у них имеется один существенный недостаток – жесткость алгоритмов, используемых в компьютерных программах. В результате в таких алгоритмах потеря информации хотя бы по одному измерительному каналу приводит к отказу в решении задачи, в которой использовался ранее потерянный параметр.

Рассматривается задача повышения надежности диагноза путем использования в системе диагностирования таких элементов искусственного интеллекта, как нейронные сети. Предлагается способ обучения искусственных нейронных сетей распознаванию образов-дефектов и неисправностей проточной части двигателя с помощью диагностических матриц на основе физической линейной математической модели двигателя.

Ключевые слова: нейронные сети, надежность, диагностика авиационных двигателей

1. Введение

Надежность летательных аппаратов зависит не только от обеспечения надежности работы его частей (планера, двигателей), но и от надежности обеспечивающих эту работу систем, в частности, систем контроля. Потеря контроля ставит под вопрос обеспечение безопасности полета летательного аппарата, особенно, с двигателями 5-го поколения, имеющими высокие параметры рабочего процесса (степень сжатия воздуха в компрессоре порядка 45, температура газа перед турбиной порядка 850К). Для своевременного принятия решения в полете при нарушении нормальной работы авиадвигателя необходим постоянный мониторинг его технического состояния, т.е. обработка поступающей от него информации в режиме реального времени для выделения опасных неисправностей, которые могут привести к отказу двигателя в полете.

2. Методы диагноза авиационных двигателей

Одной из задач автоматизированных систем диагностирования (АСД) самолета является контроль термогазодинамических параметров по тракту двигателя. Простая оценка замеряемых в полете параметров двигателя (по записям МСРП) – это *допусковый контроль* (обработка среднестатистических замеряемых в полете отклонений параметров от нормы). При этом, чем больше повторений замеров, тем достовернее контроль, но, во-первых, полет на разных участках траектории ограничен по времени, а, во-вторых, увеличение времени работы двигателя приводит к износу его частей и, вследствие этого, дополнительному изменению параметров. Последние проверяются от полета к полету – это так называемый *трендовый контроль*. Недостаток допускового контроля по замеряемым параметрам – это оценка работы двигателя в целом без диагностирования (локализации) причины этих отклонений. Для установления диагноза чаще всего применяют статистические модели, увязывающие отклонения критериев, оценивающих дефекты в узлах, с отклонениями замеряемых параметров, (выбор критериев – это самостоятельная задача) в виде регрессионной модели дефектов:

$$\delta A = W_{a1} \cdot \delta x_1 + W_{a2} \cdot \delta x_2 + W_{a3} \cdot \delta x_3 + \dots + W_{an} \cdot \delta x_n \quad (1)$$

$$\delta B = W_{b1} \cdot \delta x_1 + W_{b2} \cdot \delta x_2 + W_{b3} \cdot \delta x_3 + \dots + W_{bn} \cdot \delta x_n \quad (2)$$

где $W_{a1}, W_{a2}, W_{a3}, \dots, W_{an}, W_{b1}, W_{b2}, W_{b3}, \dots, W_{bn}$ – коэффициенты влияния (весовые коэффициенты).

Таблицу коэффициентов влияния называют *диагностической матрицей* (ДМ). Здесь же встает вопрос об оптимальном числе измеряемых параметров. С одной стороны, чем больше число замеров, тем достовернее диагноз, но и тем больше вероятность отказа какого-либо канала поступления информации (засорение датчика замера давления, обрыв электрической цепи и т.д.). В результате диагностирование по всем критериям прекратится, т.е. алгоритм АСД по данной задаче перестает работать. Проблема осложняется еще тем, что для новых двигателей такой статистики по дефектам еще нет. В работе [1] рассмотрено получение ДМ на основе не статистической, а физической линейной математической модели двигателя (см. Таблицу 1). Там же обосновано необходимое для решения системы линейных уравнений число измеряемых параметров, зависящее от конструктивной схемы двигателя (числа валов, степени двухконтурности и т.п.).

ТАБЛИЦА 1. Диагностическая матрица двигателя ТВ7-117С с дополнительными замерами параметров P^*_{TK} и $T^*_{К}$ (N=1470 кВт)

Отклонения параметров	∂n_{TK}	∂T^*_{TK}	∂G_T	∂P^*_K	$\partial P^*_{TC} = \partial P^*_{TK}$	∂T^*_K
$\partial \bar{\eta}^*_K$	0,189	0,148	0,097	0,482	0,000	-1,148
$\partial \bar{G}_B$	-2,480	-1,490	0,927	0,053	0,000	-0,105
$\partial \eta^*_{TK}$	0,000	-0,708	0,000	-0,551	0,551	0,805
∂F^{TK}_{CA}	0,000	-1,176	1,000	-1,000	0,000	0,037
$\partial \eta^*_{TC}$	0,000	0,530	-1,000	0,000	-0,947	0,130
∂F^{TC}_{CA}	0,000	-1,030	1,000	0,000	-1,000	-0,130

3. Нейронные сети в системе диагностирования

Но и в последнем случае при решении системы уравнений в программе ЭВМ с обычной логикой должно соблюдаться одно условие: число определяемых (неизвестных) параметров не может превышать числа уравнений, заложенных в программу. Исчезло или появилось одно неизвестное – и машина заходит в тупик. «Элементы современных электронных машин идиотски логичны» – сказал по этому поводу кибернетик Шмидт [2]. Один из способов, позволяющих расширить «интеллектуальные возможности» ЭВМ – это эвристический подход, при котором машине приходится в определенный момент нарушить железную логику своих рассуждений и начать действовать «наугад», например методом Монте-Карло. Но и здесь подобные действия ЭВМ должны быть специально запрограммированы. Актуальность проблемы состоит в том, что добавление новых программ вступает в противоречие с возможностями бортовых ЭВМ при необходимости их работы в полете в режиме реального времени, особенно для контроля будущих высоконагруженных двигателей 5-го и 6-го поколений. Выходом из этого нами видится в применении в бортовых АСД компьютерных систем с элементами искусственного интеллекта в виде искусственных нейронных сетей (ИНС) [3-6] не вместе, а вместо программы обнаружения в полете опасных дефектов, с помощью, например, ДМ. Однако это не означает отказа от ДМ, а предлагается их использовать в наземной части АСД для обучения ИНС поиску (распознаванию) дефектов и неисправностей авиационного двигателя. Нами проанализированы алгоритмы организации диагноза по ДМ и с помощью ИНС и выявлена интересная аналогия. Искусственный нейрон (Рисунок 1) умножает каждый i -й вход x_i на вес W_i и суммирует взвешенные входы, т.е. его действия аналогичны поиску дефекта по уравнению модели (1).

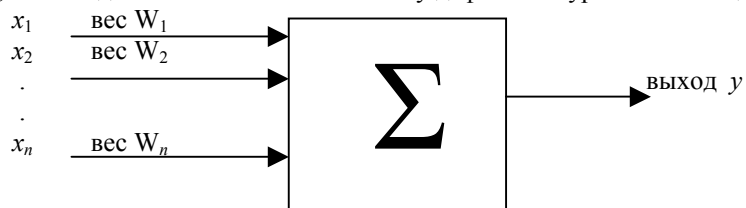
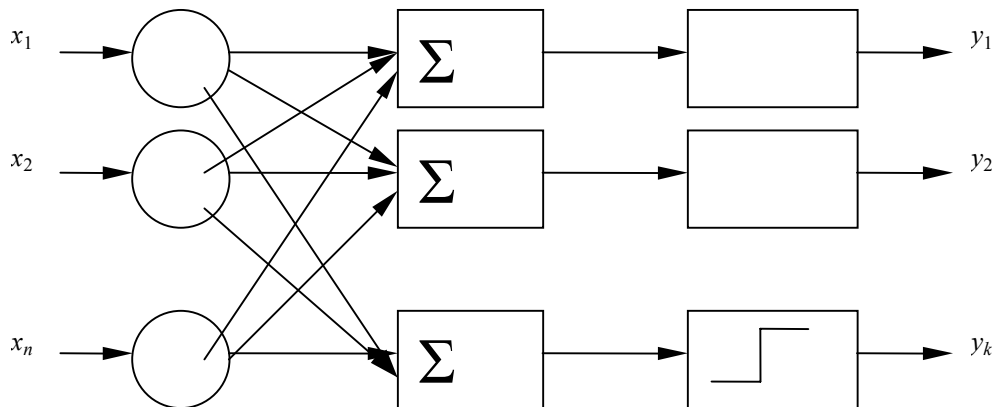


Рисунок 1. Искусственный нейрон

А в целом, локализация дефектов с помощью ДМ подобна работе системы нейронов, которая получила название персептрона (Рисунок 2). При этом каждый нейрон в простейшем случае модифицирует вычисленную сумму с помощью активизационной функции в виде сигнала наличия (1) или отсутствия (0) дефекта. Но на этом аналогия в работе ДМ и персептрона заканчивается, т.к. ДМ имеет жесткий алгоритм обработки информации, а искусственные нейронные сети могут менять свое поведение в зависимости от внешней среды. После предъявления входных сигналов совместно с известным выходом они могут самонастраиваться



(обучаться), чтобы получить требуемую реакцию. Однако организация процесса обучения в каждом конкретном случае является проблемой.

Рисунок 2. Однослойный персептрон с n входами и k выходами

4. Способ обучения нейронных сетей с помощью диагностических матриц

Ниже рассмотрен способ обучения ИНС распознаванию образов-дефектов и неисправностей проточной части двигателя с помощью разработанной нами ДМ на основе физической линейной математической модели (ММ) двигателя [1]. Особенностью предлагаемой ММ является ее способность (чувствительность) к изменению технического состояния двигателя. Это достигнуто путем введения в уравнение системы членов, учитывающих относительный сдвиг характеристик компрессоров в виде частного относительного изменения коэффициента полезного действия $\delta\bar{\eta}_k^*$ и производительности компрессора (расхода воздуха) $\delta\bar{G}_B$. При этом общее изменение этих величин может быть вызвано появлением дефекта в другом узле двигателя и в связи с этим изменением режима течения по всему тракту двигателя. Характеристика узла изображается на плоскости, сдвиг ее характеризуется не одним, а двумя представленными выше критериями комплексно в виде векторов возможных дефектов (Рисунок 3).

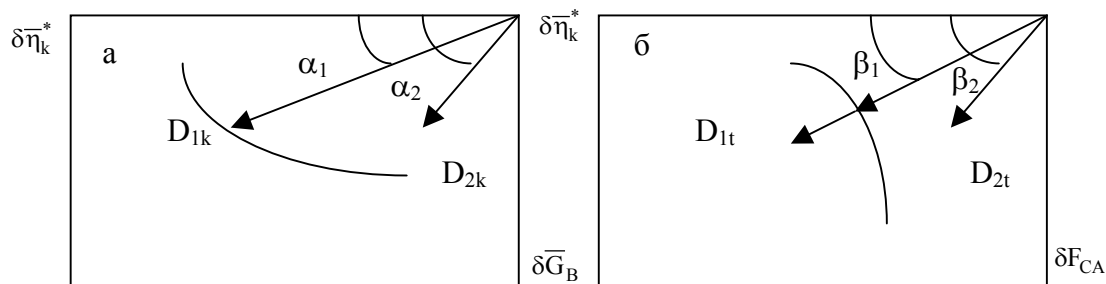


Рисунок 3. Вектора возможных дефектов: a – компрессора, b – турбины

Для турбин, сопловые аппараты которых обычно работают на критических режимах, сдвиг характеристик незначителен, поэтому их дефекты можно оценивать в виде комплекса общих изменений коэффициентов полезного действия и проходных площадей сопловых аппаратов (Рисунок 3 б). При этом можно установить предельно допустимые изменения параметров, исходя из возможности опасного нарушения работы двигателя в целом в полете. Причем важно, что

предельные отклонения можно ввести в ДМ по результатам испытаний отдельных узлов (и их деталей), а не по испытаниям двигателя в целом до разрушения.

Информация для наземного обучения многослойных ИНС производится в следующей последовательности. Сам алгоритм построения ДМ на основе физической линейной ММ двигателя изложен в [1] и аналогичен работе многослойной ИНС. Для получения ДМ система линейных уравнений преобразуется следующим образом. В левую часть уравнений переносятся члены с отклонениями параметров, которые не измеряются (в том числе с критериями дефектов), а в правую часть - с отклонениями измеряемых параметров. Далее составляются две таблицы (матрицы) коэффициентов влияния при этих параметрах. При этом коэффициенты влияния вычисляются по специальным формулам для исходного (бездефектного) технического состояния двигателя. Матрицу коэффициентов при критериях дефектов можно представить как таблицу весовых коэффициентов единичного слоя персептрона (так же как и матрицу коэффициентов при отклонениях измеряемых параметров), а саму ДМ - как результат работы многослойного персептрона. При этом для обучения предлагается в данном случае использовать сеть обратного распространения. Обучающий алгоритм представляет собой последовательность отключения единичного или парного сигналов (отклонений замеров) датчиков при заданных отклонениях критериев выбранного для обучения дефекта - «желаемых» выходных сигналов сети. Задача осложняется тем, что если для дефектов, обнаруженных в процессе испытаний двигателя, известны отклонения оставшихся измеряемых параметров, то для моделируемых теоретически отклонений критериев дефектов такие отклонения неизвестны. Поэтому для обучения предлагается формировать вспомогательную матрицу коэффициентов влияния критериев дефектов на отклонения измеряемых параметров. Для этого исходная линейная система уравнений (ММ) преобразуется так, что в левую часть уравнений переносятся члены с отклонениями всех (в том числе и измеряемых) термодинамических параметров, а в правую часть – только члены с отклонениями независимых друг от друга параметров (коэффициентов потерь в отдельных узлах и т.п.), в том числе и с выбранными комплексными критериями дефектов узлов. После математических преобразований обращения первой матрицы и перемножения ее со второй матрицей получается необходимая матрица коэффициентов влияния отклонений независимых параметров на отклонения термогазодинамических (в том числе и измеряемых в разных сечениях по тракту двигателя значений ρ^* и T^* параметров):

$$\delta\rho_i^* = W_{1p} \cdot \delta k_{1i} + W_{2p} \cdot \delta k_{2i} + W_{2p} \cdot \delta k_{3i} + \dots + W_{np} \cdot \delta k_{ni} \quad (3)$$

$$\delta T_i^* = W_{1T} \cdot \delta x_1 + W_{b2} \cdot \delta k_{2i} + W_{b3} \cdot \delta k_{3i} + \dots + W_{bn} \cdot \delta k_{ni} \quad (4)$$

где i - номер i -го дефекта какого-то узла.

Задавая комплексно разные величины критериев дефектов (Рисунок 3) и получая величины отклонений измеряемых на двигателе параметров, можно произвести первый этап обучения диагностической ИТС. Второй этап обучения заключается в последовательном отключении сигналов измеряемых параметров, при этом целью процедуры обучения сети является такая подстройка ее весов, чтобы приложение некоторого множества входов приводило к требуемому множеству выходов (векторов дефектов). Даже если за каким-то узлом пропали замеры, а в других узлах нет дефектов, ИНС после подбора весов по сочетаниям отклонений оставшихся измеряемых параметров после обучения указывает не только наличие дефекта в узле, но и предполагаемый характер дефекта). Важным свойством ИНС является нечувствительность (до некоторой степени) отклика сети после обучения к небольшим изменениям входных сигналов (погрешностям измерения). Такая система позволяет преодолеть требование строгой точности, предъявляемое обычным компьютерам, и открывает путь взаимодействия с миром хаоса, в котором мы живем.

5. Выводы

Важно отметить, что ИНС делает обобщения автоматически благодаря своей структуре, а не с помощью использования «человеческого интеллекта» в форме специально написанных компьютерных программ. ИНС могут эффективно существовать, объединяясь с Экспертными системами, где каждый подход используется для решения тех задач, с которыми он лучше

справляется. Поэтому перспективной для двигателей следующего 6-го поколения будет применение на борту не только компьютерной прогнозирующей системы, а компьютерной системы принятия решений (СПР), а человеку останется функция контроля этих систем и взятие на себя функции принятия решения в случае отказа системы.

Литература

- [1] Кузнецов Н.С., Лабендик В.П. (1993) Особенности формирования диагностических матриц для контроля состояния проточной части авиационных ГТД. *Изв. ВУЗОВ "Авиационная техника"*, 3, 89-93.
- [2] Уоссермен Ф. (1992) Нейрокомпьютерная техника: Теория и практика. Москва
- [3] Копытов Е., Кабелев Н. (2000) A method of adaptive re-configuration of multi-layer perceptron in real-time learning system/ *Computer Modelling & New Technologies* 4, No.1, 7-14.
- [4] Копытов Е., Лабендик В., Кабелев Н.. (2001) Neural Network Applications in Aircraft Engine Diagnostics. **In:** Scientific Proceedings of the Scientific-technical Union of Mechanical Engineering, vol. 2 (57). Third International Congress "Mechanical Engineering Technologies'01", June 24-26, 2001, Sofia, Bulgaria, pp. 558-560.
- [5] Haykin S. (1994) *Neural Networks: A Comprehensive Foundation*. Macmillan College Publishing, New York
- [6] Zurada J.M. (1992) *Introduction to Artificial Neural Systems*. West Publishing C., St.Paul

Received on the 17th of December 2001

ВЫСОКОИЗБИРАТЕЛЬНЫЕ ЦИФРОВЫЕ ПОЛИФАЗНЫЕ ФИЛЬТРЫ

В.П.ЕРЕМЕЕВ, Э.В. МАТОСОВ, С.Г. ТИМОНИН

*Институт транспорта и связи, департамент электроники
ул. Ломоносова 1, LV-1019, Рига, Латвия*

Предложен новый способ построения цифровых многоканальных фильтров на базе цифровых высокоизбирательных рекурсивных ФНЧ. Показана возможность упрощения полифазной структуры. Выбрана оптимальная процедура расщепляющего преобразования. Проведено детальное сопоставление реализаций на основе рекурсивного и нерекурсивного прототипов.

Ключевые слова: цифровые многоканальные фильтры

We suggest the new method design of digital multichannel filters that based on digital high selection low-band FIR filters. We showed also possibility for polyphase structure simplification. Filters have optimal procedure of decompose transform. In article we compare in detail the FIR and IIR filter realization.

Keywords: digital multichannel filters

1. Введение

Эффективное разделение сигналов на отдельные частотные полосы является актуальной задачей во многих приложениях [1,2,5,6]. Наиболее рациональной является структура, основанная на полифазной форме построения [2,4,5,6-9]. Для нерекурсивных структур определение полифазных компонент осуществляется достаточно тривиально – прореживанием коэффициентов импульсной характеристики фильтра с интервалом, равным общему числу компонент. Для рекурсивных высокоизбирательных структур эта задача более актуальна и сложна [2, 5, 6].

Ранее нами описан новый способ выделения полифазных компонент передаточной функции цифровых рекурсивных фильтров [3]. Разработана методика синтеза многоканальных рекурсивных полифазных фильтров, причем подзадача разбиения исходного рекурсивного прототипа на полифазные компоненты хорошо алгоритмизирована. Синтезируемые фильтры в полной мере наследуют свойства прототипа. Напоминаем, что имеет место ограничение: количество полифазных компонент и количество каналов системы должны быть кратными степени двойки. Вначале рассчитывается устойчивый рекурсивный цифровой прототип с чебышевской, баттервортовской, золотаревской, бесселевской, либо другой требуемой характеристикой. Далее, передаточная функция прототипа разделяется на полифазные компоненты и, наконец, используется соответствующее разделяющее преобразование (быстрое вещественное ОДПФ).

В *приложении* приводится пример и программы детализированного расчета параметров оптимальной реализации восьмиканальной фильтрующей цифровой полифазной структуры. Оптимизация связана с уменьшением числа операций расщепляющего преобразования.

2. Сравнение нерекурсивных и рекурсивных полифазных структур по вычислительной сложности

Традиционные полифазные структуры строятся на основе цифровых нерекурсивных фильтров, которые рассчитываются, например, с помощью алгоритма Ремеза или методами линейного программирования. При этом для получения высокоизбирательных характеристик требуются фильтры весьма большого порядка, что обуславливает высокую вычислительную сложность полифазной структуры в целом.

Известно, что рекурсивные фильтры обеспечивают требуемую избирательность при гораздо меньших порядках. Поэтому, применяя рекурсивный цифровой НЧ-прототип для синтеза полифазной структуры, можно ожидать упрощения многоканальной реализации.

Ниже в Таблице 1 показаны результаты сравнения рекурсивных и нерекурсивных структур по вычислительной сложности. Предметом сравнения являются количество умножений, сложений и ячеек памяти.

Обозначения :

- М – число каналов.
- № - паспорт многоканального фильтра.
- Далее указаны параметры цифрового НЧ фильтра-прототипа:
 w_1 – частота среза, w_k – контрольная частота, A_{min} – минимум затухания в полосе задержки, A_{max} – максимум затухания в полосе пропускания, K_p – коэффициент прямоугольности по уровням A_{min} и A_{max} , N – порядок, N_1 – порядок полифазной части фильтра.

ТАБЛИЦА 1

Требования к частотной избирательности полифазных фильтров							Нерекурсивные полифазные фильтры				Рекурсивные полифазные фильтры				
№	М	w_k	K_p	w_1	A_{max}	A_{min}	N	Умножений	Сложений	Ячеек памяти	N	Умножений	Сложений	Ячеек памяти	N1
1	8	0,0625	0,08601	0,0053756	0,0851412	40	55	28	48	55	3	52	36	51	49
2	8	0,0625	0,04418	0,0027613	0,0272554	50	71	36	64	71	3	52	36	51	49
3	8	0,0625	0,05099	0,0031869	0,0428964	60	79	40	72	79	3	52	36	51	49
4	8	0,0625	0,02083	0,0013019	0,0160815	75,1	95	48	88	95	3	52	36	51	49
5	8	0,0625	0,02684	0,0016775	0,0136463	70	95	48	88	95	3	52	36	51	49
6	8	0,0625	0,01923	0,0012019	0,015568	81,6	103	52	96	103	3	52	36	51	49
7	8	0,0625	0,01666	0,0010413	0,013962	95,57	119	60	112	119	3	52	36	51	49
8	8	0,0625	0,01562	0,0009763	0,0131676	102,43	127	64	120	127	3	52	36	51	49
9	16	0,03125	0,08601	0,0026878	0,0851328	40	111	56	96	111	3	100	68	99	97
10	16	0,03125	0,04424	0,0013825	0,0272874	50	143	72	128	143	3	100	68	99	97
11	16	0,03125	0,02499	0,0007809	0,0141221	61,76	159	80	144	159	3	100	68	99	97
12	16	0,03125	0,02083	0,0006509	0,0162089	75,45	191	96	176	191	3	100	68	99	97
13	16	0,03125	0,01923	0,0006009	0,0156528	82,3	207	104	192	207	3	100	68	99	97
14	16	0,03125	0,01666	0,0005206	0,0140098	95,89	239	120	224	239	3	100	68	99	97
15	16	0,03125	0,01562	0,0004881	0,0132058	102,73	255	128	240	255	3	100	68	99	97
16	32	0,015625	0,08601	0,0013439	0,0851275	40	223	112	192	223	3	196	132	195	193
17	32	0,015625	0,04426	0,0006916	0,0272921	50	287	144	256	287	3	196	132	195	193
18	32	0,015625	0,02286	0,0003572	0,0068999	60	319	160	288	319	3	196	132	195	193
19	32	0,015625	0,01938	0,0003028	0,0014273	70	383	192	352	383	3	196	132	195	193
20	32	0,015625	0,00843	0,0001317	6,48E-04	80	415	208	384	415	3	196	132	195	193
21	32	0,015625	0,00684	0,0001069	1,36E-04	90	479	240	448	479	3	196	132	195	193
22	32	0,015625	0,00296	4,625E-05	6,18E-05	100	511	256	480	511	3	196	132	195	193
23	64	0,0078125	0,08602	0,000672	0,0851415	40	447	224	384	447	3	388	260	387	385
24	64	0,0078125	0,04427	0,0003459	0,0272943	50	575	288	512	575	3	388	260	387	385
25	64	0,0078125	0,02345	0,0001832	0,0068208	60	639	320	576	639	3	388	260	387	385
26	64	0,0078125	0,01882	0,000147	0,0014113	70	767	384	704	767	3	388	260	387	385
27	64	0,0078125	0,00856	6,688E-05	6,41E-04	80	831	416	768	831	3	388	260	387	385
28	64	0,0078125	0,00687	5,367E-05	1,34E-04	90	959	480	896	959	3	-	-	-	-
29	64	0,0078125	0,00312	2,438E-05	6,11E-05	100	1023	512	960	1023	3	-	-	-	-
30	128	0,0039063	0,08603	0,0003361	0,085157	40	895	448	768	895	3	772	516	771	769
31	128	0,0039063	0,04427	0,0001729	0,02729	50	1151	576	1024	1151	3	772	516	771	769
32	128	0,0039063	0,0238	9,297E-05	0,00678	60	1279	640	1152	1279	3	772	516	771	769
33	128	0,0039063	0,01924	7,516E-05	0,001403	70	1535	768	1408	1535	3	772	516	771	769
34	128	0,0039063	0,00863	3,371E-05	6,37E-04	80	1663	832	1536	1663	3	772	516	771	769
35	128	0,0039063	0,00689	2,691E-05	1,34E-04	90	1919	960	1792	1919	3	-	-	-	-
36	128	0,0039063	0,00308	1,203E-05	6,07E-05	100	2047	1024	1920	2047	3	-	-	-	-

В Таблице 1 приведены данные оптимальных по характеристикам и вычислительным затратам рекурсивных и нерекурсивных цифровых полифазных фильтров

На Рисунке 1 дано сопоставление вычислительных затрат для рекурсивных (РФ) и нерекурсивных (НФ) 8-канальных полифазных фильтров. Видно, что рекурсивные реализации значительно эффективнее. Для структур с большим количеством каналов результаты аналогичны.

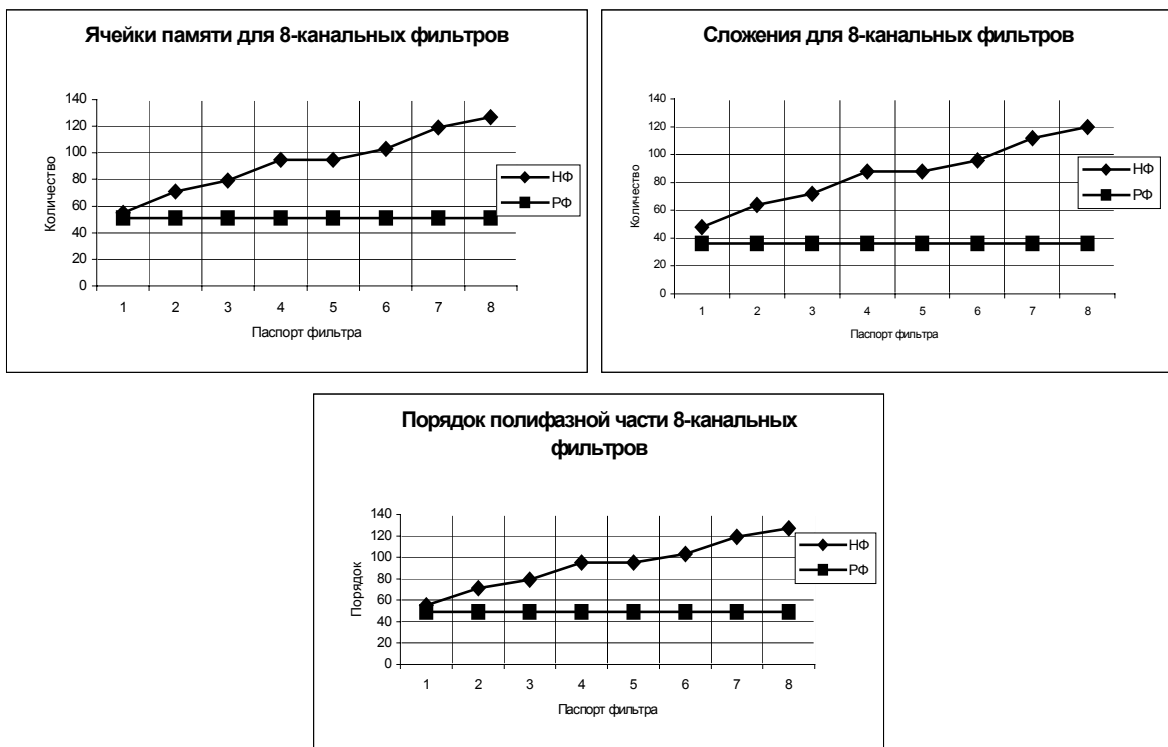


Рисунок 1. Параметры реализации 8-канальных структур.

Таким образом, при одних и тех же исходных требованиях сложность реализации нового класса многоканальных фильтров существенно ниже по сравнению со структурами, базирующимися на традиционных нерекурсивных цифровых фильтрах.

Литература

- [1] Renfors M. and Saramäki T. (1997) Recursive N – band Digital Filters. *IEEE Transactions on circuits and systems*, Vol. Cas-34, No. 1, January 1987.
- [2] Витязев В.В. (1993) Цифровая частотная селекция сигналов. Радио и связь. Москва.
- [3] Еремеев В.П., Матосов Э.В., Тимонин С.Г. (2000) Рекурсивные полифазные цифровые фильтры. *Computer Modelling and New Technologies* 4, No. 2, 57-60.
- [4] Еремеев В.П., Матосов Э.В. (1998) Квадратурные полифазные фильтры. *Сборник научных трудов РАУ*, Рига
- [5] Вайдьянатхан П.П. (1990) Цифровые фильтры, блоки фильтров и полифазные цепи с многочастотной дискретизацией. Методический обзор. *ТИИЭР* 78, № 3, март, 77-120.
- [6] Vaidyanathan P.P. (1993) *Multirate systems and filter banks*. Prentice Hall, Englewood Cliffs, N.-Y.
- [7] Еремеев В.П., Касьянов В.В. (1996) Синтез цифровых фильтров для обработки многоканальных сигналов. *Труды международной конференции "Авиация, экология, техносфера – взгляд в третье тысячелетие"*, Рига, с. 116-119.
- [8] Еремеев В.П., Матосов Э.В. (1999) Реализации многоканальных полифазных узкополосных фильтров. *Computer Modelling and New Technologies* 3, 59-65.
- [9] Еремеев В.П., Матосов Э.В. (2000) Модификации полифазных фильтров. Цифровая обработка сигналов и ее применение. *Доклады межд. конф. "Цифровая обработка сигналов"*, Москва, Том 3, 203-211.

Приложение

Пример оптимальной реализации 8-канального рекурсивного полифазного цифрового фильтра с оптимальным блоком ОДПФ

Исходные требования к низкочастотному фильтру-прототипу :

- затухание в полосе пропускания $a_{max} = 0,01$ дБ
- затухание в полосе непропускания $a_{min} = 40$ дБ
- коэффициент прямоугольности $K_n = 0,7$
- нормированная контрольная частота $\Omega_c = 0,0625$
- нормированная частота среза $\Omega_f = 0,04375$

Коэффициенты 8-канального фильтра:

ТАБЛИЦА 2. Коэффициенты входных блоков.

Номер каскада	Коэф-ты при z^0	Коэф-ты при z^{-16}	Коэф-ты при z^{-32}
1	1	-0.0911	0
2	1	0.0711	0.0328
3	1	0.6924	0.2121
4	1	1.3657	0.6580

ТАБЛИЦА 3. Коэффициенты полифазных блоков.

№ полиф. комп.	z^0	z^{-16}	z^{-32}	z^{-48}	z^{-64}	z^{-80}	z^{-96}	z^{-112}
1	0.0027	0.0354	0.1086	0.1320	0.0705	0.0152	0.0009	1.8116e-006
2	0.0046	0.0417	0.1149	0.1309	0.0660	0.0133	0.0007	0
3	0.0038	0.0424	0.1157	0.1272	0.0612	0.0116	0.0006	0
4	0.0041	0.0452	0.1180	0.1239	0.0567	0.0100	0.0004	0
5	0.0050	0.0493	0.1210	0.1208	0.0523	0.0086	0.0003	0
6	0.0064	0.0542	0.1243	0.1175	0.0482	0.0074	0.0003	0
7	0.0081	0.0594	0.1274	0.1142	0.0443	0.0063	0.0002	0
8	0.0100	0.0647	0.1301	0.1105	0.0405	0.0054	0.0001	0
9	0.0119	0.0700	0.1323	0.1067	0.0370	0.0045	0.0001	0
10	0.0140	0.0752	0.1340	0.1026	0.0336	0.0038	0.0001	0
11	0.0161	0.0801	0.1351	0.0983	0.0304	0.0032	4.7905e-005	0
12	0.0183	0.0848	0.1357	0.0938	0.0274	0.0026	3.2300e-005	0
13	0.0205	0.0892	0.1356	0.0892	0.0245	0.0022	2.1155e-005	0
14	0.0228	0.0933	0.1350	0.0845	0.0219	0.0018	1.3407e-005	0
15	0.0251	0.0972	0.1338	0.0797	0.0195	0.0014	8.2077e-006	0
16	0.0275	0.1007	0.1321	0.0748	0.0172	0.0011	4.8872e-006	0

Реализация блока ОДПФ: $a = 0.923879532$; $b = 0.382683432$; $c = 0.707106781$.

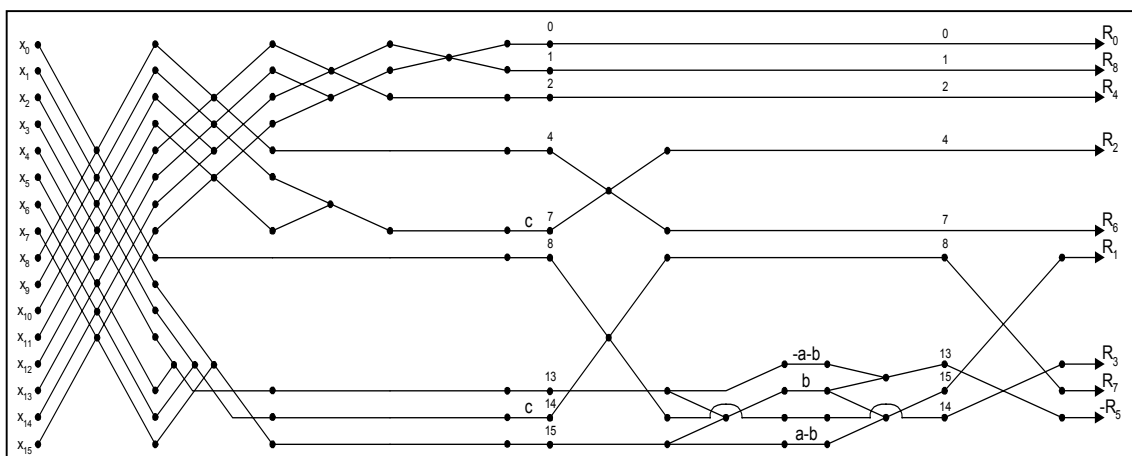


Рисунок 2. Граф сверхбыстрого преобразования Фурье (вещественная часть).

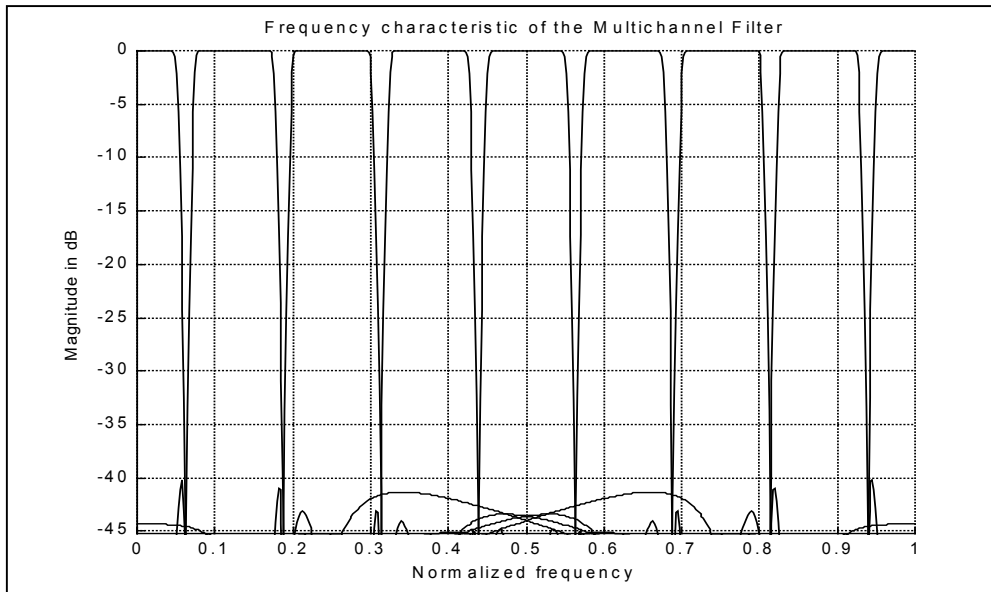


Рисунок 3. Амплитудно-частотные характеристики 8-канальной системы фильтров.

Программа оптимального вещественного преобразования Фурье на 16 точек в кодах системы MATLAB-5

```
function R = vhrfft(x)

a = 0.923879532; b = 0.382683432; c = 0.707106781;
R = zeros(16, 1);

M = x(1); x(1) = x(1) + x(9); x(9) = M - x(9);
M = x(2); x(2) = x(2) + x(10); x(10) = M - x(10);
M = x(3); x(3) = x(3) + x(11); x(11) = M - x(11);
M = x(4); x(4) = x(4) + x(12); x(12) = M - x(12);
      x(5) = x(5) + x(13);
M = x(6); x(6) = x(6) + x(14); x(14) = M - x(14);
M = x(7); x(7) = x(7) + x(15); x(15) = M - x(15);
M = x(8); x(8) = x(8) + x(16); x(16) = M - x(16);

M = x(1); x(1) = x(1) + x(5); x(5) = M - x(5);
M = x(2); x(2) = x(2) + x(6); x(6) = M - x(6);
M = x(3); x(3) = x(3) + x(7);
M = x(4); x(4) = x(4) + x(8); x(8) = M - x(8);
      x(16) = x(10) - x(16);
      x(15) = x(11) - x(15);
      x(14) = x(12) - x(14);

M = x(1); x(1) = x(1) + x(3); x(3) = M - x(3); %R5
      x(2) = x(2) + x(4); x(8) = x(6) - x(8);

M = x(1); x(1) = x(1) + x(2); x(2) = M - x(2); %R1 R9

x(8) = c*x(8); x(15) = c*x(15);

M = x(5); x(5) = x(5) + x(8); x(8) = M - x(8); %R3 R7
M = x(9); x(9) = x(9) + x(15); x(15) = M - x(15);

      M = x(14) + x(16); M = b*M;
x(14) = (a + b)*x(14); x(16) = (a - b)*x(16);
x(16) = M + x(16); x(14) = M - x(14);

M = x(9); x(9) = x(9) + x(16); x(16) = M - x(16); %R2 R8
M = x(14); x(14) = x(14) + x(15); x(15) = M - x(15); %R4 -R6

R(1) = x(1);
R(2) = x(9);
R(3) = x(5);
R(4) = x(14);
```

```

R(5) = x(3);
R(6) = -x(15);
R(7) = x(8);
R(8) = x(16);
R(9) = x(2);

for k = 2:8, R(18 - k) = R(k); end

```

Программа расчета 8-канального эллиптического фильтра

```

clear, home

%=====
% Количество каналов и полифазных компонент в многоканальном фильтре

NCh = 8; M = 2*NCh;

%=====
% Требования к частотной избирательности цифрового НЧ-прототипа

Kp = 0.7;
amax = 0.01;
wk = 1/M;
w1 = Kp*wk;
amin = 40;

amin = amin + 0.13*amin; % коррекция АЧХ в полосе задержки

clear Kp
%=====
% Определение порядка цифрового НЧ-прототипа

K = cot(0.5*pi*w1);
Wk = K*tan(0.5*pi*wk);
k = 1/Wk;
k1 = sqrt(1-k^2);
Q0 = (1 - sqrt(k1))/(2*(1 + sqrt(k1)));
Q = Q0^4;
Q = (((569*Q + 50)*Q + 5)*3*Q + 2)*Q + 1)*Q0;
Y = (10^(0.1*amin) - 1)/(10^(0.1*amax) - 1);
N = ceil(log10(16*Y)/log10(1/Q));

%=====
% Определение коэффициентов цифрового НЧ-прототипа

M0 = 10*log10(1 + 16*(10^(0.1*amin) - 1)*Q^N);
L = log((10^(0.05*M0) + 1)/(10^(0.05*M0) - 1))/(2*N);
T = 2*Q^0.25/sqrt(k);
f0 = T*sinh(L);
f = 2*cosh(2*L);
G = 1;
for J = 1:25
    G = f0*G*(1 - f*Q^(2*J) + Q^(4*J))/(1 - f*Q^(2*J - 1) + Q^(4*J - 2));
    f0 = 1;
end
G = abs(G);
if rem(N,2) == 0
    R = N/2;
    m = 0.5;
    H0 = 10^(-0.05*M0);
else
    R = (N - 1)/2;
    m = 0;
    H0 = G;
end
for i = 1:R
    S(i) = T*sin(pi*(i - m)/N);
    C(i) = 2*cos(2*pi*(i - m)/N);
    X = 1;
    for J = 1:25
        X = X*(1 - C(i)*Q^(2*J) + Q^(4*J))/(1 - C(i)*Q^(2*J - 1) + Q^(4*J - 2));
    end

```

```

W(i) = S(i)*X;
V(i) = sqrt((1 - (k*W(i))^2)*(1 - W(i)^2));
A(i) = 1/((k*W(i))^2);
B(i) = (2*G*V(i))/(1 + (k*G*W(i))^2);
C(i) = (G^2 + W(i)^2)/(1 + (k*G*W(i))^2);
H0 = H0*C(i)/A(i);
end
if rem(N,2) == 0
    b{1} = H0;
    a{1} = 1;
else
    g = G + K;
    a{1}(2) = 1;
    a{1}(1) = (G - K)/g;
    b{1}(2) = H0/g;
    b{1}(1) = b{1}(2);
end
for i = 2:R + 1
    d = K^2 + B(i - 1)*K + C(i - 1);
    a{i}(3) = 1;
    a{i}(2) = 2*(C(i - 1) - K^2)/d;
    a{i}(1) = (d - 2*B(i - 1)*K)/d;
    b{i}(3) = (K^2 + A(i - 1))/d;
    b{i}(2) = 2*(A(i - 1) - K^2)/d;
    b{i}(1) = b{i}(3);
end
end

clear A B C S V W G H0 J K L M0 Q Q0 T X Y Wk d f f0 h k k1 h m w g

%=====
% Расщепление рекурсивной передаточной функции на полифазные компоненты

it = nextpow2(M);
for i = 1:R+1
    for k = 1:it
        y = a{i};
        len = length(y);
        if i == 1, len = 1; else len = (len + 1)/2; end
        y(len) = - y(len);
        a{i} = conv(y, a{i});
        b{i} = conv(b{i}, y);
    end
end

clear len y

%=====
% Деление числителя передаточной функции на полифазные компоненты

Xm = 1;
for i = 1:R + 1
    Xm = conv(Xm, b{i});
end
Xm = [zeros(1,M - 1) Xm]; Xm = fliplr(Xm);
Xp = reshape(Xm, M, N + 1); Xp = fliplr(Xp);

clear b Xm

%=====
% Разбиение полифазных компонент на сомножители

for k = 1:M
    if k == 1, c = 1; else c = 2; end
    f = Xp(k, c:N + 1);
    [p{k}, s{k}, q{k}] = polyfact(f);
    p{k} = fliplr(p{k});
    s{k} = fliplr(s{k});
    if isempty(p{k}) == 1, p{k} = 1; else p{k} = p{k}; end
    if isempty(s{k}) == 1, s{k} = 1; else s{k} = s{k}; end
end

clear f c Xp

```

```

=====
% Импульсная характеристика входных блоков полифазного фильтра

    Ym = 1;
for i = 1:R + 1, Ym = conv(Ym, a{i}); end
    Ym = fliplr(Ym);
    NP = 64*M;
    X = [1 zeros(1, NP - 1)];
    X = filter(1, Ym, X);

        clear Ym a

=====
% Импульсная характеристика полифазных компонент

    Pc = zeros(M, NP); dch = 2^it - 1;
    X = X(find(X)); lng = length(X);
for k = 1:M
    x = X; x = x*q{k};
    sz = size(p{k});
for n = 1:sz(1), x = filter(p{k}(n,:), 1, x); end
    sz2 = size(s{k});
for n = 1:sz2(1), x = filter(s{k}(n,:), 1, x); end
    ch = k - 1;
for i = 1:length(x), Pc(k, i + ch) = x(i); ch = ch + dch; end
    end

clear x X

    sz = size(Pc);
    for k = 1:sz(2), y(:, k) = vhrfft(Pc(:, k)); end
    y = y + y;
y(1,:) = 0.5*y(1,:); y(NCh + 1,:) = 0.5*y(NCh + 1,:);

        clear p s q sz

=====
% Частотная характеристика многоканального фильтра

figure(2), hold on, NP = NP/2 - 1;
for k = 1:NCh + 1
    Sy = 20*log10(abs(fft(y(k,:))));
    plot((0:NP)/NP, Sy(1:NP + 1))
    end
    grid on, hold off
title('Frequency characteristic of the Multichannel Filter')
ylabel('Magnitude in dB')
xlabel('Normalized frequency')
axis([0 1 -amin 0])
zoom
=====

```

Программа разбиения полифазных компонент на множители

```

function [ap,as,h] = polyfact(a)

    n = length(a)-1;
    z = roots(a);          y = imag(z);
    m = 1; l = 1; ap = []; zp = ap; zs = ap; as = ap;
    for k = 1:n
if abs(y(k)) > 2*eps,    zp(m,1) = z(k,1); m = m+1;
    else,                zs(l,1) = z(k,1); l = l+1;    end, end
    for k = 1:(l-1),      as = [as; poly(zs(k,1))];    end
    for k = 1:2:(m-1),    h = poly([zp(k,1) zp(k+1,1)]);
    ap = [ap; h];        end
    h = a(1);

```

Received on the 1st of December 2001

НОВЫЕ СТРУКТУРЫ МАЛОЧУВСТВИТЕЛЬНЫХ ЦИФРОВЫХ ФИЛЬТРОВ

В. ЕРЕМЕЕВ, А. ГУМЕНЮК, Т. МАМИРОВ

*Институт транспорта и связи, департамент электроники
ул. Ломоносова 1, LV – 1019, Рига, Латвия*

Предложены новые структуры для реализации цифровых фильтров - каскадное соединение субструктур первого порядка. Передаточные функции таких фильтров имеют комплексные коэффициенты. Практически реализуемые полосы пропускания при прочих равных условиях на несколько порядков меньше, чем у биквадных реализаций.

Ключевые слова: цифровые фильтры, передаточные функции

We propose new structures for digital filters realization – cascade combination of first-order substructures. The transfer functions of these filters have complex coefficients. Practically realized pass-bands in equal conditions are some orders lower than biquad realizations passbands.

Keywords: digital filters, transfer functions

При проектировании малочувствительных цифровых фильтров с большим динамическим диапазоном возникают проблемы, связанные как с выбором соответствующего класса передаточных характеристик, так и выбором структуры реализации. На наш взгляд, создание робастных систем - это, прежде всего, проблема выбора эффективной структуры.

Ориентация на малочувствительные реализации связана даже не столько с тем, что предполагается использовать в процессорах "короткую арифметику", но в большей степени с желанием получить цифровые фильтры с рекордными характеристиками: либо с очень крутыми амплитудно-частотными характеристиками (АЧХ), либо с максимизацией динамического диапазона, либо, наконец, с предельно узкополосными АЧХ. В дальнейшем для иллюстрации эффективности новых предлагаемых структур мы остановимся на синтезе сверхузкополосных цифровых фильтров нижних частот с классическими характеристиками.

Единственным сегодня известным техническим решением подобного класса задач является применение волновых фильтров [1]. Однако чрезмерная избыточность, сложность проектирования и моделирования оставляют актуальным поиск альтернативных решений. Концептуально проблема выбора новой структуры решена обобщенным сопоставлением двух традиционных реализаций - прямой и биквадной [1-4].

Одна и та же передаточная функция может быть записана для прямой реализации следующим образом:

$$H(z^{-1}) = \frac{b_0 + b_1 z^{-1} + b_2 z^{-2} + \dots + b_N z^{-N}}{1 + a_1 z^{-1} + a_2 z^{-2} + \dots + a_N z^{-N}} \quad (1)$$

Для эквивалентной биквадной реализации соответственно четного и нечетного порядков имеем:

$$H(z^{-1}) = \prod_{k=1}^{N/2} \frac{b_{0k} + b_{1k} z^{-1} + b_{2k} z^{-2}}{1 + a_{1k} z^{-1} + a_{2k} z^{-2}} \quad (2)$$

$$H(z^{-1}) = \frac{b_0 + b_1 z^{-1}}{1 + a_1 z^{-1}} \prod_{k=1}^{(N-1)/2} \frac{b_{0k} + b_{1k} z^{-1} + b_{2k} z^{-2}}{1 + a_{1k} z^{-1} + a_{2k} z^{-2}} \quad (3)$$

Блок-диаграммные реализации прямой и биквадной структур показаны на Рисунках 1 и 2.

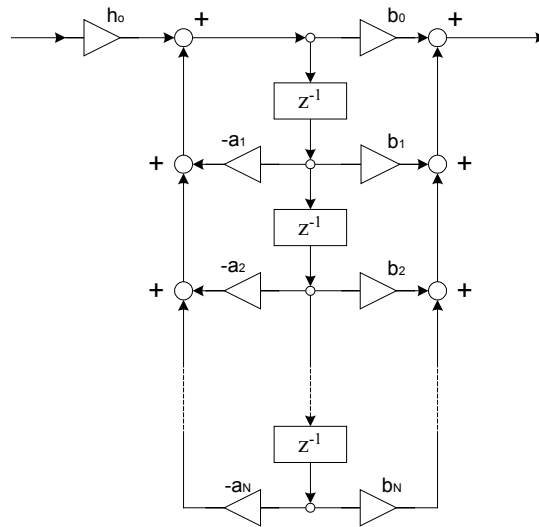


Рисунок 1. Блок-диаграмма прямой структуры

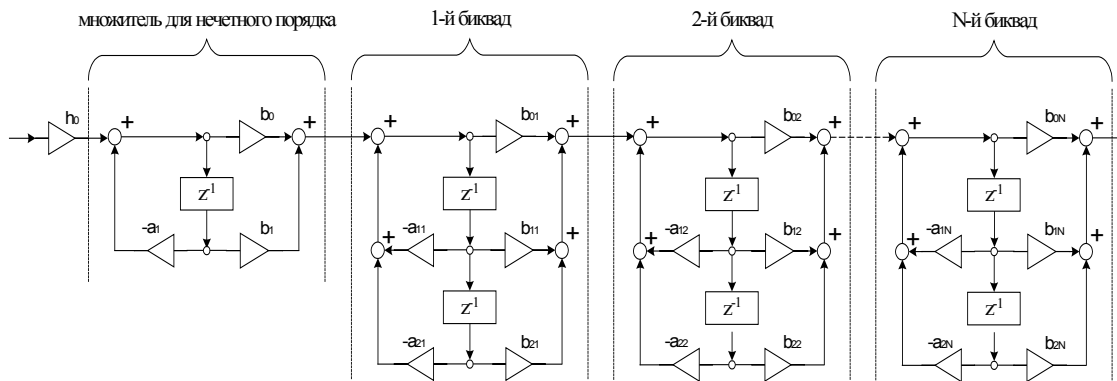


Рисунок 2. Блок-диаграмма биквадной структуры

Для определения частотных характеристик целесообразно использовать встроенную функцию **freqz.m** пакета MatLab-6, в которую передаются рабочий диапазон частот, а также векторы коэффициентов числителя и знаменателя передаточной функции, и которая возвращает комплексный вектор рассчитанных значений передаточной функции. С ее помощью для фильтров Чебышева I-го и II-го рода, а также эллиптического были исследованы АЧХ НЧ – фильтров при уменьшении их полос пропускания.

АЧХ фильтров **прямой** реализации (рис.1) при постепенном уменьшении полосы пропускания вначале не имеют искажений в полосах пропускания и задерживания, но при достижении некоторого критического значения появляются сперва слабые, а затем и все более заметные искажения АЧХ. При дальнейшем сужении полосы пропускания характеристика теряет свою первоначальную форму и, наконец, полностью «разваливается». Для стандартных требований к характеристикам фильтров ниже в таблицах будут приведены зависимости критических полос пропускания от порядка. Отметим также и известный факт, что прямая структура реализации практически нереализуема при больших порядках из-за очень большой чувствительности к точности установки ее коэффициентов и крайне плохой динамики.

Традиционным типом практических реализаций цифровых фильтров является каскадная, т.н. **биквадная** реализация (Рисунок 2). Она позволяет качественно снизить чувствительность структуры к неточностям установки параметров на несколько порядков. В частности, вполне реализуемы ЦФНЧ с критическими полосами пропускания, установленными для прямой

реализации. Полосы пропускания, при которых и у биквадных реализаций того же порядка начинают появляться искажения АЧХ, на несколько порядков меньше.

Исследуя генезис биквадных структур из прямой и рассчитывая на наследуемые при этом процессе свойства, нами сделан следующий логический шаг с намерением получить лучшую структуру. Предлагается каскадно включать звенья только первого порядка, которые в отличие от биквадов естественно именовать как **билайны (biline)**:

Передаточная функция новой реализации может быть представлена в форме:

$$H(z^{-1}) = \prod_{k=1}^N \frac{b_{0k} + b_{1k} z^{-1}}{1 + a_{1k} z^{-1}} \tag{4}$$

Коэффициенты передаточной функции при этом будут в общем случае комплексными. Это усложняет реализацию. Какова же цена такого перехода?. Исследование критических полос пропускания фильтра на билайнах при различных требованиях к его характеристикам подтвердило предположение о получении замечательных преимуществ этого типа реализации, по сравнению с прямой и биквадной. При прочих равных условиях критическая полоса пропускания структуры любого порядка на билайнах гораздо меньше (на несколько порядков!), чем у соответствующей традиционной структуры на биквадах. Подробное сопоставление параметров АЧХ для прямой, биквадной и билайновой реализаций приведены в таблицах ниже. Блок – диаграмма билайн - реализации приведена на Рисунке 3.

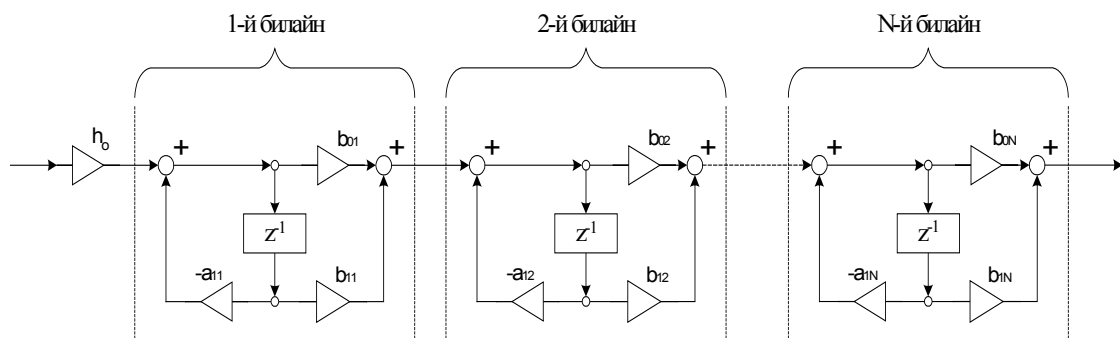


Рисунок 3. Блок-диаграмма biline - структуры

ТАБЛИЦА 1. Критические полосы пропускания для прямой, биквадной и билайн – реализаций фильтра Чебышева I-го рода

Затухание в полосе пропускания	amax, дБ	0,01	0,01	0,01	0,01	0,01	0,01	0,01
Порядок	N	5	7	9	11	13	15	17
Затухание в полосе задерживания	amin, дБ	8	20	35	55	70	85	105
Реализации:								
Прямая	W _{1с}	2,10E-03	9,00E-03	2,20E-02	5,20E-02	8,50E-02		
Биквадная	W _{1с}	6,00E-08	1,00E-07	1,20E-07	3,00E-07	2,00E-06	1,00E-06	2,00E-06
Билайновая	W _{1с}	2,00E-14	1,00E-12	4,00E-12	1,00E-12	8,00E-14	1,00E-13	2,00E-13

Затухание в полосе пропускания	amax, дБ	0,1	0,1	0,1	0,1	0,1	0,1	0,1

Порядок	N	5	7	9	11	13	15	17
Затухание в полосе задерживания	a_{min} , дБ	15	30	45	65	80	95	115
Реализации:								
Прямая	W_{1c}	1,50E-03	9,00E-03	2,80E-02	5,50E-02	9,00E-02		
Биквадная	W_{1c}	1,00E-07	2,00E-07	1,00E-07	3,00E-07	3,00E-07	2,00E-07	2,00E-07
Билайновая	W_{1c}	1,00E-14	7,00E-14	1,00E-13	1,00E-13	3,00E-13	8,00E-14	1,00E-13

Затухание в полосе пропускания	a_{max} , дБ	0,5	0,5	0,5	0,5	0,5	0,5	0,5
Порядок	N	5	7	9	11	13	15	17
Затухание в полосе задерживания	a_{min} , дБ	20	40	55	70	90	105	120
Реализации:								
Прямая	W_{1c}	1,50E-03	1,20E-02	3,50E-02	5,80E-02	9,00E-02		
Биквадная	W_{1c}	9,00E-08	2,00E-07	1,00E-07	2,00E-07	1,00E-07	4,00E-07	5,00E-07
Билайновая	W_{1c}	8,00E-15	3,00E-14	2,00E-13	8,00E-14	8,00E-14	4,00E-13	5,00E-13

ТАБЛИЦА 2. Критические полосы пропускания для прямой, биквадной и билайн – реализаций фильтра Чебышева II-го рода

Затухание в полосе пропускания	a_{max} , дБ	0,01	0,01	0,01	0,01	0,01	0,01	0,01
Порядок	N	5	7	9	11	13	15	17
Затухание в полосе задерживания	a_{min} , дБ	8	20	35	55	70	90	105
Реализации:								
Прямая	W_{1c}	6,00E-04	5,00E-03	1,60E-02	3,50E-02	5,80E-02	8,70E-02	1,10E-01
Биквадная	W_{1c}	8,00E-08	8,00E-08	1,00E-07	2,00E-07	1,00E-07	3,00E-07	2,00E-07
Билайновая	W_{1c}	9,00E-15	9,00E-15	1,00E-14	8,00E-15	3,00E-14	6,00E-14	4,00E-14

Затухание в полосе пропускания	a_{max} , дБ	0,1	0,1	0,1	0,1	0,1	0,1	0,1
Порядок	N	5	7	9	11	13	15	17
Затухание в полосе задерживания	a_{min} , дБ	15	30	45	65	80	95	115
Реализации:								
Прямая	W_{1c}	8,50E-04	6,50E-03	1,90E-02	3,90E-02	6,60E-02	9,50E-02	1,20E-01
Биквадная	W_{1c}	1,00E-07	1,00E-07	2,00E-07	1,00E-07	2,00E-07	2,00E-07	3,00E-07

Билайновая	W_{1c}	5,00E-15	8,00E-15	4,00E-14	7,00E-14	3,00E-14	3,00E-14	9,00E-15
------------	----------	----------	----------	----------	----------	----------	----------	----------

Затухание в полосе пропускания	a_{max} , дБ	0,5	0,5	0,5	0,5	0,5	0,5	0,5
Порядок	N	5	7	9	11	13	15	17
Затухание в полосе задерживания	a_{min} , дБ	20	40	55	70	90	110	125
Реализации:								
Прямая	W_{1c}	9,00E-04	8,00E-03	2,20E-02	4,20E-02	6,70E-02	9,90E-02	1,25E-01
Биквадная	W_{1c}	1,00E-07	1,00E-07	2,00E-07	1,00E-07	2,00E-07	2,00E-07	3,00E-07
Билайновая	W_{1c}	7,00E-15	1,00E-14	3,00E-14	3,00E-14	2,00E-14	3,00E-14	3,00E-14

ТАБЛИЦА 3. Критические полосы пропускания для прямой, биквадной и билайн – реализаций эллиптических фильтров

Затухание в полосе пропускания	a_{max} , дБ	0,01	0,01	0,01	0,01	0,01	0,01	0,01
Порядок	N	5	7	9	11	13	15	17
Затухание в полосе задерживания	a_{min} , дБ	20	50	80	110	140	170	200
Реализации:								
Прямая	W_{1c}	1,50E-03	9,50E-02	2,50E-02	5,20E-02			
Биквадная	W_{1c}	8,00E-08	8,00E-08	1,50E-07	2,40E-07	4,20E-07	4,20E-07	4,20E-07
Билайновая	W_{1c}	2,80E-16	2,80E-15	5,10E-14	7,00E-14	7,00E-14	8,00E-14	8,90E-14

Затухание в полосе пропускания	a_{max} , дБ	0,1	0,1	0,1	0,1	0,1	0,1	0,1
Порядок	N	5	7	9	11	13	15	17
Затухание в полосе задерживания	a_{min} , дБ	30	60	90	120	150	180	210
Реализации:								
Прямая	W_{1c}	1,40E-03	9,50E-03	2,80E-02	5,50E-02			
Биквадная	W_{1c}	1,50E-07	1,50E-07	3,00E-07	2,60E-07	4,00E-07	4,00E-07	1,00E-06
Билайновая	W_{1c}	5,80E-15	2,50E-14	7,20E-14	3,90E-14	4,00E-13	2,50E-13	3,50E-13

Затухание в полосе пропускания	a_{max} , дБ	0,5	0,5	0,5	0,5	0,5	0,5	0,5
Порядок	N	5	7	9	11	13	15	17
Затухание в полосе задерживания	a_{min} , дБ	40	70	100	130	160	190	220
Реализации:								

Прямая	W_{1c}	1,50E-03	1,00E-02	3,20E-02	6,00E-02			
Биквадная	W_{1c}	1,00E-07	1,50E-07	1,80E-07	2,50E-07	2,50E-07	3,20E-07	3,80E-06
Билайновая	W_{1c}	1,90E-14	4,70E-14	1,50E-13	1,50E-13	3,00E-13	4,50E-13	9,00E-13

В заключение отметим, что для новых структур при программных вычислениях приходится перемножать комплексные числа. Обычно эта операция приводит к четырем вещественным умножениям:

$$(a + jb)(c + jd) = ac - bd + j(bc + ad)$$

Вместо этого лучше использовать следующий алгоритм:

$$(a + jb)(c + jd) = ac - bd + j(bc + ad) = a(c + d) - d(a + b) + j a(c + d) + j c(b - a) = A_1 - A_2 + j (A_1 + A_3),$$

где $A_1 = a(c + d)$, $A_2 = d(a + b)$, $A_3 = c(b - a)$.

Здесь мы получаем 3 умножения вместо 4-х при большем числе суммирований (5 вместо 2). Более того, если необходимо выполнять умножение на комплексную константу, то число сложений можно сократить до трех. В целом предлагаемый способ лучше тривиального, так как повышается точность вычислений и уменьшаются шумы умножений.

Литература

- [1] Антонью А. (1983) *Цифровые фильтры: анализ и проектирование*. Радио и связь, Москва 320 с.
- [2] Каппелини В., Константи́нидис А. Дж, Эмилиани П. (1983) *Цифровые фильтры и их применение*. Энергоатомиздат, Москва 360 с.
- [3] Оппенгейм А.В., Шафер Р.В. (1979) *Цифровая обработка сигналов*. Связь, Москва 416 с.
- [4] Рабинер Л., Гоулд Б. (1978) *Теория и применение цифровой обработки сигналов*. Мир, Москва. 848 с.

Received on the 1st of December 2001

Authors' index

BRITAVSKAYA E.P.	85
BUDILOV K.	42
FINOGENOV A.	28
GRYAZNOV D.	28
GUMENYUK A.	124
KABASHKIN I.V.	90
KABELEV N.	119
KALNIN J.-R.	18
KIV A.E.	85
KOPYTOV E.	119
KOTOMIN E.A.	7, 18
LABENDIK V.	119
MAMIROV T.	132
MATOSOV E.V.	124
NASKIDAYEV O.	100
SHUNIN YU.N.	7, 28, 42
SYCHEV O.	7
TIMONIN S.G.	124
YATCKIV I.V.	96
YEREMEYEV V.P.	124,132
ZHUKOVSKII Yu.F.	7, 28



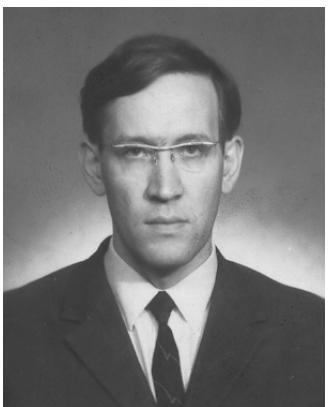
Yuri N. Shunin (b. March 6, 1951 in Riga)

- Director of General and Applied Physics Department (Transport and Telecommunication Institute Riga). *Director of specialities:* Semiconductor Electronics & Technologies, Computer simulation of semiconductor technologies, the Head of Department of natural sciences and computer modelling (Information System Management Institute). *Director of speciality:* Information Systems
- **University study:** Moscow physical and technical institute (1968-1974).
- Ph.D. (physics & mathematics) on solid state physics (1982, Physics Institute of Latvian Academy of Sciences), Dr. Sc. Habil (physics & mathematics) on solid state physics (1992, Ioffe Physical Institute of Russian Academy of Sciences).
- **Publications:** 170 publications, 1 patent.
- **Scientific activities:** solid state physics, physics of disordered condensed media, amorphous semiconductors and glassy metals, semiconductor technologies, heavy ion induced excitations in solids, mathematical and computer modelling, system analysis



Igor V. Kabashkin (born in Riga, 1954)

- Vice-rector for Research and Development Affairs of Transport and Telecommunication Institute, Professor, Director of Telematics and Logistics Institute,
- PhD in Aviation (1981, Moscow Institute of Civil Aviation Engineering), Dr.Sc.Habil. in Aviation (1992, Riga Aviation University), Member of the International Telecommunication Academy, Member of IEEE, Corresponding Member of Latvian Academy of Sciences (1998)
- **Publications:** 280 scientific papers and 67 patents.
- **Research activities:** information technology applications, operations research, electronics and telecommunication, analysis and modelling of complex systems, transport telematics and logistics



Vitaly Yeremeyev (b. 1940 in Irkutsk, Russia),

- Professor of Transport and Telecommunication Institute, Dc.Sc.Habil.
- **Publications:** 170 scientific works, 30 patents.
- **Scientific activities:** digital signal processing, fast algorithms, numerical methods in computer science, system theory, digital filtering.



Eugene Kotomin (b. September 20, 1949, Vilnius, Lithuania)

Professor, Dr. Sc. Habil., Head of Theoretical Laboratory of Institute Solid State Physics, University of Latvia

University study: University of Latvia (Faculty of Physics), 1971

Dr.habil.phys. (in Solid State Physics) (Doctor of Science in former USSR). Title of Thesis: "Theory of Defect Accumulation and Recombination in Ionic Crystals Controlled by Electron Tunnelling", Institute of Physics, Latvian Academy of Sciences, 1988.

Publications: 3 books and more than 300 papers

Interests:

- Theoretical and Statistical Physics
- Solid State Physics
- Chemical Physics of Condensed Matter
- Theory of Defects in Nonmetallic Solids

Head of Project. Physics of Metal/Oxide Interfaces. *Joint project with University College London, UK, 1998-1999.*

Head of Project. Large Scale Computer Modelling of Materials. *Joint project with Royal Academy of Sciences, Sweden, 1999-2000.*



Yuri F. Zhukovskii (b. February 2, 1949, Riga, Latvia),
Theoretical Laboratory of Institute Solid State Physics, University of Latvia

Education:

1966-75. **B.S. + M.S. degrees:** Department of Physics and Mathematics, the University of Latvia, Riga, Latvia.

1986-92. **Ph.D. degree (Dr. chem.):** Institute of Inorganic Chemistry, Latvian Academy of Sciences, Latvia,

and Institute of Physics, St. Petersburg State University, Russia.

Advisors: Dr. chem. A.K. Lokenbach (Riga) and Dr. phys. E.P. Smirnov (St. Petersburg).

Title of the Thesis: "Quantum-chemical investigations of water chemisorption on aluminum surface".

Publications: 70 papers and conference abstracts dealing with the quantum chemistry.

CONFERENCES: 32 presentations dealing with the quantum chemistry were prepared for 27 international conferences, meetings, seminars and symposiums organized in 12 countries (with 28 published abstracts).

01-03.2000. Visiting scientist, Centre for Materials Research, University College London, Great Britain;

04-05. and 10-11.2000. Visiting scientist, the Ångström Laboratory, Inorganic Chemistry, Uppsala University, Sweden

Arnold E. Kiv, professor, Dr. Sc. Habil (phys&math)



- Chief of Theoretical Physics Department and Computer Modelling Laboratory South Ukrainian Pedagogical University, professor of the Department of Materials Engineering, Ben-Gurion University of the Negev P.O.B. 653, Beer-Sheva, 84105, Israel

Scientific activities: sub-threshold radiation effects in solids. Present scientific activities: computer modelling of processes in physics, psychology and social sciences.



Eugene A. Kopytov (b. December 5, 1947 in Lignica, Poland),

- Rector of Transport and Telecommunication Institute, Professor of Computer Science Department, Doctor Habilitatus of Science, Academician of Baltic Informatization Academy,
- **Publications:** 125 publications and 1 patent.
- **Scientific activities:** computer science and information technology applications, modelling and simulation, statistical recognition and classification.



Juris-Robert Kalninsh (b. 1942 in Riga), Professor, Dr Sc. Habil.

- ◆ 1991 Dr Sc Habil. in physics.
- ◆ 1983 Dr Sc in Physics, Institute of Physics
- ◆ 1972 Ph.D. Institute of Physics

President of the Association of Latvian Scientists, Vice-rector of Social Technologies Institution of Higher Education

Scientific interests: Theoretical physics. Transport in heterogeneous media and composite materials. Kinetics of bimolecular reactions in condensed matter with focus on many-particle processes. The kinetics of the generation, annealing, migration of defects in solids under irradiation. Large-scale computer simulations of processes in condensed matter



Deniss Gryaznov (b. 1977 in Novgorod)

- BS on Electronics (Riga Aviation University, 1999)
- MS on Computer Modelling of Semiconductor Technologies (Transport and Telecommunication Institute , 2001)

Scientific activities: radiation detectors, computer modeling, scattering theory, ion implantation, chaos and applied physics.



Cyril Budilov (b. 1977 in Novgorod)

- BS on Electronics (Riga Aviation University, 1999)
- MS on Computer Modelling of Semiconductor Technologies (Transport and Telecommunication Institute , 2001)

Scientific activities: nuclear physics, computer modeling, scattering theory, ion implantation, chaos and applied physics. Also is interested in modeling of semiconductor devices



Eduard Matosov

- Master of Sciences
- University study in of Riga Aviation University (1993 - 1999).



Oleg Naskidaev (born on February 14, 1977 in Riga)

- BS on Electronics (Riga Aviation University, 1999)
- MS on Computer Modelling of Semiconductor Technologies (Transport and Telecommunication Institute , 2001)
- Service Specialist of Tieto Konts Financial Systems Ltd
- **Scientific activities:** computer modelling, programming on the C++ and Pascal, ion implantation, chaos and applied physics. Also is interested in modelling of semiconductor technologies.

Vladimir Labendik (born in Russia, 1946)

- Academic education in Riga Civil Aviation Engineering Institute, Candidate of Technical Sciences (1980, RCAEI), Dr. Sc. Habil. (1999, Riga Aviation University), 95 scientific works and 6 patents.

Scientific interests: thermodynamics, mathematical modelling of exploitation parameters of aviation engines, diagnostics of aviation engines

Oleg Sychev (b. 1974 in Lipezk, Russia)

- Master of Science
- University study in Riga Aviation University (1992-1997).

Scientific activities:

computer modelling, solid state electronics, computer sciences, solid state band structure calculations

Takhir Mamirov (b. in Almaty, Kazakhstan, May 16, 1980)

- 1st years student of Master Study Programme of Transport and Telecommunication Institute, Electronics, Telecommunication and Computer techniques Faculty, specialization – Digital Telecommunication Technologies (Latvia, Riga, Lomonosov St, 1)

Scientific interests: computer modelling, computer hardware, digital filters

COMPUTER MODELLING & NEW TECHNOLOGIES

ISSN 1407-5806 & ISSN 1407-5814(on-line)

EDITORIAL BOARD:

Prof. Igor Kabashkin (Chairman of the Board), *Transport & Telecommunication Institute, Latvia*

Prof. Yuri Shunin (Editor-in-Chief), *Transport & Telecommunication Institute, Latvia*

Prof. Adolfas Baublys, *Vilnius Gedeminas Technical University, Lithuania;*

Dr. Brent Bowen, *University of Nebraska at Omaha, USA;*

Prof. Olgierd Dumbrajs, *Helsinki University of Technology, Finland;*

Prof. Vitaly Yeremeyev, *Transport & Telecommunication Institute, Latvia*

Prof. Juris-Roberts Kalninch *Social Technologies Institution of Higher Education, Latvia;*

Prof. Arnold Kiv, *Ben-Gurion University of the Negev, Israel*

Prof. Anatoly Kozlov, *Moscow State University of Civil Aviation, Russia;*

Prof. Juris Zakis, *University of Latvia.*

Technical editor:

MS Christina Hamroon, *Transport & Telecommunication Institute, Latvia*

MS Cyril Budilov, *Transport & Telecommunication Institute, Latvia*

Host Organization:

Transport and Telecommunication Institute - Eugene Kopytov, Rector

Co-Sponsor Organizations:

PAREX Bank, Latvia - Valery Kargin, President

Information System Management Institute, Latvia - Roman Dyakon, Rector

Supporting Organization:

Latvian Transport Development and Education Association - Andris Gutmanis, President

Latvian Academy of Sciences - Juris Ekmanis, Vice-president

University of Nebraska at Omaha, USA - Brent Bowen, Director of Aviation Institute

THE JOURNAL IS DESIGNED FOR PUBLISHING PAPERS CONCERNING THE FOLLOWING FIELDS OF RESEACH:

- mathematical and computer modelling
- mathematical methods in natural and engineering sciences
- physical and technical sciences
- computer sciences and technologies
- semiconductor electronics and semiconductor technologies
- aviation and aerospace technologies
- electronics and telecommunication
- navigation and radar systems
- telematics and information technologies
- transport and logistics
- economics and management
- social sciences

Articles are presented in the journal in English (preferably), Russian, German and Latvian languages (at the option of authors). All articles are reviewed.

EDITORIAL CORRESPONDENCE

Transporta un sakaru institūts (Transport and Telecommunication Institute)
Lomonosova iela1, LV-1019, Riga, Latvia. Phone: (+371)-7100593. Fax: (+371)-7100535.
E-mail: journal@tsi.lv, <http://www.tsi.lv>

COMPUTER MODELLING AND NEW TECHNOLOGIES, 2001, Vol. 5, No.1
Scientific and research journal of Transport and Telecommunication Institute (Riga, Latvia).
The journal is published since 1996.

The Camera-Ready Copies

PREPARATION OF CAMERA-READY TYPESCRIPT: COMPUTER MODELLING AND NEW TECHNOLOGIES

A Guide for Authors

A.N. AUTHOR

*Affiliation
Institute address*

Abstract reviews the main results and peculiarities of a contribution. Abstract is presented always in English or in English and the second (presentation) language both.

1. Introduction

These instructions are intended to provide guidance to authors when preparing camera-ready submissions to a volume in the **CM&NT**. Please read these general instructions carefully before beginning the final preparation of your camera-ready typescript.

Two ways of preparing camera-ready copy are possible:

- (a) preparation on a computer using a word processing package;
- (b) printed copy fitted for scanning.

2. Printer Quality, Typing Area and Fonts

IMPORTANT:

If you produce your camera-ready copy using a laser printer, use a 15 x 23 cm typing area (in A4 format: 37 mm - left, 30 mm- right, 30 mm- top, 30 - bottom, line spacing - single), as in these instructions, in combination with the **10 points Times** font. The pages will then be reproduced one to one in printing.

Fonts

The names and sizes of fonts are often not the same on every computer system. In these instructions the Times font in the sizes 10 points for the text and 8 points for tables and figure legends are used. The references section should be in the 10 points font.

3. Format and Style

The text should be in clear, concise English (or other declared language). Please be consistent in punctuation, abbreviations, spelling (**British English**), headings and the style of referencing.

Camera-ready copy will be printed exactly as it has been submitted, so please make sure that the text is proofread with care.

In general, if you prepare your typescript on a computer using a word processing package, use styles for the font(s), margin settings, headings, etc., rather than inserting these layout codes every time they are needed. This way, you will obtain maximum consistency in layout. Changes in the layout can be made by changing relevant style(s).

4. Layout of the Opening Page

A sample for the opening page of a contribution is shown in Figure I on page 3. Requirements for the opening page of a contribution are (see also Figure 1) : the titles should always be a centered page and should consist of: the title in capital letters, bold font, flush center, on the fourth text line; followed by the subtitle (if present) in italics, flush center, with one line of white above. The author's name(s) in capitals and the affiliation in italics, should be centered and should have two lines of white space above and three below, followed by the opening text, the first heading or the abstract.

5. Headings

Please distinguish the following four levels of headings:

1. First-order Heading

This heading is in bold, upper and lowercase letters, numbered in arabic figures, and has two lines of space above and one line below. The text begins full out at the left margin.

1.1. SECOND-ORDER HEADING IN CAPITALS

This heading is in roman capitals, numbered in arabic figures and has one line of space above and below. The text begins full out at the left margin.

1.1.1. *Third-order Heading in Italics*

This heading is in italics, upper and lower case letters, numbered in arabic figures and has one line of space above and no space below. The text begins full out at the left margin.

Fourth-order Heading in Italics. This heading is in italics, upper and lowercase letters, with one line of space above the heading. The heading has a full stop at the end and the text runs on the same line.

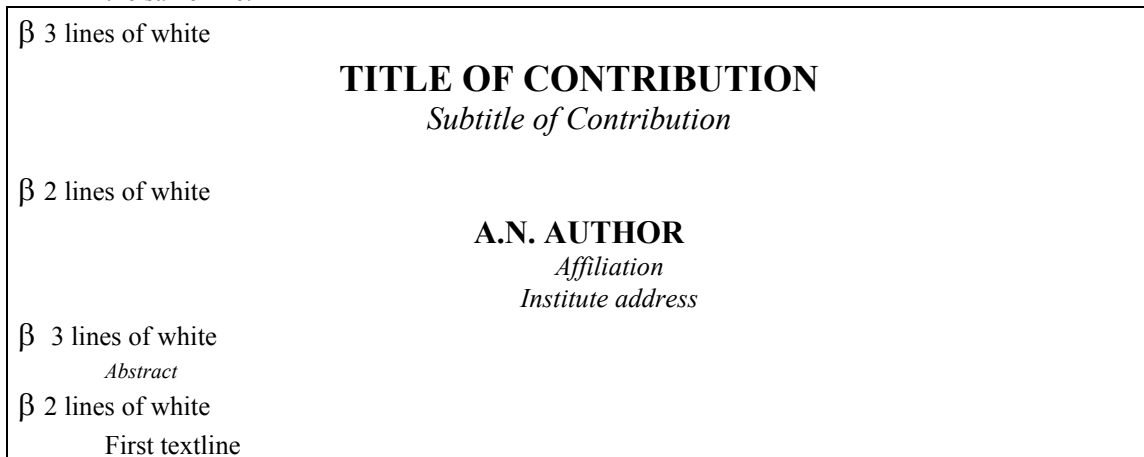


Figure 1. Example of an opening part of contribution to a Volume of RAU Scientific Reports.

6. Figures and Photographs

- *Line drawings* must be submitted in original form, on good quality tracing paper, or as a glossy photographic print.

- *Halftone photographs* must be supplied as glossy prints.

- *Colour illustrations.* Colour illustrations are more expensive and the author is expected to cover the extra costs . Please consult with Editors about this.

Mount all illustrations directly into the text at the appropriate places. Alternatively, it is acceptable to leave the appropriate space blank in the text, and submit the illustrations separately. In this case You

must put the figure numbers in pencil in the open spaces in the text and on the back of the figures. Also indicate the top of the illustration.

For computer plotting the ORIGIN Software is preferable.

- Legends for figures/illustrations should not be incorporated in the figure itself and they should be listed in numerical order (headed as "Figure 1.", "Figure 2.", etc.). The legends should be set centered, below the figure.

7. Displayed Equations

Displayed equations should be in the left side of the page, with the equation number in parentheses, flush right.

$$E_{int} = \iint \psi^+(\mathbf{x})\psi(\mathbf{x})K(\mathbf{x} - \mathbf{x}')(-div\mathbf{P}(\mathbf{x}'))d^3x d^3x' , \quad (1)$$

$$K(\mathbf{x} - \mathbf{x}') = C_0 \frac{\exp(-\lambda(|\mathbf{x} - \mathbf{x}'|))}{|\mathbf{x} - \mathbf{x}'|} . \quad (2)$$

Font sizes for equations are: 12pt -full, 7pt - subscripts/superscripts, 5pt - sub- subscripts/superscripts, 18pt - symbols, 12pt - subsymbols .

8. Tables

Please center tables on the page, unless it is necessary to use the full page width. Exceptionally large tables may be placed landscape (90° rotated) on the page, with the top of the table at the left-hand margin. An example of a table is given below:

TABLE 1. National programs of fusion research [1]

Experiment	Type	Laboratory	Task	Begin of operation
JET	tokamak	Joint European Torus, Culham, UK	Plasma physics studies in the region close to ignition	1983
TEXTOR	tokamak	FA, Jülich. Germany	Studies of plasma-wall interaction	1982
TORE SUPRA	tokamak	CEA, Cadarache, France	Testing of super-conducting coils, stationary operation	1988
ASDEX Upgrade	tokamak	IPP, Garching, Germany	Plasma boundary studies in divertor plasmas	1990
WENDELSTEIN 7-AS	stellarator	IPP, Garching, Germany	Testing the principles of "advanced stellarator"	1988
WENDELSTEIN 7-X	stellarator	IPP, Greifswald, Germany	Testing feasibility of "advanced stellarator" for power station	2004

9. References

The References should be typeset in a separate section as a numbered list at the end of your contribution in the following style:

Journal articles should consist of: author's name, initials, year, title of article, journal title, volume number, inclusive page numbers, e.g.:

- [1] Dumbrajs O. (1998) Nuclear Fusion. *RAU Scientific Reports & Computer Modeling & New Technologies 2, aa-zz*
- [2] Kiv A.E. , Polozovskaya I.A., Tavalika L.D. and Holmes S. (1998) Some problems of operator-machine interaction.. *RAU Scientific Reports & Computer Modelling & New Technologies 2, aa-zz*
- [3] Shunin Yu.N. (1996) Elementary excitations and radiation defects in solids induced by swift heavy ions. *RAU Scientific Reports & Solid State Electronics & Technologies 1, 15-35*
- [4] Schwartz K. (1996) Excitons and radiation damage in alkali halides. *RAU Scientific Reports &*

Book references should consist of: author's name, initials, year, title of book, publisher, place of publication, e.g.:

[5] Schwartz K. (1993) *The Physics of Optical Recording*. Springer-Verlag, Berlin Heidelberg New York

[6] Shunin Yu.N. and Schwartz K.K. (1997) Correlation between electronic structure and atomic configurations in disordered solids. In R.C. Tennyson and A.E. Kiv (eds.). *Computer Modelling of Electronic and Atomic Processes in Solids*. Kluwer Academic Publishers, Dordrecht, pp. 241-257 .

Unpublished papers should consist of: author's name, initials, year (or: in press), title of paper, report, thesis, etc., other relevant details, e.g.:

[7] Shunin Yu.N. (1995) Elementary Excitations in amorphous solids accompanying the swift heavy ions passages. Private communication. GSI Seminar. Darmstadt

The references above should be cross-referenced by numbers within square brackets:

...as cited in [1], or Kiv *et al.* [2]... The use of author initials for cross-references is not encouraged.

10. Authors Index

Editors form the author's index of a whole Volume . Thus , all contributors are expected to present personal colour photos with the short information on the education , scientific titles and activities.

11. Submission

Check your typescript very carefully before it is submitted. Submit two copies of the typescript to the Editors of the Volume. Always retain a copy of all material submitted as backup.

11.1. DISK FORMATS AND WORD PROCESSING PACKAGES

If you want to present contributions electronically please before submitting accord with the Editors the details on your computer system, your word processing package and version (MS Word 6 and above versions are preferable) and the way of transfer on the information (disk or Internet).

Acknowledgements

Acknowledgements (if present) mention some specialists , grants and foundations connected with the presented paper. The first page of the contribution should start on page 1 (right-hand, upper, without computer page numbering). Please paginate the contributions, in the order in which they are to be published. Use simple pencil only.